Finite element model updating of bridge structures using game theory based algorithm

Ereiz, Suzana

University of Zagreb
Faculty of Civil Engineering

Suzana Ereiz

FINITE ELEMENT MODEL UPDATING OF BRIDGE STRUCTURES USING GAME THEORY BASED ALGORITHM

DOCTORAL DISSERTATION

Zagreb, 2023.

University of Zagreb
Faculty of Civil Engineering

Suzana Ereiz

FINITE ELEMENT MODEL UPDATING OF BRIDGE STRUCTURES USING GAME THEORY BASED ALGORITHM

DOCTORAL DISSERTATION

Supervisors: Assoc. prof. Ivan Duvnjak, Ph.D.
Assoc. prof. Javier Fernando Jiménez Alonso, Ph.D.

Zagreb, 2023.

Sveučilište u Zagrebu
Građevinski fakultet

Suzana Ereiz

Poboljšanje modela konačnih elemenata mostova primjenom algoritma temeljenog na teoriji igara

DOKTORSKI RAD

Mentori: Izv. prof. dr. sc. Ivan Duvnjak,
Izv. prof. dr. sc. Javier Fernando Jiménez Alonso

Zagreb, 2023.

Statement of the originality

The work contained in this thesis has not been previously submitted for a degree or diploma at any other higher education institution. To the best of my knowledge and belief, the thesis contains no material previously published or written by another person except where due references are made.

Suzana Ereiz, M. S. CE.

Supervisor information

Ivan Duvnjak was born in Sinj in 1984. After primary and secondary, he enrolled at the Faculty of Civil Engineering at the University of Zagreb, where he graduated in Structural Engineering in 2008. In 2015, he completed his PhD at the same faculty on the topic "Damage assessment on plate structures using dynamic parameters" under the supervision of prof. Mladenko Rak.

In June 2016 he became an assistant professor at the University of Zagreb, Faculty of Civil Engineering, and in October 2021 he was promoted to associate professor. He is the Lecturer in charge at graduate and postgraduate study programs at the University of Zagreb, Faculty of Civil Engineering in the subjects Theory of Elasticity and Plasticity, Mechanics of Materials and Methods of Theory of Elasticity and Plasticity.

As an author and co-author, he has published more than 80 scientific papers in journals and at international and national scientific conferences. He is one of the authors of the university textbook "Theory of elasticity and plasticity with methods for solving tasks". He is actively involved in ten international and national scientific research projects. In his scientific work, he develops in the field of testing and damage detection of structures, model updating and structural health monitoring of structures. He is currently a reviewer for six international and one national scientific journal and has served as a guest editor in scientific journals. He recently spent a short period at international institutes (Eucentre TREES Lab) and universities (Lulea LTU, Barcelona UPC, Aveiro) in Europe. Besides his scientific and teaching activities, he is actively involved in professional work. Since 2018 he is head of the Structural Testing Laboratory and head of Chair for Mechanics of Materials and Testing of Structures since 2022.

He is an active member of the international working group AG9 (Testing and Structural Health Monitoring) at FIB and the International Association for Bridge and Structural Engineering (IABSE).

Supervisor information

Javier Fernando Jiménez Alonso was born in 1976 in Almeria, Spain. After graduating from high school, he enrolled at the Higher Technical School of Civil Engineering in Granada, where he graduated with a master's thesis on "Marine Structures Design". In October 2007, he was accepted as a research and teaching assistant at the Higher Technical School of Building Engineering, Department of Building Structures of the University of Seville. In 2011 he started his postgraduate studies at the Higher Technical School of Engineering, University of Seville. In December 2015 he defended his PhD thesis entitled "Proposal and calibration of a biodynamic model of human-structure interaction by the resolution of the inverse dynamic problem: application to pedestrian bridges" under the supervision of prof. Andres Sáez. In April 2019, he became an assistant professor at the Technical University of Madrid, Higher Technical School of Civil Engineering. In 2020 he was academic secretary of the Department of Continuum Mechanics and Structural Analysis, Technical University of Madrid. In February 2021 he became an assistant professor at the University of Seville, Higher Technical School of Engineering. Since the beginning of his work at the University, he has been actively involved in scientific research projects. He collaborated in 6 Spanish research projects, published 26 articles in scientific journals and more than 50 conference papers as author or co-author. He is the Lecturer in charge at graduate and postgraduate study programs at University of Seville, Higher Technical School of Engineering in the subjects Aircraft Structures, Airport Structures I, Airport Structures II, Concrete-Steel Composite Structures and Computational Methods for Fatigue Analysis. In addition to teaching and participating in scientific research projects, he has experience in many professional projects, including in-situ monitoring of footbridges, in which he had a leading role. His professional activities also include the design of multiple civil engineering structures, with a special focus on footbridges. Additionally, he has taken part in several projects about retrofitting and improving the dynamic performance (vibration control) of civil engineering structures. He is a member of the Spanish Association of Civil Engineers.

Abstract

In this research, an implementation of game theory has been developed as a computational tool to assist designers in solving the maximum likelihood finite element model updating problem of bridge structures. Finite element model updating is usually performed using the deterministic maximum likelihood method by defining the updating problem as an optimization problem in terms of a single or multi-objective function. In this way, a numerical model is obtained that reflects the actual structural behaviour. Despite its widespread use, the maximum likelihood method has some limitations that are directly related to the performance of the updating process. To overcome these limitations, game theory has been considered herein. For this purpose, the conventional updating problem, formulated as either a single or a multi-objective function, has been transformed into a game theory problem, considering three different game models: non-cooperative, cooperative and evolutionary. The performance of the proposal has been assessed on two case studies the simple finite element model of the laboratory bridge and a high-fidelity finite element model of the real pedestrian suspension bridge. As a result of this research, game theory has proven to be an efficient tool to improve the performance of the finite element model updating process under the maximum likelihood method, as it ensures a reduction in computational time without compromising the accuracy of the solution.

Keywords: *finite element model updating, game theory, maximum likelihood method, structural dynamic parameters, bridge structures*

Prošireni sažetak

U okviru ove doktorske disertacije razvijen je deterministički pristup poboljšanja modela konačnih elemenata mostovnih konstrukcija temeljen na metodi najveće vjerojatnosti koji uključuje transformaciju klasičnog optimizacijskog problema poboljšanja modela konačnih elemenata u problem teorije igara. Poboljšanje numeričkih modela provodi se s ciljem kako bi se dobio model konačnih elemenata čije ponašanje odgovara stvarnoj konstrukciji. Varijacije u svojstvima materijala, starenje i već postojeća oštećenja konstrukcije mosta utječu na parametre modela koji ga opisuju te time dovode u pitanje njegovu daljnju primjenu. Zbog brige o starenju i degradaciji velikog broja mostova, u posljednje vrijeme sve je intenzivniji rad na praćenju njihova stanja kroz razne pristupe. Među tim pristupima jedan od sve popularnijih jest analiza dinamičkih parametara (frekvencija i oblika titranja konstrukcije). Navedeno je iniciralo upotrebu podataka dobivenih ispitivanjem konstrukcije u svrhu poboljšanja modela konačnih elemenata i njihovu daljnju upotrebu. Ovaj postupak, tzv. poboljšanje numeričkih modela (eng. *Finite element model updating*, FEMU) može se provesti kroz niz pristupa koji se dijele na determinističke i stohastičke. U inženjerskoj praksi, obično se primjenjuje deterministički pristup najveće vjerojatnosti. Primjenom navedenog pristupa problem ažuriranja modela konačnih elemenata formulira se kao optimizacijski problem definiranjem jednociljne (eng. *single*) ili višeciljne (eng. *multi*) objektivne funkcije. Funkcija s jednim ciljem definira se u obliku sume reziduala eksperimentalno određenih i numerički predviđenih dinamičkih parametara konstrukcije pomnoženih težinskim faktorima. U višeciljnoj objektivnoj funkciji, svaki njen član odgovara jednom rezidualu. Optimizacija objektivnih funkcija rezultira vrijednostima parametara numeričkog modela za čije vrijednosti on odgovara stvarnom ponašanju konstrukcije. Provodi se primjenom prirodom inspiriranih algoritama zbog njihove učinkovitosti u rješavanju nelinearnih problema optimizacije. Bez obzira na široku i učestalu primjenu za poboljšanje numeričkih modela, deterministički pristup metode maksimalne vjerojatnosti ima nekoliko ograničenja koja su izravno povezana s učinkovitošću procesa poboljšanja te načinom definiranja problema optimizacije. Glavni problemi formulacije optimizacijskog problema kao jednociljne objektivne funkcije vezani su uz definiranje

vrijednosti težinskih faktora koji se pridružuju rezidualu vlastite frekvencije i rezidualu modalnih oblika te potrebu provođenja analize utjecaja različitih vrijednosti težinskih faktora na rezultat optimizacije. Definiranje poboljšanja numeričkih modela u obliku višeciljne objektivne funkcije povezan je s problemom vremena potrebnog za proračun skupa optimalnih rješenja (Pareto skup) i problemom odabira najboljeg rješenja iz Paretovog skupa optimalnih rješenja (eng. *knee point*). Kako bi se navedeni problemi riješili, u ovom istraživanju usvojen je pristup teorije igara kao računalnog alata. U tu svrhu, za rješavanje nedostataka definiranja optimizacijskog problema poboljšanja numeričkog modela kao objektivne funkcije s jednim ciljem uzet je u obzir kooperativni model igara. Uz to, testirana su tri modela igara: nekooperativni, kooperativni i evolucijski kako bi se savladali nedostaci definiranja optimizacijskog problema kao objektivne funkcije s više ciljeva. Učinkovitost predloženog pristupa najprije je testirana u okviru poboljšanja numeričkog modela jednostavnog laboratorijskog mosta. Testiranjem je potvrđena učinkovitost primjene teorije igara u rješavanju problema poboljšanja numeričkih modela definiranog kao objektivna funkcija s jednim ili više ciljeva. U usporedbi s konvencionalnim pristupom, teorija igara pokazala se vrlo učinkovitom u smislu smanjenja vremena proračuna, bez da se njime utječe na točnost rješenja. Nadalje, primjena teorije igara omogućava direktno pronalaženje najboljeg optimalnog rješenja bez potrebe određivanje cijelog skupa optimalnih rješenja. Usporedba različitih modela igara pokazala je kako je evolucijski model igara najefikasniji rezultirajući vremenom proračuna vrlo bliskom kooperativnom modelu, ali dajući rješenje koje je najbliže najboljem optimalnom rješenju Pareto skupa. Uspoređujući formulaciju objektivne funkcije s jednim ciljem i objektivne funkcije s više ciljeva kao problem teorije igara, objektivna funkcija s više ciljeva pokazala se boljom, bez obzira na nešto duže vrijeme proračuna, ali dajući optimalno rješenje koje je najbliže najboljem optimalnom rješenju. Zbog toga je ovaj model igara odabrana za rješavanje problema poboljšanja numeričkog modela visoke točnosti na studiji slučaja visećeg pješačkog mosta. Kroz navedenu primjenu na stvarnoj mostovnoj konstrukciji i usporedbu s konvencionalnom metodom poboljšanja numeričkih modela, potvrđena je primjena teorije igara u rješavanja problema poboljšanja numeričkih modela visoke točnosti složenih tipova mostovnih konstrukcija kao što su viseći mostovi. Kao krajnji rezultat ovog istraživanja, pokazalo se da je teorija igara vrlo učinkovit alat za unaprjeđenje izvedbe poboljšanja modela konačnih elemenata temeljenih na deterministčkom pristupu metode maksimalne vjerojatnosti.

Ključne riječi: *poboljšanje modela konačnih elemenata, teorija igara, metoda maksimalne vjerojatnosti, dinamički parametri konstrukcije, mostovne konstrukcije*

Contents

Statement of the originality i
Supervisor information ii
Supervisor information iii
Abstract iv
Proširenі sažetak v
Contents vii
Notations x
Glossary xix
Chapter 1. Introduction 1
1.1. Problem statement 1
1.2. Objectives, scope, and hypotheses of the research 8
1.3. Methodology and plan of research 9
1.4. Organization of the thesis 11
Chapter 2. FEMU using the conventional methods 13
2.1. Main terms in FEMU procedure and their relationship 13
2.2. Selection of the updating parameters and model class 14
2.3. Definition of FEMU problem 16
2.3.1. Iterative deterministic MLM 17
2.4. Nature inspired computational optimization algorithm 19
2.4.1. Genetic algorithm 19
2.4.2. Particle swarm optimization 24
2.4.3. Simulated annealing 28
2.4.4. Harmony search 31
2.4.5. Hybrid local-global optimization algorithm 33
Chapter 3. GT for FEMU optimization 37
3.1. Main terms in GT 37
3.2. GT for SO optimization 39
3.3. GT for MO optimization 40
3.3.1. General problem 41

3.3.2. Determination of the game player's strategy space ... 42
3.3.3. NCGT model ... 44
3.3.4. CGT model ... 46
3.3.5. EGT model ... 48
Chapter 4. Laboratory application ... 51
4.1. Description of the structure ... 51
4.2. Initial numerical model of laboratory footbridge ... 52
4.3. Experimental identification of modal properties of the laboratory footbridge ... 54
4.4. Comparison between initial FE model and experimental test results ... 55
4.5. Sensitivity analysis and sorting variables in strategy space ... 56
4.6. Solution of the FEMU problem based on a conventional optimization method ... 57
4.6.1. Solution of the SO FEMU problem ... 58
4.6.2. Solution of the MO FEMU problem ... 59
4.7. Solution of the FEMU problem based on the GT ... 60
4.7.1. Solution of the SO FEMU problem based on GT ... 60
4.7.2. Solution of the MO FEMU problem based GT ... 61
4.8. Discussion of the results ... 63
4.8.1. Solution of SO FEMU problem ... 63
4.8.2. Solution of MO FEMU problem ... 64
4.8.3. SO vs MO optimization based on GT algorithm ... 66
Chapter 5. Case study on real structure ... 67
5.1. Description of the structure ... 68
5.2. Initial numerical model ... 70
5.3. Experimental identification of the pedestrian suspension bridge ... 74
5.3.1. Determination of the force magnitude in the hangers ... 74
5.3.2. Determination of the force magnitude in the anchorage cables ... 78
5.3.3. Determination of the natural frequency in the down main cables ... 80
5.3.4. Determination of the natural frequencies of the pylons ... 81
5.3.5. Determination of the dynamic parameters of the characteristic edge slab ... 82
5.3.6. Determination of the dynamic parameters of the characteristic span slab ... 84
5.3.7. Determination of the structural dynamic parameters ... 86
5.4. Comparison between the initial FE model and experimental test results ... 90
5.5. Sensitivity analysis and sorting variables in strategy space ... 91
5.6. Solution of the MO FEMU problem based on the conventional optimization methods ... 93
5.7. Solution of the FEMU problem based on the EGT model ... 93
5.8. Discussion of the results ... 94
Chapter 6. Conclusion and future research ... 96
6.1. Conclusions ... 96
6.2. Recommendations for future research ... 98

A. Appendix 100
A. I. Measured natural frequencies and calculated force value in hangers 100
A. II. The force values in the upper main cables 103
A. III. Edge slab mode shapes 108
A. IV. Span slab mode shapes 111
References 115
Curriculum vitae 139

Notations

Lower case Latin characters

a	Action in game	[-]
d_{BL}	Distance from boundary line	[-]
d_{EP}	Distance from equilibrium point	[-]
$dg_1, \dots, dg_m$	Design m goals	[-]
$d(j,i)$	Space distance of θ_j to f_i	[-]
f_t^{exp}	Experimental natural frequency for corresponding mode t	[Hz]
$f_{H,no}^{exp}$	Experimentally determined natural frequency of the hanger number no.	[Hz]
f_t^{num}	Numerical natural frequency for corresponding mode t	[Hz]
$f_t^{upd,HS}$	Natural frequency value obtained by updating numerical model using the multi objective harmony search	[Hz]
$f_t^{upd,NCGT}$	Natural frequency value obtained by updating numerical model using the multi objective non-cooperative game model	[Hz]
$f_t^{upd,CGT}$	Natural frequency value obtained by updating numerical model using the multi objective cooperative game model	[Hz]
$f_t^{upd,EGT}$	Natural frequency value obtained by updating numerical model using the multi objective evolutionary game model	[Hz]
$f_t(\boldsymbol{\theta}_t^*)$	Optimal values of the residual	[-]
$f_t(\boldsymbol{\theta}_t^{**})$	The worst values of objective function residuals	[-]
$f_{nt}(\boldsymbol{\theta})$	Normalized objective function residual	[-]
$\overline{f_i}$	Reference value of the objective function	[-]
f_i^g	Value of the objective function in g^{th} game round	[-]
g	Game round	[-]

g_{best}	The position of the particle that was closest to the target in the whole particle swarm	[-]
k	Node number	[-]
k_L	Equivalent longitudinal stiffness	[N/m]
k_T	Equivalent transversal stiffness	[N/m]
l_{best}	Position of the particle that was closest to the target only in its neighbourhood	[-]
i	Game players	[-]
n	Total number of modal properties	[-]
n_f	Total number of the natural frequencies	[-]
n_m	Total number of mode shapes	[-]
p	Number of the equality constraints non-upper limit and non-low limit	[-]
q	Number of the inequality constraint's non-upper limit and non-low limit	[-]
r_t^f	Natural frequency residual	[-]
r_t^m	Mode shape residual	[-]
$rand_1$, $rand_2$	Random numbers between the zero and one	[-]
t_{SOA}^{GT}	Simulation time single objective game theory based optimization required	[s]
t_{SOA}^{HS}	Simulation time single objective conventional method based optimization required	[s]
t_{NCGT}	Simulation time multi objective non-cooperative game model based optimization required	[s]
t_{CGT}	Simulation time multi objective cooperative game model based optimization required	[s]
t_{EGT}	Simulation time multi objective evolutionary game model based optimization required	[s]
t_{HS}	Simulation time multi objective harmony search based optimization required	[s]
t_{HS_PSBO}	Simulation time multi objective harmony search based optimization required for solving the pedestrian suspension bridge updating problem	[s]

t_{EGT_PSBO}	Simulation time multi objective evolutionary game model based optimization required for solving the pedestrian suspension bridge updating problem	[s]
t- IRS	Enhanced instantaneous response surface	[-]
t_{of}	Objective function tolerance	[-]
u	Utility function	[-]
$u_m(a)$	The utility u player m receives from arriving at a particular outcome	[-]
$v_{\kappa\iota}^{n+1}$	Updated velocity of the particle swarm	[m/s]
w_{ij}	Degree of the cooperation	[-]
$x_{\kappa\iota}^{n}$	Position of the particle in the iteration n	[-]
$\boldsymbol{z}$	Vector of the output response	[-]
$\boldsymbol{x}$	Any input vector of the numerical model	[-]
w_t	Weighted factor of modal properties for corresponding mode t	[-]
w_t^f	Weighted factor for natural frequencies residual for corresponding mode t	[-]
w_t^m	Weighted factor of mode shapes residual for corresponding mode t	[-]

Upper case Latin characters

A	Strategic profiles	[-]
A_{cs}	Cross section area	[mm^2]
BL	Boundary line	[-]
C_1, C_2	Learning factors	[-]
CCGA	Cooperative coevolutionary genetic algorithm	[-]
CGT	Cooperative game theory model	[-]
D	Downstream	[-]
DOF	Degree of freedom	[-]
E_P	Modulus of elasticity of polyurethane	[GPa]
E_S	Modulus of elasticity of steel	[GPa]
E_C	Modulus of elasticity of concrete	[GPa]

E_{CA}	Modulus of elasticity of the cable elements	[GPa]
E_R	Modulus of elasticity of rigid connection	[GPa]
EFDD	Enhanced Frequency Domain Decomposition	[-]
EGT	Evolutionary game theory model	[-]
ELD	Encoding by location for damage detection approach	[-]
EP	Equilibrium point	[-]
$F(\boldsymbol{\theta})$	Objective function	[-]
$F_1(\boldsymbol{\theta})$	First residual of the objective function	[-]
$F_2(\boldsymbol{\theta})$	Second residual of the objective function	[-]
$F_{A,no}^{exp}$	Calculated force value in the anchorage cable based on the experimentally determined natural frequency	[kN]
$F_{A,no}^{exp,30}$	Horizontal force component in the anchorage cable for an angle of 30° based on the experimentally determined natural frequency	[kN]
$F_A^{num,30}$	Horizontal component of the force in the anchorage cable for an angle of inclination of 30° from the static calculation	[kN]
$F_{H,no}^{exp}$	Calculated force value in the hanger elements based on the experimentally determined natural frequency	[kN]
F_{UMC}	Force value in upper main cable previous segment	[kN]
F''_{UMC}	Force value in upper main cable observed segment	[kN]
FDD	Frequency Domain Decomposition	[-]
F_{wt}	Weighted objective function	[-]
FE	Finite element	[-]
FEM	Finite element model	[-]
FEMU	Finite element model updating	[-]
FRF	Frequency Response Function	[-]
G	Game	[-]
G_{best}	The best positions achieved by the agent closest to the target since the beginning of the process	[-]
GA	Genetic algorithm	[-]
GAHA	Genetic annealing hybrid algorithm	[-]

GT	Game theory	[-]
GEP	Gene expression programming	[-]
HGA	Hybrid genetic algorithm	[-]
HMCR	Harmony memory consideration rate	[-]
HS	Harmony search	[-]
IDFT	Inverse discrete Fourier transformation	[-]
IL	Influence line	[-]
IRR	Implicit redundant representation	[-]
IEPSO	Immunity-based particle swarm optimization	[-]
I_{max}	Maximum number of iterations	[-]
K_B	Boltzmann constant	[$m^2kgs^{-2}K^{-1}$]
$K_1, K_2, \ldots$	Weights of the weighted function components	[-]
L	Length	[m]
$\boldsymbol{M}$	Model operator which describes the input-output behaviour	[-]
$\boldsymbol{M}(\boldsymbol{\theta_{opt}})$	Outputs of the numerical model with the optimal model parameters	[-]
$\widetilde{M}$	q-component vector of experimental data sets	[-]
MAC	Modal Assurance Criterion	[-]
MF	Modal flexibility	[Hz^{-2}]
MI	Maximum improvisation parameter	[-]
MLM	Maximum likelihood method	[-]
MO	Multi objective	[-]
$Mo(j)$	Comprehensive degree of influence of θ_j to all objective functions	[-]
MPR	Modal participation ratio	[%]
MPSO	Multistage particle swarm optimization	[-]
MSE	Modal strain energy	[J]
MWFEM	Multivariable wavelet finite element modelling method	[-]
N	Set of players	[-]

NCGT	Non-cooperative game theory model	[-]
NM	Nelder-Mead's simplex method	[-]
NN-PSO	Neural network particle swarm optimization	[-]
NSGA-II	Non-dominated sorting genetic algorithm	[-]
P_M	Model parameter space	[-]
P_O	Model output response space	[-]
P_r	Metropolis Hastings acceptance ratio	[-]
PAR	Pitch adjustment rate	[-]
POE	Pareto optimal equilibrium	[-]
POS	Pareto optimal solution	[-]
PS	Population size	[-]
PSO	Particle swarm optimization	[-]
$P_{s,new}$	New population size	[-]
P_{best}	The best positions achieved by the agent closest to the target since the beginning of the process	[-]
$S_1, S_2, \dots, S_m$	Game strategy	[-]
S_f	Strategy space of natural frequency residual	
S_{ms}	Strategy space of mode shape residual	
SA	Simulated annealing	[-]
SAA	Simulated annealing algorithm	[-]
SC	Super criterion	[-]
SCO	Sine-cosine optimization algorithm	[-]
SGA	Simple genetic algorithm	[-]
SHM	Structural Health Monitoring	[-]
SO	Single objective	[-]
T_C	Constant temperature value in Kelvin	[-]
T_{min}	Global minimum temperature	[-]
U	Upstream	[-]
UKF-HS	Unscented Kalman filter harmony search	[-]

V	Number of fragments	[-]
VBDD	Vibration based damage detection	[-]
X_{κ}^{n}	Vector of the position of the particle κ in the iteration n	[-]

Greek characters

$\alpha_1, \alpha_2, \alpha_3, \alpha_4$	Angle between the suspension bridge cables	[°]
β	Band angle	[°]
Δ	Relative error between the experimental and numerical values	[-]
$\Delta(j,i)$	Impact index	[-]
ΔE	Energy change	[J]
Δf_t	Relative difference between the experimental and numerical natural frequency for mode t	[%]
$\lvert\Delta f_t^{HS}\rvert$	Relative difference between the experimental and numerical natural frequency obtained by updating numerical model using the multi-objective function and harmony search algorithm, for mode t	[%]
$\lvert\Delta f_t^{NCGT}\rvert$	Relative difference between the experimental and numerical natural frequency obtained by updating numerical model using the multi-objective function and non-cooperative game model, for mode t	[%]
$\lvert\Delta f_t^{CGT}\rvert$	Relative difference between the experimental and numerical natural frequency obtained by updating numerical model using the multi-objective function and cooperative game model, for mode t	[%]
$\lvert\Delta f_t^{EGT}\rvert$	Relative difference between the experimental and numerical natural frequency obtained by updating numerical model using the multi-objective function and evolutionary game model, for mode t	[%]
$\Delta\theta_j$	Step length of the fragments	[-]
$\boldsymbol{\varepsilon}$	Vector of model uncertainty	[-]
$\boldsymbol{\theta}$	Vector of the structural model updating parameters	[-]
θ_l	Lower bound of the structural model updating parameters vector	[-]
θ_u	Upper bound of the structural model updating parameters vector	[-]

$\boldsymbol{\theta}_{opt}$	Vector of the optimal structural model parameters	[-]
$\theta^{*}_{MO\_HS}$	Knee point of the multi-objective problem solved using Harmony search	[-]
$\theta^{*}_{SO\_GT}$	Single objective optimal solution obtained using the game theory	[-]
$\theta^{*}_{MO\_HS\_PSBO}$	Knee point of the multi-objective problem of pedestrian suspension bridge solved using Harmony search	[-]
$\theta^{*}_{EGT\_PSBO}$	The optimal solution of the multi-objective problem of pedestrian suspension bridge solved using evolutionary game model	[-]
$\theta^{0}_{initial}$	Initial strategy for game theory models	[-]
$\theta^{0}_{initial\_PSBO}$	Initial strategy for evolutionary game model for solving the pedestrian suspension bridge model updating optimization problem	[-]
$\Theta(j,i)$	Effect of θ_j on the objective f_i	[-]
κ	Particle	
λ	Threshold of moment	[-]
$\boldsymbol{\mu}$	Vector of measurement uncertainty	[-]
$\boldsymbol{\mathcal{M}_m}$	Model in the structural model class	[-]
$\boldsymbol{\mathcal{M}_m}(\boldsymbol{\theta}_{opt})$	Model in the structural model class for optimal set of the model parameters, $\boldsymbol{\theta}_{\mathrm{opt}}$	[-]
ν_S	Poisson ratio of steel	[-]
ν_P	Poisson ratio of polyurethane	[-]
ν_C	Poisson ratio of concrete	[-]
ν_{CA}	Poisson ratio of cable elements	[-]
ν_R	Poisson ratio of rigid connection	[-]
ξ	Convergence criterion	[-]
ρ_S	Material density of steel	[kg/m^3]
ρ_P	Material density of polyurethane	[kg/m^3]
ρ_C	Material density of concrete	[kg/m^3]
ρ_{CA}	Material density of cable elements	[kg/m^3]
ρ_R	Material density of rigid connection	[kg/m^3]

m'	Cable mass	[kg/m']
ζ_t^f	Standard deviation of the natural frequency	[Hz]
ζ_1^c	Standard deviation of the damping ratio	[%]
$\boldsymbol{\Phi}$	Solution that best optimize the general optimization problem defined as weighted objective function	[-]
ϕ_t^{exp}	Experimentally obtained normalized mode shape vector	[-]
$\left(\phi_t^{exp}\right)^T$	Transpose vector of experimentally obtained normalizes mode shape	[-]
ϕ_t^{num}	Numerically obtained normalized mode shape vector	[-]
$(\phi_t^{num})^T$	Transpose vector of numerically obtained normalizes mode shape	[-]

Additional notations

{ }	Vector
$\{\ \}^T$	Transpose vector
[ ]	Matrices
$[\ ]^{-1}$	Inverse Matrices

Glossary

Finite element model	Numerical model of the structure developed in the Ansys software
Finite element model updating	The process of iterative changes of the numerical model physical parameters to obtain numerical modal analysis results that correspond to those obtained through experimental investigation of dynamic parameters of real structure
Updating parameters	Parameters of the numerical model selected based on the sensitivity analysis which values are iterated during the finite element model updating process
Structural dynamic parameters	Natural frequencies and mode shapes of the real structure obtained by performing the experimental investigation using operational modal analysis
Structural behaviour	Term used to define the structural performance as its global stiffness, i.e., dynamic parameters (natural frequencies and mode shapes)
Game theory	Mathematical discipline that provides tools for analysing situations in which game participants make decisions that are interdependent. In this thesis it is used as tool for solving the finite element model updating problem.
Players	The participants of the game. From the aspects of the implementation of game theory for finite element model updating application, the players are natural frequencies and mode shape residuals.
Strategy set	The updating parameters of the numerical model which affect the natural frequency or mode shape residuals. The union of the natural frequency and

	mode shape residuals strategy space gives the complete space of the selected updating parameters. There is no updating parameter that is in both strategy spaces.
Game round	The step in game in which the value of the natural frequency and mode shapes residuals are tested for the selected values of the updating parameters.
Decision	The value of the updating parameters that each player selects in each game round.
Utility	The value of natural frequency and mode shape residuals for the selected values of the updating parameters (decision)
Non-cooperative game theory model	Game model in which the players (natural frequencies and mode shapes) do not cooperate, and they make their decision independently of each other.
Cooperative game theory model	Game model in which the natural frequency and mode shape residual cooperate. The value of the mode shape utility function is depended on the natural frequencies' values.
Evolutionary game theory model	Game model in which the natural frequency and mode shape residual change their behaviour (they choose to cooperate or not) during the game according to their utility after each game round.

Chapter 1. Introduction

At the time of designing bridges up to date, the density and magnitude of the load, especially traffic, have increased, and the requirements for regulation have also become more stringent. To ensure the essential requirements, especially the mechanical resistance and stability, the numerical modelling of the bridges is carried out according to the current regulations. Due to various assumptions, idealization, discretization, and parameterizations that are introduced during numerical modelling, obtained numerical model may not always reflect the actual structural behavior. By combining experimental investigations (static or/and dynamic tests) and FEMU methods, the differences between the actual and the predicted structural behavior could be minimized [1].

1.1.Problem statement

Numerical models can serve as an effective modern tool for continuous monitoring of structures, damage detection, prediction of service life, and determination of an optimal maintenance strategy. The increasing number of new and the progress of existing numerical modeling methods have led to increasing demands on the reliability of models and results. Therefore, the errors and uncertainties associated with model assumptions that most often lead to inaccuracies must be quantified. Their evaluation is important to determine the degree of reliability and accuracy of the numerical model. This has led to the development of finite element model updating (FEMU) methods. The main aim of this method is to calibrate the numerical model based on the actual behavior of the structure determined as a part of static and/or dynamic testing of structure. In the context of different types of structures, numerical modelling is usually performed using finite element (FE) method [2]. This type of models is used to analyze the internal forces, stresses, displacements, and structural dynamic parameters [3]. While updating the FE models, there are two possible uncertainties, one related to the predicted FE model and one related to the experimentally obtained data. Uncertainties associated with the FE model include differences between the predicted behaviour (numerical

model) and the actual behaviour of the structure. In practice, this error can be reduced but never eliminated. Modelling uncertainties can be generally divided into the uncertainties of the model parameters, the model structure, and the model code [4]. Uncertainty in model parameters is usually arise due to incorrect assumptions of model parameters such as material properties; section properties, and thickness of shell or plate elements [5]. The uncertainty of the model structure arises from incorrect assumptions of the mechanical properties and physical behaviour (linear/nonlinear) of the structure. Such erroneous assumptions arise from different idealization and simplification of the structure, inaccurate assumption of mass distributions, incorrect modelling of mesh connections, boundary conditions, joints [6]–[8], and so on. Incorrect assumptions of loads, geometric shape, and structural behaviour (nonlinear/linear) can also lead to obvious uncertainty in the model structure [9]. These types of errors can be eliminated by introducing appropriate modelling assumptions. Some differences and unreliability can be minimized by developing a more detailed FE model or so called a high-fidelity finite element model [10]. Detailed modelling can minimize the degree of uncertainty in the model and the number of parameters that need to be updated. On the other hand, detailed modelling can increase the complexity of the model and increases the computational effort. Thus, this part of modelling must rationally defined according to the type of calculation, analysis and further use of the obtained model.

The experimental methods and their results most used to update the finite element model include static and dynamic structural tests or data and results obtained as a part of Structural Health Monitoring (SHM). However, since they are very good indicators of structural global stiffness, dynamic parameters - natural frequencies and corresponding mode shapes are most often used. The errors that are most common in this field include those due to the imperfection of measuring equipment, random measurement noise, signal processing, and, in general, the problem of post-processing the measured data [11]–[13]. In order to obtain a numerical model that represents the actual structural behaviour as best as possible, its quality must be evaluated [14]. This assessment consists of three steps. In the first step, the assessment of the idealization and numerical method errors is performed in order to eliminate or reduce these two types of errors. Then, the correlation analysis between the numerical model predictions and the experimental test results is performed. In this way the differences and the degree of correlation between the predictions and the test results and design parameters of the numerical model that affect the output results are determined. In the third step, the quality of the numerical model is assessed after updating the selected design parameters.

The definition of FEMU is not uniformly established in the literature. Marwala et al. [15] wrote in their study that model updating is developed to correct and improve the FE model of the structure according to its actual behavior. Shahbaznia et al. [16] define FEMU as the process of updating the original numerical model of a structure to better reflect the measured response of the real structure. Schommer et al. [17] defined model updating as an optimization method. In this method, through optimization of defined objective function differences between the structural behavior predicted by the numerical model and the actual structural behavior are minimized. Mottershead and Friswell [18] define FE model updating as a procedure to update the numerical model to better reproduce the measured response of the real structures. In another paper [19], the same authors define model updating as the process by which the response of a FE model gradually approximates the response of the real structure by gradually updating the physical parameters. So, the definition is not uniform, but more or less all authors have the common basis of the definition: updating the numerical model based on the experimentally obtained test results to obtain the actual structural behaviour numerically (Figure 1.1).

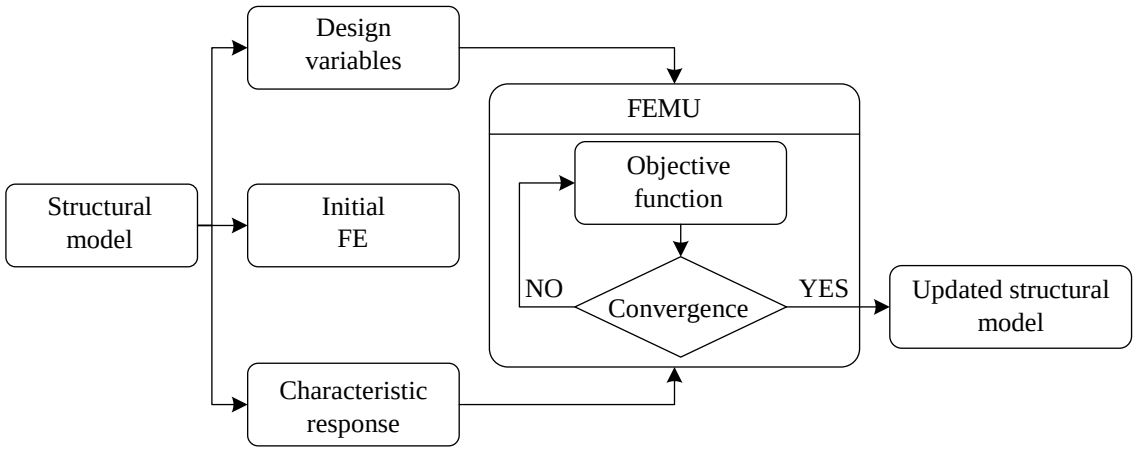

Figure 1.1. General flowchart of performing the FEMU

General division of FEMU methods divide them into the manual and automated methods. Although this is a very general classification, it is still very important, because often a combination of these methods leads to much better results and they are often used together [20]–[24]. This combination of automated and manual methods is usually used to bring the initial numerical model as close as possible to the actual behavior of the structure using manual updating, while automated model updating is performed to further reduce these differences and obtain a more reliable estimate of the unknown parameters. In addition, this combination can improve complete process of model updating and speed up computational time [21] [22]. Generally, manual methods rely on trial and error in the selection of structural parameters such

as geometry, material properties and boundary conditions. They are used when the number of parameters to be updated is small [25]. This method is not able to provide a reasonable physical explanation for the changes in the results. This can lead to inefficient results despite its simplicity [26]. When more parameters are considered, it is recommended to use automated methods. These methods are commonly used to reduce idealization errors [6] and they are introduced with two sub-methods. The first one is a global FEMU and the second one is a local FEMU. The global model updating assumes that the uncertainty parameters in the overall model have a single value for each selected element. The local model updating assumes that each mesh element has its own value for the uncertainty parameters [27].

The second classification is a bit more concrete. It divides FEMU methods into non-iterative (direct) and iterative (indirect). Direct model updating methods are the oldest methods used to update numerical models [28] [29]. They are used to directly update the FEM of structure by changing the structural stiffness matrix and the mass matrix. Without the use of iterative procedures, these methods can reproduce accurate experimental data, which makes them computationally efficient. These methods include the matrix update methods [30], the optimal matrix methods [31], the eigenstructure assignment methods [32], and the Langrage multiplier method [33]. As there are no direct changes in physical parameters of FEM when the model updating is performed under direct methods, the importance of the numerical model decrease, i.e., its ability for simulation decreases [34]. Despite the computational efficiency demonstrated in numerous studies [30], [35], [36] the use of the direct model updating method has decreased, and it has been replaced by indirect (iterative) methods [35]. Indirect (iterative) methods are referred to parameter identification or estimation [37]. According to this, FEMU methods are classified into the deterministic Maximum Likelihood Method (MLM) and stochastic Bayesian method. When the MLM [38] is used to perform FEMU each selected updating parameter returns to its expected values, these estimators are so-called point estimators. In stochastic Bayesian model updating [39], each selected updating parameter returns on the interval in which its value lies, or on the probability density function. Therefore, these estimators are also called interval estimators. Accuracy and the computational time required for FEMU of a complex structure have caused that the MLM is commonly used [39]. This method is based on transformation of the FEMU problem into an optimization problem with the aim of finding the selected updating parameter values that optimize the differences between the structural behaviour predicted by the numerical model and its actual behaviour. Most often, the differences between the structural behaviour predicted by numerical model and its actual

behaviour are described in form of residuals. Two types of them are used: frequency residuals $\left(r_t^f\right)$ and mode shape residual (r_t^m). They can be defined in different way, but most often it is defined as the absolute relative difference when the natural frequency is considered, while the mode shape residuals are defined using the different combination of the Modal Assurance Criterion (MAC). Such examples of the natural frequency and mode shape residual can be defined as follows:

$$r_t^f(\boldsymbol{\theta}) = |\Delta f_t| = \left|\frac{f_t^{num} - f_t^{exp}}{f_t^{exp}}\right| \tag{1.1.}$$

$$\text{MAC}\,(\phi_t^{exp},\phi_t^{num}) = \frac{\left|(\phi_t^{num})^T \phi_t^{exp}\right|^2}{\left((\phi_t^{num})^T(\phi_t^{num})\right)\cdot\left(\left(\phi_t^{exp}\right)^T\left(\phi_t^{exp}\right)\right)} \tag{1.2.}$$

$$r_t^m(\boldsymbol{\theta}) = \sqrt{\left(\frac{\left(1-\sqrt{\text{MAC}\,(\phi_t^{exp},\phi_t^{num})}\right)^2}{\text{MAC}\,(\phi_t^{exp},\phi_t^{num})}\right)} \tag{1.3.}$$

In the Eq. (1.1.) t is a mode number, f_t^{num} is the t[th] numerically obtained natural frequency value, f_t^{exp} is the t[th] experimentally obtained natural frequency. In the equation (1.2.) the ϕ_t^{num} is the t[th] numerically obtained normalized mode shape vector and ϕ_t^{exp} is the experimentally obtained one, while $(\phi_t^{num})^T$ and $\left(\phi_t^{exp}\right)^T$ are their transpose vectors. The influences of the previous residuals from the Eq. (1.1.) and the Eq. (1.3.) on the objective function (function that define the differences between the actual and predicted structural behaviour) can be defined via two approaches: (1) single objective (SO) (Eq. (1.4.)) and the multi- objective (MO) (Eq. (1.5.)).

$$F(\boldsymbol{\theta}) = \sum_{t=1}^{n} w_t F_t(\boldsymbol{\theta})^2 = \left(\sum_{t=1}^{n_f} w_t^f r_t^f(\boldsymbol{\theta})^2 + \sum_{t=1}^{n_m} w_t^m r_t^m(\boldsymbol{\theta})^2\right) \tag{1.4.}$$

$$F(\boldsymbol{\theta}) = (F_1(\boldsymbol{\theta}) \quad F_2(\boldsymbol{\theta})) = \left(\sum_{t=1}^{n_f} r_t^f(\boldsymbol{\theta})^2 \quad \sum_{t=1}^{n_m} r_t^m(\boldsymbol{\theta})^2\right) \tag{1.5.}$$

In the SO approach (Eq. (1.4.)) the objective function is defined as a sum of the weighted residuals between the structural dynamic parameters obtained numerically and their counterpart obtained experimentally. The values of the proposed weighted factors which are assigned to

different residuals can be selected using some statistical criterion [40] or by using the trial and error method [41]. In order to successfully determine the value of the unknown design variables using the SO approach, it is important to properly define the weighted factors value. This requires the performing of sensitivity analysis as well as engineering judgment, while their sum must meet the condition $\sum w_t = \sum\left(w_t^f + w_t^m\right) = 1$. The optimization of the SO function is most often performed using the nature-inspired computational algorithm due to their good performance when they are used to find a global solution of a nonlinear optimization problem [42]. Optimizing such defined function, the single solution, vector of the updated design variables is obtained. Despite the extensive use, this method presents the two main limitations related to the weighted factors: properly selection of the weighted factor values and the necessity of performing the sensitivity analysis to test the influence of different values of weighted factors to the results of SO optimization. Due to the fact that this approach cannot yield rational optimal design, it was overheled by MO (Eq. (1.5.)) optimization approach [43]. According to the MO the updating problem may be formulated as the combination of two sub-problems: a bi-objective optimization sub-problem; and a decision-making sub-problem. The bi-objective function is usually defined in terms of the residuals between the experimental and numerical modal properties. With this approach different objective functions are used with respect to the different residuals, and it does not require determination or suggestion of the values of the weighted factors. The optimization of such defined function leads to a set of possible solutions, called the Pareto front, from which the best solution is selected based on the selected decision-making strategy [44]. This solution, among the different elements of the Pareto front, may be determined as the best-balanced solution (balance between the variations of the different residuals). It allows updating the numerical models to better reproduce the actual behaviour of the structure. The selection of the preferred solution among the Pareto optimal front is not straightforward and, as it is mentioned before, requires a decision making strategy which is not sometimes uniformly defined and depends on additional, qualitative experience driven and subjective requirements [45]. The most preferred solution of the MO optimization problem is selected as a knee point [46] of the Pareto optimal front. In addition to the selection of a knee point, there are several approaches that are used as a criterion and those include the minimum distance from equilibrium point [47], maximum band angle [48], maximum distance from boundary line [49] and fuzzy satisfying approach [50]. The graphical representation of some of them can be found on the following figure (Figure 1.2).

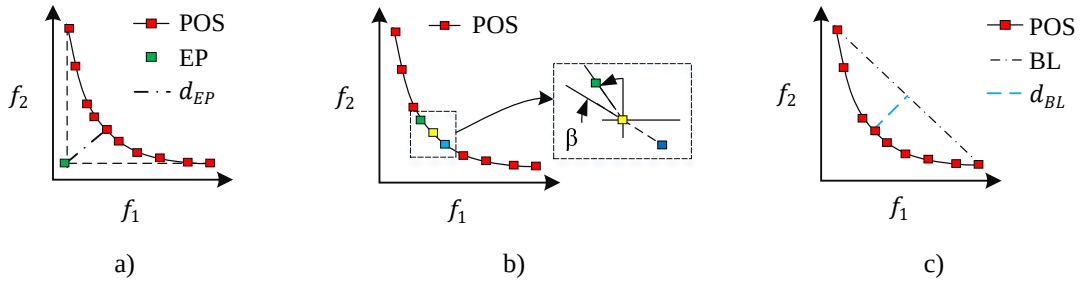

Figure 1.2. Graphical representation of the criterion a) maximum distance from equilibrium point; b) maximum band angle; c) maximum distance from boundary line for finding the optimal solution on the Pareto optimal front of optimization problem defined with the objective functions f_1 and f_2 (Legend: POS-Pareto optimal solution; EP-Equilibrium point; d_{EP}- distance from equilibrium point; β- band angle; BL-boundary line; d_{BL}- distance from boundary line)

Regardless the method chosen for selecting the optimal solution, performing the FEMU optimization under the MO approximation has two main limitations: the high simulation time required to compute the Pareto optimal front; and the necessity of solving a subsequent decision-making problem (the selection of the best solution among the different elements of the Pareto front). Therefore, a discussion has been opened on the potential determination of the optimal solution without the need to determine the entire set of the Pareto optimal front. The currently proposed methods are based on the weighted sum [47]. Thus, Christodoulou et al. [51] investigated the relation between the MO optimization and weighted sum SO method. They proposed the optimally weighted method in order to select the most preferred model from Pareto optimal set. Kim and Weck [52] proposed an adaptive weighted sum method by changing the weights adaptively and specifying additional constraints. On the other hand, Ponsi et al. [45] proposed a method for direct estimation of the preferred solution without need to determine the whole Pareto front. It is based on solving the MO optimization problem formulated as a combination of different objectives solved through SO approach. In addition to the most commonly weighted sum methods, some other methods that are most often used to perform the transformation of the MO optimization into the SO optimizations are: min-max method [53], ideal point [54], weight square [55], virtual objective [56]. In addition to the previous, there are also the methods such as feasible direction, centre and interactive programming method [57]. To solve defined FEMU optimization problem under the MLM, different types of optimization algorithms have been proposed [39]. Same as it is for solving the SO approach, among different types of optimization algorithms, nature inspired computational algorithms have been widely used to solve this problem. Some of the most commonly used are genetic algorithm [58], particle swarm optimization [59], harmony search [60], simulated annealing [61], etc. Due to their good performance, these algorithms are still present and extensively used in practical engineering applications, but their main drawback is

high computational cost. In order to reduce the simulation time, three alternatives are currently considered to improve the efficiency and solve this problem (i) the parallelization of the problem [38] (ii) the hybridization of the algorithm - the advantages of local based gradient and global optimization algorithms are combined [59], and (iii) the collaborative combination of different optimization and machine learning tools [62].

Although very commonly used for structural applications, the MLM has several major drawbacks. In SO approach, these problems are related to the selection of weighting factors and the need to perform a sensitivity analysis to determine the impact of different values of the weighting factors on the optimization results. The main drawbacks of MO optimization are the time required to find a set of optimal solutions and the need to solve a subsequent decision-making problem. On the other hand, the mathematical discipline of Game Theory (GT) has been very successfully applied in solving the optimization problems in various other fields of science and even in engineering practice to achieve the efficiency of optimization algorithms. Therefore, in order to solve the previous mentioned problem of the FEMU under the MLM and to improve their computational efficiency, the application of the GT discipline opens up. It has been research in this work and implemented in FEMU discipline.

1.2. Objectives, scope, and hypotheses of the research

Hypotheses of research:

By applying the GT, the MLM FEMU of civil engineering structures (in particular bridges) can be solved more efficiently minimizing the computational cost without compromising the accuracy of the adjustment (differences between the experimental and numerical dynamic behaviour of the considered structure) and better agreement with the results of experimental tests can be achieved.

Objectives of research:

- Develop an algorithm based on MLM and GT considering three different approaches (non-cooperative (NCGT), cooperative (CGT) and evolutionary (EGT)) for performing FEMU of bridge structures using the structural dynamic properties.
- Improve the computational efficiency of FEMU of laboratory and real bridge structures in compared to conventional nature-inspired computational algorithms.
- Achieve better agreement between the numerical model predictions and experimental test results.

1.3. Methodology and plan of research

This study used several scientific methods that can be classified as quantitative methods. The mathematical methods, the modelling method, the analytical method is used to determine the method and procedure that can be used to solve the problems of the conventional method and the algorithms for performing the updating of the finite element model of the bridge structures. In the experimental part of the research, the experimental method, the observation method, and the measurement method were used to determine the structural dynamic properties of the bridge. Appropriate conclusions can be drawn from the quantitative analysis carried out and the analysis of the data obtained from the experimental part.

The research was carried out in six stages, which is briefly described below:

Stage 1: Overview of research conducted hitherto

A review of foreign and domestic literature in the field of structural FEMU is presented. Within the review, emphasis is placed on the on scientific research that deal with the topic of FEMU of bridge structures and the model updating under the MLM. Of greatest interest are research that present experimental investigations of real structures, those in which FEMU is performed using the structural dynamic properties - natural frequencies and mode shapes. In addition, research on GT is discussed, especially those in which this mathematical discipline has been used to solve an optimization problem.

Stage 2: Numerical analysis of the initial finite element model of the selected bridges

For the selected bridges (laboratory and full-scale), all available documentations required for the development of the numerical model are collected. Based on the collected documentations, initial numerical models are developed in commercial software (Ansys). Its interface can be connected with the mathematical programming language interface (Matlab), which makes it easier to update the numerical models. After the development of the initial numerical models, numerical modal analysis is performed to determine the dynamic properties-natural frequencies and mode shapes. Also, a sensitivity analysis is performed to select the physical model parameters whose iterative changes of values are used to perform the model updating.

Stage 3: Experimental investigation

Experimental part of this research is carried out in several steps:

- In the first step, an experimental investigation program of the structural dynamic properties is developed. The elements of the structure are defined, the characteristics of which, in

addition to the frequencies and mode shapes, are additionally experimentally examined.

- In the second step, the test defined in the experimental investigation are carried out using the equipment adequate for measuring the dynamic parameters. The vibration measurements are carried out using the accelerometers placed on the suitable locations, analog-digital converter, and a personal computer. In order to determine the dynamic properties of elements and whole bridge structure an operational modal analysis is carried out.
- In the third step, by analysing the data collected in the second step, the natural frequencies value of the real structure and their corresponding mode shapes are determined.

Stage 4: Development and validation of the FEMU based on GT

Given to the high computational cost of implementing the MLM in performing the FEMU for practical engineering applications, its performance is improved in this phase by re-formulating the optimization problem into the GT one. GT has been successfully applied in many scientific field (politics, sociology, biology, etc.) to solve various optimization problem. Based on the available information on successful applications, a GT has been adopted as computation tool to improve the updating process. For this purpose, the updating problem has been reformulated as a GT problem considering three different game models (i) non-cooperative, (ii) cooperative, and (iii) evolutionary. The performance of the proposal has been assessed when it is implemented for the model updating of the laboratory footbridge and real, pedestrian suspension bridge. In addition to comparing the results of SO and MO optimization problems obtained with different game models, they have also been compared with the results obtained using conventional optimization algorithms.

Stage 5: FEMU of a real bridge

To generalize the use of the proposed method for FEMU of complex civil engineering structures, the best one approach (SO/MO) and game model from the previous phase is implemented on the real bridge. First, using the results of the sensitivity analysis, both the updating parameters and the MO function (in terms of differences between the experimental and numerical dynamic properties) are defined. The updating of the numerical model is carried out via the iterative updating of selected updating parameters. The optimization problem is transformed into the GT problem. Finally, the performance of the selected game model is compared with the results obtained using conventional algorithms.

Stage 6: Conclusions and recommendations for future research

After analysing the obtained results and applying different GT model, conclusions are drawn about its efficiency to improve the performance of the updating process under the MLM since it allows a direct estimation of the solution, do not require the performing the analysis to determine the effect of the different weights to the optimization results and reduce the simulation time without compromising the accuracy of the solution. Based on the knowledge obtained through all stages of the doctoral thesis, the hypothesis is confirmed or rejected. Finally, the thesis presents the recommendations and guidelines for future research.

1.4. Organization of the thesis

For a better understanding of the structure of the work, this subchapter provides a brief description of the topic covered in each chapter.

- Chapter 2 introduces the main terms and fundamentals important for understanding the FEMU. The selection of the updating parameters and the most commonly used algorithms used to optimize defined objective functions under the MLM are discussed.
- Chapter 3 contains a theoretical background of the GT discipline and possibilities of its application for solving optimisation problems. It also discusses the transformation of the optimisation problem into a GT problem. Three game models focusing on non-cooperative, cooperative and evolutionary model for solving the bi-objective optimisation problems and cooperative game model for solving the SO problems are described and discussed. Algorithm steps for each game model and each objective function are described.
- Chapter 4 provides an overview of the application of the three game models to solving the FEMU problem of the laboratory bridge. This section provides the description of the following topics: (i) the initial numerical model of the laboratory footbridge; (ii) the dynamic tests addressed to identify experimentally the modal properties of the structure; (iii) the sensitivity analysis performed to select appropriately the updating parameters; (iv) the FEMU of the structure considering the two mentioned methods (the GT method considering the three different models and a conventional SO and MO optimization algorithm based on the Pareto front); and (v) the comparison of the results obtained using both methods. The obtained results are discussed at the end of chapter.
- Chapter 5 presents the real structure application of the GT. For this purpose, the pedestrian suspension bridge is selected. It contains the description the structure, the development of

the high-fidelity numerical model, the description of the performed experimental investigations, and results of the FEMU using the conventional method and the GT. At the end of chapter, the obtained results are discussed.

- Chapter 6 presents a conclusions and recommendations for future research regarding the improving the currently developed GT based model updating methodology and its application.

Chapter 2. FEMU using the conventional methods

The FEMU problem is generally defined as the difference between the structural behaviour predicted by the numerical model and the actual structural behaviour. Depending on the method used, whether iterative stochastic or deterministic, this problem is defined as an optimization or statistical problem. This section gives an overview of definition of FEMU problem using the iterative (deterministic) MLM.

2.1. Main terms in FEMU procedure and their relationship

The main terms and elements important for understanding the process of FEMU include the model, model class, measured data and model updating.

Experimental datasets $\widetilde{M}$ is a q-component vector that can compress one type of dataset (homogeneous) or multiple types of datasets (heterogeneous). This vector is based on the output quantities such as the natural frequency and mode shapes, while it can also be based on the strains and displacements.

Considering the structural properties as input variables and the results of numerical analysis as the output variables, the model can be generally described as the input-output function between the updating design variables and output results. Input variables considering the structural model parameters θ, while the output response z is defined as the output (i.e., displacements, strains, natural frequency, mode shapes…) due to the any input vector x. To sum the previous, the output response can be generally defined by the equation that connects the input and the output variables in the following form:

$$\mathbf{z} = \mathbf{M}(\boldsymbol{x}, \boldsymbol{\theta}) \tag{2.1.}$$

where **M** is model operator which describes the input-output behaviour. In the FEMU procedure it is often working with the output results which are independent of vector **x**, and the previous relation can be expressed as:

$$\mathbf{z} = \mathbf{M}(\boldsymbol{\theta}) \tag{2.2.}$$

Model parameter vector $\boldsymbol{\theta}$ represents a class of models $\mathcal{M}_m$ and ranges over a subset P_M. The model in the structural model class can be defined as:

$$\boldsymbol{\mathcal{M}_m} = \{\boldsymbol{\mathcal{M}_m}(\boldsymbol{\theta}) | \boldsymbol{\theta} \in P_M\} \tag{2.3.}$$

Each of the associated model in model class maps the model parameter space P_M into the model output response space P_O. After defining the experimental data sets, model, model class, the model updating can be defined as a process of parameter estimation of specific model class. If considering the vector of model uncertainty ($\boldsymbol{\varepsilon}$) and vector of measurement uncertainty ($\boldsymbol{\mu}$), the vector of measured data sets can be defined as follows:

$$\widetilde{\boldsymbol{M}} = \boldsymbol{M}(\boldsymbol{\theta}) + \boldsymbol{\varepsilon} + \boldsymbol{\mu} \tag{2.4.}$$

For optimal value of model parameters, $\boldsymbol{\theta_{opt}}$, the outputs of numerical model $\boldsymbol{M}(\boldsymbol{\theta_{opt}})$ represent a model $\boldsymbol{\mathcal{M}_m}(\boldsymbol{\theta_{opt}})$ for the experimentally obtained data sets $\widetilde{\boldsymbol{M}}$.

The next subchapter describes the process of the selection of the numerical model parameters $\boldsymbol{\theta}$ which optimal values, $\boldsymbol{\theta_{opt}}$, lead to the numerical model, $\boldsymbol{M}(\boldsymbol{\theta_{opt}})$, that correspond to the actual structural behaviour $\widetilde{\boldsymbol{M}}$.

2.2.Selection of the updating parameters and model class

The selection of an appropriate set of parameters of the numerical model, whose values are updated during the model updating is a non-trivial procedure. The selected parameters of the numerical model should represent the unknown structural properties, but their number is also be limited to avoid ill-conditioned problems.

Regardless of the method used to perform model parameterization, problems arise during updating that lead to non-unique solutions. Parameter estimation is constrained when the amount of measured data is insufficient. This leads to an underdetermined system of equations in deterministic methods or unidentified parameters in stochastic iterative methods [14][63]. Regularization is often used to update the deterministic finite element model, but parameterization is also preferred [64]. Regardless of the simplicity or complexity of finite element models, they often have many parameters, including the material properties and cross section of the element, the connection of model elements and boundary condition properties, and the model geometry, which can be selected as updating parameters. Model parameterization

has a significant impact on reducing errors and simplifying the finite element models. According to Mottershead and Friswell [18] in order to meet the requirements for the accuracy and reliability of the numerical model and the performance of the model updating procedure, the parameterization procedure should meet the following criteria:

- to overcome the ill-conditioned problems, a limited number of parameters should be selected for updating,
- the uncertainties model should be corrected by model parameterization,
- the outputs of the numerical model must be sensitive to selected updating parameters.

Model parameterization that includes sensitivity analysis of the model, has the great advantage of providing sensitive parameters and suppressing the problem of inadequacy. This group of parameterization methods includes the subset selection method [65] and the parameter clustering method [66]. In the subset selection method, a reduced number of parameters of the finite element model are selected to be used as updating parameters. The parameters that do not affect the output results are excluded from the model updating process. Originally, this approach was used in regression analysis [67]. Since it is not practical or possible to test all possible subsets for a large number of parameters, heuristics are used [68]. In these approaches, parameters are selected by an orthogonalization process based on the similarity of their sensitivity vector corresponding to the columns of the sensitivity matrix. The orthogonalization process ensures that each parameter has a different effect on the residual reduction. In addition, there are methods based on the decomposition of the sensitivity matrix [69] and the method that uses global sensitivity analysis for subset selection in model updating [65]. The second sensitivity-based method, the clustering method [66], is based on grouping the parameters of a numerical model with similar sensitivity into a cluster, each of which changes with an updating parameter [70]. Selected updating parameters from the same cluster have the same effect on the model updating process. To link similar sensitivities, the unweighted pair group method (UPGMA) is used along with the arithmetic mean [71]. This method allows grouping parameters into binary clusters and then all uncertain parameters are normalized to specific values based on their physical values. To obtain an updated model for further analysis, the updated parameters are multiplied by their initial value. In addition to the previously described parameterization methods based on sensitivity analysis, some other iterative methods are also used for parameterization, such as Bayesian [72] and particle swarm parameterization [73].

Despite the proposed techniques, the selection of updating parameters depends mainly on the

understanding of structural principles, good engineering judgment, and test objectives [14] [74]. In order to obtain a physically accurate model, avoid convergence difficulties and ill-conditioned problems, the number of updating parameters must be limited and correspond to the test objective. Ultimately, it should provide an updated analytical model that represents a real structure and its actual behavior [23] [75].

In addition to properly defining parametrization and selection of the updating parameters, properly performing the selection of the class of the structural model is also important for the successful and efficient updating procedure. The class of numerical model represents a set of probable input-output models of the modelled system with respect to the various parameterizations of the structure [76]. To perform the model class selection different methods can be used such as the sensitivity-based method [77], the Bayesian approach [78], and the Particle Swarm Optimization [73]. Most often, the model class selection is performed using the Bayesian approach due to the fact that it gives a quantitative expression that can be used to set those simpler models to be preferred over unnecessarily complicated [72]. According to this method, the model class with the highest probability is selected for further use. It often happens that a complex model class is better than one that has less adjustable uncertain parameters, which is a problem. If the selected model class, which is considered optimal in each class, minimizes the rate of fitting error between the output data and the corresponding predictions, the choice of model will tend to those that have more efficient free parameters. Therefore, in choosing the optimal model class, it is very important to penalize the complicated model, which is a great challenge [78]. This topic is very important in order to select the numerical model which best describes the actual structure without compromising the computational efficiency of the model updating process and the accuracy of the adjustment [79]. This procedure is very important in model updating and the closely related procedure of selecting a model class that most accurately describes the actual behavior of the structure without compromising the complexity of the model, the computational efficiency of the improvement method, and ultimately the results of the model updating.

2.3. Definition of FEMU problem

The FEMU problem is generally defined as the difference between the structural behavior predicted by the numerical model and the actual structural behavior. Depending on the method used, whether iterative stochastic or deterministic, this problem is defined as a statistical or an optimization problem. This section gives an overview of the definition of FEMU problem using

the iterative deterministic method.

2.3.1. Iterative deterministic MLM

In practical engineering applications, FEMU is performed using the MLM, which transforms the model updating problem into an optimization problem. As part of the transformation, an objective function is defined in terms of residuals between different types of numerically predicted and experimentally obtained data sets [42]. These data sets include the structural dynamic properties [80]–[87], static data sets [88]–[91] or their combination [17], [92]–[95]. The most often the structural dynamic properties - natural frequencies and mode shapes are used. These data sets are the best indicators of the actual behaviour of the structure. When there are changes to the structure, this leads to a change in the structural stiffness (structural flexibility). Changes in structural flexibility led to changes in the structural dynamic properties. These changes are not large and emphasize. Therefore, it is very important to achieve high accuracy when performing experimental investigation of the structure. In addition to the natural frequencies and mode shapes, the formulation of the objective using the frequency response function (FRF) in FEMU is also very popular [82], [96]–[102] and offers some advantages in the application. These advantages are related to the fact that the FRF can adequately reproduce the dynamic properties. Moreover, by using the FRF, the FEMU avoids the error caused by modal fitting and does not require any fitting between the predicted and measured mode shapes [82]. Other widely used forms of the objective function are the modal flexibility residuals (MF) [84], [85], [103]–[105]. Comparing the influence of different possible residuals (frequency, mode shapes, and modal flexibility and their combination), the authors [84] conclude that the objective function that considers all three residuals shows the best performance in model updating. In addition to the previously mentioned dynamic properties and their derivatives, the objective function can also be defined using the modal strain energy (MSE) [86], [87], [106]–[108]. Measured acceleration is most commonly used for damage detection and estimation of remaining capacity in combination with some of the FEMU methods for structures subjected to traffic-induced vibrations [109]–[111]. In addition to the use of structural dynamic properties, which are more suitable for complex structures, displacements and strains obtained from in-situ static tests have also been successfully used for FEMU [88]–[91]. These types of data sets may be combined with the structural dynamic properties to perform model updating [7], [17], [21], [92], [95], [112]–[116].

To account for the relative contributions and uncertainties associated with an experimental

estimate of a dynamic or static structural parameter to the objective function, the residuals are weighted in SO approach, Eq. (1.4). The weighting of the residuals is very important to obtain more accurate FEMU-a results. When the natural frequencies are taken into account, their values can be determined experimentally very easily and with high accuracy. Therefore, weighting factors with a high value are assigned to them. On the other hand, compared to the natural frequencies, the mode shapes are less sensitive to changes in structural stiffness and have about 10 times greater influence due to noise [36]. In order to achieve a possible correlation between the experimentally and numerically obtained data sets, the weighting factors of the mode shapes must be analyzed to obtain their optimal values [117]. Since the optimal value of the weighting factors is not known in advance, they can be obtained by the trial-and-error method [115] or by statistical criteria [118]. Usually, it is assumed that the optimal value is between 0 and 1 [119]. The use of these values ensures the best correlation between experimentally and numerically determined mode shapes. In another work, it was assumed that the optimal value of the weighting factors is different [21]. In damage detection based on FEMU, it is also difficult to define an objective function and choose appropriate weighting factors for mode shapes or natural frequencies when structural dynamic parameters are involved, since it is not known which of them are important for a particular damage detection problem [120]. On the other hand, MO approach, Eq. (1.5.), uses different objective functions with respect to the different residuals [121]. The general aim of this approach is to find the optimal solution in the Pareto optimal front [122]. To determine the best solution, a reasonable criterion must be defined. In a FEMU problem defined with two sub-objective functions (bi-criterion problems), an additional constraint is applied in most cases, mainly based on the decision-making strategy [123]. This approach tries to find good compromises or "trade-offs" between conflicting objective functions in an optimal manner. Moreover, the most commonly used criteria consider the edge knee point [46]. This criterion is based on finding a solution where a small improvement in one objective would lead to a large deterioration in at least one other objective [46].

To compare the effectiveness of SO and MO functions, authors usually perform FEMU using both approaches. To overcome the disadvantage of the computational cost and the unique dependence between the updated model and the objective function considered, Jiménez-Alonso et al. [124] performed a study on a laboratory model of footbridge using both a SO and a MO function. Based on the research performed, they concluded that the MO approach is the best option for the FEMU. It allows a large search space, reduces the computational time, and

provides a better balance of the influence of two sets of considered natural frequencies and mode shapes residuals. Naranjo-Pérez et al. [125] validated the performance of the new hybrid algorithm by comparing it with three different computational intelligence algorithms performed for the same real structure as in [124]. The comparison was based on the speed of convergence and accuracy of matching, using both SO and MO functions. They also concluded that the MO approach is better than the SO approach. Jin et al. [126] performed the comparison between the SO and MO approaches and concluded that all the updated models of the SO objective approach are behind the optimal Pareto front (far from the origin). On the other hand, it is also found that the weighting factors should balance the sub-objective functions, but in some cases deviate from this expectation. In addition, the updated parameters of the MO approach appeared to contain physical significance with fewer objective function values, while the SO approach resulted in about 50% of the updated parameters being close to constraints.

2.4. Nature inspired computational optimization algorithm

Iterative FEMU techniques are based on the use of changes in the physical structural parameters to perform the model updating and produce the models that are physically realistic [12]. As mentioned earlier, these methods are based on solving an optimization problem for which computational optimization algorithms are usually used to find the global optimum. In this chapter, the Genetic algorithm (GA), Particle Swarm Optimization (PSO), Simulated Annealing (SA), Harmony search (HS), and some hybrid local-global optimization algorithms are discussed in detail. For more information and application of the other algorithms and methods, the readers are referred to the following [9].

2.4.1. Genetic algorithm

Genetic algorithm represents a stochastic global searching technique based on the global evolution process and Darwin natural selection [129] that was first presented and simulated for FEMU application by Levin and Lieven [130]. It operates to find a solution of an optimization problem for population of possible solutions. In most of the optimization problems, GA works with the initial population size. This population covers a good representation of the updating solution space, and its size should depend on the nature of the optimization problem. The nature of the optimization problem is determined by a set of structural model parameters, which may be updating parameters. From the initial population through the crossover, mutation and selection phases a better generation are iteratively formed. Through phase of crossover, new

individuals are generated by combining the random parent chromosomes. Mutation phase is used as an auxiliary method that creates new individuals to avoid the information that is lost in selection and crossover phases. In the crossover phase, the parts of the parent chromosomes are selected and inverted. In this way, new information is introduced into the population [39], diversity of population is maintained, and the local search ability of GAs is improved [131]. To grow a new population from each generation, selection is performed using the fitness-based method. The population that is fitter has a higher probability of being selected. Selection can be done by ranking the fitness of each solution and selecting the best solution or by ranking a randomly selected sample of the population (computational efficiency) using methods such as uniformly order selection [39], stochastic tournament selection [131] or roulette wheel selection [132]. The previous phases are repeated until the stopping criteria is reached (Figure 2.1). Commonly used stopping criteria include the maximum number of generations/iteration [133]–[136], the minimum fitness value [137] [138] or any combination of these criteria.

Most early studies focus on using the GA in performing model updating searching for the properties of structural materials [20], investigating the effect of temperature on the modal frequency [5], to help in understanding the current state of structural restauration [139], etc. Ye and Chen [5] performed the FEMU of the TV tower based on GA to investigate the effects of the different effects of temperature on the modal frequency under two situations. In the first case, they proposed that temperature only affects the elastic modulus, while in the other case, they proposed that it only affects the geometric stiffness of structures. The first situation was considered more important because of the significant frequency change. In the second case, the frequency change was very small, and it was suggested to be ignored. Genetic Algorithm can be very useful for structural identification of the historical buildings and SHM performed on it. Bianconi et al. [20] performed the FEMU of the bell tower using the GA for the automatic calibration of the elastic parameters to reduce modelling error following the model assurance criterion. In addition to automated FEMU, the authors also performed manually calibration. Comparing the results obtained using both FEMU methods, it was concluded that with the GA the numerical model was much improved, but the frequencies had a higher deviation. The obtained results of comparison authors connected with the possible influence of soil structure interaction. To obtain an accurate and robust numerical model of the Baptistery of San Giovanni in Firenze, Lacanna et al. [26] performed FEMU based on GA using ambient vibration test data. Jiménez-Alonso and Sáez [139] used GA to performed the FEMU and help understand the actual state of structural conservation of the reinforced concrete truss bridge to select the

appropriate retrofitting technique. Costa et al. [140] calibrated a numerical model of stone masonry arch railway bridge with GA by using dynamic modal parameters estimated from an ambient vibration test. Sabamehr et al. [141] used GA to identify system properties and find correlations between the structural frequencies and changes in the sectional properties of the bridge segment. Pachón et al. [142] used GA to adjust the numerical model of the E. Torroja's bridge to the experimental results with a reduced number of sensors. Hernández-Díaz et al. [143] used GA to obtain the numerical acceleration at the mid span of the footbridge under different pedestrian flows. Gentilini et al. [144] proposed a procedure based on dynamic testing, added masses and genetic algorithm (GA) to identify the tensile force, the modulus of elasticity of the material and the rotational stiffness of restrains for structural characterization of the tie rods.

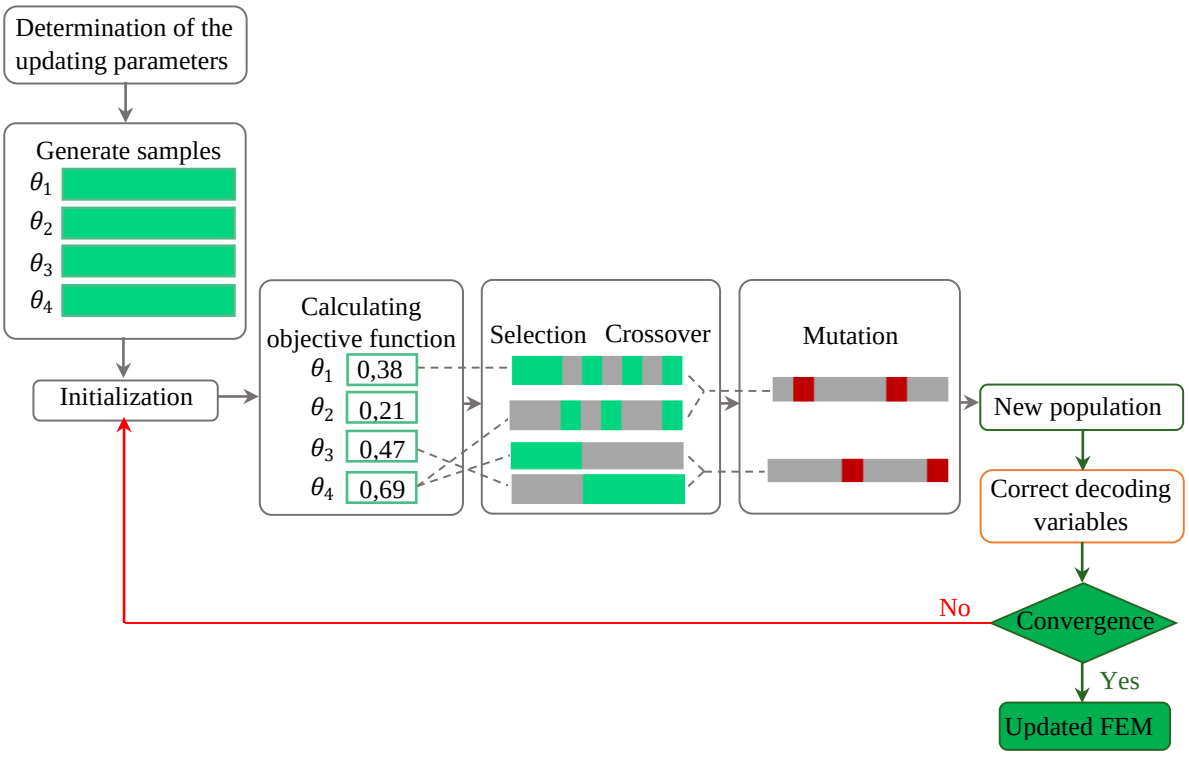

Figure 2.1. Flowchart of Genetic Algorithm method

Yang et al. [145] use GA, to solve the optimization problem of surrogate-based FEMU of a three-story structure using the frequency response function. Kim et al. [115] employed a FEMU method based on static and dynamic data sets to improve the identification of structural updating parameters. They used GA to identify the updating parameters for the conventional FEMU method and verified the effectiveness of the proposed FEMU method on a simply supported plate girder prestressed bridge deck. Sun et al. [146] used a genetic algorithm to evaluate the Pareto-optimal solution of the updating parameters to perform fuzzy FEMU to

accurately evaluate the mechanical state of an in-service cable-stayed bridge. Oh et al. [147] proposed a dynamic displacement based FEMU using a motion capture system to find parameters that minimize the difference between the updated model and the direct measurement. To minimize the combined error functions with the same number of modes simultaneously, non-dominated sorting genetic algorithm-II was used. Cui et al. [148] proposed a FEMU method of structural multi-scale monitoring model based on MO optimization using the non-dominated sorting genetic algorithm- II (NSGA-II) to obtain the optimal parameter values of the large shell structure of Zhuhai Opera House. Wang et al. [149] used a non-dominated sorting GA to perform a multi scale model updating of the transmission tower structure using the measured dynamic response as well as the static displacement and strain response. Luong et al. [150] used a GA, to update the steel truss structures using vibration-based data and identified axial forces in all members. Sun and Xu [94] used a non-dominated sorting GA, to perform the FEMU of a long-span aqueduct structure based on the MO optimization. Tran-Ngoc et al. [133] performed the FEMU of the bridge using GA and particle swarm optimization (PSO), analyzed and evaluated the effects of different joint assumptions on large-scale truss bridge. The comparison of the results obtained with both FEMU methods showed that the PSO algorithm provides a better result and reduces the computation time. In addition, the authors confirmed that the dynamic analysis results are extremely sensitive to the assumptions for the joints. To perform a preliminary evaluation of the bridge structure in terms of its mechanical resistance and stability after an earthquake damage, Mosquera et al. [151] used GA, to perform a high fidelity finite element modal updating. In addition, GA is also used to update the finite element model for damage detection. Srinivas et al. [108] identified and quantified damage on beam and plane truss structures by implementing a multi stage approach based on modal strain ratio change using GA. To minimize the differences between the analytical and experimental modal properties of a concrete-filled steel tubular arch bridge, Zhou et al. [92] used three artificial intelligence algorithms to calibrate uncertain parameters. These three algorithms were the simple genetic algorithm (SGA), the simulated annealing algorithm (SAA), and the genetic annealing hybrid algorithm (GAHA). The results of this study showed that the use of GAHA gave the best performance. In addition, the arch bridge could be efficiently calibrated using a combination of SGA and SAA. Park et al. [152] used GA, to solve the optimization problem of the proposed damage detection method based on FEMU. The proposed method is based on the modal participation ratio (MPR), which is defined as an indicator of the extent of modal contribution. This ratio was used to define the objective

function as the differences between the MPR extracted from the sensors and the MPR estimated from the numerical model. Jeenkour et al. [153] proposed encoding by locations (ELD) and damage factor using GA to determine the location and extent of damage on the beam element where the location and damage extent were used as a decision variable in GA. Wang et al. [107] proposed a multilayer genetic algorithm for damage detection of truss structures to solve this problem. In the proposed method, the damage detection is divided into several groups for optimization purposes. Comparing the proposed method with GA, the advantages of the proposed method such as computational efficiency, less possibility of local optima, a small size of search for each group can be highlighted. In general, when updating the finite element model, the most important thing is to find a computationally efficient algorithm that can solve the proven FEMU optimization problem. For complex structures (cable-stayed bridges, suspension bridges and other complex structures), model updating with GA is very difficult to perform in terms of computation time and obtaining accurate results. For this reason, there are many studies where the genetic algorithm has been combined with another method to reduce the computation time and provide the required accuracy of the numerical model. Erdogan et al. [113] used GA, to solve the inverse fuzzy model updating problem of the benchmark test structure using static and dynamic data sets under different loads and conditions. Jin et al. [126] [48] used GA to solve the SO problem and NSGA-II to solve the MO problem of FEMU of highway bridge structures using modal properties. Yu et al. [154] used GA, to perform the FEMU of the cable stayed bridge response surface model using SHM data. In addition, there are examples of research reporting the use of a genetic algorithm for optimal sensor placement for structural identification and damage detection. Soman et al. [155] proposed the implementation of GA to improve the coverage of sensor networks for damage detection using guided waves. The first step of the proposed method was to determine the minimum number of sensors based on the quality of the signal processing algorithm. The second step involved determining the optimal sensor placement by improving the implementation of GA. Hou et al. [156] used GA to define the optimal sensor placement for determining the modal parameters used for L1-regulated damage detection of cantilever beams and three-story frame structures. Nasr et al. [138] proposed a method for optimal sensor placement by combining GA with the Ensemble Kalman filter for structural system identification and damage detection.

The FEMU under the GA optimization shows that this method is widely used and frequently applied in solving such problems as model updating, damage detection, and optimal sensor placement. This is mainly due to its ease of use and integration in the computational software,

Matlab, most commonly used for model updating and solving optimization problems. On the other hand, the main problem is the computational effort required to solve the optimization problem. Several studies have compared the computational efficiency of GA with that of other optimization algorithms in solving SO and MO optimization problems, and it was found that it takes the most computational time.

2.4.2. Particle swarm optimization

Particle swarm optimization was introduced by Kennedy and Eberhart [157], inspired by the social behaviour and movement dynamics of animals and insects. It represents an efficient global optimization method for continuous variable problems that can be easily implemented with very few parameters. It is successfully applied in various types of optimization problems and in solving the FEMU optimization problem. The basic term in this method is the particle that stores the best position data it has ever visited, and the particle that was closest to the target in the whole particle swarm (global PSO-g_{best}) or only in its neighborhood (local PSO-l_{best}), determined by its position and velocity. Based on the information the particle gathers, it decides on the speed of movement to the new position. Position, X_κ^n, is the solution reached by the κ - th particle out of a total of swarm particles in the n-th iteration. Position is defined by coordinates in s-dimensional space, where s represents the number of variables, $x_{\kappa\iota}^n$, that make up the solution $X_\kappa^n = \{x_{\kappa 1}^n, x_{\kappa 2}^n, \dots, x_{\kappa s}^n\}, \kappa = 1,2, \dots, p$. The velocity of the particles is represented by the ratio of the position changes. A graphical representation of the PSO optimization algorithm can be seen in Figure 2.2, where the main steps can be summarized as follows:

- definition of the number of particles, initialization of the algorithm constants (position and velocity),
- definition of an objective function as the difference between the current position and the target position,
- recording and updating the best particle position and the best position ever reached by the swarm members,
- updating the velocity of the particle swarm according to the equation: $x_{\kappa\iota}^{n+1} = x_{\kappa\iota}^n + v_{\kappa\iota}^{n+1}$, where $v_{\kappa\iota}^{n+1}$ is the velocity, $x_{\kappa\iota}^{n+1}$ is the position in the iteration n+1, and $x_{\kappa\iota}^n$ is the position in the iteration n. The velocity is calculated with the next equation:

$$v_{\kappa\iota}^{n+1} = w v_{\kappa\iota}^n + C_1 rand_1(Pbest_{\kappa\iota} - x_{\kappa\iota}^n) + C_2 rand_2(Gbest_\iota - x_{\kappa\iota}^n) \quad (2.5.)$$

In the previous equation, C_1 and C_2 represent learning factors. These factors are positive weighting coefficients used to balance the influence of individual and social experiences. The $rand_1$ and $rand_2$ are random numbers between zero and one, while P_{best} and G_{best} are the best positions achieved by the κ^{th} agent closest to the target since the beginning of the process,

- update the position of each particle based on social behaviour to match the environment by constantly returning to the most promising identified region,
- repeat steps the previous steps until the termination criteria is met.

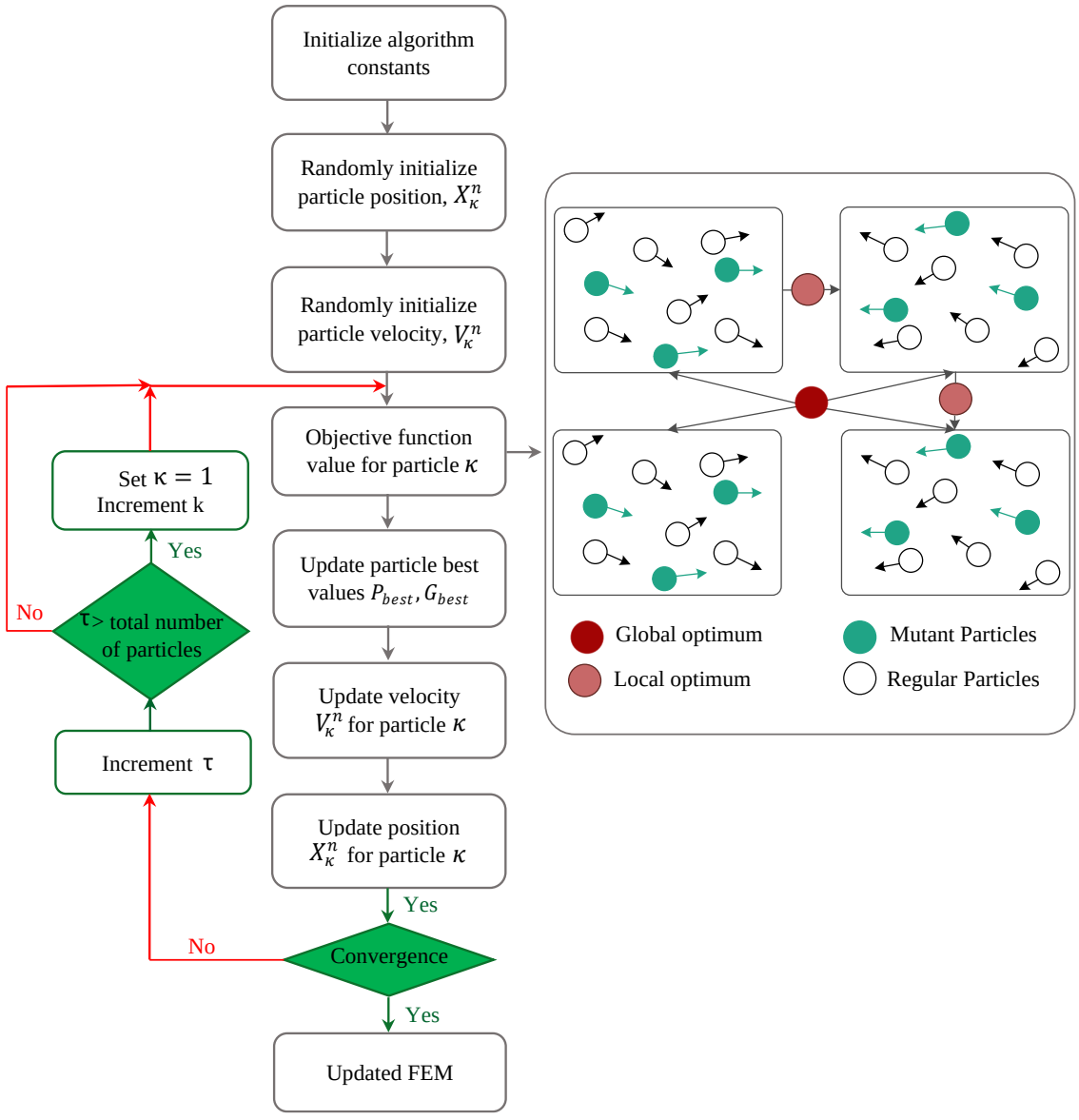

Figure 2.2. Flowchart of Particle swarm optimization

Tran-Ngoc [133] used particle swarm optimization (PSO) to update the model of Nam O Bridge using vibration-based SHM to build a reliable model for health condition assessment and operational safety management of the bridge. They mainly focused on the stiffness conditions

of typical joints of truss structures and concluded that adopting semi-rigid joints (using rotational springs) can most accurately represent the dynamic behaviour of the truss bridge.

Many studies that deal with the application of the PSO algorithm in FEMU show that it can be used for both simple and complex damage detection models. Gökdağ and Yildiz [158] proposed a dynamic parameters based model updating for damage detection of a Timoshenko beam using a particle swarm optimization algorithm. Marwala et al. [159] used PSO to perform model updating damage detection of simply supported beam and H-shaped structures. The damage detection performed and the comparison with GA and Simulated Annealing (SA) showed that PSO has better performance. In addition, the combination of Nelder-Mead's simplex method (NM) and PSO has been shown to be very effective in damage detection, using PSO for global optimization and NM for local optimization. Jiménez-Alonso et al. [124] compared three optimization algorithms Harmony search, genetic algorithm and PSO by performing model updating of a laboratory steel footbridge. From the comparison, it was found that the accuracy of PSO and HS algorithm is similar and greater than that of GA. Mohan et al. [160] presented a robust finite element damage detection method using FRF as input response in the objective function and evaluated for beam and plane frame structures. Seyedpoor [161] proposed a two-stage method using modal strain energy and PSO to correctly detect structural multiple damage. In the first stage, the modal strain energy was calculated based on the modal analysis obtained from finite element modelling. Based on the data obtained in the first stage, the extent of damage was determined in the second stage using the PSO algorithm. The success of the method was investigated on a cantilever beam and a planar truss. Nanda et al. [162] used the particle swarm optimization algorithm to identify damage in a frame structure by varying the flexibility and modal data. Zhang et al. [163] proposed a FEMU method for damage detection based on multivariable wavelet FEM method and PSO optimization. In the first step of the proposed method, the multivariable wavelet FEM (MWFEM) method was used to model the structure with the crack. In the second step, the values of the natural frequencies were obtained, which were combined using the PSO to determine the location and size of the crack. Gerist and Maheri [164] introduced a two-stage structural damage detection using PSO optimization. In the first stage, preliminary identification of structural damage is performed using sparse recovery. The results obtained in the first stage are improved to the exact location and extent in the second stage using the micro-search (MS) embedded in the PSO search. The effectiveness of the proposed method has been tested on several different types of the model. Nouri Shirazi et al. [165] proposed an adaptive multi-stage particle swarm optimization (MPSO) method to detect

damage based on changes in natural frequencies. In the proposed method, the PSO deals with real values of damage variables. Perera et al. [166] proposed a method to solve the MO finite element model for damage detection on frame-like structures when modelling errors. First, the formulation of the objective function was developed using the modal parameters sensitive to modelling errors. Then, multi objective PSO (MOPSO) was applied to a multi-objective framework.

Apart from using PSO for model updating, finding optimal values of unknown parameters and damage detection, other possibilities of the PSO algorithm have also been researched. Cancelli et al. [167] proposed a new approach to extract and analyze the vibration characteristics of the structure in order to obtain the condition assessment of the bridge girder. As part of the proposed approach, FEMU was performed using particle swarm optimization to fit the extracted reduce order stiffness matrix and modal properties. The proposed approach was found to be very effective in locating and quantifying damage along the beam with very high accuracy. Mthembu et al. [73] proposed the application of particle swarm optimization to the problem of selecting optimal FEM. An optimal model is the one that has the smallest number of updated parameters and the smallest deviation of the parameter variables from the mean material properties. To overcome the problem of local optimization and premature convergence of traditional learning algorithms, Chatterjee et al. [168] proposed a particle swarm optimization based approach for training Neural Network (NN-PSO). In this method, PSO was used to select the optimal weights for the neural network classifier. The proposed method was evaluated on a multi-story RC building and was found to be very effective in predicting structural failure.

Previous studies which have dealt with PSO-based FEMU showed that it is a very efficient method for solving the FEMU optimization problem. Moreover, it does not require any knowledge of the function, or its derivatives and it can explore multiple possible solutions in parallel manner in the same sequence. Since it is a global method, its performance does not depend on the initial population solutions. Notwithstanding the foregoing, these methods also have their drawbacks. The first is related to the solution obtained, i.e., there is no guarantee that it is more optimal than the other solution, nor is there convergence to the overall optimal value. The second one is related to the definition of the parameters, because all other algorithms require the definition of parameters that ultimately affect the final performance.

2.4.3. Simulated annealing

Simulated annealing is an optimization method proposed by Kirkpatrick et al. [61]. It is a probabilistic algorithm used to approximate the global optimum of a function by searching for the global extrema of a constrained function around a certain configuration range. The basic concept of this approach comes from annealing in metallurgy. The metal is slowly heated and cooled under controlled conditions until the desired properties are achieved. The process of controlled slow cooling is called annealing. Through a cooling process that promotes diffusion, the metal progresses toward a state of thermal equilibrium, reaching a state of minimum energy. Rapid cooling keeps the metal in a metastable state and prevents the metal's phase transition. Metropolis et al. [169] described how to simulate a group of molecules in thermal equilibrium at a constant temperature T_c. In a simulation, a randomly selected molecule is randomly shifted, after which the energy change ΔE [J] of the entire group is calculated. The most important result is the Metropolis acceptance criterion, which defines the probability of acceptance of a simulated energy change, P_r as it follows:

$$P_r\{\Delta E\} = \begin{cases} 1, & \Delta E \leq 0 \\ e^{-\Delta E/K_B T_c}, & \Delta E \geq 0 \end{cases} \tag{2.6.}$$

According to the above Eq (2.6.) if the energy gain is negative the total energy of the system is accepted. On the other hand, if the change increases the total energy of the system, then it is accepted with the probability$e^{-\Delta E/K_B T}$, where K_B is the Boltzmann constant. If the simulation is performed for a sufficient number of random motions, the final arrangement of the molecules is close to that in thermal equilibrium or steady state. This is the global minimum temperature T_{min} [K]. The formal proof of convergence model describes simulation as a homogeneous Markov chain whose steady state is shown to correspond thermal equilibrium. Theoretically, convergence is achieved only for an infinite number of simulations. The three assumptions under which thermal equilibrium is achieved according to the Metropolis algorithm are (1) Reversibility (symmetry) - the probability of choosing the next state is the same as the probability of returning from the next state to the current state; (2) Ergodicity - the random displacements of the molecules are such that the molecules can reach any position in their configuration space; (3) Convergence to the canonical distribution - the probabilities in the acceptance criterion are such that the ensemble weights on average in the Boltzmann (Gibbs) distribution. The simulated cooling process is performed using the Metropolis algorithm which is performed through following steps: (1) Melt a system optimized to a high temperature; (2)

At very high temperatures, all energy states are almost equally probable; (3) Slowly lower the temperature until the system freezes and there are no more changes; (4) At each temperature, the Metropolis simulation must be run until the system reaches a steady state at that temperature. The process of the simulated annealing optimization algorithm is shown on Figure 2.3.

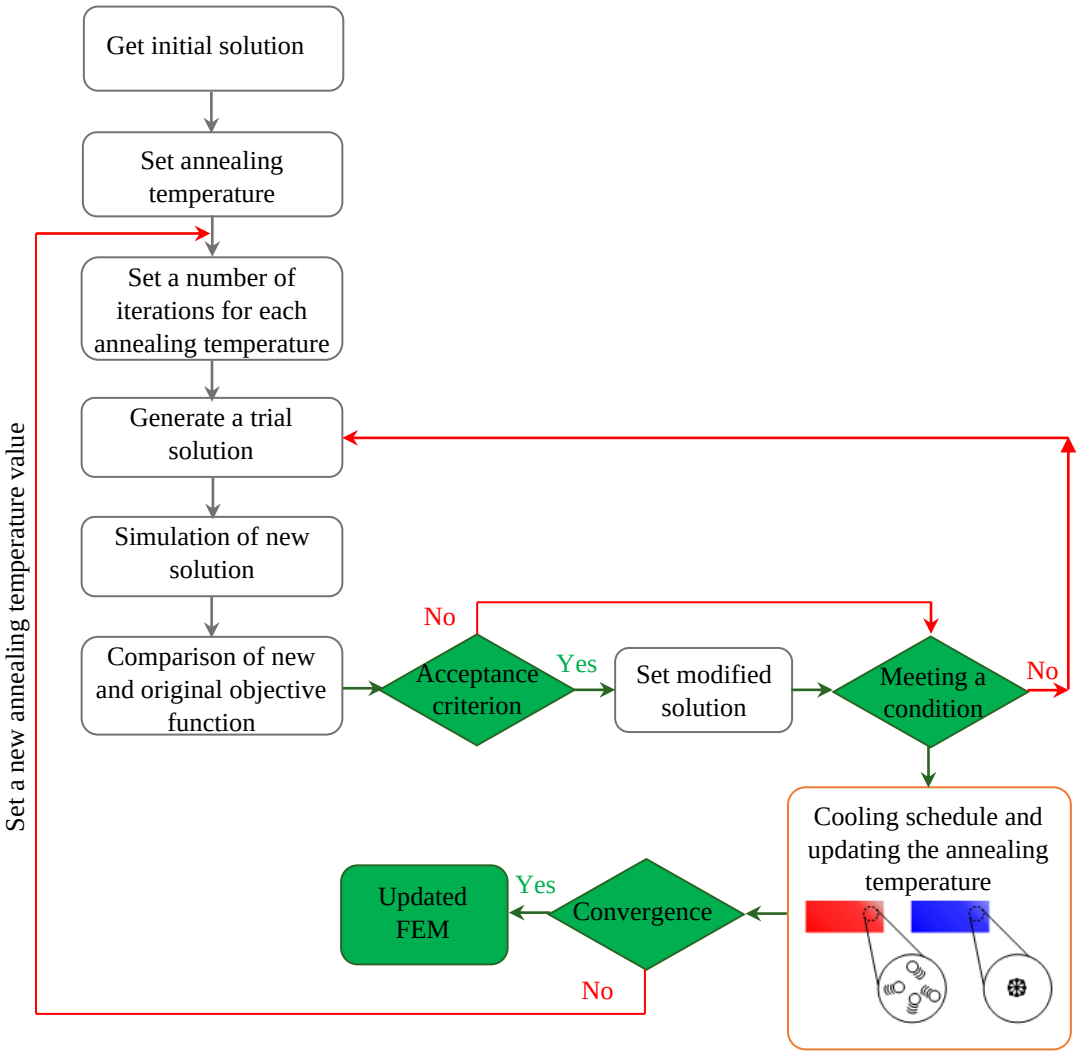

Figure 2.3. Flowchart of Simulated annealing optimization algorithm

Levin and Lieven [170] performed a comparison of two powerful optimizations genetic algorithms and simulated annealing to perform the model updating in the frequency domain. Based on the performed comparison they found that the SA is better than conventional GA and that the accuracy of model updating is dependent on the appropriate selection of the updating parameters. Marwala [171] performed the comparison of computational efficiency of Simulated Annealing, genetic algorithms and Response Surface method on an H-shaped structure. The comparison shows that the response surface method is 2.5 times faster than the genetic algorithm and 24 times faster than simulated annealing. Zhou et al. [92] presented ambient vibration measurements to develop a baseline model for a newly constructed arch bridge by

performing the updating of numerical model using three algorithms: the simple genetic algorithm (GA), the simulated annealing algorithm (SAA) and genetic annealing hybrid algorithm (GAHA). The SAA converged on an infeasible design because it began from a random point and then worked its way toward the minimum, meaning that a local minimum is more likely to be reached. Kourehli [172] proposed a damage detection method based on the simulated annealing using three different objective functions based on static and dynamic measurements, which is verified on a four-story steel frame (IASC-ASCE benchmark structure).

Some of the other authors work on improving the computation efficiency of the FEMU process under simulated annealing. Zimmerman and Lynch [173] increased the computational efficiency of SA, by dividing the annealing into a series of steps, each of which is executed on each computer node. The efficiency of the algorithm was tested on three-story structures, and it was found that the larger number of sensors in the network resulted in efficiency gains. There are studies in which simulated annealing is used in combination with stochastic Bayesian model updating. Thus, Lam et al. [174] used the simulated annealing to propose a Bayesian FEMU damage detection based on structural dynamic properties. Huang et al. [175] use simulated annealing to obtain maximum a posteriori values of posterior probability density function of design variables for characterizing damage and quantifying uncertainty. Green [176] proposed in his work a new Markov Chain Monte Carlo algorithm, "Data Annealing". It is based on the input of the likelihood of training data, so that its effects on the posterior are introduced gradually. Moreover, the proposed approach reduces the computational effort and the probability that local search will get stuck in local traps. Chiu and Lie [19] developed an algorithm based on simulated annealing to cope with the problem of finding the optimal sensor placement under the minimum cost limitation.

Based on the literature review conducted on the use of Simulated Annealing to perform model updating and closely related processes such as damage detection and optimal sensor placement, it can be highlighted that this method has not received as much attention as other computational optimization algorithms such as GA and PSO. This is mostly due to the SA requirements of a large number of annealing cycles and a slow convergence speed. These problems question the limitations of the applicability of SA to complex types of structures. However, it can be seen in the literature that authors make efforts to solve this problem and combine the advantages of SA to develop some hybrid optimization algorithms by taking advantage of SA, such as its strength in solving combinational problems and good performance in hill climbing for the optimal

solution.

2.4.4. Harmony search

Harmony search [177] is an optimization algorithm proposed by Geem et al. [60], primarily intended to imitate a simplified model of improvisation where there are no chords or modes, only notes or tones. Each tone represents a value of a design variable, and each musician represents a design variable. The vector for optimizing a particular objective function forms the entire harmony. Given the notes that the musician has already played, he chooses a new note to change the harmony. These changes can also be made by pitch or by playing an adjacent tone. The harmony search algorithm consists of three steps. In the first step, a random population of possible solutions is created, which is stored in the Harmonic Memory Matrix. In the second step, an objective function is evaluated for each of the possible solutions. In the third step, a new harmony is created at each iteration, the maximum number of which is determined by the maximum improvisation (MI) parameter. The evaluation of the objective function for each new harmony is performed in the fourth step. By comparing the original and the new harmonies, the harmony memory matrix is updated in the fifth step. Until the convergence criteria are met, steps 3-5 are repeated. For the third step and the development of a new harmony, three mechanisms can be used. These include random selection, memory selection, and pitch adjustment [178]. Each design variable of the new vector can be determined from previous values stored in the harmony memory matrix or from a new random value. The probability of selecting the previous element of the harmony memory matrix is determined by the Harmony Memory Consideration Rate, HMCR. When the value is taken from the previous value, it changes according to the pitch adjustment rate, PAR, considering a predefined range of possible values. The complete process of harmony search is shown in the Figure 2.4. This optimization process is characteristic of SO optimization, while in MO optimization, both the harmony memory consideration and the pitch adjustment rate are used in each iteration to define a new value for the design variables. To rank the solutions of MO optimization, non-dominant sorting [179] and crowding distance [180] are used.

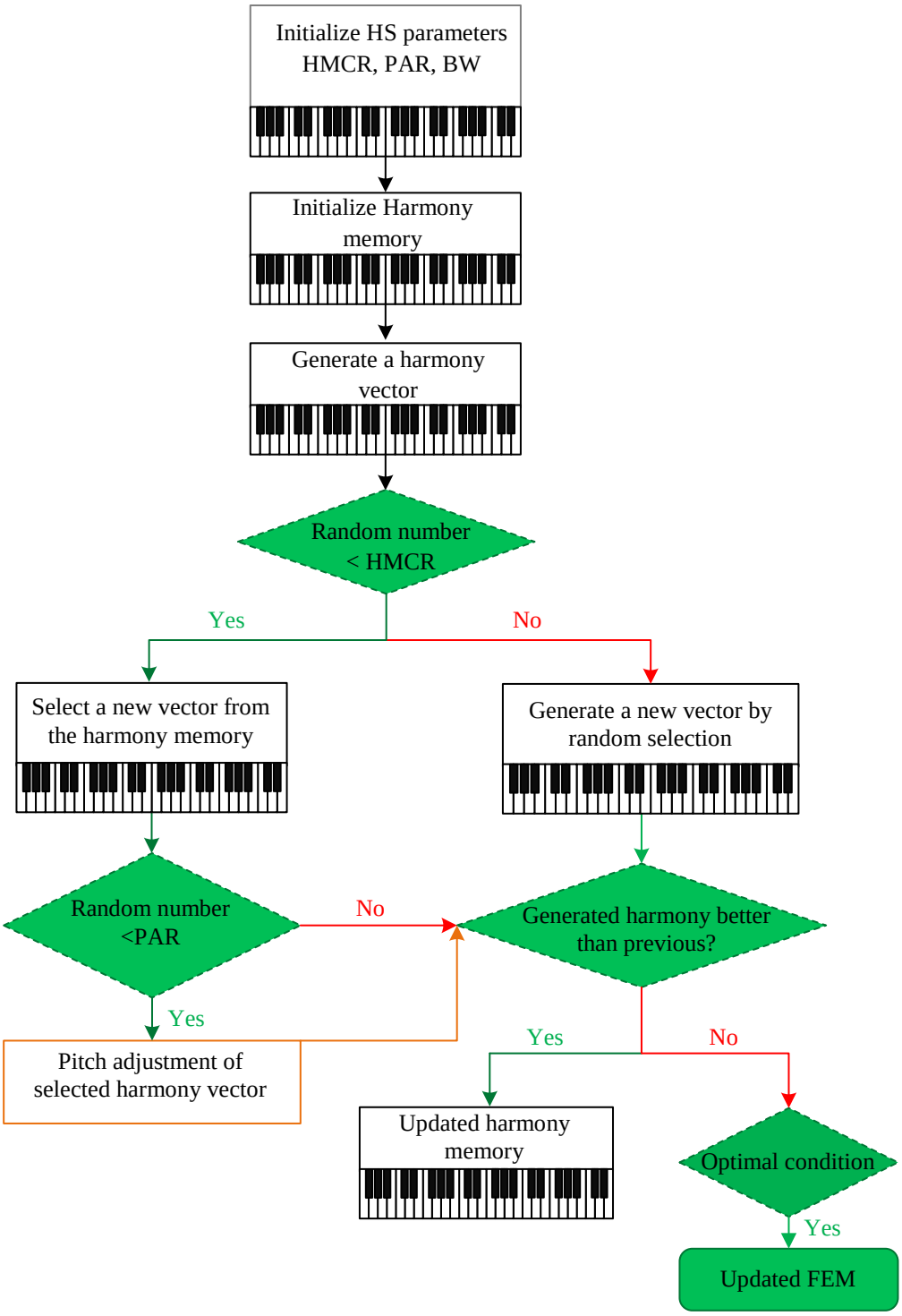

Figure 2.4. Flowchart of Harmony search optimization algorithm

As for the application of the Harmony search algorithm in solving the FEMU optimization problem and the related global problem, there are few studies [125], [181]–[184] in which it is used for this purpose. Most of the papers [125], [182], [183] focus on combining harmony search with other algorithms to improve the computational efficiency. When compared to the conventionally used optimization algorithms (GA, PSO) [124] as standalone algorithms, it can

be seen that HS is the most efficient among them when comparing the computational cost and accuracy of the adjustment. This subsection has served only as an introduction for mathematical background and description of steps of the harmony search algorithm, while its application and examples of studies will be more discussed in the following section.

2.4.5. Hybrid local-global optimization algorithm

As can be seen from the previous subsections dealing with the implementation of model updating and closely related processes such as damage detection, the use of the discussed algorithms as stand-alone algorithms is very computationally intensive. Moreover, the search for solutions can often get stuck in local traps. To solve the above problems, many studies and researches have proposed hybrid local-global algorithms that can successfully solve this problem by combining the advantages and disadvantages of the standalone algorithms.

As for the Genetic algorithm, their hybridization in order to perform model updating more efficiently, Jung and Kim [41] proposed a hybrid genetic algorithm (HGA) by combining GA with Nelder-Mead's modified simplex method to improve the FE model of the bridge structure. Using a Kriging model, Qin et al. [134] proposed a hybrid algorithm to perform the FEMU of complex bridge structures. To increase the chance of finding the global minima and finding the minimum that best describes the system Shabbir and Omenzetter [137] used a combination of GA and sequential niche technique which was tested to perform FEMU of simple laboratory structures and a full-scale pedestrian bridge.

To deal with the damage detection, Boonlong [185] proposed a cooperative coevolutionary genetic algorithm (CCGA) capable for solving an optimization problem with a large number of decision variables, as an optimizer for damage detection on beam element. In the proposed method, each population contains several types of subpopulations. Using the populations, the proposed method explores the search space with a smaller number of generated solutions. As in the classical genetic algorithm, each species is independently involved. Cha and Buyukozturk [120] proposed a damage detection approach using a MO hybrid genetic algorithm based on MSE to determine the exact location and extent of damage on 3D steel structures. Shallan et al. [186] used Hybrid GA in combination with sequential quadratic programming, interior point, and active set to minimize the objective function, and performed the localization and quantification of damage of beam and simple frames using static datasets from a limited number of sensors. Raich et al [135] presented the FRF-based damage detection method using the implicit redundant representation (IRR) GA, which identifies both the location and severity of

the damage using the limited amount of measurement information. The effectiveness of the proposed method was demonstrated on cantilever beam, two-span continuous beam, and frame structure. The application of the optimization-based approaches for damage detection is slow to converge and requires a large amount of computation.

The Particle swarm optimization algorithm is also successfully used to propose hybrid local-global optimization algorithms to solve, most often, FEMU and damage detection method. As a combination of GA and sequential niche technique, Shabbir and Omenzetter [187] also proposed a method that combine sequential niche technique with PSO. In this way, the authors made a possible systematic search for multiple minima and their confidence in finding the global minima was increased. In order to solve the damage detection problem, Luo and Yu [188] proposed a sparse regularization method based on particle swarm optimization to detect structural damage. The proposed method consisted of two steps. In the first step, the FEM is updated based on the sensitivity analysis while the damage location is determined by the PSO. In the second step, the possible damage location and PSO are used to determine the extent of damage in subsequent iterations. Numerical simulations on a cantilever beam show the robustness and applicability of the proposed method. Vakil-Baghmisheh et al. [189] used a hybrid particle swarm Nelder Mead algorithm to perform damage detection in a cantilever beam by minimizing the objective function based on the differences in natural frequencies. Saada et al. [190] proposed a modified particle swarm optimization algorithm for damage detection in beam structures to facilitate the performance of FEMU in accordance with experimentally determined natural frequencies. The main idea of the modified method was to identify multiple optima by running the algorithm a predetermined number of times, each time identifying an optimal location. Jena and Parhi [191] modified the PSO technique with the strategy of squeezing the physical domain of the search space to perform an inverse analysis of damage identification based on natural frequency. Kang et al. [192] improved a PSO by combining it with the artificial immune system and developed a new immunity-based particle swarm optimization (IEPSO) algorithm for model updating damage detection. Compared with the classical PSO algorithm and various evolutionary algorithms, the proposed method showed better performance in determining the location and extent of damage of simply supported beams and truss structures. Kaveh et al. [183] proposed a mixed particle swarm ray optimization combined with harmony search for model updating damage detection of a five-story frame space truss 3D structures. To solve the damage prediction problem for structures with irregular shape, Alkayem et al. [136] combined PSO and the sine-cosine optimization (SCO) algorithm

and developed a new hybrid optimization algorithm. Using the social interaction between PSO and SCO, the highly nonlinear and multimodal optimization problem of FEMU - based damage detection was overcome. The reliability of the developed approach was tested on irregularly shaped 3D modular structures and proved to be very efficient. Li and Chen [193] proposed a PSO-t-IRS to study time-varying reliability-based design optimization problems, which are also associated with high computational cost and difficulty in modelling. This method combines the PSO and the enhanced instantaneous response surface (t-IRS). Enhanced instantaneous response surface was used to construct the extended surrogate model for the instantaneous response, while the PSO was integrated with the extended surrogate model and used to find the optimal solution for the time-varying reliability-based design optimization. The effectiveness of the proposed approach was demonstrated in several examples, including a simply supported beam, a two-bar frame, a six-bar indeterminate truss structure, and a 23-bar truss structure.

The other nature inspired computation algorithms advantages are also used to propose and develop some better, more computational effective hybrid local-global optimization algorithms. Thus, He and Hwang [194] combined Genetic algorithm and Simulated annealing in order to propose a new hybrid algorithm for finding actual damage. The results of the validation of the proposed hybrid method showed its efficiency when the measured data are free of error. When the measured data has an error that is acceptable, the proposed method provides less accurate but still acceptable and reasonable results. In order to increase the quality of the solution and the speed of convergence, Rong and Shun [195] proposed a new algorithm that combines the advantages of genetic and the simulated annealing algorithm. The efficiency was tested on a helical spring optimization design case and system identification problem described by auto regressive and moving average exogenous model. Astroza et al. [196] combine simulated annealing with the unscented Kalman filter in their work to reduce the computational cost. The results show that the proposed combination saves significant computational time without affecting the estimation performance.

To reduce the high computational time for model updating of complex structures under the harmony search optimization algorithm, Naranjo-Pérez et al. [125] proposed a novel hybrid Unscented Kalman Filter- Harmony Search (UKF-HS). The performance of the proposed algorithm was tested on the benchmark footbridge under the context of SO and MO optimization and compared with three computational optimization algorithms. In another work, Naranjo-Pérez et al. [182] combine MO harmony search, active set algorithms, artificial neural network and principal component analysis to solve the problem of high computational time and

uncertainties associated with selecting the best updated model among all Pareto-optimal solutions. Kaveh et al. [183] proposed a new optimization algorithm for damage detection that combines mixed particle swarm ray optimization with harmony search. Miguel et al. [184] proposed a new vibration based method that combines a time-domain modal identification technique with the evolutionary harmony search algorithm. The proposed method was verified on a numerical example and three cantilever beams with different damage scenarios and noise levels. The results show that the proposed method can be efficiently used for structural damage detection and remaining life prediction.

Chapter 3. GT for FEMU optimization

Game Theory is a mathematical discipline that deals with the decision under conflicting or partially conflicting conditions, when the interdependence of the actions of two or more participants determines all individuals' outcomes [197]. This theory is used to solve different types of the optimization problems in sociology, politics, economics, biology, philosophy, engineering, etc. Originally, it referred to zero-sum games with two games in which one subject's loss equals the other subject's gain. Using the GT, Morgenstern and Neuman [198] modelled the interactions that occur in economics. Comparing the economy and game, in both discipline, there are some rules, such as what is/is not allowed, the handling of information (which is/is not available), and choice that can be made. Most important, decision always depend on the outcome and what our teammate will do. The general idea is to create the mathematical formulation of a described phenomenon in a simplified version. Following those concepts of a Morgenstern and Neuman there are several attempts to describe other phenomena and interactions in biology, sociology, politics, and other scientific fields in a similar way. These phenomena are also defined as optimization problems, or rather, many algorithms inspired by the mentioned phenomena are used to solve the different types of optimization problems. Based on the various studies and successful application of GT in solving optimization problems, the potential of its application in solving the FEMU optimization problems opens.

3.1. Main terms in GT

Using the GT, some nature phenomena are modelled as a game. Each of these terms have some rules, what is or is not allowed. There is information that may or may not be available, decision that are made, and the most important, these decisions have an outcome that depends on the decision of the other players. The main terms of game are players, strategies, utility, available information, and equilibrium (Table 3-1.). The optimal solution of a game is the optimal strategy, i.e., action that maximizes the player's utility, considering that there are other players.

Table 3-1. Main terms in GT [199].

Game element	Description
Game	Any set of circumstance whose outcome depends on the actions of two or more decision makers (players). Order pair (A, u) where A note a set of strategic profiles, while u denote the utility function
Players	A strategic decision-maker within the context of game. A set $M = \{1, \dots, m\}, i \in M$ is called a set of players.
Strategy	A complete plan of action *a* player will take given the set of circumstances that might arise within the game $a = a_1 \times \dots \times a_m$
Utility	The utility u player m receives from arriving at a particular outcome (can be in any quantifiable form) for strategy a in state s $u_i(a) = Q_i^*(s, a)$
Information set	The information is available at a given point in the game
Equilibrium	The point in a game at which the players made their decision and result has been reached

The main idea of solving the optimization problem using the GT is to transform the optimization problem into the GT taking into account the objective functions as players, design variables of objective functions as their strategy, the objective function values for different set of design variable as utilities [200].

Table 3-2. Relation between the main terms in GT and the optimization problems

Game element	Minimization problem
Game	Optimization problem
Players	Objective function residuals
Strategy	Set of design variables
Utility	Objective function values for different design variable set

For solving the optimization problem of several different game models, non-cooperative (NCGT), cooperative (CGT) and evolutionary game (EGT) models are used. As the name implies, the NCGT model [201], is a game model in which players do not cooperate, while in the CGT model [202] there are players who cooperate during the game. In addition to the NCGT and CGT models, which propose a fixed behaviour of players during the game, i.e., they cooperate or not there is also EGT model. This game model assumes that players change their behaviour during the game as the game evolute, i.e., they decided whether they cooperate or not [203]. If the MO optimization is considered, compared to conventional optimization methods that obtains solutions by merging MO functions, GT optimization methods obtain solutions by partitioning design variables. Each game player is assigned selected design

variables that can show the correlations between each optimization goal and corresponding design variable. In this way, a high-dimensional optimization problem is transformed into the several low-dimensional problems, reducing problem complexity.

3.2. GT for SO optimization

The transformation of the classical SO optimization problem into the GT problem is performed by defining the objective function as a weighted function [204]. Components of the weighted function are obtained by minimization, maximization, and normalization of defined objective function residuals. The whole process consists of five steps (Figure 3.1) which can be summarized as a previous mentioned three steps extended with the formulation of the weighted objective function and its optimization.

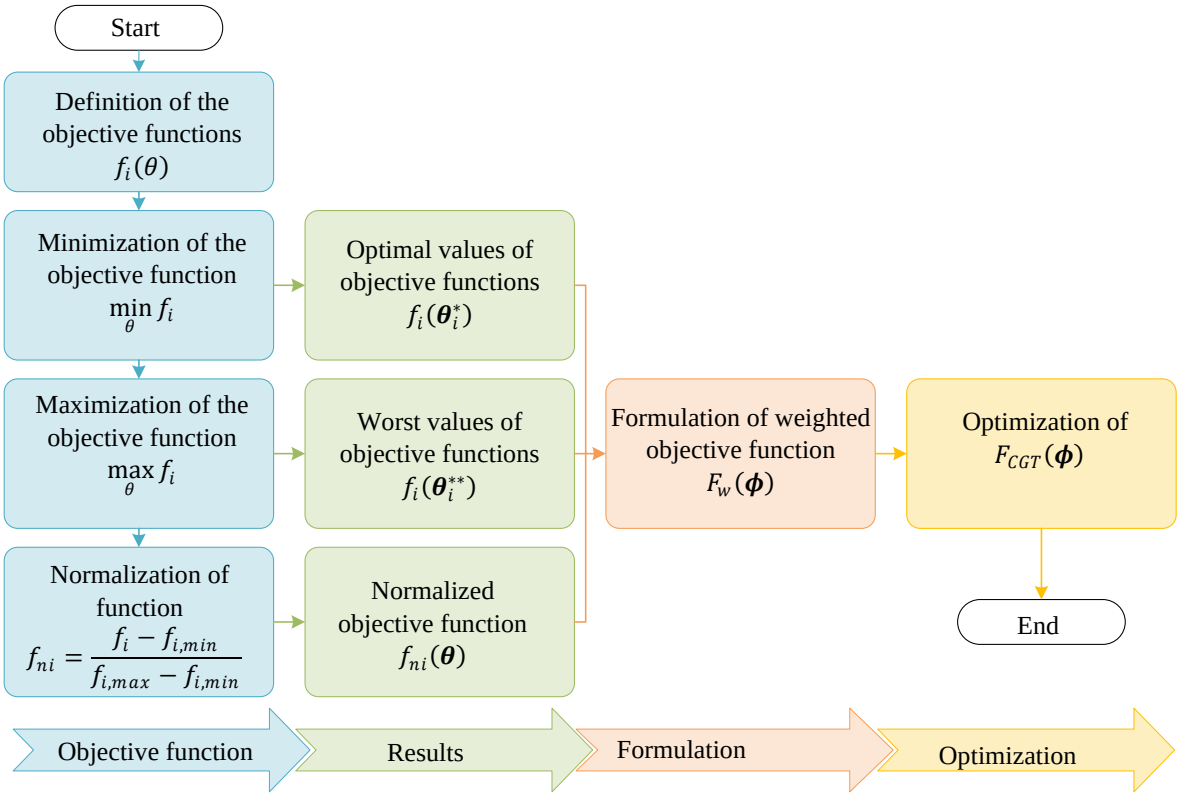

Figure 3.1. Detailed flowchart of the GT approach for solving the SO optimization problem based on the CGT model

- The first step of the method is based on the minimization of defined SO function, i.e., its residuals, using the nature inspired computational optimization algorithm. The HS optimization algorithm has been considered in this research due to its computational efficiency. In this way, the optimal values of the residuals are determined as $f_i(\boldsymbol{\theta}_i^*)$.
- In the second step the maximization of defined objective function residuals is performed

using the HS algorithm. In this way the worst values of objective function residuals, $f_i(\boldsymbol{\theta}_i^{**})$, are determined.

- Based on the results obtained in the previous two steps, in the third step normalization of each defined objective function residuals is performed following the Eq. (3.1.)

$$f_{ni}(\boldsymbol{\theta}) = \frac{f_i(\boldsymbol{\theta}) - f_i(\boldsymbol{\theta}_i^{*})}{f_i(\boldsymbol{\theta}_i^{**}) - f_i(\boldsymbol{\theta}_i^{*})} \tag{3.1.}$$

- The normalized objective function residuals are used for formulation of the weighted objective function using the following equation:

$$F_w(\boldsymbol{\theta}) = K_1 f_{n1}(\boldsymbol{\theta}) + K_2 f_{n2}(\boldsymbol{\theta}) \tag{3.2.}$$

where K_1 and K_2 represent the weighted factors of residuals for which the following applies:

$$K_2 = 1 - K_1 \text{ with } 0 \leq K_i \leq 1 \text{ and } \sum_{i=1}^{2} K_i = 1 \tag{3.3.}$$

In order to ensure that the normalized objective function residuals from the Eq. (3.1.) is as far away as possible from its worst possible value, the new criterion, so called the super criterion is introduced.

$$F_{sc}(\boldsymbol{\theta}) = \prod_{i=1}^{2} [1 - f_{ni}(\boldsymbol{\theta})] \tag{3.4.}$$

Based on the defined super criterion from the previous equation (Eq.(3.4.)), the new objective function, $F_{CGT}(\boldsymbol{\Phi})$, is defined as follows:

$$\begin{aligned} &F_{CGT}(\boldsymbol{\Phi}) = F_w(\boldsymbol{\theta}) - F_{SC}(\boldsymbol{\theta}), \\ &\boldsymbol{\Phi} = [\theta_1 \;\; \theta_2 \;\; \ldots \theta_n \;\; K_1 \;\; \mathrm{K}_2\,]^T \\ &\boldsymbol{\Phi_l} \leq \boldsymbol{\Phi} \leq \boldsymbol{\Phi_u} \end{aligned} \tag{3.5.}$$

where, $\boldsymbol{\Phi}$ is the vector of new design variables while $\boldsymbol{\Phi_l}$ and $\boldsymbol{\Phi_u}$ are respectively the lower and upper bounds of the search domain of these design variables.

- In the last step, the minimization of the new defined function $F_{CGT}(\boldsymbol{\Phi})$ is performed, which leads to the $\boldsymbol{\Phi}$ that best optimize the general optimization problem.

3.3. GT for MO optimization

To solve the limitations of the MO formulation: the high simulation time to compute the Pareto optimal front and necessity of solving a subsequent decision-making problem, the updating problem can be re-formulated as several utility function. For this purpose, three different game

models: NCGT, CGT and EGT have been considered. The following subsections describe the process of re-formulating the MO approach into a GT and gives a description of each of the three mentioned game models.

3.3.1. General problem

The GT method is based on the transformation of the classical MO optimization problem into the GT problem by defining the objective function as a several utility function. The general MO optimization problem of *m* objective functions and *n* design variables can be written as follows:

Find the design variables $\boldsymbol{\theta} = [\theta_1 \quad \theta_2 \quad \dots \quad \theta_n]$ which minimizes the objective function $F(\boldsymbol{\theta}) = [f_1(\boldsymbol{\theta}) \quad \dots \quad f_m(\boldsymbol{\theta})]$ subjected to constraint $\theta_l \leq \theta_\gamma \leq \theta_u \ (\gamma = 1, \dots, n)$; $h_d(\boldsymbol{\theta}) = 0 \ (d = 1, \dots, p)$ and $g_e(\boldsymbol{\theta}) = 0 \ (e = 1, \dots, q)$ where θ_γ represent design variable, θ_l and θ_u lower and upper bound, n is a total number of design variables, p is number of the equality constraint's non-upper limit and non-low limit and q is number of the inequality constraint's non-upper limit and non-low limit.

If the given classical MO optimization problem is transformed into the GT problem, the *m* design goals are the *m* game players. Design variable θ can be divided into the game strategy $S_1, S_2, \dots, S_m$. The values of the objective functions for a particular set of design variables are the corresponding utility in the game. Constraints in the MO optimization problem are constraints in a game. Mathematically, the MO optimization problem, as a GT problem can be written as follow:

Game is presented as a $G = \{S_1, \dots, S_m; \ dg_1, \dots, dg_m\}$ where $S_1, \dots, S_m$ are a strategy set and $dg_1, \dots, dg_m$ are *m* design goals. The following applies to the strategic set $S_1 \cup \dots \cup S_m = \boldsymbol{\theta}$ and $S_{\boldsymbol{u}} \cap S_{\boldsymbol{v}} = 0 \ (u, v = 1, \dots, m; u \neq v)$

To perform the transformation of the MO optimization problem into the GT problem it is important to perform the division of the design variable set $\boldsymbol{\theta}$ into each player strategy space $(S_1, \dots, S_m)$. This can be done using different methods: (i) fuzzy clustering [205], (ii) spatial game method [206], (iii) sorting partition method under the threshold limit [207], (iv) k-means cluster method [208]. Herein the determination of the game player's strategy space is performed using the sorting partition method due to its ease implementation and good performance when it has been implemented to solve structural optimization problems [208].

The general flowchart to solve a multi-objective optimization problem according to the GT

method considering the three mentioned game models (NCGT, CGT and EGT) is shown in Figure 3.2. The step by step procedure for each mentioned game model is described in detail in: section 3.3.3 for NCGT model; section 3.3.4 for CGT model; and section 3.3.5 for EGT model.

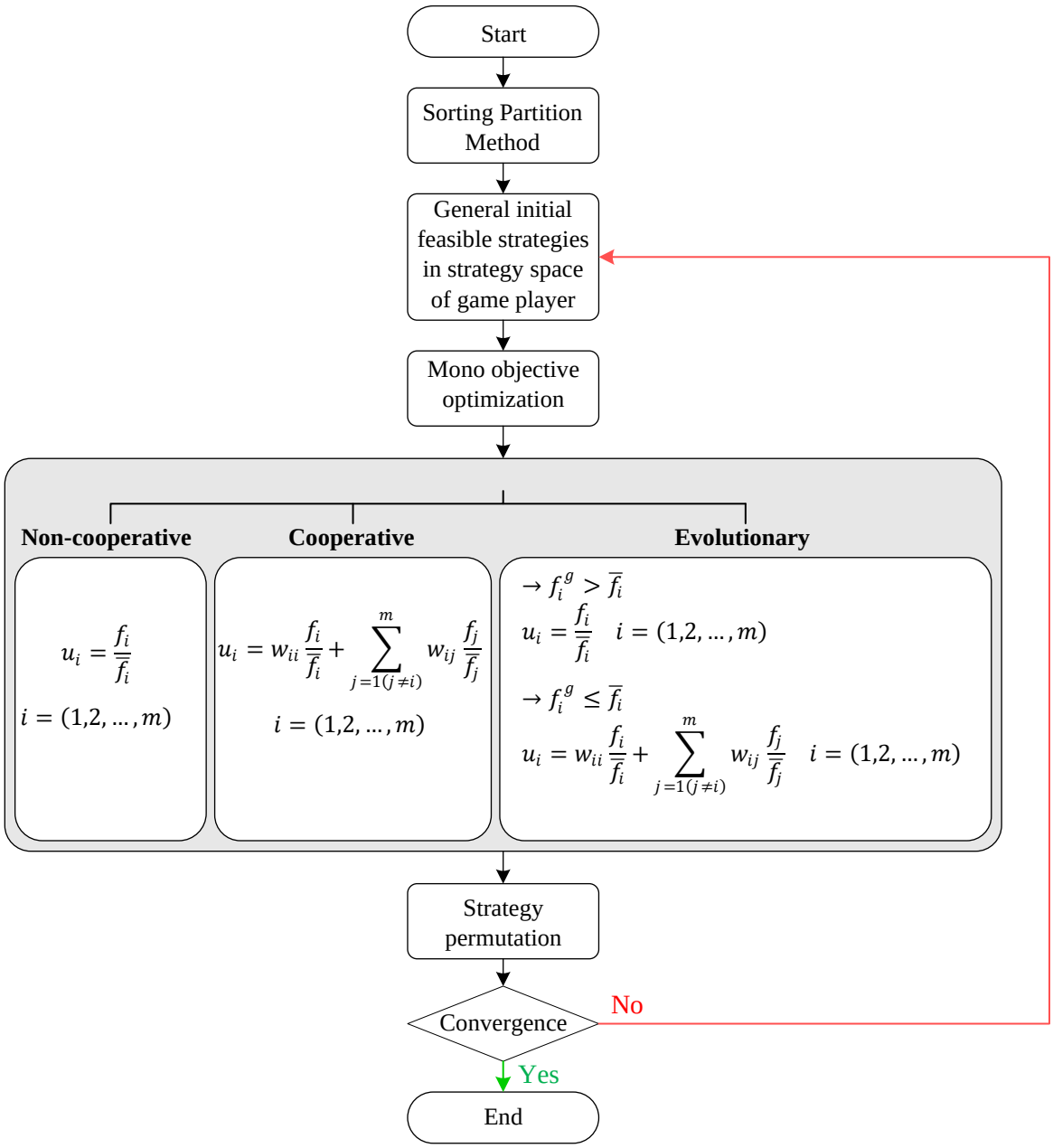

Figure 3.2. General flowchart of the GT method to solve the MO optimization problem considering the three mentioned game models: NCGT, CGT, and EGT.

3.3.2. Determination of the game player's strategy space

Before starting the definition of the objective function considering the GT method, it is important to perform the division of the selected design variables $\boldsymbol{\theta}$ into the strategy space

$(S_1, \dots, S_m)$ of each game player i $(i = 1,2, \dots, m)$. Herein this is performed via the sorting partition method [206] which sort the item based on the utility, *U(i, a)*, of item *a* for player *i* according to the following steps:

- Optimize *m* SO, and then obtain the optimal solution $f_1(\theta_1^*), f_2(\theta_2^*), \dots, f_m(\theta_m^*)$, where $\theta_i^* = \{\theta_{1i}^*, \theta_{2i}^*, \dots, \theta_{ni}^*\}(i = 1,2, \dots, m)$
- Every θ_j is divided into V fragments with a step length $\Delta\theta_j$ in its feasible space. The effect of θ_j on the objective f_i is computed as follows:

$$\Theta(j,i) = \frac{\sum_{v=1}^{V}\left|f_i\left(\theta_{1i}^*, \dots, \theta_{(j-1)i}^*, \theta_j(v), \theta_{(j+1)i}^*, \dots, \theta_{ni}^*\right)\right|}{\mathrm{V} \cdot \Delta\theta_j} - \frac{f_i\left(\theta_{1i}^*, \dots, \theta_{(j-1)i}^*, \theta_j(v-1), \theta_{(j+1)i}^*, \dots, \theta_{ni}^*\right)}{\mathrm{V} \cdot \Delta\theta_j} \tag{3.6.}$$

The normalization gives an impact index $\Delta(j,i)$ defined as follows:

$$\Delta(j,i) = \frac{\Theta(j,i)}{\sum_{l=1}^{n}\Theta(l,i)} \quad (j = 1,2, \dots, n; i = 1,2, \dots, m) \tag{3.7.}$$

- $d(j,i)$ is defined as the space distance of θ_j to f_i as follows:

$$d(j,i) = \frac{\frac{1}{\Delta(j,i)}}{\sum_{h=1}^{m}\frac{1}{\Delta(j,h)}} \quad (j = 1,2, \dots, n; i = 1,2, \dots, m) \tag{3.8.}$$

$Mo(j)$ is defined as the moment of θ_j to all objective functions. It represents the comprehensive degree of influence of θ_j to all objective functions as follows:

$$Mo(j) = \frac{1}{\sum_{h=1}^{m}\frac{1}{\Delta(j,h)}} \quad (j = 1,2, \dots, n) \tag{3.9.}$$

The component λ is defined as the threshold of moment as follows:

$$\lambda = \frac{\sum_{j=1}^{n} Mo(j)}{2} \tag{3.10.}$$

The determination of the game player's strategy space, i.e. sorting of all the design variables to each objective function, is achieved based on the descending order of *d (j, i).* If different design variables have the same space distance to the same objective function, the sorting of the design variables is performed according to the impact index following the rule: the higher ranking is assigned to the objective function that has the greater impact index. The selection of the design variable is performed until the accumulative moment is greater or equal than the moment threshold, λ. The following rules must be considered for the assignment of the design variables to each game player's strategy space:

- the design variable $\theta_j (j = 1,2, \dots, n)$ is assigned to the strategy space of the player for whom it has the highest rank,
- the design variable $\theta_j (j = 1,2, \dots, n)$ is assigned to the strategy space based on the highest impact index $\Delta(j, i)$ if it has the same highest ranking among different game players.

The following sub-sections describe in detail the three mentioned game models (NCGT, CGT and EGT). Thus, a literature review has been included for each model.

3.3.3. NCGT model

In the non-cooperative game theory model (NCGT), players' benefits are based on their NC behaviour. Therefore, the solution of the game can be found via the application of either the Nash or the Stackelberg equilibrium [209]. The main difference between these two criteria is the players' position: all players share the same position according to the first criterion; and there is a leader according to the second criterion. Thus, each player makes his decision independently of the other players according to the Nash equilibrium. While, according to the Stackelberg equilibrium the players make their decision based on the leader's decision.

Using NCGT model Özyildirim and Alemdar [201] have performed optimization of the non-renewable resources model based on the Nash equilibrium optimization method. Bezoui et al. [210] proposed a new method for solving bi-objective optimization problem which transforms a MO linear optimization problem into a GT problem that can be solved using the Nash equilibrium methods. Based on a gene expression programming (GEP) and Nash Equilibrium, Xiao et al. [211] have proposed a new approach for MO multidisciplinary design optimization (MDO) problems in non-cooperative environments. Chatterjee and Khas [212] in their study have shown that Nash equilibrium of finite n-person NCGT model is equivalent to an optimal solution of the optimization model with zero optimal value. Spallino and Rizo [205] proposed a NCGT method based on evolutionary strategy in order to solve the MO optimization problem of composite laminated structures. In their method, each game players are an equal body and eventually found a Nash equilibrium point through negotiation function. Compared to the evolution strategy and SO optimization, authors showed the efficiency of the proposed method. Using three different game model, Holmerg et al. [213] have developed a GT approach robust to uncertain loading and exemplified the design of both 2D and 3D structures. The authors showed that the nature of the proposed NCGT, between the structure and the external loads, is such that convergence is difficult to obtain. This is due to the fact that an element may be very

important for some loads but completely unnecessary for others. This typically leads to oscillations in the design variable values. Merging genetic algorithms and Nash strategy, Sim and Kim [214] introduced the Nash genetic algorithm in order to find a Nash equilibrium through a genetic process in which agent populations can evolve into evolutionarily stable strategies (ESS) through the Darwinian selection process.

Regardless of the successful implementation of the NC game model in solving optimization problems, a Nash equilibrium is usually a local optimal profile. If it is not unique, it is not sufficient to ensure a global optimum solution [215]. In order to ensure a global optimal solution, some more powerful algorithms need to be developed such as the use of GT metaheuristic [216] and a better determination of the strategy space [217].

The transformation of the FEMU optimization problem into NCGT model is based on the optimization of the utility function formulated as it follows:

$$u_i = \frac{f_i}{\overline{f_i}} \quad i = (1,2,\dots m) \tag{3.11.}$$

where f_i is defined objective function (residuals), while $\overline{f_i}$ is its reference value, which can eliminate differences in magnitude for each objective function. The initial design value is most often chosen to be $\overline{f_i}$. Based on the SO optimization of each game player utility function the best solution (best strategy) is obtained. For the proposed game model, after determination of the strategy space and generation of the initial feasible strategy, the SO optimization of utility function (Eq.(3.11)) is performed in strategy space of i^{th} game player fixing the supplementary set according to the player's utility. After that, the permutation of the defined strategies is performed, and its feasibility is assessed according to all constraints. If feasibility is dissatisfied, the new initial feasibility is formulated, otherwise, the convergence criterion is checked. If the convergence criterion (Eq.(3.12.)) is satisfied, the game is over, otherwise, the SO optimization is repeated until all conditions are met.

$$\sqrt{\sum_{i=1}^{m}\left(f_i^{g} - f_i^{g-1}\right)^2} \leq \xi = 0{,}001 \tag{3.12.}$$

The complete flowchart to solve the FEMU problem considering the NCGT model is shown in (Figure 3.3).

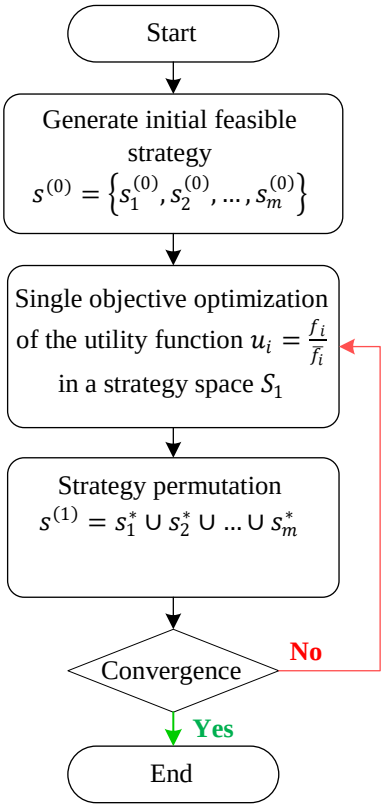

Figure 3.3. General flowchart of the GT method to solve the multi-objective optimization problem based on the NCGT model

3.3.4. CGT model

In the cooperative game theory model (CGT), players cooperate and abide by a binding agreement. Therefore, players' benefits are based on their cooperation. In this game model, there are three types of agreements: competitive; coalition; and selfless agreement [218]. The main characteristics of the mentioned game model are: self-interest for competitive game; mutuality for coalition game model, and collectivistic for selfless agreement [207]. The CGT model is used more frequently than the NCGT model. Dhingra and Rao [219] combined the CGT model and fuzzy set theory to develop a new MO optimization method to deal with the design of high-speed mechanisms. Xie et al. [217] proposed a four-step GT - based method for MO optimization based on the idea that design objectives are used as players and that design variables are decomposed into a set of strategies of all players. By introducing the induced game and transforming the bi - objective optimization problem into the two-player game problem Monfared et al. [220] ensure the finding the Pareto optimal equilibrium (POE) point more precisely. The authors showed that there is at least one POE point for the class of linear bi-objective optimization problems and that the objective space of MO optimization problem is

exactly the payoff space. Rao [221] presented a method for solving the MO optimization problem using the CGT model and concepts for generating the Pareto optimal solution. Vincent [222] studied the role of GT in the process of engineering design and multi-criteria optimization. Cheng and Li [43] used a CGT model to find the compromise solution among conflicting objective and combining this game model with the genetic algorithm to propose a new MO optimization algorithm.

The transformation of the FEMU optimization problem with the complete process of calculation is shown in Figure 3.4.

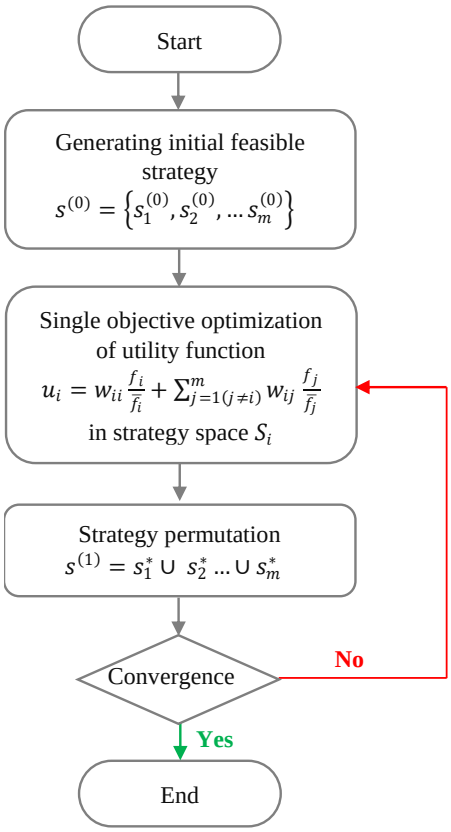

Figure 3.4. General flowchart of the GT method to solve the multi-objective optimization problem based on the CGT model

It is based on the optimization of the utility function formulated as follows:

$$u_i = w_{ii}\frac{f_i}{\bar{f}_i} + \sum_{j=1(j\neq i)}^{m} w_{ij}\frac{f_j}{\bar{f}_j} \quad i = (1,2,\dots m) \tag{3.13.}$$

where $\sum_{j=1}^{m} w_{ij} = 1$ are weighted factors. The value of w_{ij} refers to the degree of the cooperation. The greater this value is, the degree of cooperation is lower. It is worth noting that the w_{ii} and w_{ij} are self-interest and altruistic factors, respectively. Their choice in the collusive CGT should follow two general principles: principles of equilibrium (the self-interest factor is

the sum of all altruistic factors) and the principle of consistency (all game players select the same altruistic factor during the construction of the utility function). Based on the single-objective optimization of each player's utility function, the best strategy is obtained.

3.3.5. EGT model

In the evolutionary game theory model (EGT), the players' behaviour evolve as a game evolves , i.e., the players change their behaviour during the game [203]. Thus, they cooperate or not according to the outcome (results) of the game. This game model consists of two main components: evolutionary stable strategy [223] and replicator dynamic [224].

On the one hand, in evolutionary stable strategy, a population composition is observed that is resistant to the emergence of individuals pursuing a strategy unrelated to the strategy pursued by other individuals in the population (the so-called mutants). For mutants within a population, it is very important that the efficiency they achieve by following their strategy is lower than the efficiency achieved by the rest of the population. On the other hand, replicator dynamics is concerned with the question of whether an equilibrium is reached in a population that is out of equilibrium and, if so, which strategies lead to this equilibrium.

Xie et al. [225] proposed a three steps optimization method based on the EGT model. The first step consists of defining the players using the design objectives and determination of design variables. In addition, using the fuzzy clustering design variables are divided in strategy space. The second step is reserved for selection of the player's behaviour using the evolution rules according to which the players change their behaviour as a game evolute. In his/her strategy space, each player takes his/her utility function as a SO and introduces this formulation of function in optimization obtaining the best strategy upon other players. In this round, all players' strategies confirm the group strategy. Based on convergence criterion and through the multi round game the final equilibrium is obtained. Meng et al. [207] proposed a novel computationally efficient method to form the solution strategy space of game players called sorting partition method under threshold limit. The proposed method is presented with the game profit functions constructed according to both non-cooperative and cooperative behaviour. The proposed method enables the EGT method to converge potentially faster. In addition, it was shown that the complexity of the problem can be reduced by transforming the original high-dimensional optimization problem into three low-dimensional optimization problems. Jin et al. [226] used an EGT model in order to transform the optimization problem into the game strategic problem using adaptable dynamic game evolution process intelligently obtains the optimized

strategy. They proposed a large frequency offset estimation precision using the MO optimization theory and evolutionary game optimization. Greiner et al. [227] give a review of the evolutionary algorithms and metaheuristic techniques based on GT covering NCGT (Nash equilibrium and Stackelberg game) and CGT (Pareto optimality). Meng et al. [202] compared the three mentioned game models (NCGT, CGT and EGT). For the optimum design of four bar joist rack structures, *m* design objectives were considered as *m* game players, while the design variables were divided into the players' strategy space using fuzzy clustering. Based on the three mentioned GT models, authors concluded that the EGT model is the best model in terms of computational efficiency and accuracy. Both CGT and NCGT models have limitations. Regarding CGT model, its efficiency is limited, and domain decomposition does not significantly help improve efficiency, as the objective functions of all the domains are related. Regarding the NCGT model, the optimal solution in its own domain may be inconsistent with the global optimal solution. This is due to the fact that each optimization algorithm aims to obtain the optimal in its own domain without considering the other domains.

Two characteristics of a player's behaviour alternate when the EGT model is used to solve the FEMU problem. These characteristics depend on the value of the individual player's utility function and whether the player's benefits is computed according to either a NCGT Eq (3.11.), or CGT model, Eq (3.13.).

In the EGT (Figure 3.5), game starts as either a NCGT (Figure 3.3) or a CGT (Figure 3.4), determining each player's game strategy and establishing the utility function according to the equation Eq. (3.13.). The first round of the game is characterized by the cooperative behaviour. In the g^{th} game round, if the value of the objective function is higher than those one of the initial design, $\left(f_i^{(g-1)} > \overline{f_i}\right)$, then game player selects the NCGT model, Eq. (3.11.), while otherwise the player chooses the CGT model, Eq. (3.13.). According to both selected behaviour (CGT/NCGT models) and the corresponding utility function, u_i, the single objective optimization in strategy space, S_i, which belongs to the player i is performed. The optimal values obtained are combined and their feasibility is tested. If it is dissatisfied then each player's strategy space is randomly generated, while otherwise the convergence criterion, Eq (3.12.), is checked. If it is reached, the game is over, while otherwise, the single-objective optimization is performed again. The complete flowchart to solve the FEMU problem considering the EGT model is shown in Figure 3.5.

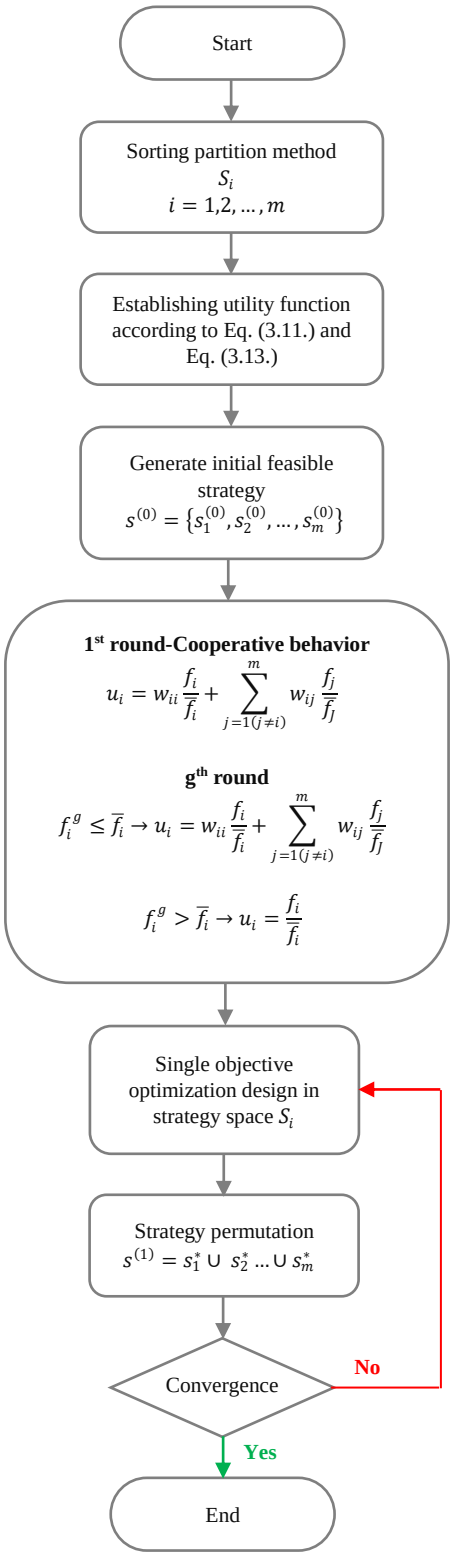

Figure 3.5. General flowchart of the GT method to solve the multi-objective optimization problem based on the EGT model

Chapter 4. Laboratory application

The performance of GT optimization is assessed when it is implemented to update the model of the laboratory footbridge. First, the SO optimization is performed using the method from the Chapter 3.2, and then the MO optimization is performed using the three-game model (Chapter 3.3). To validate the results of the GT based optimization, the FEMU is also performed using the conventional Harmony Search (HS) optimization algorithm. The results obtained using conventional HS algorithm and the proposed approach were compared to determine the most efficient game model, which is used to update the high-fidelity finite element model of real bridge structures in the Chapter 5.

4.1. Description of the structure

The observed single span footbridge is located at the laboratory of the Vibration Engineering Section of the University of Exeter (UK). The length of the span is 15 m (Figure 4.1.) It consists of two UB 457 x 191 x 82 beams designed to be made from two 7.5 m long beams connected to each other. The bridge span is covered with the Sandwich Plate System (SPS) bolted to the UB 457 x 191 x 82 beams. At the beginning and at the end of the structure there are transverse UC 203 x 203 x 60, while between those two transverse beams at each 1.25 m there are the splice plate with a section of 200 mm x 12 mm. The supports of the structure consist of a column section with stub cantilever which is directly pinned to the floor. For a detailed description of the laboratory footbridge the readers are referred to [228].

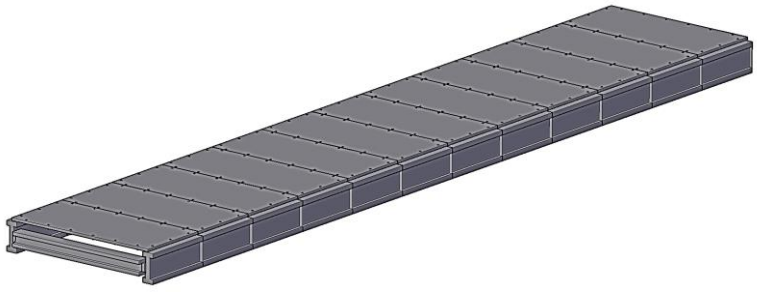

a)

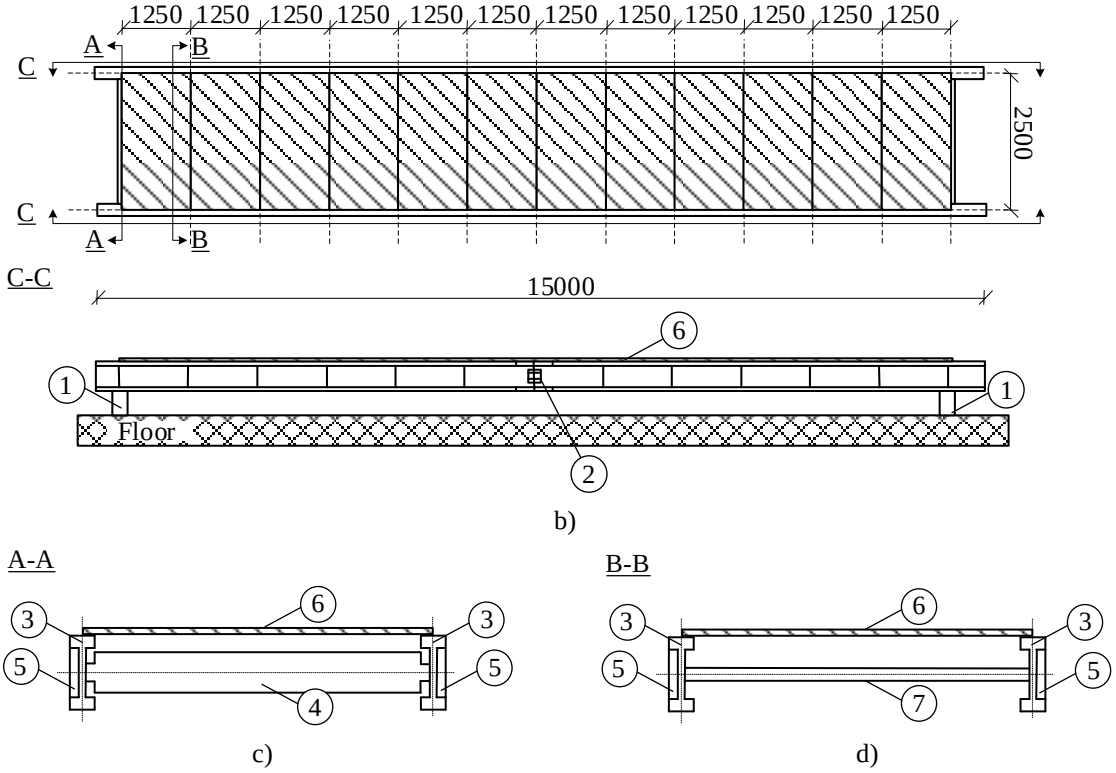

Legend: 1-connection with the floor; 2-connection between UB 457x191x82; 3-UB 457x191x82; 4-UC 203x203x60; 5-transversal stiffeners; 6-SPS panels; 7-Splice plate

Figure 4.1. a) 3D laboratory footbridge model with b) ground plan and characteristic cross-section C-C of the laboratory footbridge c) characteristic cross section A-A, d) characteristics cross section B-B (All dimensions are in millimetres)

4.2. Initial numerical model of laboratory footbridge

Numerical modelling of the laboratory pedestrian bridge structure is performed using the commercial FE package ANSYS [229] and personal computer with processor of 3.59 GHz and a 16 GB RAM memory. Finite element model is developed using the following elements:

- the 3D linear beam elements, BEAM 188, for modelling the bolts that configure the connections between the steel structures and SPS panels,
- four node shell elements with six degrees of freedom, SHELL181, for modelling the lateral beam, transversal plates and SPS panels (first order shear deformation theory),
- COMBIN14 for modelling support with lateral and longitudinal spring elements, while it is assumed that the vertical displacements were constrained.

The developed finite element model is meshed using 31903 elements.

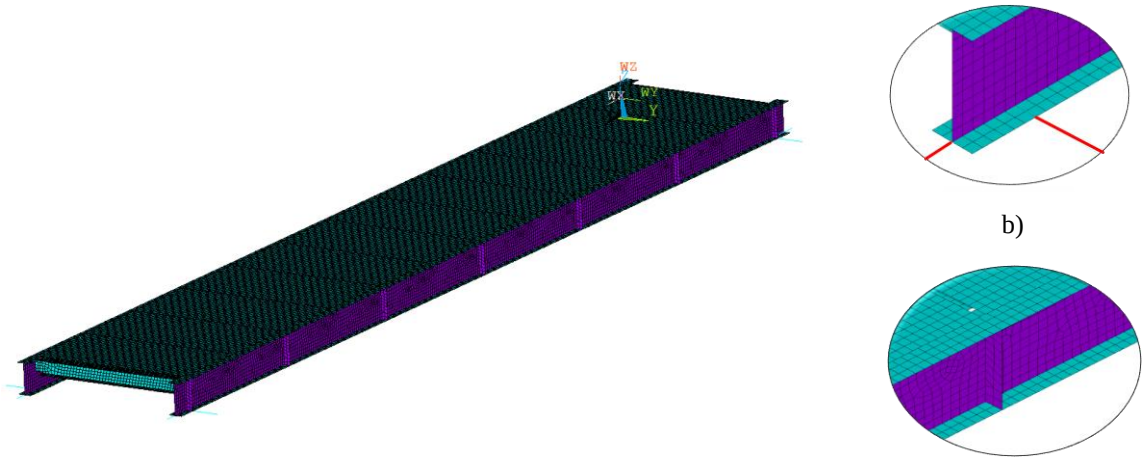

Figure 4.2. a) 3D FE model of the laboratory footbridge with b) detail of connections and of c) detail of transverse stiffeners placed at every 1.25 m along the length of the longitudinal beam

The initial values of the mechanical properties of the numerical model were assumed as follows. For steel components: (i) the modulus of elasticity was proposed as E_S =210 GPa; (ii) the material density, ρ_S =7850 kg/m^3; and (iii) the Poisson ratio, ν_S =0,3. For polyurethane components: (i) the modulus of elasticity was proposed as E_P =0,75 GPa; (ii) the material density, ρ_P =1100 kg/m^3; and (iii) the Poison ratio, ν_P=0,5. The spring stiffness was determined based on the results of a FE analysis of a column element. Both an equivalent longitudinal, k_L=5,5x10^7 N/m, and transversal, k_T=1,9x10^7 N/m, stiffness was obtained. On the developed FE model of the laboratory bridge, a numerical modal analysis was performed to obtain the natural frequencies (f_t^{num}) and the mode shapes (ϕ_t^{num}) for each considered mode *t*. The results of the numerical modal analysis are shown in Figure 4.3.

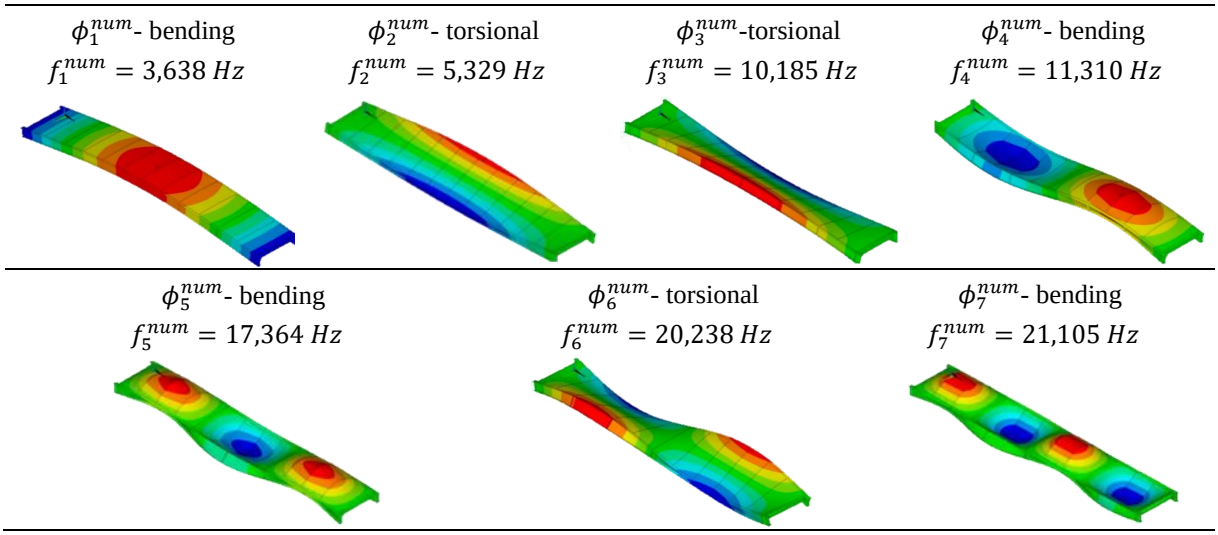

Figure 4.3. Numerical natural frequencies (f_t^{num}) and mode shapes (ϕ_t^{num}) obtained from the initial FEM of the laboratory footbridge for t=1, …,7

4.3. Experimental identification of modal properties of the laboratory footbridge

The modal properties (natural frequencies and mode shapes) of the laboratory footbridge were experimentally identified via a forced vibration test (Figure 4.4.).

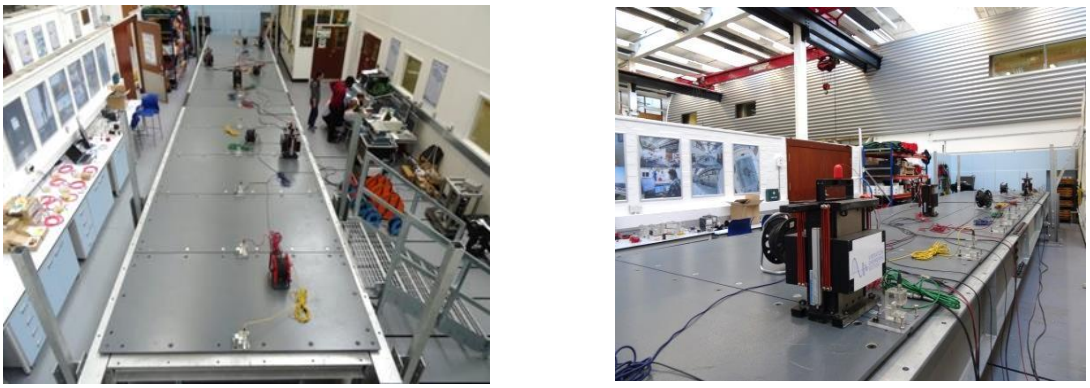

a) b)

Figure 4.4. Laboratory footbridge: a) view on the footbridge; and b) Proof mass actuators APS Dynamics model 400 [124]

For this purpose, two types of proof mass actuators (two APS Dynamics model 400 with 30 kg of inertial mass and one APS Dynamics model 113 with 13 kg of inertial mass) and several roving accelerometers (Honeywell QA700 and QA750) were used. The actuators were driven simultaneously with uncorrelated random signals generated and recorded using a Data Physics SignalCalc Mobilyzer spectrum analyser. The layout of the experimental dynamic test is shown in Figure 4.5.

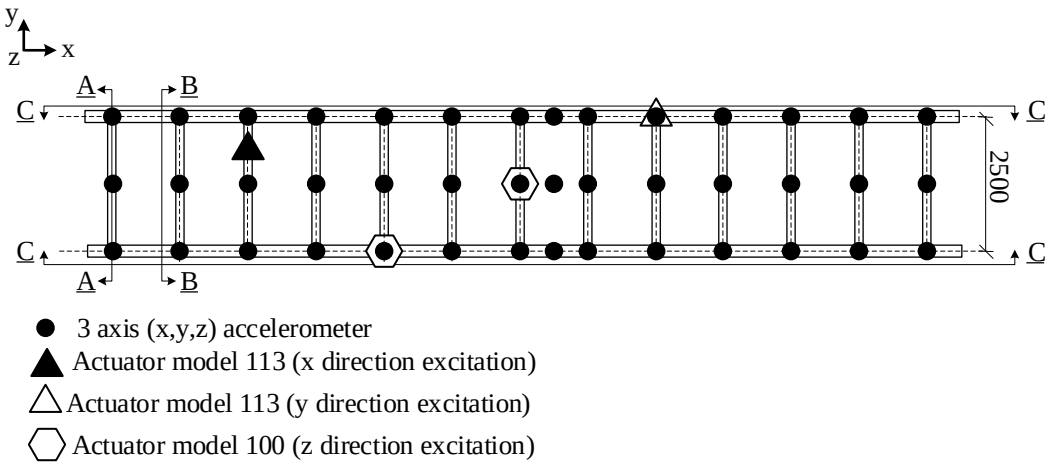

Figure 4.5. Layout of the dynamic test performed to identify experimentally the modal properties of the laboratory footbridge

As result of the identification process, the experimental natural frequencies $\left(f_t^{exp}\ \ t = 1, \dots, 7\right)$ and associated mode shapes $\left(\phi_t^{exp}\right)$ are shown in Figure 4.6. For a detailed description of the experimental investigation together with the forced vibration test, readers are referred to [228].

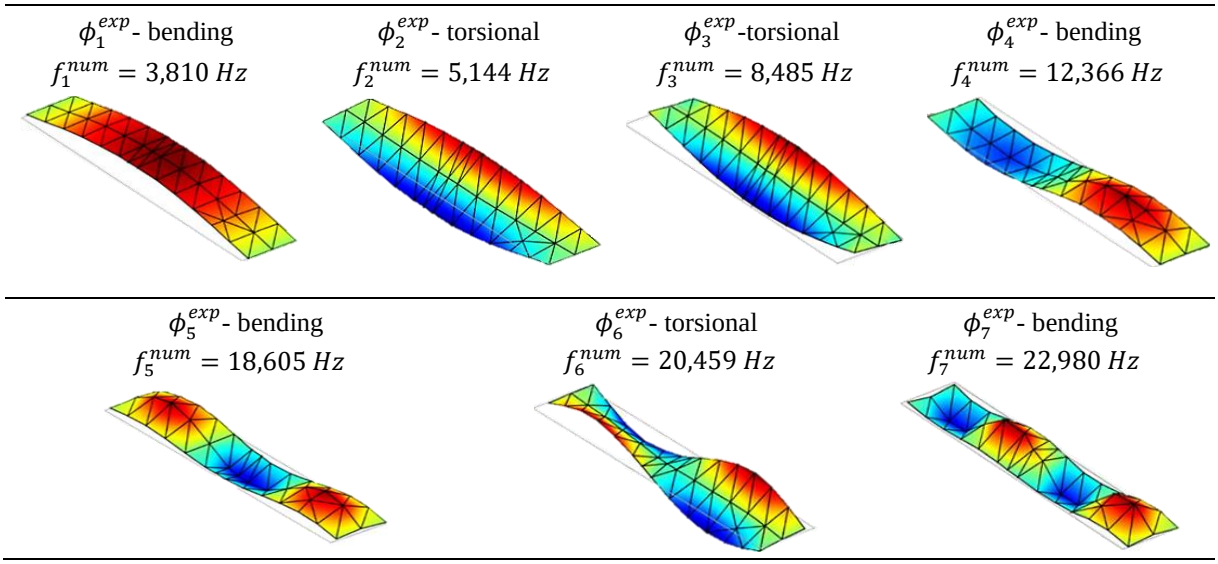

Figure 4.6. Experimental modal properties of the laboratory footbridge –experimental natural frequencies (f_t^{exp}) and associated mode shapes (ϕ_t^{exp}) for t=1, …,7 [76]

4.4. Comparison between initial FE model and experimental test results

In order to assess both the performance of the initial numerical model and the accuracy of its predictions, a comparative analysis was performed. Among the different comparison methods [230], a correlation analysis between the experimental and numerical modal properties of the structure was performed. Herein this correlation analysis is performed based on the Eq. (1.1.), for natural frequencies, and the Eq. (1.3.), for the mode shapes. The results of the correlation analysis are shown in (Table 4-1).

Table 4-1. Comparison of the laboratory footbridge behaviour predicted by initial numerical model and experimental test results based on the relative differences between the natural frequency, (Δf_t) and the modal assurance criterion $MAC\ (\phi_t^{exp}, \phi_t^{num})$

Mode shape t	f_t^{num} [Hz]	f_t^{exp} [Hz]	$\lvert\Delta f_t\rvert$ [%]	MAC $(\phi_t^{exp},\phi_t^{num})$ [/]
1	3,638	3,810	4,51	0,999
2	5,329	5,144	3,60	0,994
3	10,185	8,485	20,03	0,990
4	11,310	12,366	8,54	0,877
5	17,364	18,605	6,67	0,985
6	20,238	20,459	1,08	0,993
7	21,105	22,980	8,16	0,910

Although the deviations for the initial numerical model are not significant, it is still possible to achieve better matches with the experimentally obtained results in order to reduce the relative difference of natural frequencies and increase the value of the MAC coefficient. In this way the common reference value for sum of the relative differences of natural frequencies (5%) and MAC factor (greater than 0,9) will be achieved. Thus, the initial numerical model will be

improved via FEMU. Herein, this was performed using the three different GT models NCGT, CGT and EGT. The performance of the GT models has been analysed in detail. Both the accuracy of the solution obtained and the required computational time have been compared for this purpose Additionally, the results obtained have been compared with the ones obtained via a conventional optimization method based on the computation of the Pareto front and the subsequent decision making problem [76].

4.5. Sensitivity analysis and sorting variables in strategy space

Before starting with the FEMU process, it is important to select the most relevant updating parameters. This parameter selection can be performed using different methods [231]–[233]. Herein, a sensitivity analysis has been performed for this purpose (Figure 4.7). As selection criterion, the ratio between the modal strain energy associated with physical parameters and the overall modal strain energy (MSE) of the structure has been considered. The selection analysis was performed in two steps. In the first step, a preliminary selection was performed based on engineering judgement. In the second step, this set of parameters was reduced based on the model strain energy (MSE) ratio.

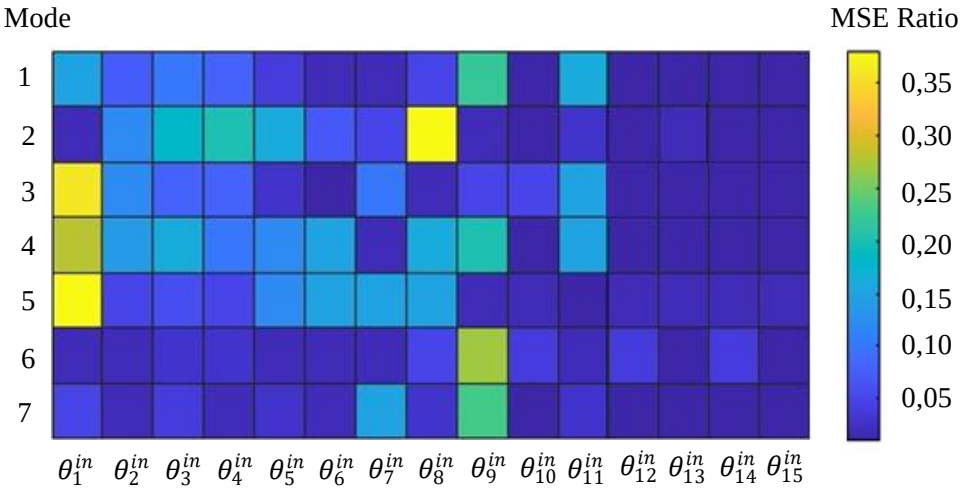

Figure 4.7. Sensitivity analysis performed on the laboratory footbridge model for initial selected 15 updating parameters

For the first step, the preliminary set of parameters consists of the same fifteen parameters $\left(\theta_{1,2,\ldots,15}^{in}\right)$ considered in previous studies [80]. After performing the sensitivity analysis (second step), instead of the selected fifteen parameters (Figure 4.7) only ten of them were included in the FEMU process (Table 4-2, Figure 4.8). The remaining five (those for which the maximum value of the MSE ratio is less than 0,05) were excluded due to their reduced effects on the modal properties of this structure.

Table 4-2. List of the selected updating parameters of the FE model their description and assigned initial values based on the previous studies [125][124]

Parameter	Description	Initial value
θ_{1-6}^{in}	Young modulus of elasticity of steel (longitudinal beam)	210 [GPa]
θ_{7}^{in}	Young modulus of polyurethane of SPS panels	0,75 [GPa]
θ_{8}^{in}	Young modulus of elasticity of steel bolts	210 [GPa]
θ_{9}^{in}	Equivalent longitudinal stiffness of support	$5{,}5 \cdot 10^7$ [N/m]
θ_{10}^{in}	Equivalent transversal stiffness of support	$1{,}9 \cdot 10^7$ [N/m]

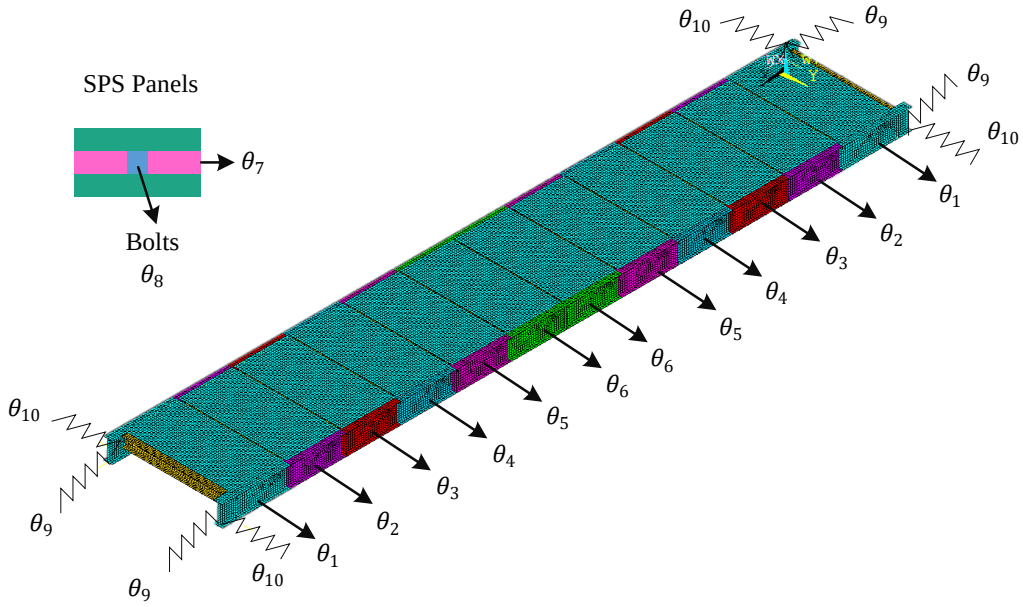

Figure 4.8. Selected updating parameters of the FE model of laboratory footbridge

4.6. Solution of the FEMU problem based on a conventional optimization method

To validate the computational efficiency of the GT algorithms, the FEMU is also performed using a conventional bi-objective optimization method based on the computation of the Pareto front together with a subsequent decision-making problem (for the determination of the "knee" point). As optimization algorithm, HS algorithm has been considered herein due to the high performance shown to solve the FEMU problem of civil engineering structures [76]. The updating process was performed linking a FE analysis software, Ansys [229], with a mathematical software, Matlab [234]. The following parameters of the HS algorithms were established to perform the optimization process [76]: population size PS=100; maximum number of iterations I_{max}=50; objective function tolerance $t_{of} = 1 \cdot 10^{-4}$; new population size $P_{s,new} = 40$; harmony memory pitch adjustment $HMCR = 0{,}9$ and pitch adjusting rate $PAR = 0{,}3$.

4.6.1. Solution of the SO FEMU problem

Using the SO function, the optimization problem of the laboratory footbridge is defined as follows:

Find $\vec{\theta} = \{\theta_1\ \theta_2\ \theta_3\ \theta_4\ \theta_5\ \theta_6\ \theta_7\ \theta_8\ \theta_9\ \theta_{10}\}^T$ which minimizes $F(\boldsymbol{\theta})$ (4.1.)

where

$$F(\boldsymbol{\theta}) = \sum_{t=1}^{n} w_t F_t(\boldsymbol{\theta})^2 = \left(\sum_{t=1}^{n_f} w_t^f r_t^f(\boldsymbol{\theta})^2 + \sum_{t=1}^{n_m} w_t^m r_t^m(\boldsymbol{\theta})^2 \right) \quad (4.2.)$$

The optimization of such defined function is performed taking into account the influence of different values of the natural frequencies (w_t^f) and mode shapes (w_t^m) weights on the updated value of physical parameters (Table 4-3.) and consequently on the values of the residuals (Table 4-3., Figure 4.9.). The position of the results obtained using the different values of weighting factors is shown on the Figure 4.9.

Table 4-3. Updated value of the physical parameters of the model and values of the residuals in terms of the weighting factors under the SO approach

w_t^f	w_t^m	θ_1	θ_2	θ_3	θ_4	θ_5	θ_6	θ_7	θ_8	θ_9	θ_{10}	$\sum r_t^f$ $[10^{-3}]$	$\sum r_t^m$ $[10^{-3}]$
1,0	0	1,100	0,982	1,034	0,989	0,922	0,979	0,750	2,484	0,763	1,000	21,18	4,51
0,9	0,1	1,097	1,012	1,099	0,901	0,944	1,013	0,754	1,133	0,860	0,787	15,98	4,54
0,8	0,2	1,093	0,910	1,085	0,953	1,089	1,029	1,342	2,181	0,754	0,824	8,76	4,97
0,7	0,3	1,097	0,988	0,912	0,997	1,022	1,032	1,385	1,955	0,861	0,835	10,08	4,80
0,6	0,4	1,085	1,086	1,098	1,084	0,986	1,056	1,274	1,996	0,848	0,837	10,02	5,01
0,5	0,5	1,079	0,952	0,941	0,908	1,083	1,044	1,263	2,106	0,750	0,844	9,34	5,03
0,4	0,6	1,073	0,922	1,093	0,981	0,936	1,013	1,265	2,183	0,789	0,764	8,79	5,11
0,3	0,7	1,066	1,077	0,990	1,039	1,065	0,995	1,027	2,496	0,813	0,777	10,56	5,07
0,2	0,8	1,071	0,966	1,092	0,991	0,971	0,930	1,087	1,985	0,785	0,756	10,14	5,04
0,1	0,9	1,068	1,055	1,078	1,047	1,056	1,061	1,170	2,437	0,791	0,792	9,33	5,14
0	1,0	1,055	0,927	0,934	0,910	0,900	1,094	1,325	2,394	0,826	0,797	9,00	5,27

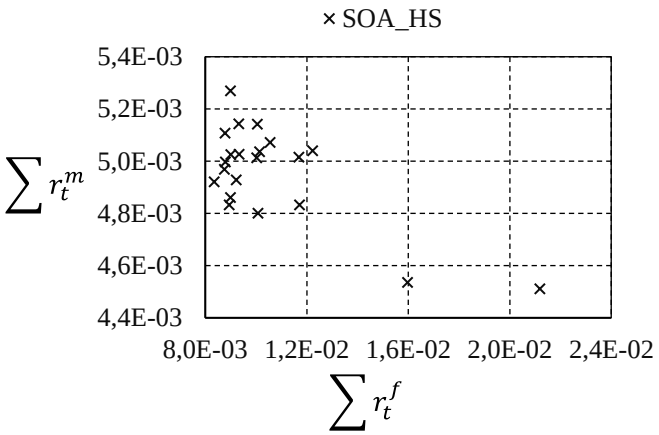

Figure 4.9. Comparison among different residuals in the function space considering Harmony search optimization algorithm and SO function approach

According to the performed SO FEMU optimization the results vary from the minimum values $\theta_{SO_{HS}}^{min}$ = [221,6; 191,10; 191,50; 189,21; 189; 195,30; 0,5625; 237,93; 4,14· 10^7; 1,44·10^7] till the maximum $\theta_{SO_{HS}}^{max}$ = [231; 228,06; 230,79; 227,64; 227,69; 229,74; 1,039; 524,16; 4,74· 10^7; 1,91·10^7]. The computational time the conventional optimization algorithms required to solve the updating problem formulated as the SO function was 41432 s.

4.6.2. Solution of the MO FEMU problem

The initial finite element model of the laboratory footbridge was also updated under the MO approach. The same design variables as those selected for the SO objective approach were adopted. The optimization problem of the laboratory footbridge using the MO approach is defined as follows:

Find $\vec{\theta} = \{\theta_1\ \theta_2\ \theta_3\ \theta_4\ \theta_5\ \theta_6\ \theta_7\ \theta_8\ \theta_9\ \theta_{10}\}^T$ which minimizes $F(\boldsymbol{\theta})$ (4.3.)

where

$$F(\boldsymbol{\theta}) = (F_1(\boldsymbol{\theta}) \quad F_2(\boldsymbol{\theta})) = \left(\sum_{t=1}^{n_f} r_t^f(\boldsymbol{\theta})^2 \quad \sum_{t=1}^{n_m} r_t^m(\boldsymbol{\theta})^2 \right) \tag{4.4.}$$

As result of this updating problem, Figure 4.10 shows the Pareto front of the two terms of the MO function. Additionally, the "knee" point of this Pareto front (the most balanced solution) has been included in Figure 4.10. Therefore, the knee point is computed as $\theta^*_{MOA\_HS}$= [1,062; 0,995; 0,979; 0,976; 1,009; 1,893; 1,009; 2,043; 0,771; 0,784] that correspond to the following values of the numerical model physical properties [223,02; 208,95; 205,59; 204,96; 211,89; 397,53; 0,75675; 429,03; 4,25· 10^7; 1,50·10^7].

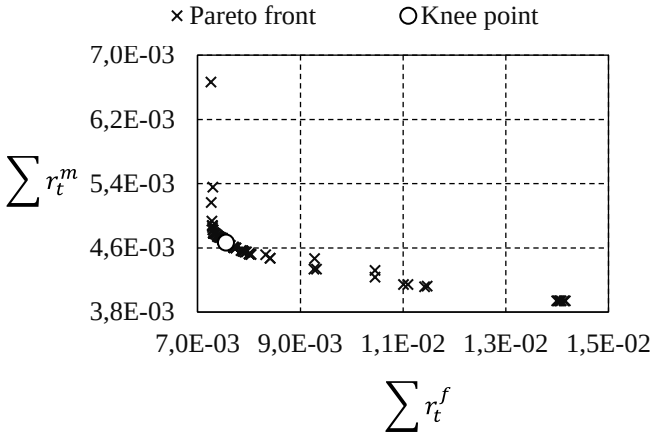

Figure 4.10. Comparison among different residuals in the function space considering Harmony search optimization algorithm and MO function approach

The total computational time required to obtain the Pareto front considering the HS optimization algorithm has been recorded 27 289 s.

4.7. Solution of the FEMU problem based on the GT

After performing FEMU with the conventional algorithm, the following subchapters describe FEMU according to the GT approach based on transforming the SO function into the weighted function and the MO function into the utility function, as well as different game models: NCGT; CGT; and EGT. For both function definitions and all three game models for the optimization process, the nature-inspired harmony search algorithm is used according to the set of variables defined in Chapter 4.6. while the convergence criterion for all three game models is set according to Eq. (3.12.). The same design variables are considered as it is for the SO and MO approach under the conventional approach.

4.7.1. Solution of the SO FEMU problem based on GT

For defined optimization problem of the laboratory footbridge the optimization is performed under the GT approach described in the Chapter3.2. The problem is formulated as follows:

$$\text{Find } \vec{\theta} = \{\theta_1\ \theta_2\ \theta_3\ \theta_4\ \theta_5\ \theta_6\ \theta_7\ \theta_8\ \theta_9\ \theta_{10}\}^T \text{ which minimizes } F(\boldsymbol{\theta}) \tag{4.5.}$$

where function $F(\boldsymbol{\theta})$ is defined as it is in the Eq (4.2.). As part of standard procedure of SO optimization using the GT, the minimization, maximization, and normalization of defined natural frequency $\left(r_t^f\right)$ and mode shape (r_t^m) residuals is performed (Table 4-4). According to the normalized residuals, the weighted objective function is formulated introducing the new updating parameter, *K*, whose value represent the weight factor values of the normalized natural frequency residual. The, *1-K*, represent the weight factor values of the normalized mode shape residual.

Table 4-4. SO optimization using GT

	r_t^f	r_t^m
Minimization	0,007899	0,004646
Maximization	0,050766	16,79360
Normalization	$r_{t,n}^f = \frac{r_t^f - 0{,}007899}{0{,}042867}$	$r_{t,n}^m = \frac{r_t^m - 0{,}004646}{16{,}78895}$

Based on the performed minimization, maximization and normalization of defined natural frequency, r_t^f, and mode shape, r_t^m, residuals the weighted objective function is defined as follows in Eq (4.6.).

$$F_{w,t}(\boldsymbol{\Phi}) = K \cdot r_{t,n}^{f} + (1-K) \cdot r_{t,n}^{m} - \left(1 - r_{t,n}^{f}\right) \cdot \left(1 - r_{t,n}^{m}\right) \quad (4.6.)$$

Optimizing the formulated weighted objective function, the optimal design variable values are obtained. It is assigned to the vector $\theta^{*}_{\text{SOA\_GT}}$ = [1,088; 0,992; 0,979; 1,072; 1,019; 0,913; 1,236; 2,427; 0,791; 0,782] that correspond to the following values of the numerical model properties [228,48; 208,32; 205,59; 225,12; 213,99; 191,73; 0,927; 509,67; $4{,}251 \cdot 10^{7}$; $1{,}49 \cdot 10^{7}$]. The optimal value of the natural frequency residual weight factor is $K = 0{,}243$. The position of the solution of the optimization SO function using GT, i.e., the values of the objective functions $f_1(\theta) = \sum r_t^f$ and $f_2(\theta) = \sum r_t^m$ is shown on the Figure 4.11. The total computational time required to perform the optimization of a SO function using GT was recorded as 10 559 s. Based on the previous, some initial conclusions can be drawn regarding the possibility of performing FEMU using GT and the time required for the simulation, which is lower than the time the application of conventional algorithms required.

4.7.2. Solution of the MO FEMU problem based GT

The solution method for the MO problem using the GT starts with the definition of the strategy space of each objective function according to the method describe in the Chapter 3.3.2. Accordingly, each term of the MO function (the natural frequency residual r_t^f, the mode shape residual r_t^m was optimized). The impact index (Δ), space distance (d) and space moment (Mo) were computed. According to the mentioned partition rules, the strategy space of each term of the MO function is determined as follows:

$$S_f = \{\theta_2, \theta_3, \theta_4, \theta_5, \theta_6, \theta_7, \theta_8\}$$

$$S_{ms} = \{\theta_1, \theta_9, \theta_{10}\}$$

where S_f represents the natural frequency residual strategy space, while the S_{ms} represents the mode shape strategy space. The detailed information and illustration of the exploration of the strategy space are shown in the Table 4-5. Subsequently, after the determination of each player's strategy space, the updating problem has been solved using the three GT models (NCGT, CGT and EGT). As mentioned, the GT method transforms the bi-objective optimization problem into two SO optimization problems. As in the previous section, HS algorithm has been selected as global optimization algorithm to solve these SO optimization problems. The three GT models start from the same initial strategy $\theta^{0}_{initial}$ = [1, 1, 1, 1, 1, 1, 1, 1, 1, 1].

Table 4-5. Impact index, Δ, space distance, d, space moment, Mo and ranking of design variables

Design variable	$f_1(\boldsymbol{\theta})$			$f_2(\boldsymbol{\theta})$			Mo(j)
	Δ(j,1)	d(j,1)	ranking	Δ(j,2)	d(j,2)	ranking	
θ_1	0,0999826	0,5000757	10	0,1000129	0,4999243	1	0,0499989
θ_2	0,1000049	0,4999847	2	0,0999988	0,5000153	9	0,0500009
θ_3	0,1000049	0,4999847	3	0,0999988	0,5000153	5	0,0500009
θ_4	0,1000049	0,4999847	4	0,0999988	0,5000153	6	0,0500009
θ_5	0,1000049	0,4999847	5	0,0999988	0,5000153	7	0,0500009
θ_6	0,1000049	0,4999847	6	0,0999988	0,5000153	8	0,0500009
θ_7	0,1000011	0,499987	7	0,0999959	0,500013	4	0,0499993
θ_8	0,100006	0,4999817	1	0,0999987	0,5000183	10	0,0500012
θ_9	0,0999934	0,5000146	8	0,0999993	0,4999854	3	0,0499982
θ_{10}	0,0999921	0,5000176	9	0,0999992	0,4999824	2	0,0499978

For each model, the calculation is performed until the convergence criterion is (Eq. (3.12.)) meet. Herein this convergence criterion, $\xi = 0.001$, was set. For the CGT and EGT models, the degree of the cooperation was established as $w_{11}= w_{22}= w_{12}= w_{21}= 0,5$ according to the rules described in the Chapter 3.3.4. For the sake of simplicity, only the first and last round of each model are shown in (Table 4-6).

Table 4-6. Results of GT based MLM for FEMU of laboratory footbridge

Design variable	Initial Strategy	NCGT		CGT		EGT	
		1st Round	7th Round	1st Round	3rd Round	1st Round	3rd Round
θ_1	1	1,099	1,056	1,061	1,087	1,072	1,069
θ_2	1	1,025	0,930	0,925	0,975	0,925	0,963
θ_3	1	0,922	1,047	1,019	1,025	1,019	0,978
θ_4	1	0,903	0,919	0,940	0,948	0,941	0,968
θ_5	1	0,997	1,092	1,080	1,011	1,080	1,017
θ_6	1	1,996	1,648	1,829	1,789	1,725	1,864
θ_7	1	1,012	1,024	1,017	1,015	1,026	1,011
θ_8	1	2,499	2,262	2,464	2,368	2,415	2,036
θ_9	1	0,755	0,785	0,748	0,757	0,726	0,765
θ_{10}	1	0,799	0,767	0,784	0,771	0,784	0,774
$\sum r_t^f$	2,74E-02	7,97E-03	7,69E-03	8,50E-03	7,65E-03	8,50E-03	7,57E-03
$\sum r_t^m$	1,51E+01	1,10	4,79E-03	4,94E-03	4,74E-03	4,94E-03	4,71E-03
T [s]		21462		12276		13262	

Values of updating parameters correspond to the following values of the numerical model properties: (i) for NCGT model : [221,76; 195,3; 219,87; 192,99; 229,32; 346,08; 0,768; 475,02; $4,33\cdot10^7$; $1,46\cdot10^7$]; (ii) for the CGT model [228,28; 204,75; 215,25; 199,08; 212,31; 375,69; 0,761; 497,28; $4,17\cdot10^7$; $1,46\cdot10^7$] and (iii) for EGT [224,49; 202,23; 205,38; 203,28; 213,57; 391,44; 0,758; 427,56; $4,22\cdot10^7$; $1,48\cdot10^7$]. As result of the updating process, Figure 4.12. illustrates the solution of the updating problem for the three mentioned game model. The

total computational time required to solve the FEMU optimization problem defined as a MO function for three game models was: 21 462 s for NCGT; 12 276 s for CGT and 13 262 s for EGT model.

4.8. Discussion of the results

To assess the performance of the GT approach for solving the FEMU optimization problem of simple laboratory bridge model, the comparison of the results has to be performed. Two comparison criteria have been considered: the accuracy of the solution and the computational time required to compute the solution. Both the SO and MO functions optimized using GT were compared to the corresponding solutions obtained using the conventional algorithm, and the SO and MO function solutions obtained using GT were compared with each other.

4.8.1. Solution of SO FEMU problem

Figure 4.11 compares graphically the optimal solution provided by SO optimization using the conventional optimization process under the Harmony search algorithm and SO optimization using the GT. First, it can be remarked that the SO FEMU optimization problem can be successfully solved by adopting GT as computational tool. When comparing the pair of residuals, based on the first criterion, it can be remarked that the solution obtained by applying the GT is in the domain of the solutions obtained by applying the conventional algorithm and by varying the values of the weighting factors.

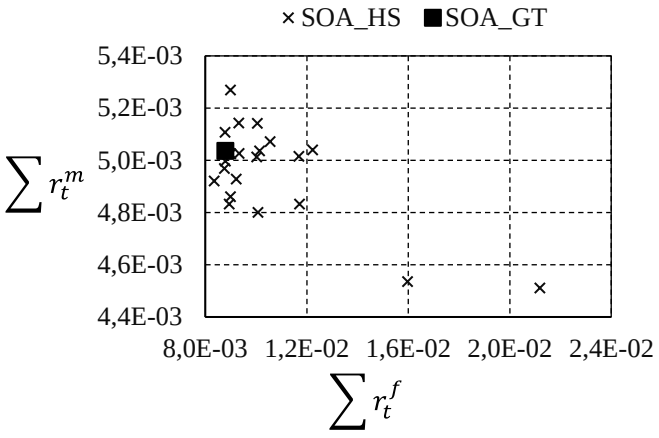

Figure 4.11. Comparison among different residuals in the function space considering Harmony search optimization algorithm and GT model for optimization SO function approach

On the other hand, the computational time required to perform the updating process according to the different methods, can be computed as: for the SO optimization using GT $t_{SOA}^{GT} = 10\,559$ s and for the conventional method $t_{SOA}^{HS} = 41\,432$ s. It can be remarked that the GT required

lower computational time than the conventional algorithms for SO FEMU optimization. Based on these two comparison criteria, it can be concluded that the GT method can be successfully used to solve the FEMU problem of simple civil engineering structures, such as an example of laboratory bridge model in this research, according to the SO MLM. The GT method allows reducing the computational time required to perform the SO FEMU process without compromising the accuracy of the solution. The time reduction is caused by the direct estimation of the weight factors without the necessity to perform the analysis of the effects of different weighted factors values on the optimization results. Finally, the numerical natural frequencies and associated mode shapes of the updated model of the footbridge, considering the updating physical parameters provided by the GT method are shown in the Table 4-7. The natural frequencies relative difference and the MAC factors of each mode shape have been computed. Both the relative differences and the MAC factors provided by the GT are similar to the ones obtained by the conventional optimization algorithms.

Table 4-7. Correlation between experimentally determined natural frequencies and updated ones obtained by optimizing the SO function using conventional HS optimization algorithm and GT model for SO optimization

Vibration mode, t	f_t^{exp} [Hz]	SOA_HS		SOA_GT		$MAC\left(\phi_t^{exp}, \phi_t^{num}\right)$	
		f_t^{upd,SOA_HS} [Hz]	$\lvert\Delta f_t^{SOA\_HS}\rvert$ [%]	f_t^{upd,SOA_GT} [Hz]	$\lvert\Delta f_t^{SOA\_GT}\rvert$ [%]	SOA_HS	SOA_GT
1	3,854	3,896	1,09	3,875	0,54	0,999	0,999
2	5,489	5,561	1,31	5,505	0,29	0,994	0,994
3	8,365	8,495	1,55	8,358	0,08	0,988	0,988
4	11,896	11,861	0,29	11,946	0,42	0,905	0,902
5	18,662	18,394	1,44	18,596	0,35	0,987	0,986
6	20,016	20,153	0,68	20,155	0,69	0,993	0,993
7	22,506	22,083	1,88	22,357	0,66	0,974	0,947

4.8.2. Solution of MO FEMU problem

The same comparison criteria, as it was for the SO optimization problem, have been considered for the MO. Figure 4.12. compares graphically the optimal solution provided by different methods. According to the comparison illustrates in Figure 4.12. the solution provided by the two methods are similar. It can be remarked that the solution provided by the EGT model is better (the nearest to the "knee point") than the one provided by the remaining game models. On the other hand, the computational time required to perform the updating process according to the different methods can be computed as: $t_{NCGT} = 21462\ s$ for the NCGT method; $t_{CGT} = 12726\ s$ for the CGT method; $t_{EGT} = 13262\ s$ for the EGT method; and $t_{HS} = 27289\ s$ for the conventional method. It can also be remarked that the CGT model is the quickest method. Based on these two criteria, it can be concluded that the GT method can be successfully used

to solve the MO FEMU problem of simple civil engineering structures such as an example of laboratory bridge model in this research. The GT method allows reducing the computational time required to perform the MO FEMU process without compromising the accuracy of the solution. The time reduction is caused by the direct estimation of the "knee point" without the necessity to compute the whole Pareto front. Additionally, it can be concluded that the EGT model is the best option to perform the MO FEMU of civil engineering structures since it is the most balanced alternative considering the two comparison criteria. Finally, the numerical natural frequencies and associated model shapes of the updated model of the footbridge considering the updating physical parameters provided by the GT method are shown in Table 4-8 and Table 4-9 respectively. Additionally, the relative differences and MAC ratio of each mode shape have been computed. The good performance of the solution provided by the GT method it is illustrated in Table 4-8 and Table 4-9 respectively. Both the relative differences and the MAC factors provided by the GT method are similar to the ones obtained by the conventional optimization algorithm.

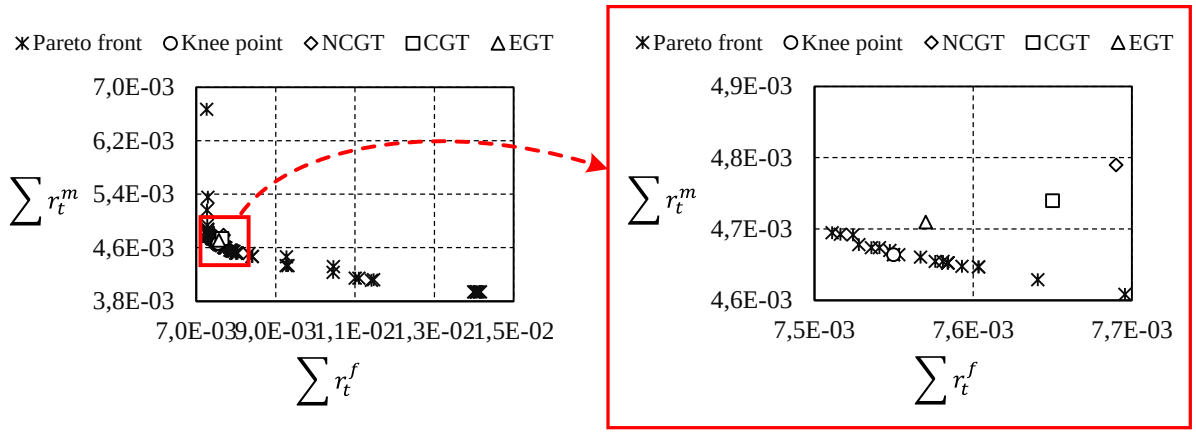

Figure 4.12. Comparison of the "knee" point obtained based on the Pareto front (conventional method) with the position of the optimal solutions obtained using the three different game models (NCGT, CGT and EGT)

Table 4-8. Correlation between experimental and updated natural frequencies using conventional HS optimization and different game models (NCGT, CGT, EGT)

Vibration mode, t	f_t^{exp} [Hz]	HS		NCGT		CGT		EGT	
		$f_t^{upd,HS}$ [Hz]	$\lvert\Delta f_t^{HS}\rvert$ [%]	$f_t^{upd,NCGT}$ [Hz]	$\lvert\Delta f_t^{NCGT}\rvert$ [%]	$f_t^{upd,CGT}$ [Hz]	$\lvert\Delta f_t^{CGT}\rvert$ [%]	$f_t^{upd,EGT}$ [Hz]	$\lvert\Delta f_t^{EGT}\rvert$ [%]
1	3,854	3,875	0,54	3,882	0,73	3,866	0,31	3,883	0,75
2	5,489	5,505	0,29	5,510	0,38	5,500	0,20	5,513	0,44
3	8,365	8,358	0,08	8,336	0,35	8,397	0,38	8,342	0,27
4	11,896	11,946	0,42	11,967	0,60	11,913	0,14	11,973	0,65
5	18,662	18,596	0,35	18,621	0,22	18,565	0,52	18,642	0,11
6	20,016	20,155	0,69	20,191	0,87	20,100	0,42	20,198	0,91
7	22,506	22,357	0,66	22,386	0,53	22,328	0,79	22,418	0,39

Table 4-9. Correlation between experimental and updated mode using conventional HS optimization and different game models (NCGT, CGT, EGT)

Vibration mode, t	HS	NCGT	CGT	EGT
1	0,999	0,999	0,999	0,999
2	0,994	0,994	0,994	0,994
3	0,988	0,988	0,988	0,988
4	0,905	0,880	0,880	0,880
5	0,987	0,987	0,987	0,987
6	0,993	0,993	0,993	0,993
7	0,974	0,961	0,968	0,972

4.8.3. SO vs MO optimization based on GT algorithm

Figure 4.13. illustrates a comparison of the position of the solutions obtained considering two approaches - SO and MO based on the GT. The pair of residuals of each of the solutions has been represented in a MO function space.

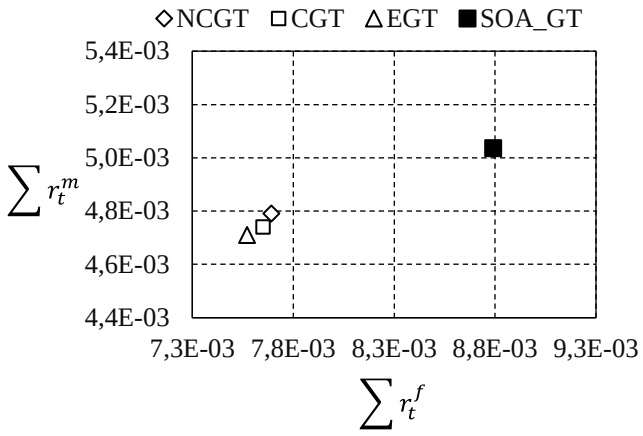

Figure 4.13. Comparison of solutions position under the SO and MO approach solved using different game models

Based on the comparison of the position it can be seen that the solution obtained by optimizing the FEMU problem defined as the SO function is far away from the solution obtained by optimizing the MO function. On the other hand, if we consider the conclusions stated in the previous subsections and compare their position with the position of the Pareto optimal front "knee point" it can be concluded that the MO approach is better option than the SO one. It can be concluded that comparing different game models – NCGT, CGT, EGT, the EGT model is the best model which can be used for solving the FEMU optimization problems of simple civil engineering structures such as presented laboratory bridge model. Regardless of the lower computational time required by the CGT model, the position of the MO FEMU problem's solution obtained by applying the EGT model makes the EGT model the best choice for FEMU of civil engineering structures. Therefore, in the next chapter, this game model will be applied to solve the complex FEMU problem of a real pedestrian suspension bridge.

Chapter 5. Case study on real structure

Among the various types of bridges, suspension bridges are increasingly used to span large spans and the richness of the architectural features and aesthetic aspects. However, their main cables and hangers may be subjected to corrosion and fatigue damage. There is a need for a simple and reliable method to detect and locate this type of damage to subsequently make structural retrofitting and prevent further damage occurring. SHM has emerged as an option that can meet this need. Current SHM system are equipped with a variety of methods to detect damage of a local and global nature. The limitations of the local methods require non-destructive and global damage detection methods. This has led to the continuous development of vibration-based damage detection (VBDD) methods in SHM systems. The basic principle of vibration based SHM is that damage changes the structural dynamic properties. Therefore, the change in structural dynamic properties can be used to detect damage. Due to the difficulty of detecting higher mode shapes in large structures such as suspension bridges, the applicability of existing damage estimates to this type of structure is limited. In addition, this type of structure oscillates in transversal, longitudinal, vertical, torsional, and combined mode shapes, making it difficult to identify the damage. According to the previous problem, a numerical model which is updated based on the experimentally determined structural behaviour is open up as a potential to cope with this problem. In the following, the experimental and numerical analysis of the suspension bridge over the Drava River in Osijek is shown. First, a brief technical description is given. After that, the performed experimental investigation and obtained results are shown. Based on the experimentally obtained results, the numerical model is developed, and the numerical analysis is performed. Both, experimentally and numerical obtained structural dynamic data sets (natural frequency, mode shapes) are compared and used to perform the FEMU of the bridge structure using the EGT model.

5.1. Description of the structure

A pedestrian suspension bridge over Drava River in Osijek (Figure 5.1) was built in 1980. A single span of 209,5 m, a statically pretensioned catenary bridges the river. A parabolic suspension cable, anchored in the blocks behind the bridge, is stretched over the 24 m high steel pylons. Prefabricated concrete hallway slabs are hung on it by inclined hangers. The corridor is 5 m width, while the total span width is 6,12 m.

a)

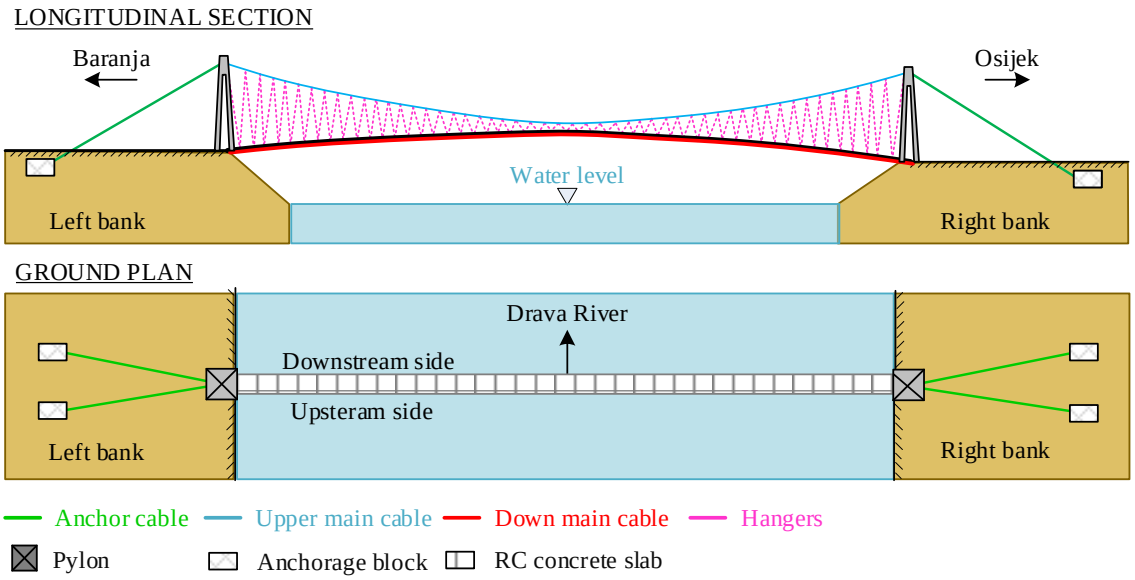

b)

Figure 5.1. a) View on the bridge from the right bank b) Longitudinal section and the ground plane of the bridge

The span consists of prefabricated concrete slabs. There are 50 of them in total and can be divided into three types. The slabs type 1 is placed at the beginning and the end of the bridge

(2 pcs). The slab type 3 is in the middle of the span (1 pcs) while all the rest slabs are type 2. These characteristic slabs have a dimension 6 x 4 m. The longitudinal and transverse ribs are divided each slab into four parts. The lateral longitudinal ribs have a rectangular cross section 26 x 50 cm. The other ribs are 16 cm high, while their width vary, 12 x 18 cm for the longitudinal ribs in the middle, 12 x 15 cm for the outer transvers ribs and 16 x 22 cm for the central transverse ribs. The design value of the concrete cover thickness of ribs is 2 cm, while the class of the concrete is MB 40. The slabs are 8 cm high, doubly reinforced, and have a design value for the concrete cover thickness of 1.5 cm. They are connected by rigid welded reinforcement in the lateral ribs. At one end the slab is suspended on the hangers (ϕ21 mm), while at its other end it is supported by a longitudinally movable mandrel (ϕ28 mm), on the adjacent slab. Under the slabs, there are a two tension cables anchored in the foundation of the pylon. The cross section of the bridge is shown on the following figure (Figure 5.2.).

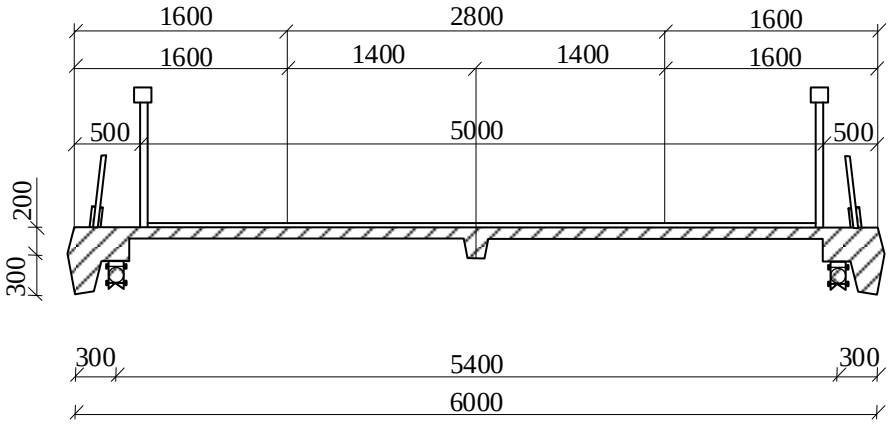

Figure 5.2. Cross section of the bridge (all dimensions are in millimetres)

The down main cable consists of 2 ϕ 61 mm cables on each side of the bridge and forms a system of pre-tensioned catenaries that reduces deformations of the deck and dampens vibrations. During the war the bridge was damaged – hangers were damaged, and two prefabricated slabs were broken through. Afterwards, the bridge was rehabilitated to its original condition. In 2009, new asphalt layer was installed, and the connection was fixed and rehabilitated. During the preparation of the concrete substructure for installation of the asphalt the concrete cover was removed in several place by hydro-demolition of the concrete surface. This year, 2022, as part of the restoration of the bridge, the connecting elements of the upper main cable were replaced, the layer of asphalt was removed, beams of the prefabricated slabs were reprofiled, the gaps between the prefabricated slabs were sealed, corrosion protection of the steel elements was renewed, and the handrail was repaired.

5.2. Initial numerical model

Initial numerical model of the bridge was developed using the commercial FE package Ansys [229]. All the numerical simulations were performed using a PC with a processor 3,59 GHz and 16 GB RAM memory. The developed model was meshed using 20787 elements. It has been developed according to the following scheme:

- three main lateral beams, transversal beams, handrail elements and rigid connection between elements have been modelled by 3D linear beam elements (BEAM 188),
- the concrete slabs have been modeled as four node shell elements with six degree of freedom (SHELL 181),
- the cable elements (upper and down main cables, hangers, anchorage cables) have been modelled by 3D uniaxial tension element with three degrees of freedom at each node (LINK 180),
- the connection between slabs, longitudinal beams, and transversal beams have been modelled using the 1-D longitudinal spring-damper with UX degree of freedom (COMBIN14),
- the boundary conditions on anchorage cables and pylons are modeled to constrain translations in the x, y, and z directions. The boundary conditions of the downstream main cables are assumed to be constrained.

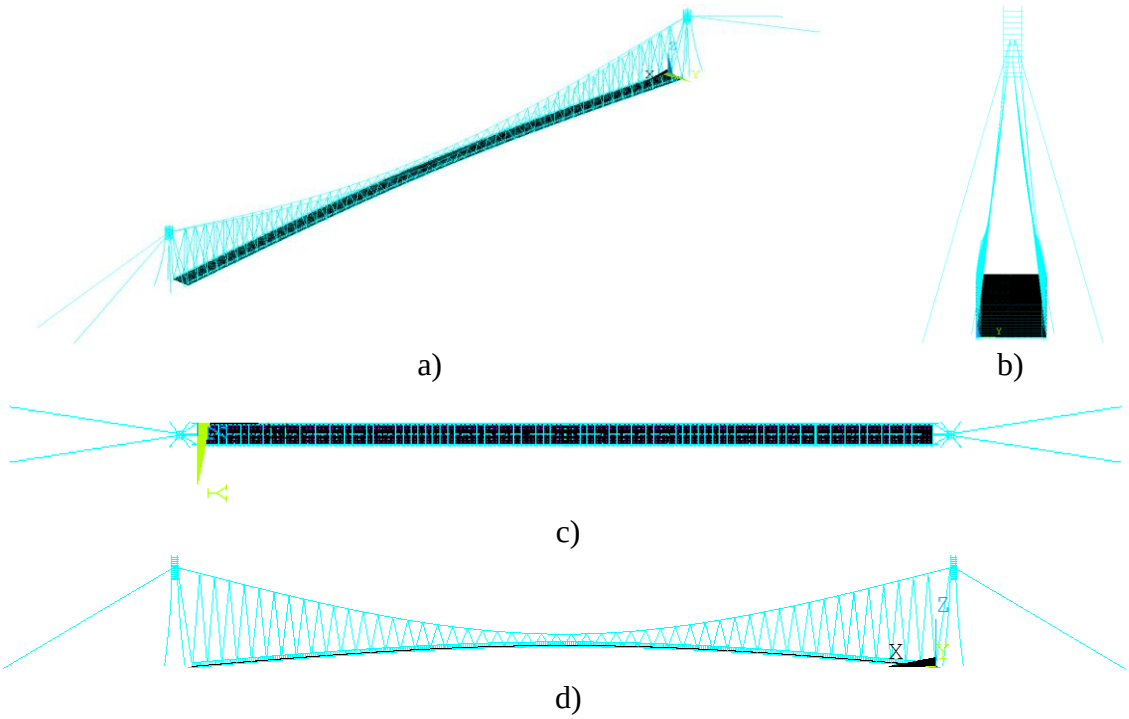

Figure 5.3. Initial numerical model of pedestrian suspension bridge over Drava River a) 3D view b) y-z plane c) x-z plane d) x-y plane

The material properties with the marked numerical model elements to which these properties are assigned are summarized in the Table 5-1.

Table 5-1. Sum of the material properties assigned to the initial numerical model elements with the description

Notation	Parameter	Units	Adopted values	Assigned element
E_{steel}	Elastic modulus	GPa	210	Pylons
ρ_{steel}	Mass density	kg/m^3	7850	
ν_{steel}	Poisson's ratio	-	0,2	
$E_{concrete}$	Elastic modulus	GPa	33	Transversal and longitudinal slab beam, longitudinal beam in the middle of span, transversal beam at each 2m and 4m, longitudinal side beam
$\rho_{concrete}$	Mass density	kg/m^3	2548	
$\nu_{concrete}$	Poisson's ratio	-	0,2	
E_{cable}	Elastic modulus	GPa	160	Anchorage cables, upper and down main cables, old and new hangers
ρ_{cable}	Mass density	kg/m^3	7850	
ν_{cable}	Poisson's ratio	-	0,3	
E_{rigid}	Elastic modulus	GPa	210000	Rigid elements
ρ_{rigid}	Mass density	kg/m^3	0,0001	
ν_{rigid}	Poisson's ratio	-	0,3	
k_{lon}	Spring stiffness	N/m	$1 \cdot 10^{10}$	Connection between the slabs, transversal beams elements, longitudinal beam elements

The cross sections with their dimensions and the remarked numerical model elements to which these properties are assigned are summarized in the Table 5-2.

Table 5-2. Sum of the dimension properties (in millimetres) assigned to the initial numerical model elements

Cross section	Dimension	Assigned element
Rectangular hollow section	736 x 736	Pylon upper part (thickness=18mm)
	736 x 736	Pylon (thickness =18mm)
	120 x 10	Horizontal handrail part (thickness =3 mm)
	50 x 50	Inclined handrail elements (thickness =4 mm)
Rectangular	80 x 80	Transversal slab beam, Longitudinal slab beam
	250 x 250	Longitudinal side beam
	160 x 160	Longitudinal beam in the middle of span and at each 4m
	26,9 x 26,9	Equivalent cross section of vertical handrail elements
Circular	ϕ 5	Rigid elements
	6 ϕ 60	Anchorage cables, Upper main cable
	ϕ 17,4	Old hangers
	ϕ 16,4	New hangers

Based on the previous measurement results, an initial state, i.e., an initial tensile stress, of cable elements is established. The hangers and the upper main cable elements have been grouped into four groups symmetrical in relation to the middle of the bridge looking at the left and right banks. The grouping is performed based on the mean force value and standard deviation determined as part of the previous experimental investigations of the bridge (Figure 5.4).

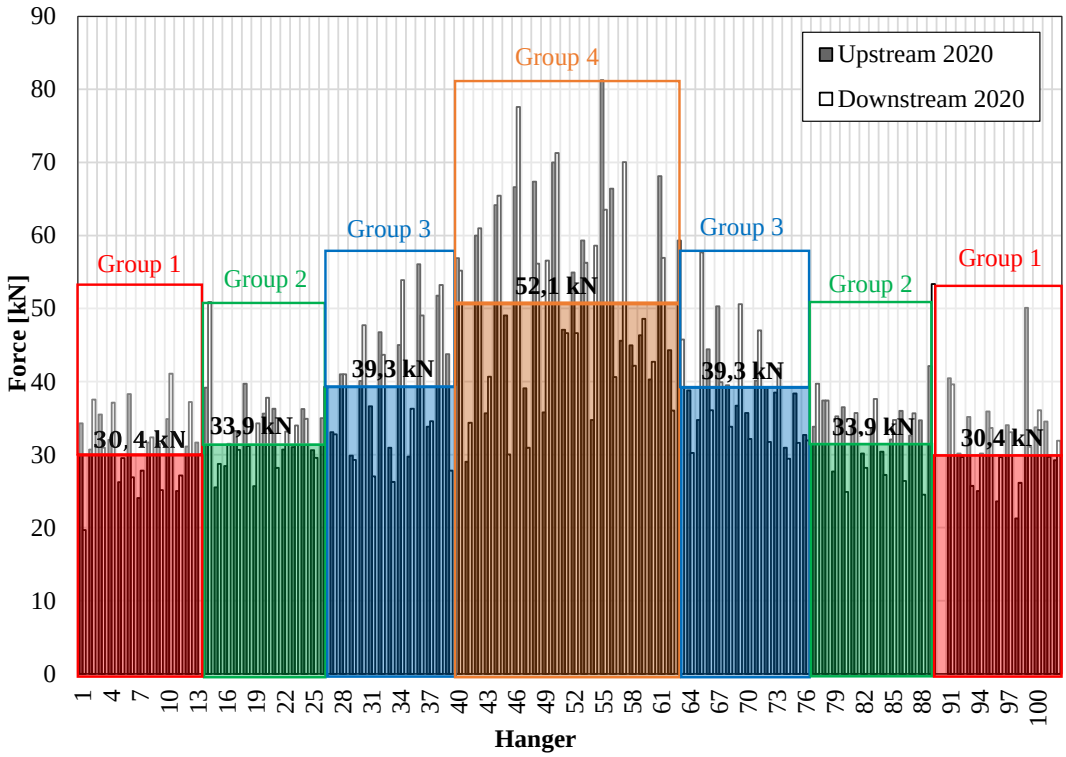

Figure 5.4. Grouping of the hangers with the highlighted (group 1 - red; group II - green; group III - blue; group IV - orange) and remarked mean values (black) and the highlighted space between the mean and maximum values (transparent white rectangles with a coloured border)

Thus, the hangers are grouped in three groups with 26 hangers and one group with 24 hangers. Mean force values are: group I – 30,4 kN; group II -33,9 kN; group III – 39,3 kN and group IV – 52,1 kN. The standard deviation of each group are as follows: group I - ±10,5 kN; group II - ±6 kN; group III – ±9 kN; group IV – ±13 kN. The force values in the upper main cables are calculated based on the equilibrium equation for each node in which hangers are connected to upper main cable (Appendix A. II.). Following the same rule as it is for hangers, the upper main cable on each side is divided into 4 groups. The first group is assigned a force value of 4852 kN with a standard deviation of 40 kN. The second group is assigned a force value of 4798 kN with the standard deviation of 14 kN. The third group is assigned the mean force value of 4744 kN with the standard deviation of 5 kN. While the fourth group is assigned the mean force value of 4766 kN with a standard deviation of 17 kN. Since the upper main cable hangs over the bridge pylons, the anchor cables are assigned the same force value and standard deviation as for group 1 of the upper main cable. The initial tensile stress in the down main cable is assigned the force values from the project documentation equal to the value of 1300 kN. The calculated standard deviation was used for determination of lower and upper bounds of the updating parameters of numerical model. On the developed FE model, the numerical modal analysis was performed to obtain natural frequencies (f_t^{num}) and mode shapes (ϕ_t^{num}) for considered mode

t. Results of the numerical modal analysis is shown on the Figure 5.5.

ϕ_1^{num}- torsional
$f_1^{num} = 0{,}335\ Hz$

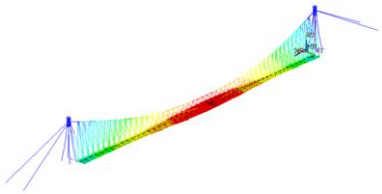

ϕ_2^{num}- vertical
$f_2^{num} = 0{,}428\ Hz$

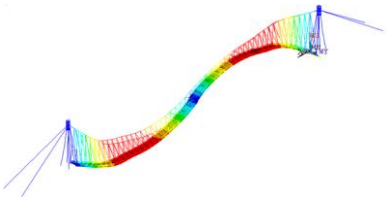

ϕ_3^{num}-torsional
$f_3^{num} = 0{,}641\ Hz$

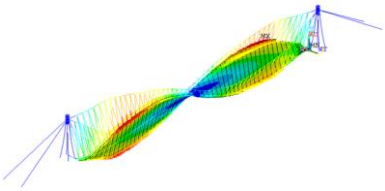

ϕ_4^{num}- torsional
$f_4^{num} = 0{,}862\ Hz$

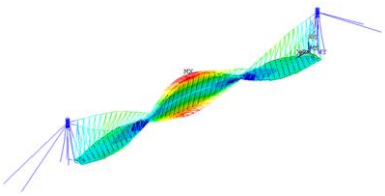

ϕ_5^{num}- vertical
$f_5^{num} = 1{,}058\ Hz$

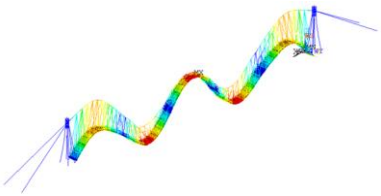

ϕ_6^{num}-vertical
$f_6^{num} = 1{,}330\ Hz$

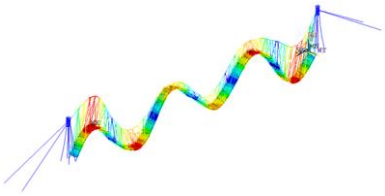

ϕ_7^{num}-vertical
$f_7^{num} = 1{,}524\ Hz$

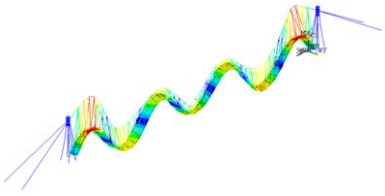

ϕ_8^{num}-vertical
$f_8^{num} = 1{,}791\ Hz$

ϕ_9^{num}-vertical
$f_9^{num} = 2{,}061\ Hz$

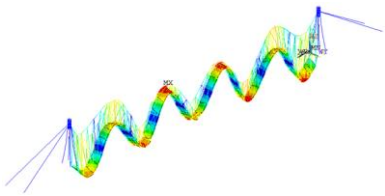

ϕ_{10}^{num}-vertical
$f_{10}^{num} = 2{,}424 Hz$

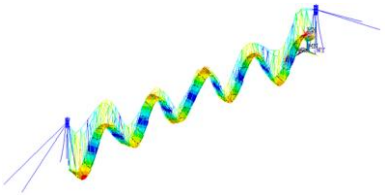

ϕ_{11}^{num}-vertical
$f_{11}^{num} = 2{,}661\ Hz$

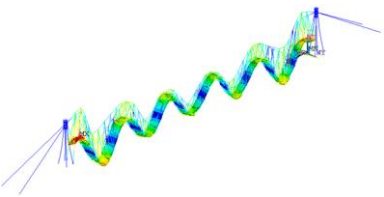

ϕ_{12}^{num}-vertical
$f_{12}^{num} = 2{,}881\ Hz$

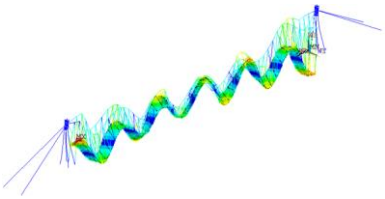

ϕ_{13}^{num}-vertical
$f_{13}^{num} = 3{,}197\ Hz$

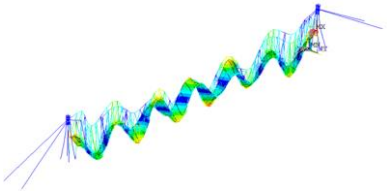

Figure 5.5. Numerically obtained natural frequencies (f_t^{num}) and mode shapes (ϕ_t^{num}) of pedestrian suspension bridge over Drava River for corresponding mode shapes *t=1, ...,13*

5.3. Experimental identification of the pedestrian suspension bridge

As a part of the experimental identification of the bridge and its elements, the following is included:

- determination of the force magnitude of all hangers on the upstream and downstream side,
- determination of the force magnitude of the main anchor cables on the right and left bank,
- determination of the natural frequency of the down main cables,
- determination of the natural frequencies of the pylons on the left and right bank,
- determination of the dynamic parameters of the characteristic edge slab,
- determination of the dynamic parameters of the characteristic slab in bridge span,
- determination of the structural dynamic parameters (natural frequencies, mode shapes, damping ratios) during the vertical excitation caused by pedestrian random walking.

5.3.1. Determination of the force magnitude in the hangers

Determination of the force magnitude in the hangers is performed using the dynamic resonant method, measuring the natural frequencies of the transverse vibration of the hanger after the pulling it out from the equilibrium position. The force values in the hangers were determined based on the correlation between the natural frequency and the stress level. The measuring of the dynamic response at each hanger (total number 2x102=204) is performed using an accelerometer attached to it according to the boundary condition (Figure 5.6.). Starting with the right bank (Figure 5.7), there is a hanger numbered 1, and at the last hanger 102 on the left bank.

a) b)

Figure 5.6. Detailed of the hangers a) connection to the slabs b) attached accelerometer for determination of the natural frequency

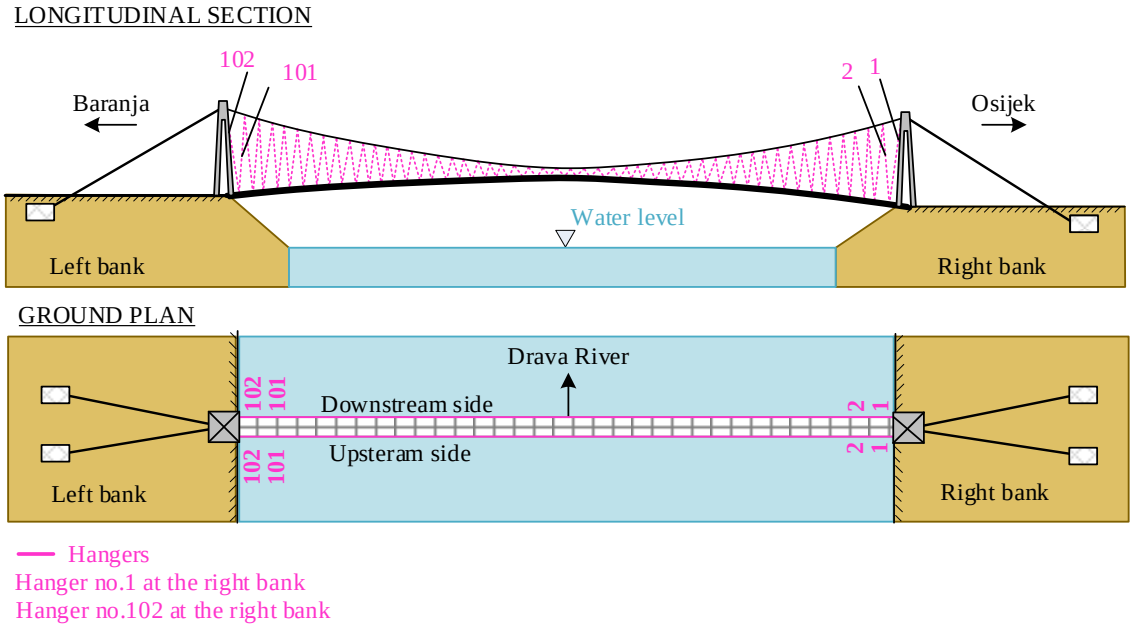

Figure 5.7. Ordinal number of the hangers-a hanger no. 1 at the right bank, and at the last hanger no. 102 located on the left bank

Detail description of the measurements and experimental investigation performed on the bridge so far is given in the following table (Table 5-3).

Table 5-3. Plan of measurements and experimental investigation carried out on the bridge so far

Measurement	Year	Description
1	1993	After the rehabilitation of the bridge destroyed during the war Measurement mark [1993]
2	2009	In March at an average daily temperature 8-10°C as part of the investigation plans of the bridge. Measurement mark [03/2009]
3	2011	In July, at the daily average temperature 30-32°C, only on individual hangers due to replacement of the connecting elements. The connecting elements of hangers 50-51 on the downstream side and the connecting elements of hangers 60-61 on the upstream side of the bridge have been replaced. Therefore, the forces on the downstream side in hangers 42-56 and the hangers 58-64 on the upstream side were determined. Measurement mark [07/2011].
4	2018	In November at an average daily temperature 6-8°C as part of the investigation plans of the bridge. Measurement mark [03/2009]
5	2020	In December at an average temperature 2-5°C as a part of the investigation plans of the bridge. Measurement mark [12/2020]
6	2022	In July at an average temperature 30°C, only on some of the hangers, due to the rehabilitation of concrete slabs. In addition to the hangers, the determination of the natural frequency is performed on the anchorage cables and down main cable Measurement mark [07/2022]
7	2022	In October at an average temperature 24°C after the restauration of the bridge Measurement mark [10/2022]

5.3.1.1. Results of determination of the force magnitude in the hangers

The results of the measured natural frequencies and the calculated force for the last measurement [10/2022] is given in the table A.I.1. in the Appendix I. of this thesis. The comparison of the measured frequencies for the measurements 1993, 03/2009, 11/2018, 12/2020 and 10/2022 is shown on the Figure 5.8. for hangers on the upstream side of the bridge, while the Figure 5.9. shows the measured frequencies in hangers on the downstream side. Based on the measured natural frequency values (measurement 10/2022) for the upstream and downstream hangers, the force values are calculated based on the equation of the string theory vibration [235] (Eq. (5.1.))

$$F_{H,no}^{exp} = 4 \cdot m' \cdot l^2 \cdot \left(f_{H,no}^{exp}\right)^2 \tag{5.1.}$$

where m' is the cable mass in kg/m, l is the cable length in meter, $f_{H,no}^{exp}$ is the experimentally determined natural frequency in Hz. The calculated force value $\left(F_{H,no}^{exp}\right)$ is given in the table A.I.1. while the graphical representation is given on the Figure 5.10.

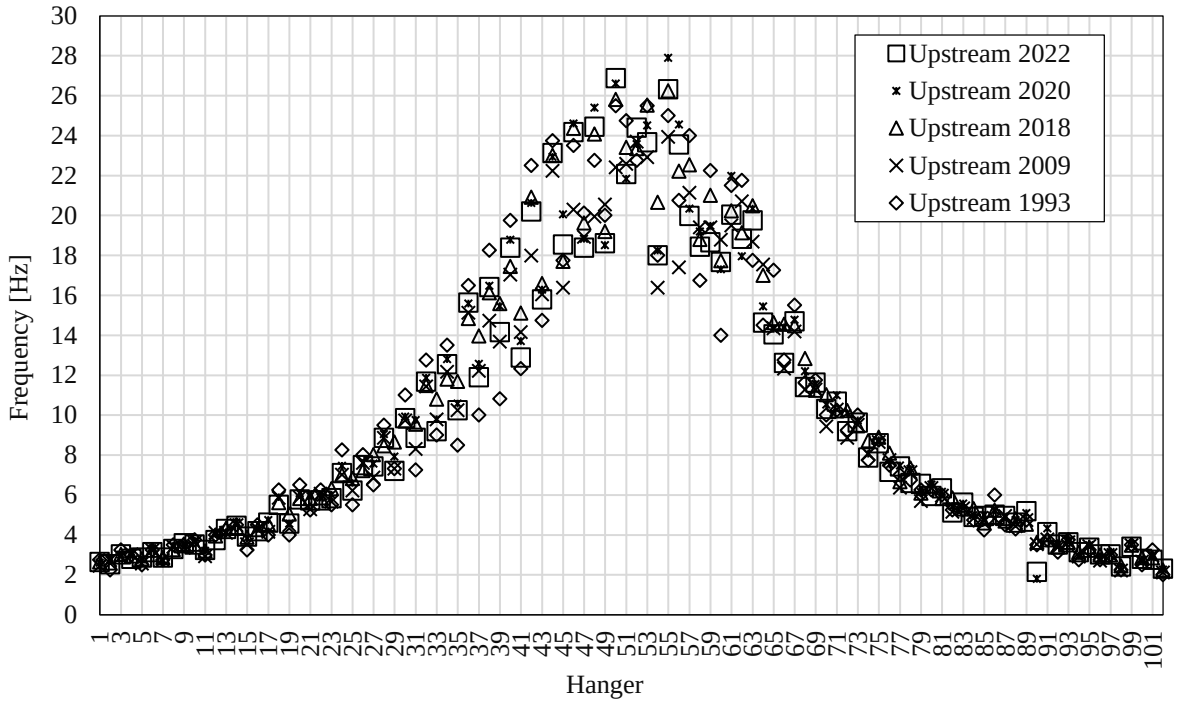

Figure 5.8. Graphical comparison of measured natural frequencies in upstream hangers for measurements 1993, 03/2009, 11/2018, 12/2020 and 10/2022

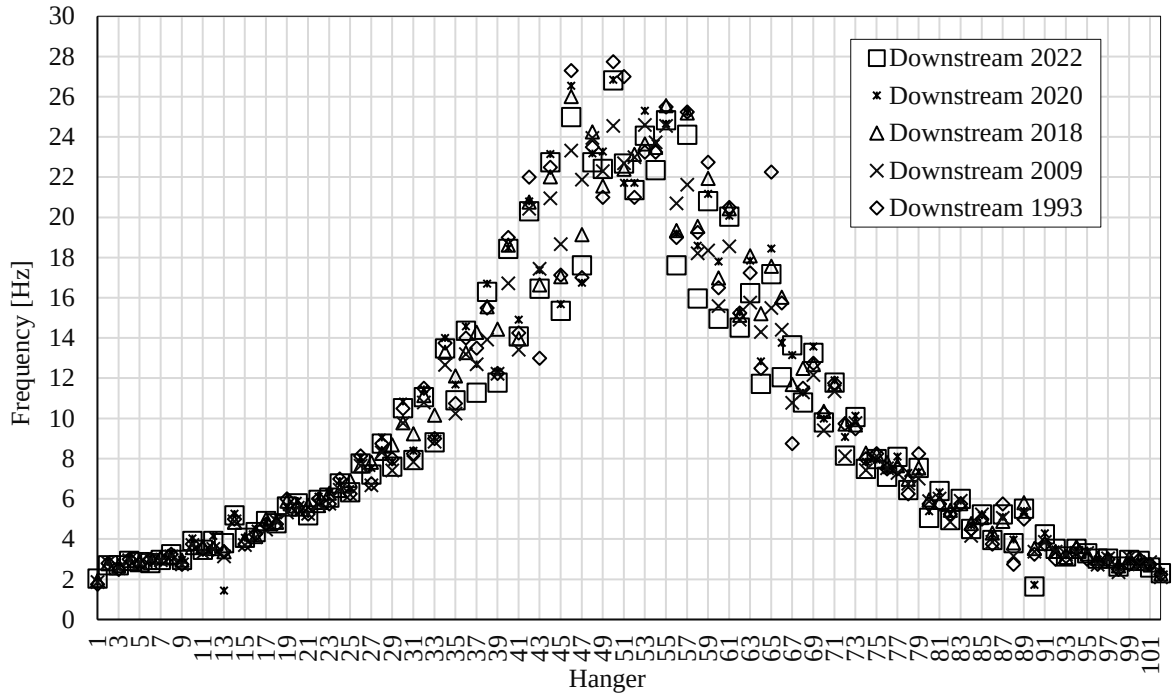

Figure 5.9. Graphical comparison of measured natural frequencies in upstream hangers for measurements 1993, 03/2009, 11/2018, 12/2020 and 10/2022

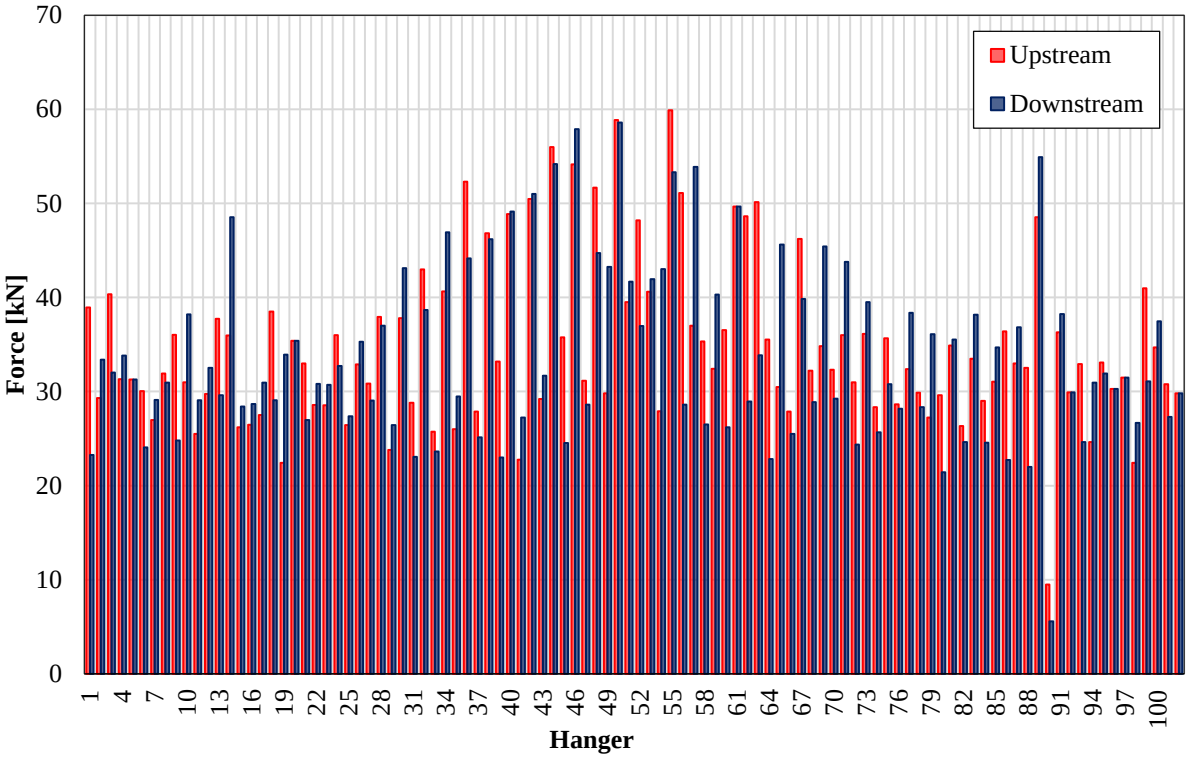

Figure 5.10. Calculated force values in the hangers on the upstream and downstream side of the bridge for the measurement 10/2022

Based on the Figure 5.10. the highest force values are in hangers which are located in the middle third of the bridge, while the lower value on the edge thirds of the bridge. Force values deviates significantly from the pair (downstream/upstream) can also be observed. Statistical analysis of

the calculated forces value in hangers for five measurement periods are given in the Table 5-4. Due to the change of force 07/2011, the magnitudes of the forces measure 03/2009 (downstream 1-41 and 57-102, upstream 1-57 and 65-102) were taken into account in combination with the magnitudes measured in hangers from 07/2011 (downstream 42-56, upstream 58-64).

Table 5-4. Statistical analysis (mean value, standard deviation, median, minimum, and maximum value) of the calculated value of force in hangers $\left(F_{H,no}^{exp}\right)$ for five measurements 10/2022, 12/2020, 11/2018, 2009/2011 and 1993

$F_{H,no}^{exp}$ [kN]	10/2022		12/2020		11/2018		03/2009,07/2011		1993	
	D	U	D	U	D	U	D	U	D	U
Mean	33,8	34,8	37,9	38,8	38,0	38,8	34,9	35,2	37,5	37,1
St. deviation	9,3	8,7	12,8	12,1	10,8	10,6	10,3	9,2	12,7	10,7
Median	31,0	32,7	34,8	35,7	34,6	35,9	32,7	33,1	32,8	34,2
Min	0	0	0	0	21,6	23,2	15,3	19,0	17,9	22,7
Max	58,6	59,9	77,6	81,2	74,5	71,9	63	60,4	80,0	73,3
Deviation of the mean value for measurement 10/2022 in comparison to previous measurements [%]			-10,8	-10,3	-11,1	-10,3	-3,2	-1,1	-9,9	-6,2

5.3.2. Determination of the force magnitude in the anchorage cables

Determination of the force magnitude in the main anchorage cables on the right and left bank are performed in the same way as on hangers. The cable vibration is excited by pulling it out from its equilibrium position.

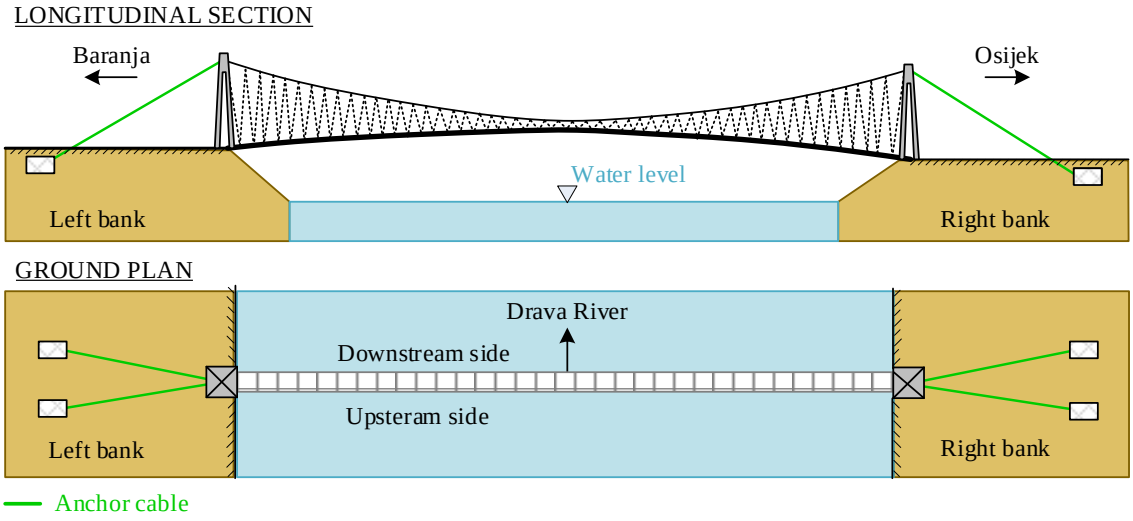

Figure 5.11. Positions of the main anchorage cables

The characteristic records for four anchor cables, based on which the natural frequency values are determined, are shown in the Figure 5.12.

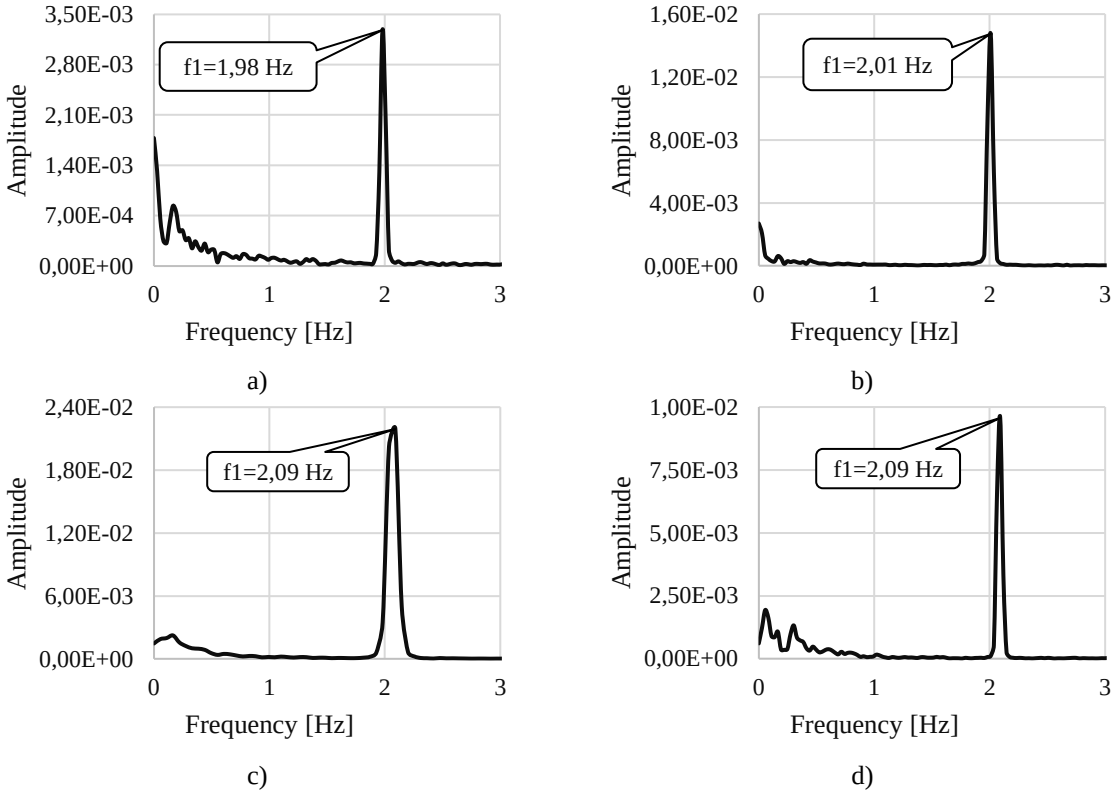

Figure 5.12. Characteristic records of measured natural frequency on the main cable a) right bank-downstream (Anchorage no.1); b) right bank-upstream (Anchorage no.2); c) left bank-downstream (Anchorage no.3); d) left bank-upstream (Anchorage no.4)

5.3.2.1. Results of the determination of the force magnitude in the anchorage cables

The following table (Table 5-5.) shows the geometrical properties of the main anchorage cables, measured natural frequency $\left(f_{A,no}^{exp}\right)$ values and the calculated force magnitudes $\left(F_{A,no}^{exp}\right)$ for measurement 10/2022. The force values $\left(F_{A,no}^{exp}\right)$ are calculated according to the equation Eq. (5.1.). Also, the value of horizontal force component $\left(F_{A,no}^{exp,30}\right)$ for an angle of 30° is calculated and compared in form of the relative error (Δ) with its counterpart from the previous measurement [12/2020].

Table 5-5. Geometrical characteristics, measured natural frequencies $\left(f_{A,no}^{exp}\right)$ and calculated force magnitudes $\left(F_{A,no}^{exp}\right)$ in the main anchorage cables for measurement [09/2022]

Anchorage no.	L [m]	A [mm^2]	$f_{A,no}^{exp}$		$F_{A,no}^{exp}$		$F_{A,no}^{exp,30}$		Δ [%]
			10/2022	12/2020	10/2022	12/2020	10/2022	12/2020	
1	53,40	14700	1,98	2,02	5187	5399	4492	4676	-3,93
2	53,40	14700	2,01	2,02	5346	5399	4629	4676	-1,01
3	53,40	14700	2,09	2,08	5780	5724	5005	4956	+0,99
4	53,40	14700	2,09	2,09	5780	5780	5005	5005	0,00

The calculated values of the horizontal component of the force for an angle of inclination of 30° $\left(F_A^{num,30°}\right)$ are known from the static calculation and are available in the report from March

2009 (number 180-92/09) of the Faculty of Civil Engineering from Zagreb. Therefore, the measured force values are also compared with those from the static calculation (Table 5-6.). The comparison is expressed in the form of the relative deviation in percentage. From the comparison results, there are very small deviations from the calculated values in the measurements 07/2022, 12/2020, 11/2018 and 03/2009.

Table 5-6. Analysis and deviations ($|\Delta|_{calc}$) of the horizontal force component of the anchorage cables ($F_{A,no}^{exp,30}$) for the five periods 10/2022, 07/2022, 12/2020, 11/2018 and 03/2009 in relation to the calculated horizontal force component ($F_A^{num,30}$) where Anch. No. represent the designation of the anchorage cable

Anch. No.	10/2022		07/2022		12/2020		11/2018		03/2009		$F_A^{num,30}$ = 4845 kN
	$F_{A,no}^{exp,30}$ [kN]	Δ_{calc} [%]	$F_{A,no}^{exp,30}$ [kN]	Δ_{calc} [%]	$F_{A,no}^{exp,30}$ [kN]	Δ_{calc} [%]	$F_{A,no}^{exp,30}$ [kN]	Δ_{calc} [%]	$F_{A,no}^{exp,30}$ [kN]	Δ_{calc} [%]	
1	4492	-7,3	4582	-5,4	4676	-3,5	4492	-7,3	4492	-7,3	
2	4629	-4,4	4582	-5,4	4676	-3,5	4584	-5,4	4583	-5,4	
3	5005	+3,3	4861	+0,3	4957	+2,3	4958	+2,3	4816	-0,6	
4	5005	+3,3	4885	+0,8	5005	+3,3	5005	+3,3	4816	-0,6	
Mean value	4783	-1,3	4727,5	-2,4	4828,5	-0,3	4759,8	-1,8	4676,8	-3,5	

5.3.3. Determination of the natural frequency in the down main cables

Determination of the natural frequency in the down main tension cables upstream and downstream on the bridge on the left and right bank of the Drava (Figure 5.13.) is performed in the same way as on the previous cases (hangers and main anchor cables). The cable is excited by pulse excitation using a rubber hammer.

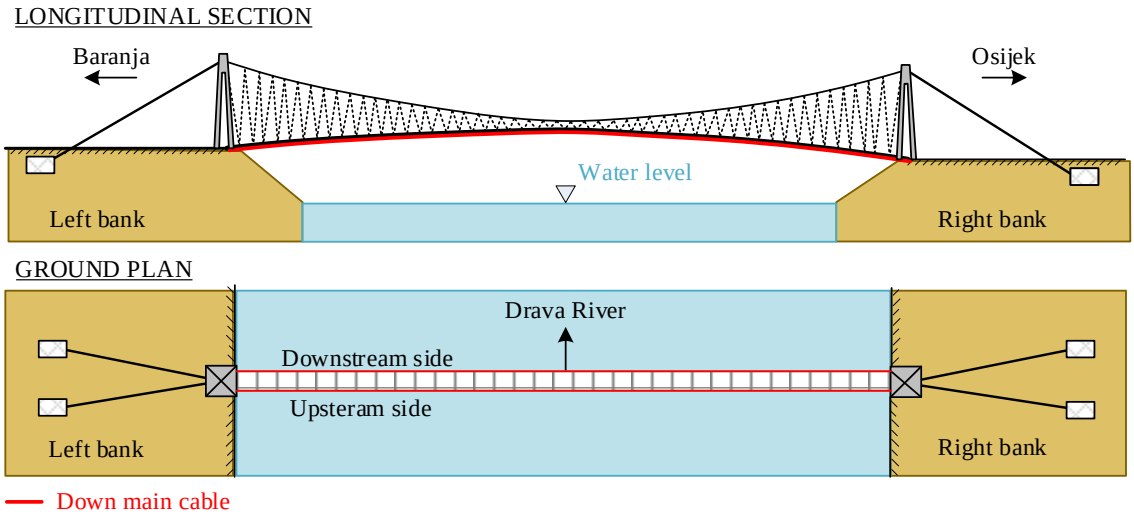

Figure 5.13. Positions of main tension cables

On the following figure (Figure 5.14.) characteristic records of the measured natural frequency of the down main upstream and downstream cable on the right and left bank of Drava River are shown.

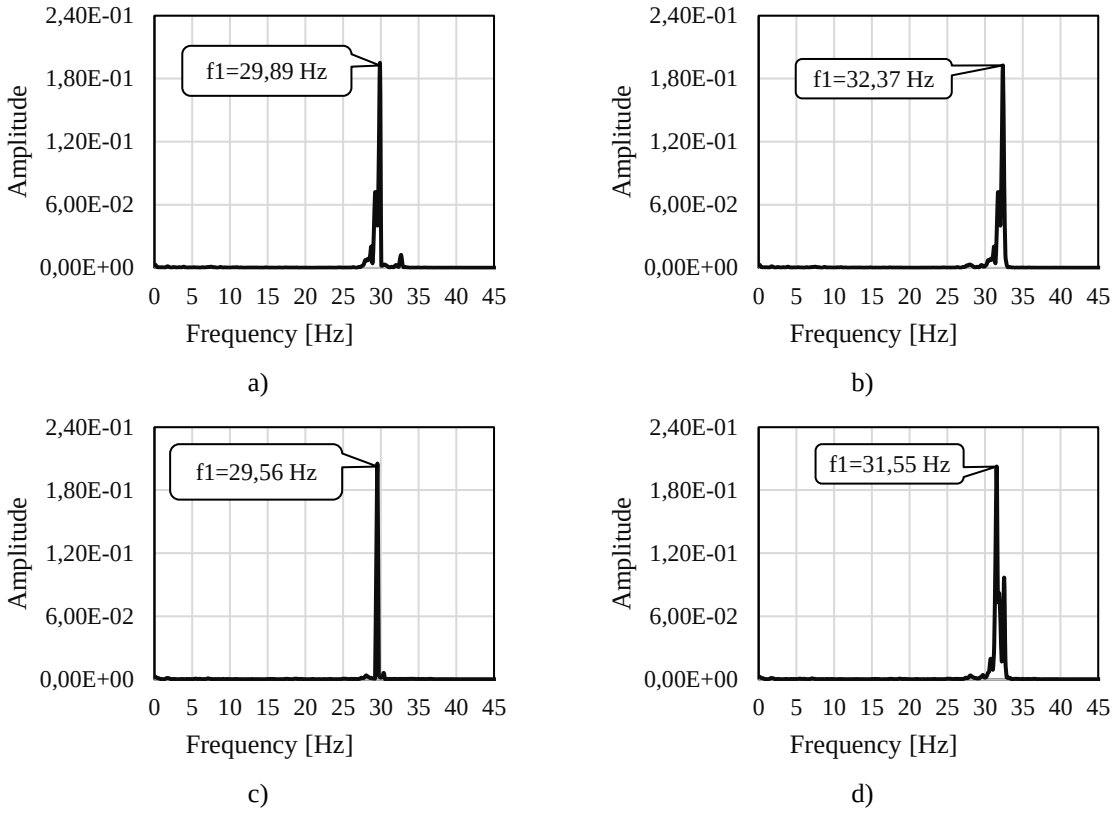

Figure 5.14. Characteristics records of the measured natural frequency of the down main cable at the a) right bank-downstream side; b) right bank – upstream side; c) left bank – downstream side; d) left bank – upstream side

5.3.4. Determination of the natural frequencies of the pylons

Determination of natural frequency of pylon was performed using two accelerometers which measured the acceleration in two perpendicular axes (in the direction of bridge span and perpendicular to it) (Figure 5.15.). The pylons were excited by randomly using a rubber hammer.

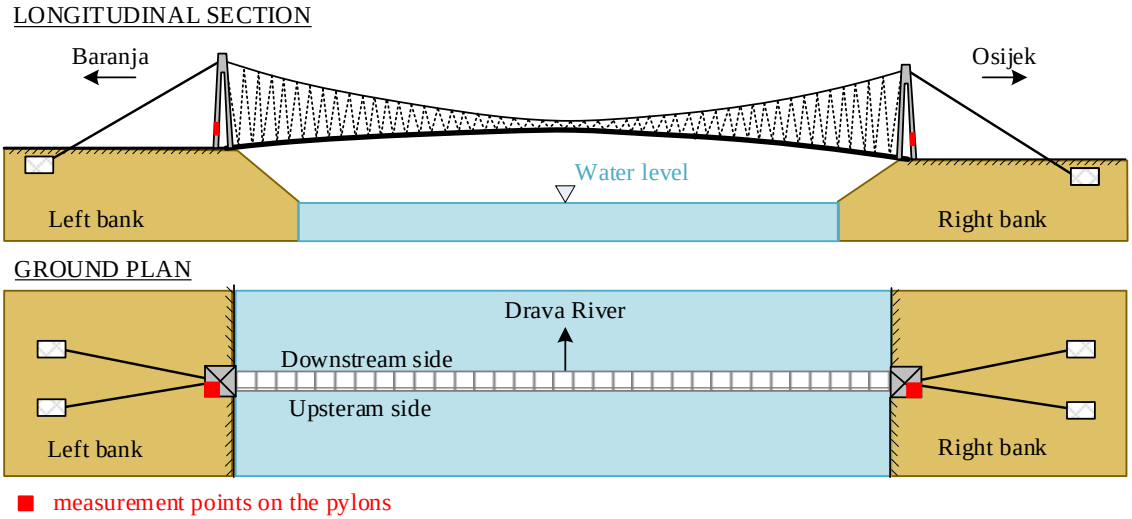

Figure 5.15. Measurement points for determination of natural frequency of pylons

Based on the performed measurement characteristic frequency domain decomposition of the pylon's records on the left (Figure 5.16. a, b) and right (Figure 5.16. c, d) bank the natural frequencies were determined (Table 5-7.).

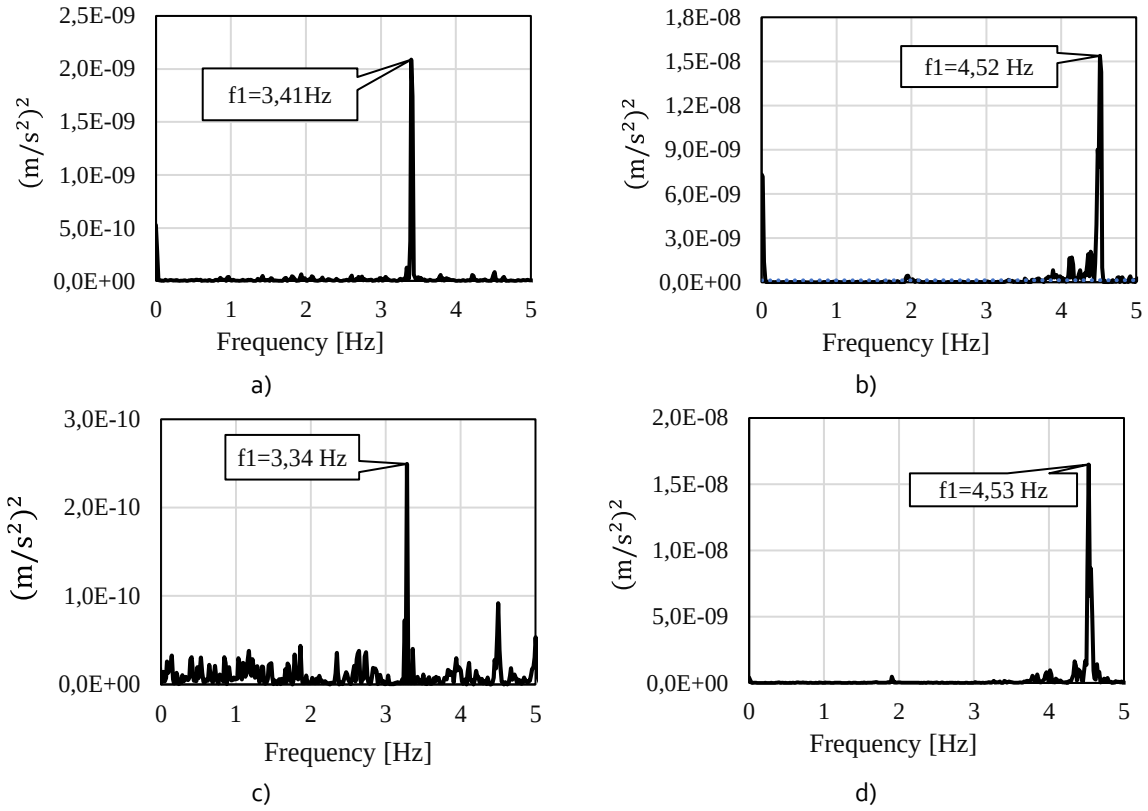

Figure 5.16. Characteristic record of FDD for determination of natural frequencies of pylons on the left bank a) left bank perpendicular to bridge b) left bank in the direction of bridge c) right bank perpendicular to bridge d) right bank in the direction of bridge

Table 5-7. The natural frequency of the pylons on the left and right banks

Orientation	Perpendicular to bridge span		In the direction of the bridge span	
Bank	Left	Right	Left	Right
Frequency [Hz]	3,41	3,34	4,52	4,53

5.3.5. Determination of the dynamic parameters of the characteristic edge slab

In addition to the previously determined modal properties of the main components of the bridge, to determine the boundary conditions of the bridge and its connection with the bank, the dynamic parameters of the edge slab (Figure 5.17.) were determined.

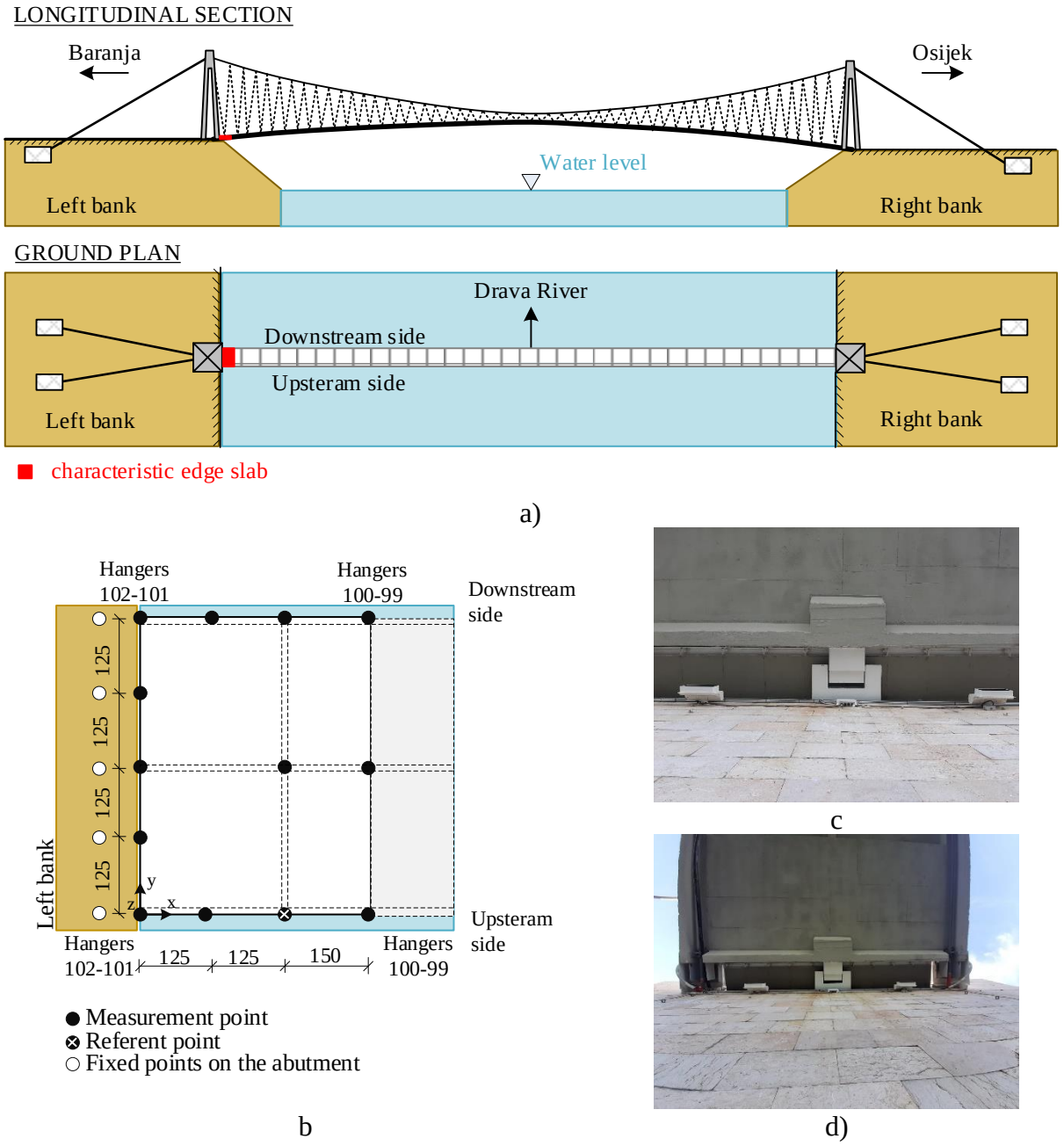

Figure 5.17. a) Position of the characteristic edge slab for which natural frequencies and mode shapes are determined b) Arrangement of the measurement points (dimensions in cm) c) boundary conditions on the left bank d) boundary condition on the right bank

Since it was determined by visual inspection that the bridge is supported in the same way on both the left (Figure 5.17. c) and right bank (Figure 5.17. d), the measurement was performed only on one slab on the left bank. Determination of structural dynamics parameters (natural frequency, mode shapes) was proposed by Frequency Domain Decomposition Methods (FDD). The procedure is based on singular decomposition of spectral density functions matrices measured during the vertical excitation caused by pedestrian random walking for 2 minutes. Measurement of accelerations during excitation was performed in total 13 measuring points

with a denser arrangement than was foreseen for the entire construction (Figure 5.17. b). The natural frequencies of the characteristic edge slab were determined as the resonant peaks of the recorded singular values of the auto spectral densities (Figure 5.18). The corresponding mode shapes are shown in Appendix A. III. of this thesis.

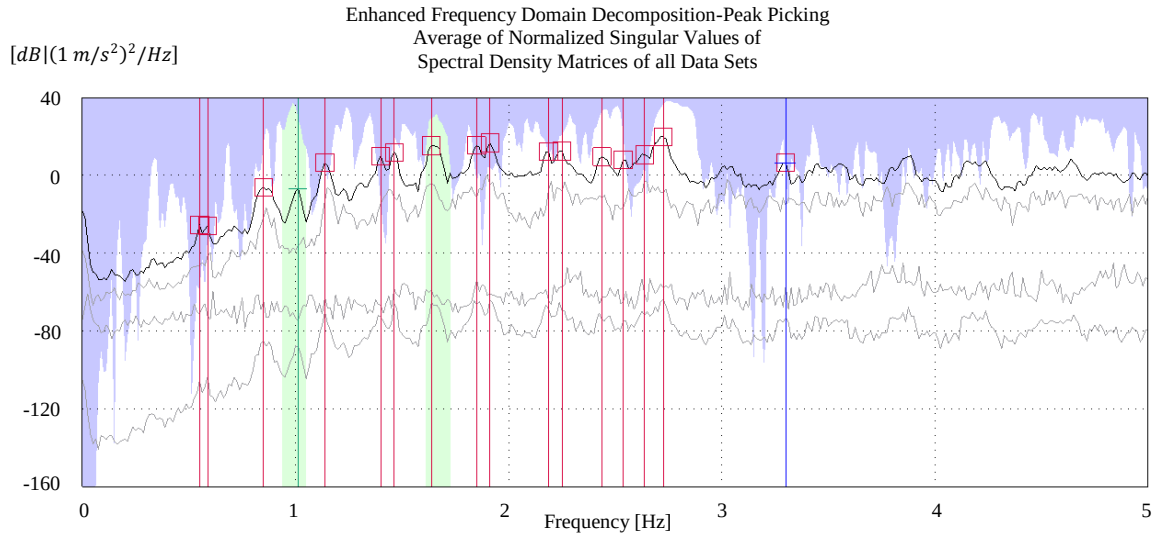

Figure 5.18. Characteristic record of Enhanced Frequency Domain Decomposition (EFDD) for the determination –average of the normalized singular values of spectral density matrices of all data sets for characteristic edge slab

5.3.6. Determination of the dynamic parameters of the characteristic span slab

In order to determine the connection between typical slabs within the bridge span, determination of the dynamic parameters of one characteristic span slab was performed. The slab was vertical excited by pedestrian random walking for 2 minutes. Measurement of accelerations during excitation was performed in total 29 measuring points in vertical direction (Figure 5.19. b).

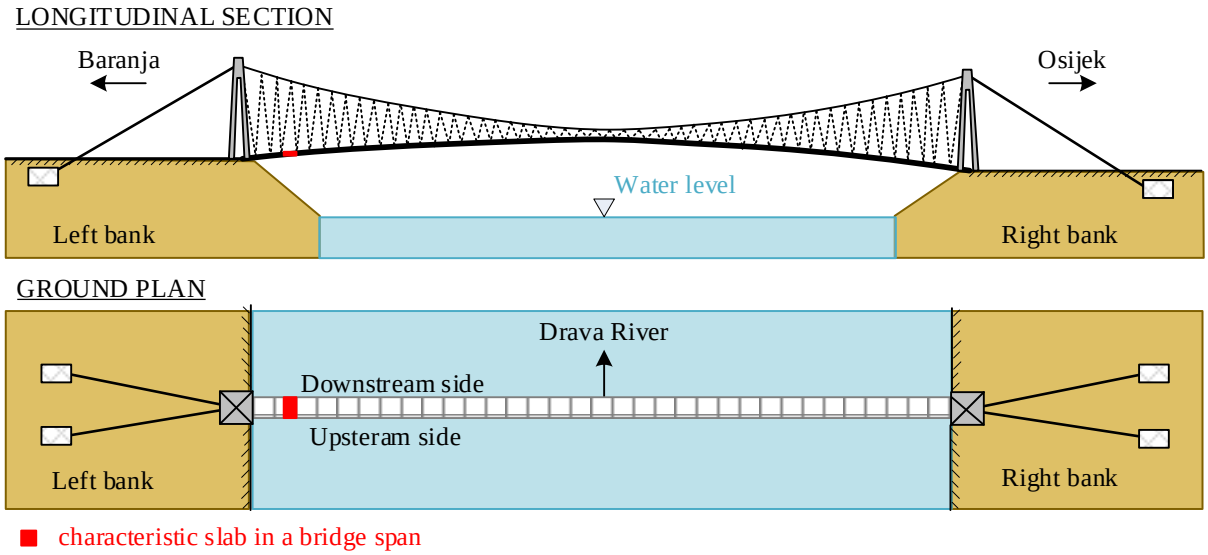

a)

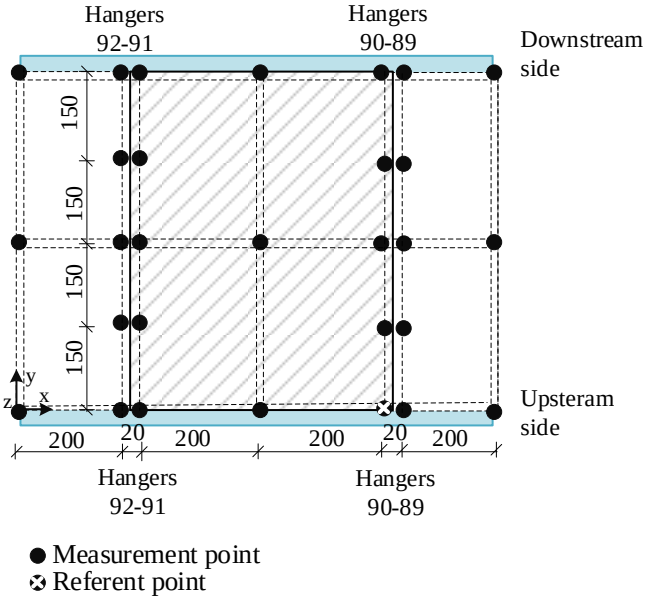

b)

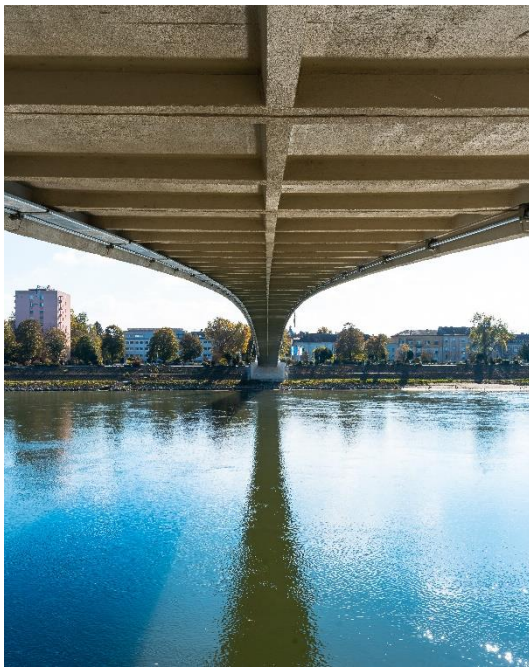

c)

Figure 5.19. a) Position of the characteristic slab in bridge span for which natural frequencies and mode shapes are determined b) Arrangement of the measurement points (dimensions in cm) c) view on the footbridge slabs

The natural frequencies of slab were determined as the resonant peaks of the recorded singular values of the auto spectral densities (Figure 5.20.). The corresponding mode shapes are shown in Appendix A. IV. of this thesis. The obtained natural frequencies and mode shapes of edge and span slab were used together with the obtained dynamic parameters of the entire bridge for FEMU of bridge initial numerical model (Chapter 5.2.).

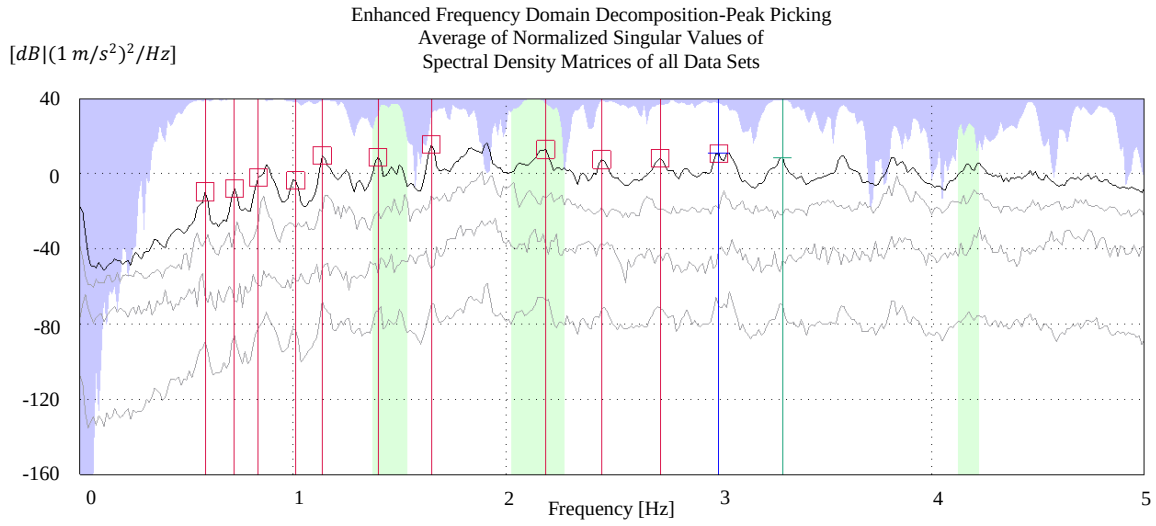

Figure 5.20. Characteristic record of Enhanced Frequency Domain Decomposition (EFDD) for the determination –average of the normalized singular values of spectral density matrices of all data sets for characteristic edge slab

5.3.7. Determination of the structural dynamic parameters

Determination of structural dynamics parameters (natural frequency, mode shapes, damping ratio) was proposed by Frequency Domain Decomposition methods (FDD). Measurement of accelerations during vertical excitation caused by random pedestrian walking was performed on the downstream (node 201-301) and upstream (node 1-101) side on the bridge in odd numbered nodes as indicated and highlighted on Figure 5.21.

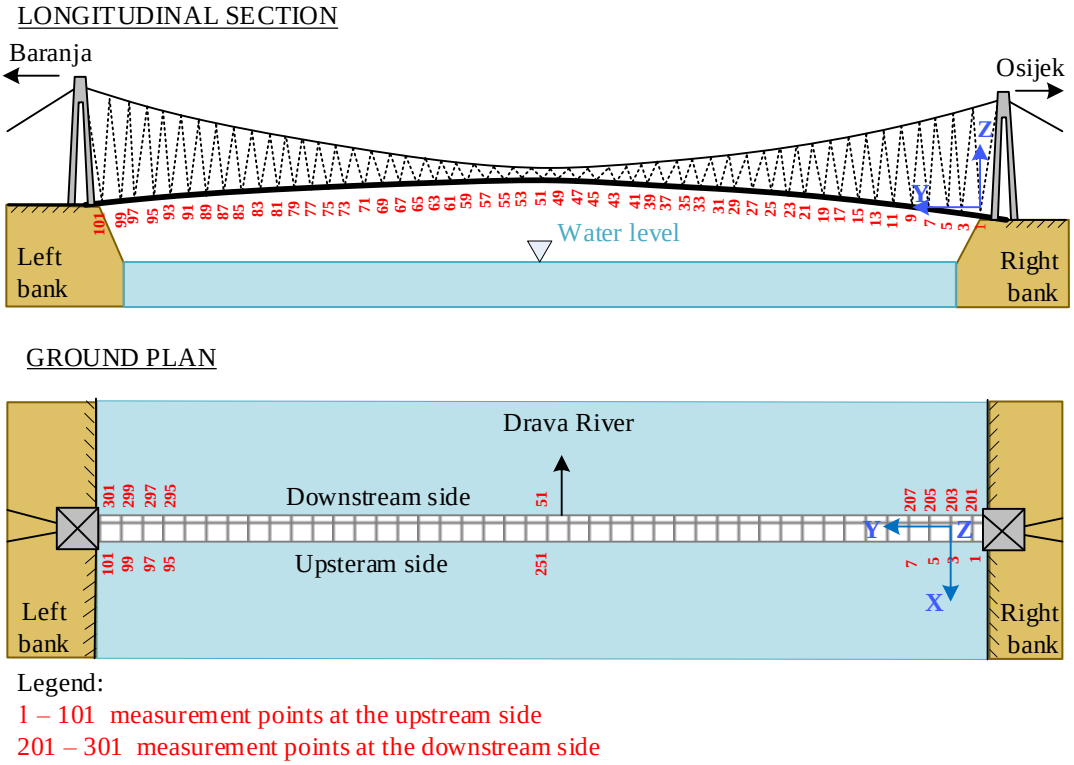

Figure 5.21. Measurement points for determination of structural dynamics parameters of suspension bridge

The structural response was measured in total 100 nodes (50 nodes on each bridge side-upstream and downstream) in two perpendicular directions (x, z), which contains a total of 200 measuring degrees of freedom during the five minutes. The first measuring node is located starting from the right bank (node 1 and 201), and the last on the left bank (node 101 and 301).

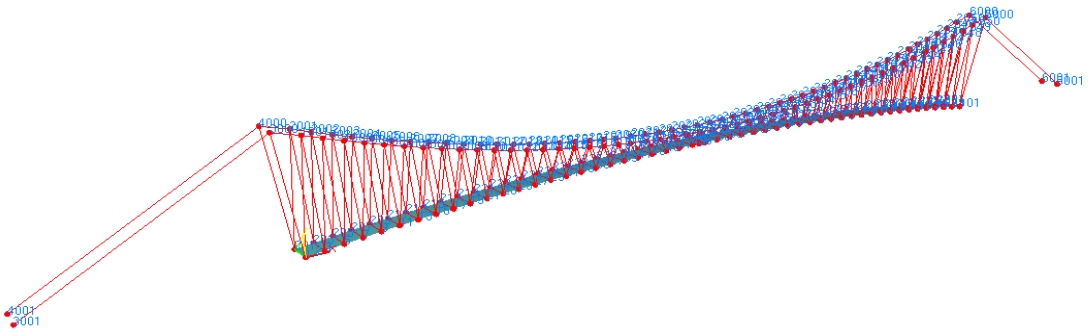

Figure 5.22. Measuring points for determination of structural dynamics parameter in Lab PULSE

The natural frequencies were determined as the resonant peaks of the recorded of singular values of the auto spectral densities (Figure 5.23.).

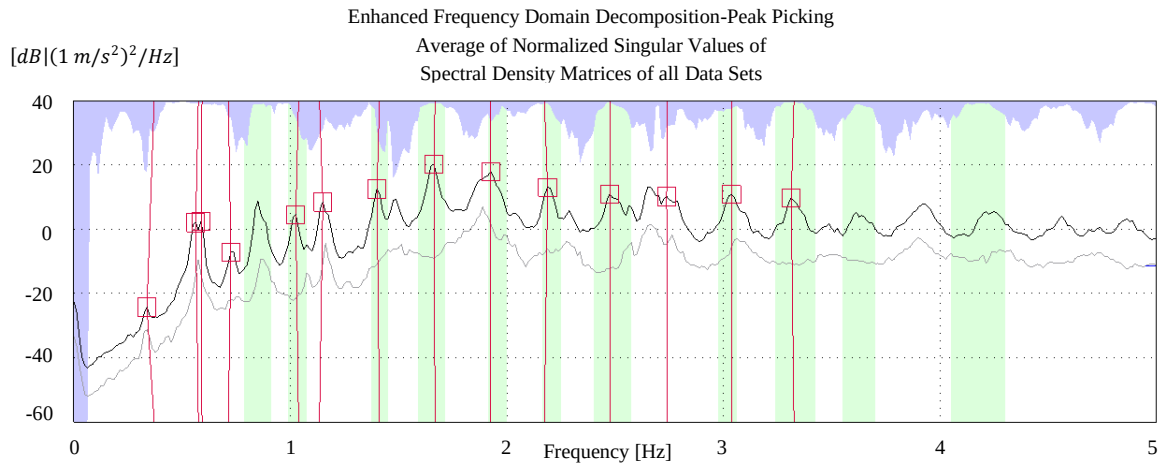

Figure 5.23. Characteristic record of Enhanced Frequency Domain Decomposition (EFDD) for the determination –average of the normalized singular values of spectral density matrices of all data sets

The damping ratios were determined using an Enhanced Frequency Domain Decomposition (EFDD) method. Near the resonance peak, i.e., the natural frequency, the power spectral density function of a single degree of freedom (DOF) system is defined. The eigenvectors around the resonance peak are compared with the eigenvector of the resonance peak itself using the MAC factor). If the value of the MAC factor is large enough, meaning that the eigenvectors match well, the individual singular value is included in the function of the single DOF system. In this way, a certain function of a single DOF system function is restored to the time domain by Inverse Discrete Fourier Transformation (IDFT), and the damping coefficient is determined from it by logarithmic decrement. The experimentally determined mode shapes and damping coefficients with corresponding natural frequencies are shown on the following figure (Figure 5.24).

ϕ_1^{exp} - Torsional / X; f_1^{exp} = 0,337 ± 0,011 Hz; ζ_1^{exp} = 3,83 ± 1,23

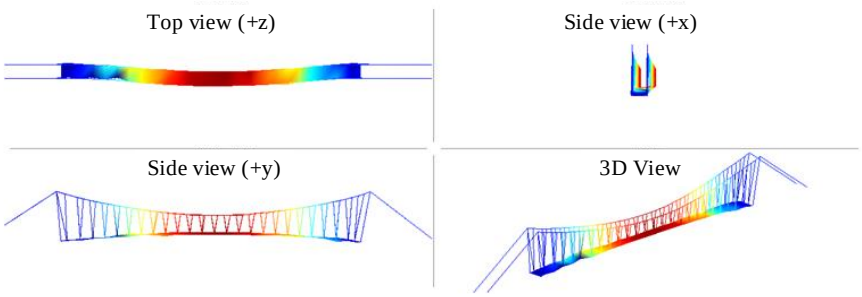

ϕ_2^{exp} - Vertical / Z; f_2^{exp}= 0,587 ± 0,06 Hz; ζ_2^{exp}= 1,746 ± 0,95

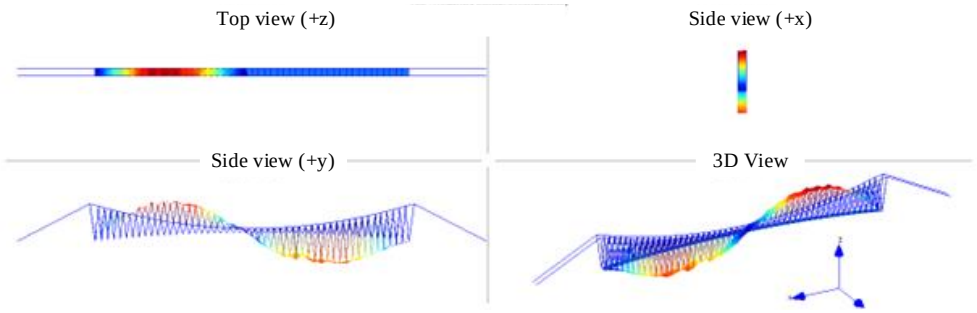

ϕ_3^{exp} - Torsional; f_3^{exp}= 0,850± 0,011 Hz; ζ_3^{exp}1,216 ± 0,52

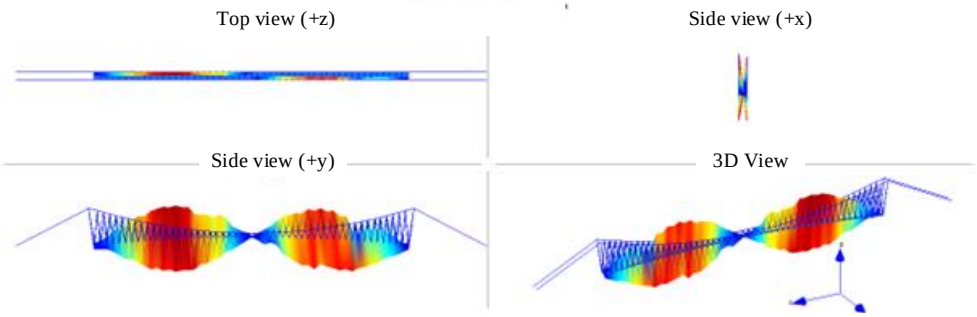

ϕ_4^{exp} – Torsional; f_4^{exp}= 1,013± 0,07 Hz; ζ_4^{exp}= 1,10± 0,23

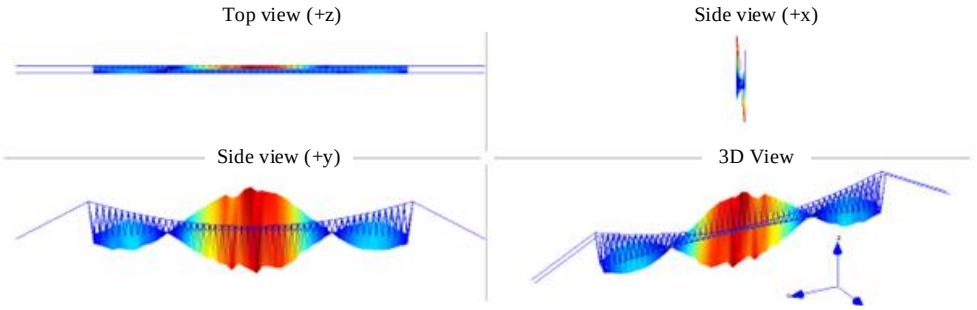

ϕ_5^{exp} – Vertical/ Z; f_5^{exp}= 1,150 ± 0,06 Hz; ζ_5^{exp}0,77 ± 0,18

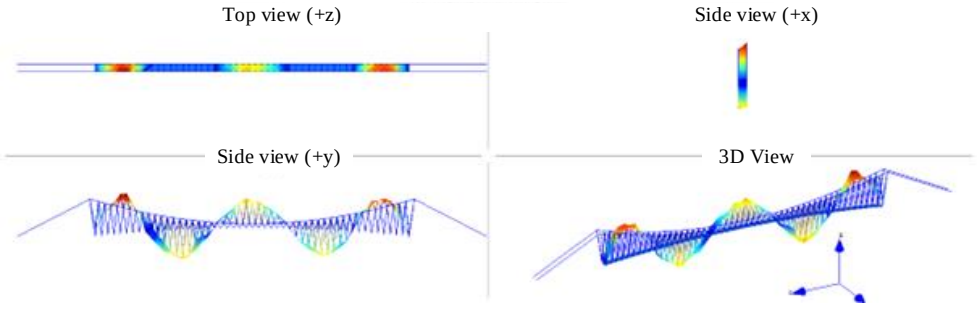

ϕ_6^{exp} – Vertical/ Z; f_6^{exp}= 1,400 ± 0,05 Hz; ζ_6^{exp}= 0,82 ± 0,24

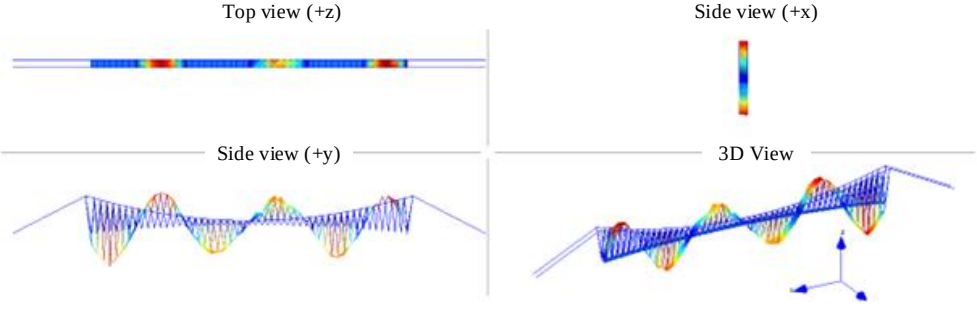

ϕ_7^{exp} – Vertical/ Z; f_7^{exp}= 1,663 ± 0,05 Hz; ζ_7^{exp}= 0,728 ± 0,40

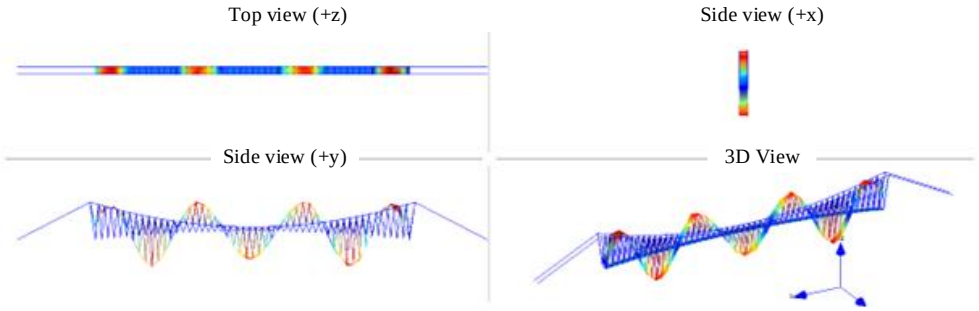

ϕ_8^{exp} – Vertical/ Z; f_8^{exp}= 1,925 ± 0,01 Hz; ζ_8^{exp}0,638 ± 0,19

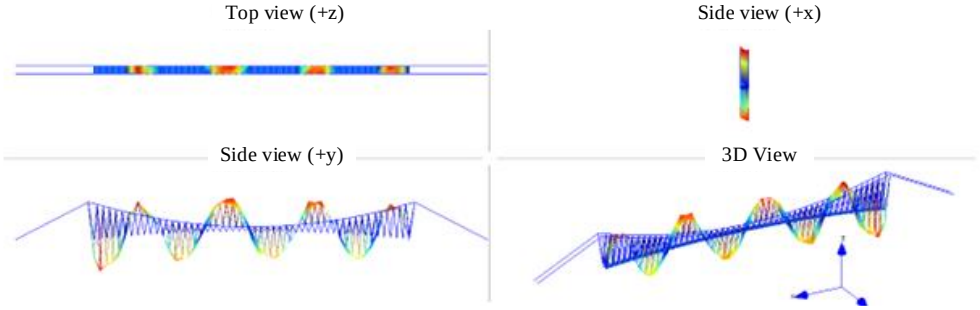

ϕ_9^{exp} – Vertical/ Z; f_9^{exp}= 2,188 ± 0,08 Hz; ζ_9^{exp}0,643 ± 0,16

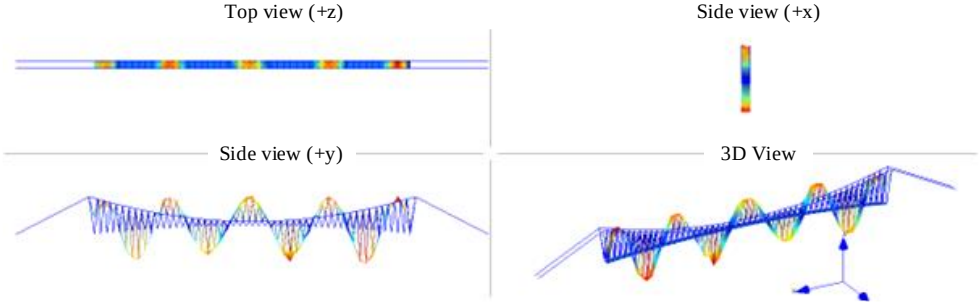

ϕ_{10}^{exp} – Vertical/ Z; f_{10}^{exp}2,475 ± 0,03 Hz; ζ_{10}^{exp}= 0,682 ± 0,34

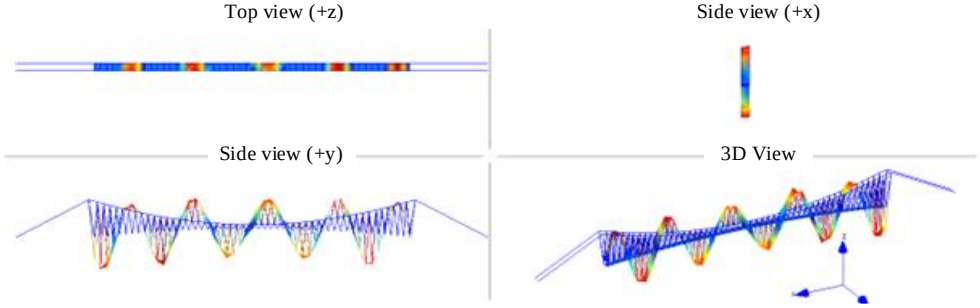

ϕ_{11}^{exp} – Vertical/ Z; f_{11}^{exp}= 2,737 ± 0,02 Hz; ζ_{11}^{exp}0,535 ± 0,18

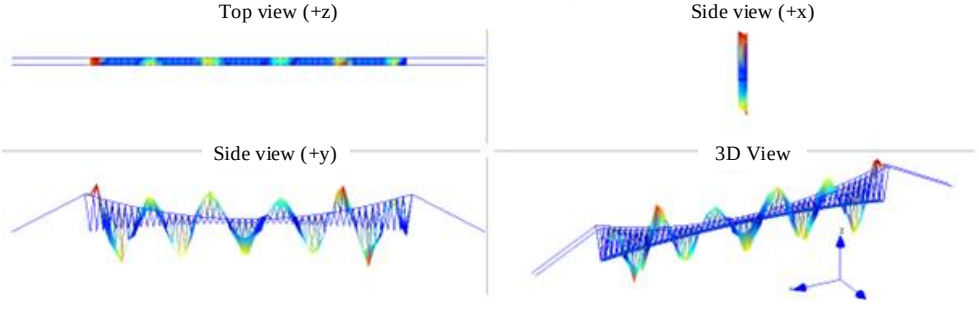

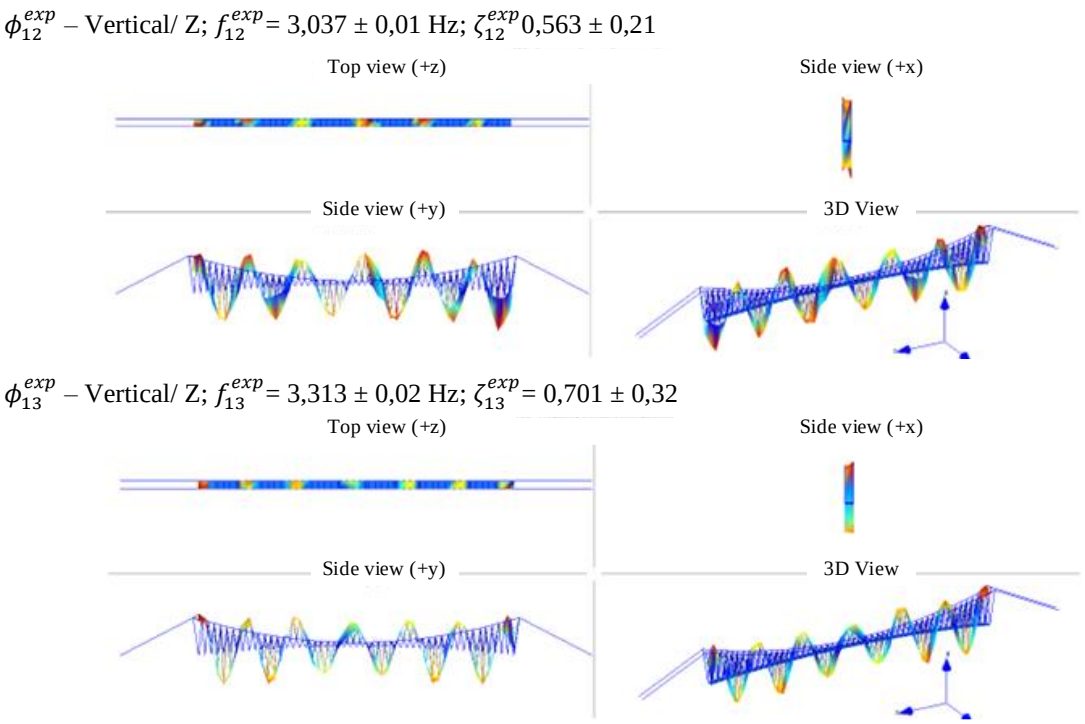

Figure 5.24. Experimentally determined natural frequency $\left(f_t^{exp}\right)$ and damping ratio $\left(\zeta_t^{exp}\right)$ of the pedestrian suspension bridge over Drava River with their standard deviation $\left(\sigma_t^f, \sigma_t^\zeta\right)$ for corresponding mode shapes $\left(\phi_t^{exp}\right)$ $(t = 1, \ldots, 13)$

Determined dynamic parameters describe the global behaviour of the bridge and represent the initial measured values. The presented results reflect the expected mode shapes with respect to the suspension bridge system and they can serve as a basis for the future measurements (natural frequencies, damping coefficients and mode shapes). The obtained dynamic parameters serve as a basis for developing/updating a numerical model to better represent the actual behaviour of the structure. The next chapter describes the comparison between the bridge behaviour predicted by numerical model and its actual behaviour, sensitivity analysis and the updating of the bridge model based on the conventional and GT FEMU method.

5.4. Comparison between the initial FE model and experimental test results

In order to assess both the performance of the initial numerical model and the accuracy of the predictions of the numerical model, a comparative analysis was performed. Herein the correlation analysis was performed based on the Eq. (1.1.) for natural frequencies, and the Eq. (1.3.) for the mode shapes. The results of the analysis are shown in the following Table 5-8. The results of the comparison indicate that the deviations for the initial numerical model are not significant, but it is still possible to achieve better matches with the experimentally obtained results in order to reduce the relative difference of natural frequencies and increase the value of the MAC coefficient.

Table 5-8. Comparison of the pedestrian suspension bridge modal parameters predicted by initial numerical model and its actual modal parameters based on the absolute relative difference between the natural frequency values (Δf_t) and modal assurance criterion MAC $(\phi_t^{exp}, \phi_t^{num})$

Mode shape t	f_t^{num} [Hz]	f_t^{exp} [Hz]	$\lvert\Delta f_t\rvert$ [%]	MAC $(\phi_t^{exp},\phi_t^{num})$ [/]
1	0,335	0,337	-0,46	0,995
2	0,569	0,587	-3,07	0,967
3	0,862	0,850	-0,94	0,960
4	1,170	1,013	15,50	0,937
5	1,142	1,150	-0,70	0,845
6	1,530	1,400	9,29	0,870
7	1,694	1,663	1,86	0,964
8	1,791	1,925	-6,96	0,802
9	2,061	2,188	-5,80	0,974
10	2,582	2,475	4,34	0,967
11	2,661	2,737	-2,78	0,953
12	2,881	3,037	-5,14	0,812
13	3,197	3,313	-3,50	0,943

Therefore, it is necessary to improve the numerical model via FEMU. This was performed using the previously presented EGT model and, in addition, using the conventional MO optimization method based on the computation of the Pareto front and the subsequent decision-making problem. The accuracy of the solution and required computational time have been compared to confirm the possibility of using the EGT model for FEMU of real case complex structures and their high fidelity FEM.

5.5. Sensitivity analysis and sorting variables in strategy space

The selection of the most relevant updating parameter is performed using the sensitivity analysis (Figure 5.25.). As selection criteria, the ratio between the modal strain energy associated with the physical parameters and the overall MSE of the structure has been considered. In the first step of the selecting process the 17 parameters were selected. Following the sensitivity analysis instead of the initially selected 17 parameters, 13 of them were selected as updating parameters $\theta = [\theta_1, \theta_2, \theta_3, \theta_4, \theta_5, \theta_6, \theta_7, \theta_8, \theta_9, \theta_{10}, \theta_{11}, \theta_{12}, \theta_{13}]$: (1) Young modulus of elasticity of the concrete elements - θ_1 [GPa]; (2) stiffness of the connection between the concrete elements - θ_2 [N/m]; (3) down main cable tension force - θ_3 [N]; (4) hangers tension force - $\theta_4 - \theta_7$ [N]; (5) Young modulus of elasticity of handrail elements - θ_8 [GPa]; (6) stiffness of the connection between the slabs and down main cables - θ_9 [N/m,]; (7) upper main cable tension force – $\theta_{10} - \theta_{13}$ [N].

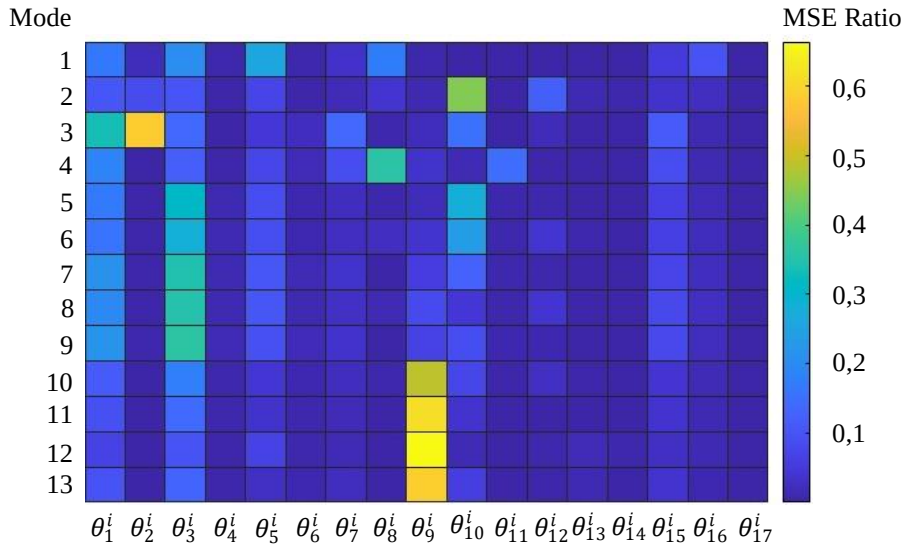

Figure 5.25. Results of sensitivity analysis performed on the pedestrian suspension bridge finite element model for initial selected $(\theta^i_{1,\dots,17})$ 17 updating parameters

To constraint defined optimization problem and guarantee the physical meaning of the updated numerical model, a search domain has been included by defining the lower $\boldsymbol{\theta^l}$ and upper $\boldsymbol{\theta^u}$ bounds of the updating parameters. The constraints are defined as follows: $\boldsymbol{\theta^l} =$ [0,9 0,1 0,8 0,6 0,6 0,6 0,6 0,9 0,8 0,8 0,8 0,8 0,8 0,8] and $\boldsymbol{\theta^u} =$ [1,1 2,0 1,2 1,1 1,25 1,5 1,8 1,1 1,2 1,2 1,2 1,2 1,2]. After performing the selection of the updating parameters, the strategy space of each natural frequency and mode shape residuals was defined using the sorting partition method described in the Chapter 3.3.2. According to the sorting method each of residuals was optimized. The impact index, space distance and space moment were computed (Table 5-9.). According to the mentioned partition rules the strategy space of natural frequency, $S_f = \{\theta_1, \theta_2, \theta_3, \theta_4, \theta_5, \theta_6, \theta_7, \theta_8, \theta_9, \theta_{11}\}$ and mode shape, $S_{ms} = \{\theta_{10}, \theta_{12}, \theta_{13}\}$ are determined.

Table 5-9. Impact index, space distance, space moment, threshold moment and ranking of all design variables

Design variable	$f_1(\boldsymbol{\theta})$			$f_2(\boldsymbol{\theta})$			Mo(j)
	Δ(j,1)	d(j,1)	ranking	Δ(j,2)	d(j,2)	ranking	
θ_1	0,167079	0,011533	2	0,001949	0,988467	13	0,001927
θ_2	0,028306	0,007474	3	0,000213	0,992526	12	0,000212
θ_3	0,127159	0,007487	8	0,000959	0,992513	10	0,000952
θ_4	0,102041	0,021810	7	0,002275	0,978190	4	0,002225
θ_5	0,085072	0,007828	6	0,000671	0,992172	1	0,000666
θ_6	0,056743	0,007762	9	0,000444	0,992238	11	0,000440
θ_7	0,042473	0,007749	5	0,000332	0,992251	5	0,000329
θ_8	0,162901	0,007690	11	0,001262	0,992310	9	0,001253
θ_9	0,130084	0,007826	1	0,001026	0,992174	6	0,001018
θ_{10}	0,098141	0,909880	4	0,990868	0,090120	7	0,089297
θ_{11}	0,081163	0,008112	10	0,000664	0,991888	8	0,000658
θ_{12}	0,054809	0,955779	12	1,184629	0,044221	3	0,052385
θ_{13}	0,041264	0,963481	13	1,088681	0,036519	2	0,039757

5.6. Solution of the MO FEMU problem based on the conventional optimization methods

To validate the computational efficiency of the EGT model when it deals with the high fidelity FEMU MO optimization problem of complex structures such as suspension bridge, the FEMU is also performed using the conventional method. As in the previous example of the laboratory bridge model, HS algorithm has been considered. The updating process was performed linking a FE analysis software Ansys [229] with a mathematical software Matlab [234].

The following parameters of the HS algorithm were established to perform the optimization process: population size PS=50; maximum number of iterations I_{max}=100; objective function tolerance $t_{of} = 1 \cdot 10^{-4}$; new population size $P_{s,new} = 25$; harmony memory pitch adjustment $HMCR = 0{,}9$ and pitch adjusting rate $PAR = 0{,}3$. As a result of this updating problem, Figure 5.26. shows the Pareto front of the two residuals of the MO function. Additionally, the "knee point" of this Pareto front (the most balanced solution) has been included in the Figure. Therefore, the "knee point" is computed as $\theta^{*}_{\text{MOA\_HS\_PSBO}}$= [0,9972 0,8895 1,0588 1,0308 0,8689 1,2284 1,7534 1,0462 0,8199 1,0219 1,0084 0,9966 1,0013] that correspond to the following values of the numerical model properties [32,908 $8{,}89 \cdot 10^{9}$ 1376,447 36,124 30,450 43,050 61,450 219,706 $1{,}721 \cdot 10^{11}$ 4864,130 4799,919 4744 4768,383]. The computational time required by HS to solve the MO FEMU problem of the pedestrian suspension bridge was recorded $t_{HS\_PSBO} = 192\,783$ s.

5.7. Solution of the FEMU problem based on the EGT model

Based on its successful application, its efficiency and accuracy of solution when it is used to solve the MO FEMU problem of simple laboratory bridge model, the EGT model is selected for solving the complex pedestrian suspension bridge high-fidelity FEMU problem.

The selected game model starts from the initial strategy $\theta^{0}_{initial\_PSBO} =$ [1 1 1 1 1 1 1 1 1 1 1 1 1] while the calculation is performed until the convergence criterion is met (Eq. (3.12.)) which is set at $\xi = 0{,}001$. The degree of the cooperation was established as w_{11}= w_{22}= w_{12}= w_{21}= 0,5 according to the rules described in the Chapter 3.3.4. In the round in which the convergence criterion is reached, the optimal values of updating parameters reach the following values: $\theta^{*}_{\text{EGT\_PSBO}}$= [0,9997 0,8917 1,0585 1,0305 0,8686 1,2281 1,7530 1,0488 0,8219 1,0221 1,0086 0,9969 1,0020] that correspond to the following values of the numerical model properties [32,991 $8{,}92 \cdot 10^{9}$ 1376,103 36,115 30,442 43,039 61,434 220,256 $1{,}732 \cdot 10^{11}$ 4865,346 4801,119 4745,186 4769,575]. The computational

time required by EGT model to solve the MO FEMU problem of the pedestrian suspension bridge was $t_{EGT\_PSBO} = 89\ 758$ s.

5.8. Discussion of the results

To compare the results obtained using conventional and proposed method for MO FEMU optimization problems, the following comparison criteria have been considered: the accuracy of the solution and the computational time required to compute the FEMU solution. The Figure 5.26. graphically compares the optimal solution provided by conventional and EGT model based method.

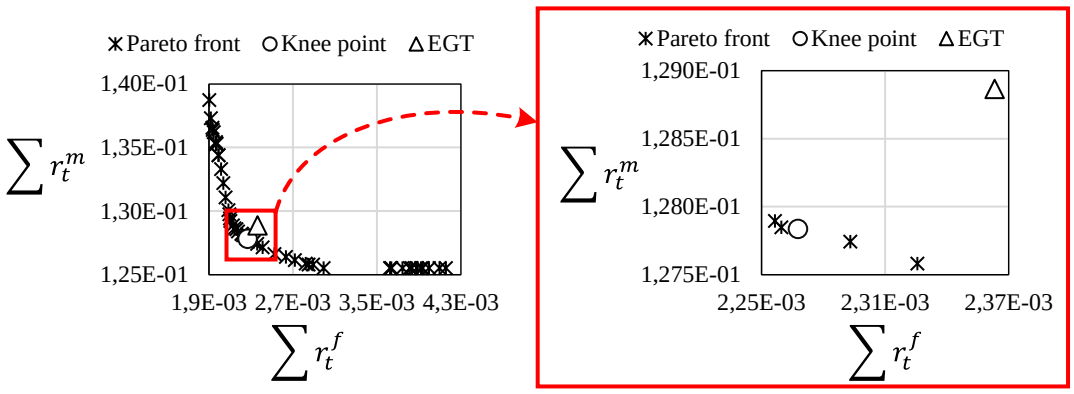

Figure 5.26. Comparison of the "knee" point obtained based on the Pareto front (conventional method) with the position of the optimal solution obtained using EGT model

According to the comparison illustrates on the Figure 5.26. it can be remarked that the solution provided by EGT model is near the best optimal solution provided by the conventional method, i.e., "knee point" as it was shown in the example of the laboratory bridge model. On the other hand, the computational time required to perform the updating process according to two methods can me computed as: $t_{HS\_PSBO} = 192\ 780$ s for conventional HS method and $t_{EGT\_PSBO} = 89\ 758$ s for EGT model. Based on those two comparison criteria, it can be concluded that the GT method can be successfully used to solve the MO FEMU optimization problem of high-fidelity model of complex type of structures such as the suspension bridge according to ML method. The computational time required to perform the high fidelity FEMU process can be significantly reduced without compromising the solution. This is ensured by direct determination of the "knee point" by using the GT without the necessity of computing the complete Pareto optimal front.

The numerical natural frequencies and associated mode shapes MAC factor of the updated model of the suspension bridge considering the updated physical parameters provided by the conventional HS and GT method are shown in the Table 5-10.

Table 5-10. Correlation between experimental and updated natural frequencies and mode shapes using conventional HS optimization and EGT model

Mode t	f_t^{exp} [Hz]	$f_t^{upd,HS}$ [Hz]	Δf_t^{HS} [%]	$f_t^{upd,EGT}$ [Hz]	Δf_t^{EGT} [%]	$MAC\ _t^{HS}$ [/]	$MAC\ _t^{EGT}$ [/]
1	0,337	0,335	-0,46	0,334	-0,89	0,997	0,997
2	0,587	0,596	1,53	0,597	1,70	0,985	0,984
3	0,850	0,842	-0,94	0,843	-0,82	0,984	0,984
4	1,013	1,025	1,18	1,025	1,18	0,954	0,954
5	1,150	1,142	-0,70	1,141	-0,78	0,986	0,987
6	1,400	1,386	-1,01	1,384	-1,14	0,982	0,982
7	1,663	1,634	-1,74	1,635	-1,68	0,957	0,957
8	1,925	1,896	-1,51	1,898	-1,40	0,972	0,971
9	2,188	2,215	1,23	2,223	1,60	0,996	0,996
10	2,475	2,427	-1,94	2,425	-2,02	0,987	0,987
11	2,737	2,692	-1,64	2,692	-1,64	0,993	0,993
12	3,037	3,054	0,56	3,042	0,16	0,964	0,964
13	3,313	3,258	-1,65	3,269	-1,33	0,993	0,992

The good performance of the solution provided by the GT method when it is implemented for solving the MO FEMU optimization problem of high-fidelity model of complex structures is illustrated in Table 5-10. Both the relative differences and the MAC factors provided by the EGT method are similar to the ones obtained by the conventional optimization algorithm when the high fidelity FEMU problem is considered.

Chapter 6. Conclusion and future research

In this work, the feasibility of using game theory as a computational tool to improve the resolution of the updating problem based on the maximum likelihood method has been analysed in detail. obtained from this research work as summarized in Section 6.1, while Section 6.2. discusses recommendations for future research to solve the outstanding problems.

6.1. Conclusions

This research presents the possibility of solving the updating problem of complex civil engineering structures (bridges) using a deterministic approach based on the implementation of game theory as computational tool to solve the maximum likelihood FEMU problem. The FEMU problem can be formulated, according to the maximum likelihood method, as an optimization problem. Thus, the implementation of game theory to cope with the updating problem involves the transformation of this optimization problem into a game theory problem. In this manner, the effectiveness (accuracy and computational time) of different game models (NCGT, CGT, EGT) in this research are implemented to solve the updating problem and results have been compared. Two different levels of case studies complexity have been compared: a simple finite element model corresponding to a laboratory footbridge and a high fidelity finite element model corresponding a complex suspension bridge. Additionally, the performance of the proposal has been compared with the results obtained via the implementation of a conventional finite element model updating based on the maximum likelihood method. Harmony search has been considered in this case as nature-inspired computational algorithm. Thus, the following conclusion can be drawn as result of this research study:

- GT has proven to be a valuable mathematical discipline that is used to successfully solve various types of optimisation problems in other scientific fields (economy, politics, etc). In this research GT has been adopted as computational tool to improve the performance of solving the FEMU optimization problems. It has been proven that by defining the objective functions as a utility function, imitating their residuals (natural frequencies

and mode shapes) as players, and finding an equilibrium point for which the solution is satisfactory to both players. The hypothesis of the research was validated through two case studies (simple and high-fidelity), and it was proven by reducing the computational time without compromising the accuracy of the solution.

- The transformation of the SO FEMU optimization problem is based on defining the so-called weighted objective function instead of the classical one. This procedure does not require performing the analysis of the influence of different weights on the optimization results. The weight values are incorporated in the optimization process which contributes that the SO problem can be successfully solved using GT, resulting in a lower computational time and in satisfying the solution which is near the optimal solution obtained by the conventional method. When comparing the conventional and GT SO optimization problems the absolute relative difference of natural frequencies are slightly higher while MAC factors are the same. The obtained solution is still optimal and lies within solution domain. The previous conclusion confirms the first part of the hypothesis. The part related to the better agreement with the results of experimental tests is unconfirmed when comparing the GT and conventional method.
- The MO FEMU problem is formulated as a GT problem considering the three different game models: NCGT, CGT and EGT. The key technology of the transforming the MO problem into the game problem is to divide the variable set (updating parameters) into each player's (natural frequency, mode shape) strategy space using the sorting partition method. Considering three different game models: NCGT, CGT, and EGT it was concluded that the solution provided by using GT and conventional MO approach is similar. It was remarked that the solution provided by EGT model is better than the other GT models as it is located the nearest to the "knee point". On the other hand, the CGT model required lower computational time to perform the updating process. When considering both criteria (computational time and accuracy) it can be concluded based on the analysis performed on the laboratory bridge case study, that the EGT model is the best option to perform the MO FEMU. Comparing the absolute relative difference of the natural frequencies and MAC factors, it can be concluded that the implementation of GT to solve the MO optimization problem leads to almost the same values obtained using the conventional methods. The difference between the dynamic parameters of the structure predicted by numerical model and the experimentally obtained is not reduced. As previously discussed, first part of the hypothesis is confirmed, while the part related

to the better agreement with the results of experimental test is unconfirmed.

- When comparing the GT solution of FEMU based on the SO function (CGT model) and MO function (EGT model) it can be concluded that the solution obtained by EGT is the nearest to the best optimal solution ("knee point") obtained using the conventional method. This conclusion is based on the results obtained by performing the FEMU of the simple laboratory bridge case study. The solution obtained using the SO approach and CGT model is an optimal, but not the best solution (it lies on the Pareto optimal front, but far from the best "knee point"). This indicates and confirms that combining the maximum likelihood MO approach with the EGT model is the best option to perform the FEMU of the simple model such as the laboratory bridge observed in this research.
- The application of the proposed MO FEMU optimization using the EGT model to solve a high fidelity FEMU optimization problem of pedestrian suspension bridges confirms its application. Moreover, when the obtained results are compared with those of the conventional method, it can be observed that EGT model leads to a solution that is very close to the best optimal solution, resulting in a significantly shorter computational time. Furthermore, the absolute relative differences of the natural frequencies and the MAC factors are almost the same when using the EGT model and the conventional method. This conclusion is based on the analysis of the results obtained from the FEMU of pedestrian suspension bridge, which is characterized by low stiffness and, consequently, low frequencies and large displacements due to environmental effects.

6.2. Recommendations for future research

Although the application of game theory in the finite element model updating through use of the deterministic maximum likelihood method has proven to be very efficient in this research, based on the results of its application in solving simple and high fidelity FEMU optimization problems, it is possible to formulate some principle issues that can be addressed in further research

- Despite the high efficiency shown by the GT method, there is a possible inconsistency in the solution due to the isolation of each player in its local domain. To tackle this problem, further studies need to improve the accuracy of the GT method by using a domain decomposition method.
- The solution obtained using SO optimization and GT results in a lower calculation time

but gives a solution that is far away from the best optimal solution ("knee point"). For further research it is recommend to improve the performance of the SO optimization based on GT in order to improve the accuracy of the solution.

- Since GT has proven to be very efficient in handling the simple and high-fidelity FEMU optimization problem under the deterministic maximum likelihood method, it is recommended for further studies to include the uncertainties in the updating process using the stochastic FEMU methods combining it with the advantages of GT.
- The objective function is usually defined as the residuals between the experimental and numerical modal properties. For this purpose, the natural frequencies and the associated mode shapes are considered. To define the mode shape residual, the Modal Assurance Criterion is normally used. For practical application, this criterion has a clear disadvantage, namely the large difference between the values of the two residuals mentioned. To overcome this limitation, it is recommended that further research be conducted to analyse the influence of different mode shape residual criteria on the updating of civil engineering structures.
- In this research FEMU is based on ambient data. When considering such a FEMU, the low amplitude of the associated vibrations typically leads to the identification of a small number of linear elastic properties what represent the problem for nonlinear systems. For this reason, it is recommended that the application of the GT and the aforementioned procedure be tested taking into account the results of static tests or other data and information about the actual structural behaviour (SHM, strain, displacements, etc).
- Due to the availability of data on the force values in the individual hangers, it is recommended for future research to include another residual value in the objective function. This residual will cover the difference between the numerically predicted force values in the hangers and the values determined based on the measured natural frequencies. It should be noted that this creates a system of underdetermined equations whose solution requires the use of other types of FEMU methods suitable for such problems.

A. Appendix

A. I. Measured natural frequencies and calculated force value in hangers

Table A. I. 1. Geometrical characteristics (length-L, A_{cs}-cross section) measured natural frequencies $\left(f_{H,no}^{exp}\right.$; no= 1,2, …102) and calculated force values $\left(F_{H,no}^{exp}\right.$; no= 1,2, …102) in hangers for measuring 10/2022

Hanger no	L(m)	A_{cs} [mm^2]		$f_{H,no}^{exp}$[Hz]		$F_{H,no}^{exp}$[kN]	
		Downstream	Upstream	Downstream	Upstream	Downstream	Upstream
1	27,30	238,35	211,85	2,04	2,64	23,66	39,62
2	24,60	238,35	211,85	2,70	2,53	33,65	29,54
3	24,10	238,35	211,85	2,70	3,03	32,29	40,67
4	22,90	238,35	211,85	2,92	2,81	34,10	31,58
5	22,50	238,35	211,85	2,86	2,86	31,58	31,58
6	21,30	211,85	238,35	2,81	3,14	24,29	30,32
7	20,90	238,35	238,35	2,97	2,86	29,39	27,25
8	19,70	238,35	211,85	3,25	3,30	31,27	32,23
9	19,30	238,35	211,85	2,97	3,58	25,06	36,41
10	18,20	238,35	238,35	3,91	3,52	38,62	31,30
11	17,90	238,35	238,35	3,47	3,25	29,43	25,81
12	16,80	238,35	211,85	3,91	3,74	32,91	30,11
13	16,50	238,35	211,85	3,80	4,29	29,98	38,22
14	15,50	238,35	238,35	5,18	4,46	49,17	36,45
15	15,10	238,35	238,35	4,07	3,91	28,81	26,59
16	14,20	238,35	238,35	4,35	4,18	29,10	26,87
17	13,90	211,85	238,35	4,90	4,62	31,45	27,96
18	13,00	238,35	211,85	4,79	5,51	29,57	39,13
19	12,70	211,85	238,35	5,62	4,57	34,53	22,84
20	11,90	238,35	211,85	5,78	5,78	36,08	36,08
21	11,60	238,35	238,35	5,18	5,73	27,54	33,70
22	10,80	238,35	238,35	5,95	5,73	31,50	29,21
23	10,60	238,35	238,35	6,06	5,84	31,47	29,23
24	9,80	238,35	211,85	6,77	7,10	33,57	36,93
25	9,60	238,35	238,35	6,33	6,22	28,17	27,19
26	8,90	238,35	238,35	7,76	7,49	36,38	33,89
27	8,70	238,35	238,35	7,21	7,43	30,01	31,87
28	8,10	238,35	238,35	8,75	8,86	38,31	39,28
29	7,90	238,35	238,35	7,60	7,21	27,49	24,75
30	7,30	238,35	238,35	10,52	9,85	44,98	39,44
31	7,10	238,35	238,35	7,93	8,86	24,18	30,18
32	6,60	238,35	238,35	11,07	11,67	40,71	45,25
33	6,50	238,35	238,35	8,81	9,19	25,01	27,22
34	6,00	238,35	238,35	13,49	12,55	49,97	43,25

Hanger no	L(m)	A_{cs} [mm^2]		$f_{H,no}^{exp}$[Hz]		$F_{H,no}^{exp}$[kN]	
		Downstream	Upstream	Downstream	Upstream	Downstream	Upstream
35	5,90	238,35	238,35	10,90	10,24	31,54	27,84
36	5,50	238,35	238,35	14,37	15,64	47,64	56,44
37	5,30	238,35	238,35	11,29	11,89	27,31	30,29
38	5,00	238,35	238,35	16,30	16,41	50,66	51,35
39	4,90	238,35	238,35	11,78	14,15	25,41	36,67
40	4,60	238,35	238,35	18,44	18,39	54,88	54,58
41	4,50	238,35	238,35	14,09	12,88	30,66	25,62
42	4,30	238,35	238,35	20,31	20,20	58,17	57,54
43	4,20	238,35	238,35	16,46	15,80	36,45	33,59
44	4,00	238,35	238,35	22,74	23,12	63,11	65,23
45	4,00	238,35	238,35	15,36	18,55	28,79	41,99
46	3,80	238,35	238,35	24,99	24,17	68,78	64,34
47	3,80	238,35	238,35	17,62	18,39	34,19	37,25
48	3,70	238,35	238,35	22,74	24,44	53,99	62,37
49	3,70	238,35	238,35	22,41	18,61	52,44	36,16
50	3,60	238,35	238,35	26,81	26,87	71,05	71,37
51	3,60	238,35	238,35	22,68	22,08	50,85	48,19
52	3,60	238,35	238,35	21,36	24,39	45,10	58,80
53	3,60	211,85	238,35	24,06	23,67	50,86	49,22
54	3,70	238,35	238,35	22,35	18,00	52,16	33,83
55	3,70	238,35	238,35	24,83	26,32	64,38	72,33
56	3,80	238,35	238,35	17,62	23,56	34,19	61,13
57	3,80	238,35	238,35	24,11	19,98	64,02	43,97
58	4,00	238,35	238,35	15,97	18,44	31,12	41,50
59	4,00	211,85	238,35	20,81	18,66	46,97	37,77
60	4,20	238,35	238,35	14,97	17,67	30,15	42,01
61	4,30	238,35	238,35	20,04	20,04	56,64	56,64
62	4,50	238,35	211,85	14,53	18,83	32,61	54,76
63	4,60	211,85	211,85	16,24	19,76	37,83	56,01
64	4,90	238,35	211,85	11,73	14,64	25,20	39,25
65	5,00	211,85	211,85	17,18	14,04	50,02	33,41
66	5,30	211,85	238,35	12,06	12,61	27,70	30,28
67	5,50	238,35	238,35	13,65	14,70	42,99	49,86
68	5,90	238,35	238,35	10,79	11,40	30,91	34,50
69	6,00	238,35	238,35	13,27	11,62	48,35	37,07
70	6,50	238,35	238,35	9,80	10,30	30,95	34,19
71	6,60	238,35	238,35	11,78	10,68	46,10	37,90
72	7,10	238,35	238,35	8,15	9,19	25,54	32,47
73	7,30	238,35	238,35	10,07	9,63	41,22	37,69
74	7,90	238,35	238,35	7,49	7,87	26,70	29,48
75	8,10	238,35	238,35	7,98	8,59	31,87	36,93
76	8,70	238,35	238,35	7,10	7,16	29,10	29,60
77	8,90	238,35	238,35	8,09	7,43	39,54	33,35
78	9,60	238,35	238,35	6,44	6,61	29,15	30,71
79	9,80	211,85	238,35	7,54	6,55	37,01	27,93
80	10,60	238,35	238,35	5,06	5,95	21,94	30,34
81	10,80	238,35	238,35	6,39	6,33	36,33	35,65
82	11,60	238,35	238,35	4,95	5,12	25,15	26,90
83	11,90	238,35	238,35	6,00	5,62	38,88	34,11
84	12,70	238,35	238,35	4,51	4,90	25,02	29,54

Hanger no	L(m)	A_{cs} [mm^2]		$f_{H,no}^{exp}$[Hz]		$F_{H,no}^{exp}$[kN]	
		Downstream	Upstream	Downstream	Upstream	Downstream	Upstream
85	13,00	238,35	238,35	5,23	4,95	35,26	31,58
86	13,90	238,35	211,85	3,96	5,01	23,11	36,99
87	14,20	211,85	211,85	5,23	4,95	37,39	33,49
88	15,10	211,85	211,85	3,80	4,62	22,32	32,99
89	15,50	238,35	211,85	5,51	5,18	55,63	49,17
90	16,50	238,35	238,35	1,65	2,15	5,65	9,60
91	16,80	238,35	238,35	4,24	4,13	38,70	36,72
92	17,90	238,35	238,35	3,52	3,52	30,28	30,28
93	18,20	238,35	238,35	3,14	3,63	24,91	33,29
94	19,30	211,85	238,35	3,52	3,14	31,29	24,90
95	19,70	238,35	238,35	3,30	3,36	32,23	33,42
96	20,90	238,35	211,85	3,03	3,03	30,59	30,59
97	21,30	238,35	238,35	3,03	3,03	31,77	31,77
98	22,50	238,35	238,35	2,64	2,42	26,91	22,61
99	22,90	211,85	238,35	2,97	3,41	31,36	41,34
100	24,10	238,35	238,35	2,92	2,81	37,77	34,98
101	24,60	211,85	211,85	2,59	2,75	27,52	31,03
102	27,30	238,35	238,35	2,31	2,31	30,33	30,33

A. II. The force values in the upper main cables

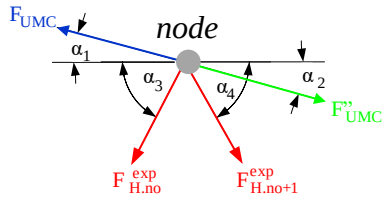

Figure A.II.1. Equilibrium of the force values in upper main cable nodes

Table A. II. 1. The force values in the upper main cable on the downstream bridge side

Node	Angle				cos (angle)				Force			
	α_1	α_2	α_3	α_4	α_1	α_2	α_3	α_4	FUMC	$F_{H,3}^{exp}$	$F_{H,2}^{exp}$	F''_{UMC}
1	18,13	17,56	84,99	85,77	0,950	0,953	0,087	0,074	4919,82	32,29	33,65	4904,76
									FUMC	$F_{H,5}^{exp}$	$F_{H,4}^{exp}$	F''_{UMC}'
2	17,56	16,47	84,75	85,05	0,953	0,959	0,092	0,086	4904,76	31,58	34,10	4876,73
									FUMC	$F_{H,7}^{exp}$	$F_{H,6}^{exp}$	F''_{UMC}'
3	16,47	15,89	84,50	84,65	0,959	0,962	0,096	0,093	4876,73	29,39	24,29	4861,97
									FUMC	$F_{H,9}^{exp}$	$F_{H,8}^{exp}$	F''_{UMC}'
4	15,89	15,27	84,04	84,30	0,962	0,965	0,104	0,099	4861,97	25,06	31,27	4848,04
									FUMC	$F_{H,11}^{exp}$	$F_{H,10}^{exp}$	F''_{UMC}'
5	15,27	14,46	83,50	83,78	0,965	0,968	0,113	0,108	4848,04	29,43	38,62	4831,2
									FUMC	$F_{H,13}^{exp}$	$F_{H,12}^{exp}$	F''_{UMC}'
6	14,46	14,01	83,00	93,27	0,968	0,970	0,122	-0,057	4831,2	29,98	32,91	4827,44
									FUMC	$F_{H,15}^{exp}$	$F_{H,14}^{exp}$	F''_{UMC}'
7	14,01	13,10	82,30	82,60	0,970	0,974	0,134	0,129	4827,44	28,81	49,17	4811,89
									FUMC	$F_{H,17}^{exp}$	$F_{H,16}^{exp}$	F''_{UMC}'
8	13,10	12,37	81,74	81,85	0,974	0,977	0,144	0,142	4811,89	31,45	29,10	4797,85
									FUMC	$F_{H,19}^{exp}$	$F_{H,18}^{exp}$	F''_{UMC}'
9	12,37	11,67	80,98	81,09	0,977	0,979	0,157	0,155	4797,85	34,53	29,57	4784,69
									FUMC	$F_{H,21}^{exp}$	$F_{H,20}^{exp}$	F''_{UMC}'
10	11,67	10,99	80,11	80,28	0,979	0,982	0,172	0,169	4784,69	27,54	36,08	4774,82
									FUMC	$F_{H,23}^{exp}$	$F_{H,22}^{exp}$	F''_{UMC}'
11	10,99	10,44	79,04	79,34	0,982	0,983	0,190	0,185	4774,82	31,47	31,50	4766,31
									FUMC	$F_{H,25}^{exp}$	$F_{H,24}^{exp}$	F''_{UMC}'
12	10,44	9,57	77,86	78,16	0,983	0,986	0,210	0,205	4766,31	28,17	33,57	4754,98
									FUMC	$F_{H,27}^{exp}$	$F_{H,26}^{exp}$	F''_{UMC}'
13	9,57	8,90	76,61	76,91	0,986	0,988	0,232	0,226	4754,98	30,01	36,38	4747,5
									FUMC	$F_{H,29}^{exp}$	$F_{H,28}^{exp}$	F''_{UMC}'
14	8,90	8,05	75,19	76,00	0,988	0,990	0,256	0,242	4747,5	27,49	38,31	4740,19
									FUMC	$F_{H,31}^{exp}$	$F_{H,30}^{exp}$	F''_{UMC}'
15	8,05	7,47	73,13	73,83	0,990	0,992	0,290	0,278	4740,19	24,18	44,98	4740,05
									FUMC	$F_{H,33}^{exp}$	$F_{H,32}^{exp}$	F''_{UMC}'
16	7,47	6,75	71,82	72,49	0,992	0,993	0,312	0,301	4740,05	25,01	40,71	4737,88
									FUMC	$F_{H,35}^{exp}$	$F_{H,34}^{exp}$	F''_{UMC}'
17	6,75	5,92	69,47	70,18	0,993	0,995	0,351	0,339	4737,88	31,54	49,97	4737,15
									FUMC	$F_{H,37}^{exp}$	$F_{H,36}^{exp}$	F''_{UMC}'
18	5,92	5,20	67,58	67,78	0,995	0,996	0,381	0,378	4737,15	27,31	47,64	4739,22
									FUMC	$F_{H,39}^{exp}$	$F_{H,38}^{exp}$	F''_{UMC}'

19	5,20	4,45	65,71	65,32	0,996	0,997	0,411	0,418	4739,22	25,41	50,66	4744,22
									F_{UMC}	$F_{H,41}^{exp}$	$F_{H,40}^{exp}$	F_{UMC}''
20	4,45	3,76	63,50	62,98	0,997	0,998	0,446	0,454	4744,22	30,66	54,88	4750,69
									F_{UMC}	$F_{H,43}^{exp}$	$F_{H,42}^{exp}$	F_{UMC}''
21	3,76	3,04	61,27	60,91	0,998	0,999	0,481	0,486	4750,69	36,45	58,17	4757,43
									F_{UMC}	$F_{H,45}^{exp}$	$F_{H,44}^{exp}$	F_{UMC}''
22	3,04	2,32	68,82	59,01	0,999	0,999	0,361	0,515	4757,43	28,79	63,11	4762,59
									F_{UMC}	$F_{H,47}^{exp}$	$F_{H,46}^{exp}$	F_{UMC}''
23	2,32	1,60	57,45	56,88	0,999	1,000	0,538	0,546	4762,59	34,19	68,78	4778,89
									F_{UMC}	$F_{H,49}^{exp}$	$F_{H,48}^{exp}$	F_{UMC}''
24	1,60	0,70	54,50	55,51	1,000	1,000	0,581	0,566	4778,89	52,44	53,99	4779,04
									F_{UMC}	$F_{H,51}^{exp}$	$F_{H,50}^{exp}$	F_{UMC}''
25	0,70	0,11	55,62	55,07	1,000	1,000	0,565	0,573	4779,04	46,62	65,85	4789,19
									F_{UMC}	$F_{H,53}^{exp}$	$F_{H,52}^{exp}$	F_{UMC}''
26	0,11	0,73	55,63	54,55	1,000	1,000	0,565	0,580	4789,19	50,86	46,63	4786,4
									F_{UMC}	$F_{H,55}^{exp}$	$F_{H,54}^{exp}$	F_{UMC}''
27	0,73	1,58	56,38	55,41	1,000	1,000	0,554	0,568	4786,4	64,38	52,16	4780,14
									F_{UMC}	$F_{H,57}^{exp}$	$F_{H,56}^{exp}$	F_{UMC}''
28	1,58	2,31	57,49	56,73	1,000	0,999	0,537	0,549	4780,14	64,02	34,19	4765,45
									F_{UMC}	$F_{H,59}^{exp}$	$F_{H,58}^{exp}$	F_{UMC}''
29	2,31	3,19	59,22	57,03	0,999	0,998	0,512	0,544	4765,45	46,97	31,12	4759,32
									F_{UMC}	$F_{H,61}^{exp}$	$F_{H,60}^{exp}$	F_{UMC}''
30	3,19	3,75	62,63	60,47	0,998	0,998	0,460	0,493	4759,32	56,64	30,15	4748,09
									F_{UMC}	$F_{H,63}^{exp}$	$F_{H,62}^{exp}$	F_{UMC}''
31	3,75	4,46	63,57	61,01	0,998	0,997	0,445	0,485	4748,09	37,83	32,61	4748,47
									F_{UMC}	$F_{H,65}^{exp}$	$F_{H,64}^{exp}$	F_{UMC}''
32	4,46	5,18	67,35	63,28	0,997	0,996	0,385	0,450	4748,47	50,02	25,20	4740,67
									F_{UMC}	$F_{H,67}^{exp}$	$F_{H,66}^{exp}$	F_{UMC}''
33	5,18	5,92	69,69	67,21	0,996	0,995	0,347	0,387	4740,67	42,99	27,70	4739,5
									F_{UMC}	$F_{H,69}^{exp}$	$F_{H,68}^{exp}$	F_{UMC}''
34	5,92	6,62	70,34	69,28	0,995	0,993	0,336	0,354	4739,5	48,35	30,91	4739,11
									F_{UMC}	$F_{H,71}^{exp}$	$F_{H,70}^{exp}$	F_{UMC}''
35	6,62	7,47	72,31	71,29	0,993	0,992	0,304	0,321	4739,11	46,10	30,95	4742,41
									F_{UMC}	$F_{H,73}^{exp}$	$F_{H,72}^{exp}$	F_{UMC}''
36	7,47	8,04	74,10	73,25	0,992	0,990	0,274	0,288	4742,41	41,22	25,54	4743,87
									F_{UMC}	$F_{H,75}^{exp}$	$F_{H,74}^{exp}$	F_{UMC}''
37	8,04	8,89	75,59	74,86	0,990	0,988	0,249	0,261	4743,87	31,87	26,70	4752,67
									F_{UMC}	$F_{H,77}^{exp}$	$F_{H,76}^{exp}$	F_{UMC}''
38	8,89	9,59	76,96	76,22	0,988	0,986	0,226	0,238	4752,67	39,54	29,10	4759,3
									F_{UMC}	$F_{H,79}^{exp}$	$F_{H,78}^{exp}$	F_{UMC}''
39	9,59	10,15	78,41	77,51	0,986	0,984	0,201	0,216	4759,3	37,01	29,15	4765,13
									F_{UMC}	$F_{H,81}^{exp}$	$F_{H,80}^{exp}$	F_{UMC}''
40	10,15	11,00	79,50	89,63	0,984	0,982	0,182	0,006	4765,13	36,33	21,94	4782,16
									F_{UMC}	$F_{H,83}^{exp}$	$F_{H,82}^{exp}$	F_{UMC}''
41	11,00	11,71	80,52	79,61	0,982	0,979	0,165	0,180	4782,16	38,88	25,15	4791,23
									F_{UMC}	$F_{H,85}^{exp}$	$F_{H,84}^{exp}$	F_{UMC}''
42	11,71	12,49	81,47	80,55	0,979	0,976	0,148	0,164	4791,23	35,26	25,02	4803,04
									F_{UMC}	$F_{H,87}^{exp}$	$F_{H,86}^{exp}$	F_{UMC}''
43	12,49	13,00	82,17	81,31	0,976	0,974	0,136	0,151	4803,04	37,39	23,11	4810,14

									FUMC	$F_{H,89}^{exp}$	$F_{H,88}^{exp}$	F_{UMC}'''
44	13,00	13,96	82,79	82,18	0,974	0,970	0,125	0,136	4810,14	55,63	22,32	4824,72
									FUMC	$F_{H,91}^{exp}$	$F_{H,90}^{exp}$	F_{UMC}'''
45	13,96	14,59	83,40	82,69	0,970	0,968	0,115	0,127	4824,72	38,70	5,65	4833,65
									FUMC	$F_{H,93}^{exp}$	$F_{H,92}^{exp}$	F_{UMC}'''
46	14,59	15,10	83,99	93,27	0,968	0,965	0,105	-0,057	4833,65	24,91	30,28	4849,89
									FUMC	$F_{H,95}^{exp}$	$F_{H,94}^{exp}$	F_{UMC}'''
47	15,10	15,88	84,44	83,77	0,965	0,962	0,097	0,109	4849,89	32,23	31,29	4867,66
									FUMC	$F_{H,97}^{exp}$	$F_{H,96}^{exp}$	F_{UMC}'''
48	15,88	16,61	84,84	84,29	0,962	0,958	0,090	0,100	4867,66	31,77	30,59	4885,5
									FUMC	$F_{H,99}^{exp}$	$F_{H,98}^{exp}$	F_{UMC}'''
49	16,61	17,30	85,21	84,80	0,958	0,955	0,083	0,091	4885,5	31,36	26,91	4902,9
									FUMC	$F_{H,100}^{exp}$	$F_{H,101}^{exp}$	F_{UMC}'''
50	17,30	17,51	85,55	85,35	0,955	0,954	0,078	0,081	4902,9	27,52	37,77	4909,06

Table A. II. 2. The force values in the upper main cable on the upstream bridge side

Node	Angle				cos (angle)				Force			
	α_1	α_2	α_3	α_4	α_1	α_2	α_3	α_4	FUMC	$F_{H,3}^{exp}$	$F_{H,2}^{exp}$	F_{UMC}''
1	18,33	17,30	85,00	85,82	0,949	0,955	0,087	0,073	4925,62	36,15	26,26	4896,93
									FUMC	$F_{H,5}^{exp}$	$F_{H,4}^{exp}$	F_{UMC}'''
2	17,30	16,48	84,57	85,28	0,955	0,959	0,095	0,082	4896,93	28,07	28,07	4875,98
									FUMC	$F_{H,7}^{exp}$	$F_{H,6}^{exp}$	F_{UMC}'''
3	16,48	15,91	84,26	84,99	0,959	0,962	0,100	0,087	4875,98	27,25	34,12	4863,06
									FUMC	$F_{H,9}^{exp}$	$F_{H,8}^{exp}$	F_{UMC}'''
4	15,91	15,24	83,70	84,69	0,962	0,965	0,110	0,092	4863,06	32,36	28,65	4847,34
									FUMC	$F_{H,11}^{exp}$	$F_{H,10}^{exp}$	F_{UMC}'''
5	15,24	14,57	83,06	84,20	0,965	0,968	0,121	0,101	4847,34	25,81	31,30	4833,56
									FUMC	$F_{H,13}^{exp}$	$F_{H,12}^{exp}$	F_{UMC}'''
6	14,57	13,76	82,52	83,29	0,968	0,971	0,130	0,117	4833,56	33,97	26,76	4815,72
									FUMC	$F_{H,15}^{exp}$	$F_{H,14}^{exp}$	F_{UMC}'''
7	13,76	13,19	82,28	82,68	0,971	0,974	0,134	0,127	4815,72	26,59	36,45	4805,75
									FUMC	$F_{H,17}^{exp}$	$F_{H,16}^{exp}$	F_{UMC}'''
8	13,19	12,39	81,59	82,01	0,974	0,977	0,146	0,139	4805,75	31,45	26,87	4790,22
									FUMC	$F_{H,19}^{exp}$	$F_{H,18}^{exp}$	F_{UMC}'''
9	12,39	11,82	80,84	81,24	0,977	0,979	0,159	0,152	4790,22	25,69	34,78	4781,56
									FUMC	$F_{H,21}^{exp}$	$F_{H,20}^{exp}$	F_{UMC}'''
10	11,82	11,01	79,91	90,40	0,979	0,982	0,175	-0,007	4781,56	33,70	32,07	4773,98
									FUMC	$F_{H,23}^{exp}$	$F_{H,22}^{exp}$	F_{UMC}'''
11	11,01	10,30	78,95	79,56	0,982	0,984	0,192	0,181	4773,98	29,23	29,21	4763,08
									FUMC	$F_{H,25}^{exp}$	$F_{H,24}^{exp}$	F_{UMC}'''
12	10,30	9,57	77,62	79,13	0,984	0,986	0,214	0,189	4763,08	27,19	32,82	4754,43
									FUMC	$F_{H,27}^{exp}$	$F_{H,26}^{exp}$	F_{UMC}'''
13	9,57	8,89	75,56	77,23	0,986	0,988	0,249	0,221	4754,43	31,87	33,89	4746,67
									FUMC	$F_{H,29}^{exp}$	$F_{H,28}^{exp}$	F_{UMC}'''
14	8,89	8,19	74,87	75,65	0,988	0,990	0,261	0,248	4746,67	24,75	39,28	4742,18
									FUMC	$F_{H,31}^{exp}$	$F_{H,30}^{exp}$	F_{UMC}'''
15	8,19	7,46	73,38	73,81	0,990	0,992	0,286	0,279	4742,18	30,18	39,44	4736,75
									FUMC	$F_{H,33}^{exp}$	$F_{H,32}^{exp}$	F_{UMC}'''
16	7,46	6,63	71,80	72,02	0,992	0,993	0,312	0,309	4736,75	27,22	45,25	4734,12

									F_{UMC}	$F_{H,35}^{exp}$	$F_{H,34}^{exp}$	F_{UMC}'''
17	6,63	6,04	69,96	70,09	0,993	0,994	0,343	0,340	4734,12	27,84	43,25	4734,02
									F_{UMC}	$F_{H,37}^{exp}$	$F_{H,36}^{exp}$	F_{UMC}'''
18	6,04	5,17	67,51	68,10	0,994	0,996	0,382	0,373	4734,02	30,29	56,44	4737,32
									F_{UMC}	$F_{H,39}^{exp}$	$F_{H,38}^{exp}$	F_{UMC}'''
19	5,17	4,62	65,40	66,20	0,996	0,997	0,416	0,404	4737,32	36,67	51,35	4740,01
									F_{UMC}	$F_{H,41}^{exp}$	$F_{H,40}^{exp}$	F_{UMC}'''
20	4,62	3,75	62,61	64,46	0,997	0,998	0,460	0,431	4740,01	25,62	54,58	4748,89
									F_{UMC}	$F_{H,43}^{exp}$	$F_{H,42}^{exp}$	F_{UMC}'''
21	3,75	3,03	59,91	61,37	0,998	0,999	0,501	0,479	4748,89	33,59	57,54	4758,11
									F_{UMC}	$F_{H,45}^{exp}$	$F_{H,44}^{exp}$	F_{UMC}'''
22	3,03	2,31	58,63	57,52	0,999	0,999	0,521	0,537	4758,11	41,99	65,23	4766,75
									F_{UMC}	$F_{H,47}^{exp}$	$F_{H,46}^{exp}$	F_{UMC}'''
23	2,31	1,43	59,44	55,09	0,999	1,000	0,508	0,572	4766,75	37,25	64,34	4775,75
									F_{UMC}	$F_{H,49}^{exp}$	$F_{H,48}^{exp}$	F_{UMC}'''
24	1,43	0,87	57,87	54,14	1,000	1,000	0,532	0,586	4775,75	36,16	62,37	4786,80
									F_{UMC}	$F_{H,51}^{exp}$	$F_{H,50}^{exp}$	F_{UMC}'''
25	0,87	0,01	57,66	53,77	1,000	1,000	0,535	0,591	4786,80	47,11	70,01	4795,85
									F_{UMC}	$F_{H,53}^{exp}$	$F_{H,52}^{exp}$	F_{UMC}'''
26	0,01	0,87	56,91	55,35	1,000	1,000	0,546	0,569	4795,85	55,38	58,80	4797,03
									F_{UMC}	$F_{H,55}^{exp}$	$F_{H,54}^{exp}$	F_{UMC}'''
27	0,87	1,44	55,99	56,07	1,000	1,000	0,559	0,558	4797,03	72,33	33,83	4776,54
									F_{UMC}	$F_{H,57}^{exp}$	$F_{H,56}^{exp}$	F_{UMC}'''
28	1,44	2,33	57,16	57,01	1,000	0,999	0,542	0,545	4776,54	43,97	61,13	4788,18
									F_{UMC}	$F_{H,59}^{exp}$	$F_{H,58}^{exp}$	F_{UMC}'''
29	2,33	2,89	59,08	59,06	0,999	0,999	0,514	0,514	4788,18	42,49	41,50	4789,80
									F_{UMC}	$F_{H,61}^{exp}$	$F_{H,60}^{exp}$	F_{UMC}'''
30	2,89	3,90	60,76	60,59	0,999	0,998	0,488	0,491	4789,80	56,64	42,01	4787,49
									F_{UMC}	$F_{H,63}^{exp}$	$F_{H,62}^{exp}$	F_{UMC}'''
31	3,90	4,45	63,34	62,79	0,998	0,997	0,449	0,457	4787,49	56,01	48,67	4787,11
									F_{UMC}	$F_{H,65}^{exp}$	$F_{H,64}^{exp}$	F_{UMC}'''
32	4,45	5,04	65,52	65,83	0,997	0,996	0,414	0,409	4787,11	33,41	34,89	4791,99
									F_{UMC}	$F_{H,67}^{exp}$	$F_{H,66}^{exp}$	F_{UMC}'''
33	5,04	6,05	67,27	67,26	0,996	0,994	0,386	0,387	4791,99	49,86	34,07	4794,00
									F_{UMC}	$F_{H,69}^{exp}$	$F_{H,68}^{exp}$	F_{UMC}'''
34	6,05	6,63	70,15	69,66	0,994	0,993	0,340	0,348	4794,00	37,07	34,50	4798,19
									F_{UMC}	$F_{H,71}^{exp}$	$F_{H,70}^{exp}$	F_{UMC}'''
35	6,63	7,31	72,01	71,43	0,993	0,992	0,309	0,318	4798,19	37,90	34,19	4803,69
									F_{UMC}	$F_{H,73}^{exp}$	$F_{H,72}^{exp}$	F_{UMC}'''
36	7,31	8,06	74,00	73,24	0,992	0,990	0,276	0,288	4803,69	37,69	32,47	4810,17
									F_{UMC}	$F_{H,75}^{exp}$	$F_{H,74}^{exp}$	F_{UMC}'''
37	8,06	8,98	75,49	75,06	0,990	0,988	0,251	0,258	4810,17	36,93	29,48	4819,66
									F_{UMC}	$F_{H,77}^{exp}$	$F_{H,76}^{exp}$	F_{UMC}'''
38	8,98	9,61	76,78	76,49	0,988	0,986	0,229	0,234	4819,66	33,35	29,60	4827,32
									F_{UMC}	$F_{H,79}^{exp}$	$F_{H,78}^{exp}$	F_{UMC}'''
39	9,61	10,17	78,23	77,68	0,986	0,984	0,204	0,213	4827,32	31,43	30,71	4835,02
									F_{UMC}	$F_{H,81}^{exp}$	$F_{H,80}^{exp}$	F_{UMC}'''
40	10,17	10,96	79,44	78,77	0,984	0,982	0,183	0,195	4835,02	35,65	30,34	4846,13
									F_{UMC}	$F_{H,83}^{exp}$	$F_{H,82}^{exp}$	F_{UMC}'''

41	10,96	11,70	80,36	79,84	0,982	0,979	0,168	0,176	4846,13	34,11	26,90	4857,09
									F_{UMC}	$F_{H,85}^{exp}$	$F_{H,84}^{exp}$	F''_{UMC}'
42	11,70	12,37	81,25	80,70	0,979	0,977	0,152	0,162	4857,09	31,58	29,54	4868,62
									F_{UMC}	$F_{H,87}^{exp}$	$F_{H,86}^{exp}$	F''_{UMC}'
43	12,37	13,15	82,02	81,48	0,977	0,974	0,139	0,148	4868,62	33,49	32,88	4883,31
									F_{UMC}	$F_{H,89}^{exp}$	$F_{H,88}^{exp}$	F''_{UMC}'
44	13,15	13,75	82,67	82,28	0,974	0,971	0,128	0,134	4883,31	43,70	32,99	4893,78
									F_{UMC}	$F_{H,91}^{exp}$	$F_{H,90}^{exp}$	F''_{UMC}'
45	13,75	14,61	83,29	82,87	0,971	0,968	0,117	0,124	4893,78	36,72	0,00	4907,64
									F_{UMC}	$F_{H,93}^{exp}$	$F_{H,92}^{exp}$	F''_{UMC}'
46	14,61	15,24	83,78	83,42	0,968	0,965	0,108	0,115	4907,64	33,29	30,28	4921,63
									F_{UMC}	$F_{H,95}^{exp}$	$F_{H,94}^{exp}$	F''_{UMC}'
47	15,24	15,91	84,32	83,91	0,965	0,962	0,099	0,106	4921,63	33,42	28,01	4936,68
									F_{UMC}	$F_{H,97}^{exp}$	$F_{H,96}^{exp}$	F''_{UMC}'
48	15,91	16,62	84,73	84,33	0,962	0,958	0,092	0,099	4936,68	31,77	27,19	4954,04
									F_{UMC}	$F_{H,99}^{exp}$	$F_{H,98}^{exp}$	F''_{UMC}'
49	16,62	17,41	85,19	84,88	0,958	0,954	0,084	0,089	4954,04	46,51	22,61	4972,68
									F_{UMC}	$F_{H,100}^{exp}$	$F_{H,101}^{exp}$	F''_{UMC}'
50	17,41	17,42	85,47	85,50	0,954	0,954	0,079	0,079	4972,68	31,03	34,98	4973,26

A. III. Edge slab mode shapes

$f_1^{exp} = 0{,}587\ Hz$

Top view (+z)

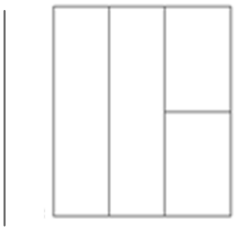

Side view (+x)

Side view (+y)

3D View

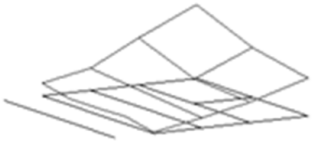

$f_2^{exp} = 0{,}850\ Hz$

Top view (+z)

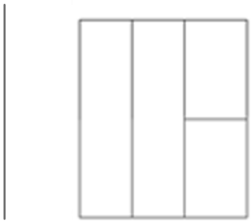

Side view (+x)

Side view (+y)

3D View

$f_3^{exp} = 1{,}013\ Hz$

Top view (+z)

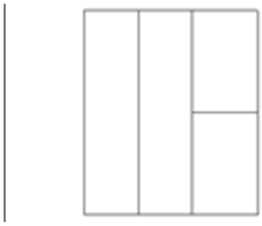

Side view (+x)

Side view (+y)

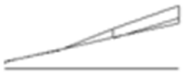

3D View

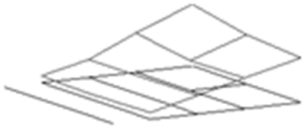

$f_4^{exp} = 1{,}462\ Hz$

Top view (+z)

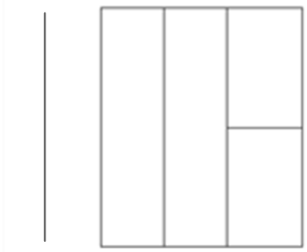

Side view (+x)

Side view (+y)

3D View

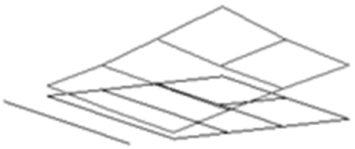

$f_5^{exp} = 1{,}850\ Hz$

Top view (+z)

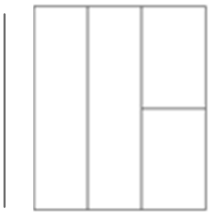

Side view (+x)

Side view (+y)

3D View

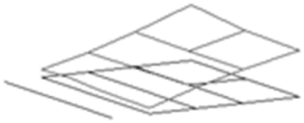

$f_6^{exp} = 2{,}188\ Hz$

Top view (+z)

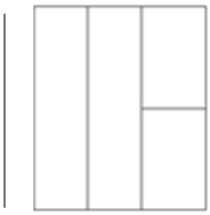

Side view (+x)

Side view (+y)

3D View

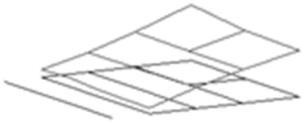

$f_7^{exp} = 2{,}725\ Hz$

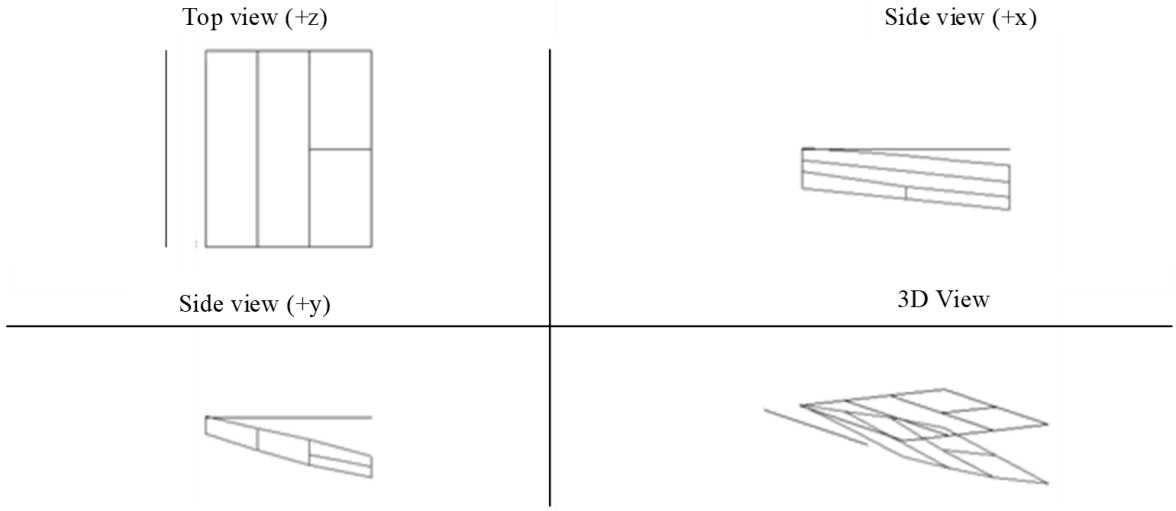

$f_8^{exp} = 3{,}313\ Hz$

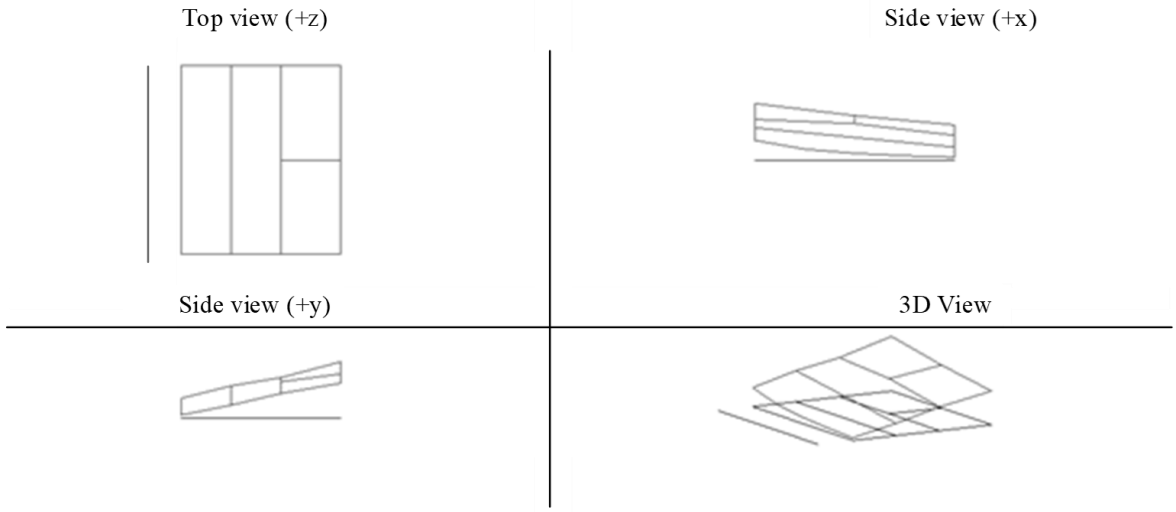

Figure A.III.1. Experimentally determined mode shapes $\left(\phi_t^{exp}\right)$ of the edge slab of pedestrian suspension bridge over Drava River for corresponding natural frequency $\left(f_t^{exp}\right)$ $(t = 1, \ldots, 8)$

A. IV. Span slab mode shapes

$f_1^{exp} = 0{,}587\ Hz$

Top view (+z)	Side view (+x)
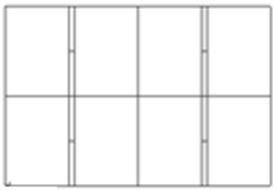	
Side view (+x)	3D View
	

$f_2^{exp} = 0{,}850\ Hz$

Top view (+z)	Side view (+x)
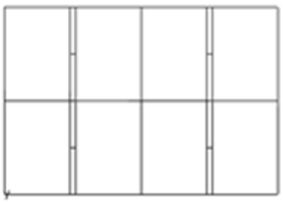	
Side view (+x)	3D View
	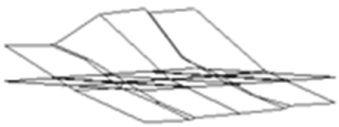

$f_3^{exp} = 1{,}013\ Hz$

Top view (+z)	Side view (+x)
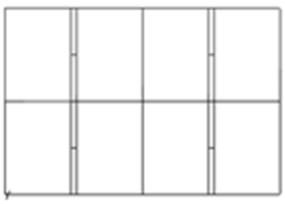	
Side view (+x)	3D View
	

$f_4^{exp} = 1{,}138\ Hz$

Top view (+z)

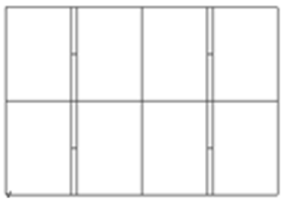

Side view (+x)

Side view (+x)

3D View

$f_5^{exp} = 1{,}400\ Hz$

Top view (+z)

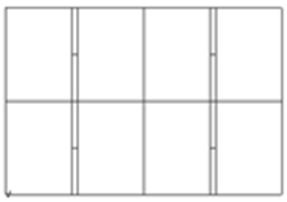

Side view (+x)

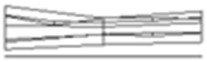

Side view (+x)

3D View

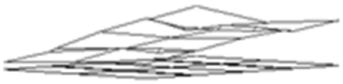

$f_6^{exp} = 1,650\ Hz$

Top view (+z)

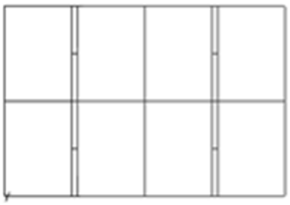

Side view (+x)

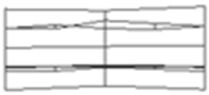

Side view (+x)

3D View

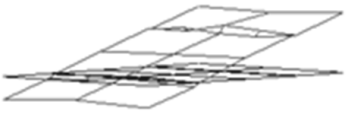

$f_7^{exp} = 2{,}180\ Hz$

Top view (+z)

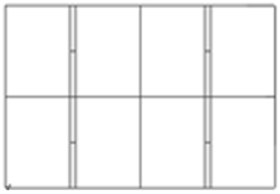

Side view (+x)

Side view (+x)

3D View

$f_8^{exp} = 2{,}475\ Hz$

Top view (+z)

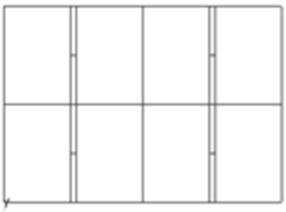

Side view (+x)

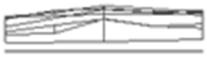

Side view (+x)

3D View

$f_9^{exp} = 2{,}725\ Hz$

Top view (+z)

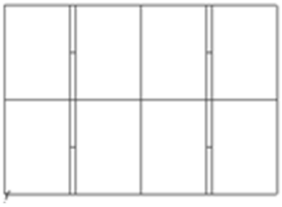

Side view (+x)

Side view (+x)

3D View

$f_{10}^{exp} = 3{,}313Hz$

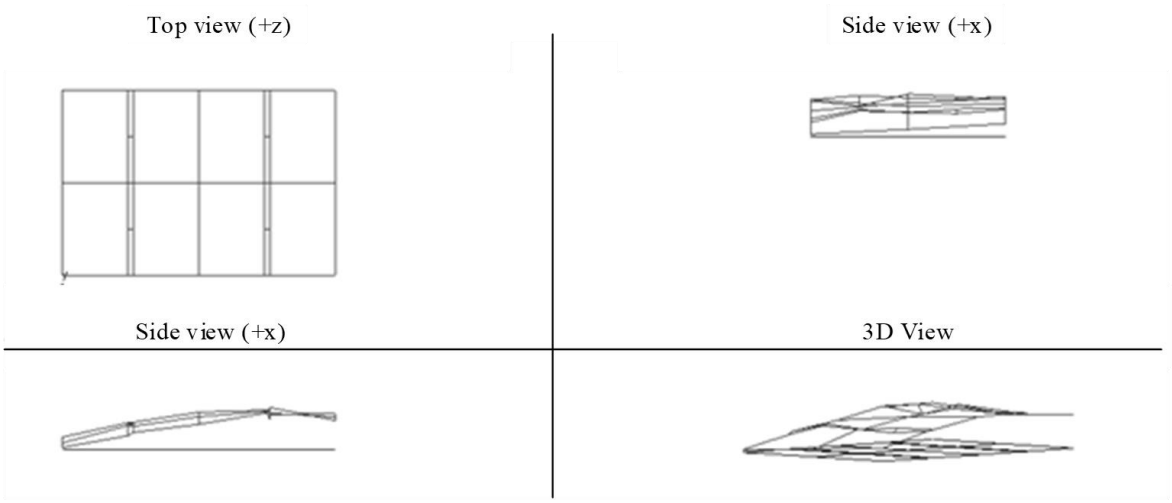

Figure A.IV.1. Experimentally determined mode shapes $\left(\phi_t^{exp}\right)$ of the span slab of pedestrian suspension bridge over Drava River for corresponding natural frequency $\left(f_t^{exp}\right)$ $(t = 1, \ldots, 10)$

References

[1] S. Ereiz, I. Duvnjak, and J. Fernando Jiménez-Alonso, "Structural finite element model updating optimization based on game theory," *Mater. Today Proc.*, Apr. 2022, doi: 10.1016/j.matpr.2022.04.401.

[2] A. Kaveh, *Computational structural analysis and finite element methods*, vol. 9783319029. 2014.

[3] K. J. Bathe, *Finite Element Procedures*, 2nd editio. Massachusetts; USA: Prentice Hall, Pearson Education, 2014.

[4] E. Simoen, G. De Roeck, and G. Lombaert, "Dealing with uncertainty in model updating for damage assessment: A review," *Mech. Syst. Signal Process.*, vol. 56, pp. 123–149, 2015, doi: 10.1016/j.ymssp.2014.11.001.

[5] X. Ye and B. Chen, "Model updating and variability analysis of modal parameters for super high-rise structure," *Concurr. Comput.* , vol. 31, no. 12, pp. 1–11, 2019, doi: 10.1002/cpe.4712.

[6] L. He, E. Reynders, J. H. García-Palacios, G. C. Marano, B. Briseghella, and G. De Roeck, "Wireless-based identification and model updating of a skewed highway bridge for structural health monitoring," *Appl. Sci.*, vol. 10, no. 7, 2020, doi: 10.3390/app10072347.

[7] L. Sun, Y. Li, and W. Zhang, "Experimental Study on Continuous Bridge-Deflection Estimation through Inclination and Strain," *J. Bridg. Eng.*, vol. 25, no. 5, p. 04020020, 2020, doi: 10.1061/(asce)be.1943-5592.0001543.

[8] M. Farshadi, A. Esfandiari, and M. Vahedi, "Structural model updating using incomplete transfer function and modal data," *Struct. Control Heal. Monit.*, vol. 24, no. 7, pp. 1–13, 2017, doi: 10.1002/stc.1932.

[9] L. Sun, Y. Li, W. Zhu, and W. Zhang, "Structural response reconstruction in physical

coordinate from deficient measurements," *Eng. Struct.*, vol. 212, no. March, p. 110484, 2020, doi: 10.1016/j.engstruct.2020.110484.

[10] D. Giagopoulos, A. Arailopoulos, V. Dertimanis, C. Papadimitriou, E. Chatzi, and K. Grompanopoulos, "Structural health monitoring and fatigue damage estimation using vibration measurements and finite element model updating," *Struct. Heal. Monit.*, vol. 18, no. 4, pp. 1189–1206, 2019, doi: 10.1177/1475921718790188.

[11] H.-P. Chen, *Structural health monitoring of large civil engineering structures*, 1st editio. Oxford: John Wiley and Sons Inc., 2018.

[12] T. Marwala, *Finite-element model Updating Using Computational Intelligence Techniques*, 1st editio. London: Springer-Verlag London, 2010.

[13] S. Dhandole and S. V. Modak, "A constrained optimization based method for acoustic finite element model updating of cavities using pressure response," *Appl. Math. Model.*, vol. 36, no. 1, pp. 399–413, 2012, doi: 10.1016/j.apm.2011.07.029.

[14] J. E. Mottershead, M. Link, and M. I. Friswell, "The sensitivity method in finite element model updating: A tutorial," *Mech. Syst. Signal Process.*, vol. 25, no. 7, pp. 2275–2296, 2011, doi: 10.1016/j.ymssp.2010.10.012.

[15] T. Marwala, I. Boulkaibet, and S. Adhikari, *Probabilistic Finite Element Model Updating using Bayesian Statistics. Application to aeronautical and mechanical engineering*, 1st editio. Chichester: John Wiley & Sons, Ltd, 2017.

[16] M. Shahbaznia, M. R. Dehkordi, and A. Mirzaee, "An improved time-domain damage detection method for railway bridges subjected to unknown moving loads," *Period. Polytech. Civ. Eng.*, vol. 64, no. 3, pp. 928–938, 2020, doi: 10.3311/PPci.15813.

[17] S. Schommer, V. H. Nguyen, S. Maas, and A. Zürbes, "Model updating for structural health monitoring using static and dynamic measurements," *Procedia Eng.*, vol. 199, pp. 2146–2153, 2017, doi: 10.1016/j.proeng.2017.09.156.

[18] M. I. Friswell and J. E. Mottershead, *Finite element model updating in structural dynamics*, 1st editio. Waterloo: Springer Netherlands, 1995.

[19] J. E. Mottershead and M. I. Friswell, "Model Updating in structural dynamics," *J. Sound Vib.*, vol. 167, no. 2, pp. 347–375, 1993.

[20] F. Bianconi, G. P. Salachoris, F. Clementi, and S. Lenci, "A genetic algorithm procedure

for the automatic updating of fem based on ambient vibration tests," *Sensors (Switzerland)*, vol. 20, no. 11, pp. 1–17, 2020, doi: 10.3390/s20113315.

[21] S. Ye, X. Lai, I. Bartoli, and A. E. Aktan, "Technology for condition and performance evaluation of highway bridges," *J. Civ. Struct. Heal. Monit.*, vol. 10, no. 4, pp. 573–594, 2020, doi: 10.1007/s13349-020-00403-6.

[22] Y. Feng, Y. Kaya, and C. Ventura, "Finite element model updating of portage Creek Bridge," *Conf. Proc. Soc. Exp. Mech. Ser.*, vol. 2, pp. 247–253, 2016, doi: 10.1007/978-3-319-29751-4_25.

[23] S. Živanović, A. Pavic, and P. Reynolds, "Finite element modelling and updating of a lively footbridge: The complete process," *J. Sound Vib.*, vol. 301, no. 1–2, pp. 126–145, 2007, doi: 10.1016/j.jsv.2006.09.024.

[24] A. C. Altunişik, F. Y. Okur, A. F. Genç, M. Günaydin, and S. Adanur, "Automated Model Updating of Historical Masonry Structures Based on Ambient Vibration Measurements," *J. Perform. Constr. Facil.*, vol. 32, no. 1, Feb. 2018, doi: 10.1061/(ASCE)CF.1943-5509.0001108.

[25] A. C. Altunişik, O. Ş. Karahasan, F. Y. Okur, E. Kalkan, and K. Ozgan, "Finite element model updating and dynamic analysis of a restored historical timber mosque based on ambient vibration tests," *J. Test. Eval.*, vol. 47, no. 5, 2019, doi: 10.1520/JTE20180122.

[26] G. Lacanna, M. Betti, M. Ripepe, and G. Bartoli, "Dynamic Identification as a Tool to Constrain Numerical Models for Structural Analysis of Historical Buildings," *Front. Built Environ.*, vol. 6, no. April, pp. 1–13, 2020, doi: 10.3389/fbuil.2020.00040.

[27] A. C. Altunişik, F. Y. Okur, A. F. Genç, M. Günaydin, and S. Adanur, "Automated Model Updating of Historical Masonry Structures Based on Ambient Vibration Measurements," *J. Perform. Constr. Facil.*, vol. 32, no. 1, p. 04017126, 2018, doi: 10.1061/(asce)cf.1943-5509.0001108.

[28] M. Baruch, "Optimization procedure to correct stiffness and flexibility matrices using vibration tests," *AIAA J.*, vol. 16, no. 11, pp. 1208–1210, 1978, doi: 10.2514/3.61032.

[29] A. Berman and E. J. Nagy, "Improvement of a large analytical model using test data," *AIAA J.*, vol. 21, no. 8, pp. 1168–1173, 1983, doi: 10.2514/3.60140.

[30] M. O. O. Jull, S. D. R. Amador, A. Skafte, J. B. Hansen, M. L. Aenlle, and R. Brincker,

"One-Step FE Model Updating Using Local Correspondence and Mode Shape Orthogonality," *Shock Vib.*, vol. 2019, 2019, doi: 10.1155/2019/1362954.

[31] D. J. Ewins, *Modal Testing: Theory, Practice and Application*, 2nd editio. Hertfordshire: Research Studies Press Ltd, 2000.

[32] S. Sen and B. Bhattacharya, "Eigen structure assignment based finite element model updating," in *International Conference on Computer Aided Engineering (CAE-2013)*, 2013, no. December 2013.

[33] F. Asma, "Finite element model updating using Lagrange interpolation," *Mech. Mech. Eng.*, vol. 23, no. 1, pp. 228–232, 2019, doi: 10.2478/mme-2019-0030.

[34] M. Girardi, C. Padovani, D. Pellegrini, M. Porcelli, and L. Robol, "Finite element model updating for structural applications," *J. Comput. Appl. Math.*, vol. 270, 2020, doi: https://doi.org/10.1016/j.cam.2019.112675.

[35] G. Heo and J. Jeon, "An Experimental Study of Structural Identification of Bridges Using the Kinetic Energy Optimization Technique and the Direct Matrix Updating Method," *Shock Vib.*, vol. 2016, 2016, doi: 10.1155/2016/3287976.

[36] E. L. Eskew and S. Jang, "Remaining stiffness estimation of buildings using incomplete measurements," *Struct. Control Heal. Monit.*, vol. 24, no. 4, pp. 1–11, 2017, doi: 10.1002/stc.1899.

[37] G. National and H. Pillars, *Parameter identification of materials and structures*. Springer Wien New York, 2005.

[38] B. Hofmeister, M. Bruns, and R. Rolfes, "Finite element model updating using deterministic optimisation: A global pattern search approach," *Eng. Struct.*, vol. 195, no. June, pp. 373–381, 2019, doi: 10.1016/j.engstruct.2019.05.047.

[39] T. Marwala, *Finite-element-model updating using computional intelligence techniques: Applications to structural dynamics*, 1st editio. London, England: Springer-Verlag London, 2010.

[40] J. E. Mottershead and M. I. Friswell, "Model updating in structural dynamics: A survey," *J. Sound Vib.*, vol. 167, no. 2, pp. 347–375, 1993, doi: 10.1006/jsvi.1993.1340.

[41] D. S. Jung and C. Y. Kim, "Finite element model updating on small-scale bridge model using the hybrid genetic algorithm," *Struct. Infrastruct. Eng.*, vol. 9, no. 5, pp. 481–495,

2013, doi: 10.1080/15732479.2011.564635.

[42] S. Ereiz, I. Duvnjak, and J. Fernando Jiménez-Alonso, “Review of finite element model updating methods for structural applications,” *Structures*, vol. 41, pp. 684–723, Jul. 2022, doi: 10.1016/j.istruc.2022.05.041.

[43] F. Y. Cheng and D. Li, “Genetic algorithm and Game Theory for multiobjective optimization of seismic structures with/without control,” in *Eleventh World Conference on Earthquake Engineering*, 1996, pp. 1–8.

[44] L. Rachmawati and D. Srinivasan, “Preference incorporation in multi-objective evolutionary algorithms: A survey,” *2006 IEEE Congr. Evol. Comput. CEC 2006*, pp. 962–968, 2006, doi: 10.1109/cec.2006.1688414.

[45] F. Ponsi, E. Bassoli, and L. Vincenzi, “A multi-objective optimization approach for FE model updating based on a selection criterion of the preferred Pareto-optimal solution,” *Structures*, vol. 33, no. April, pp. 916–934, 2021, doi: 10.1016/j.istruc.2021.04.084.

[46] J. Branke, K. Deb, H. Dierolf, and M. Osswald, “Finding knees in multi-objective optimization,” *Lect. Notes Comput. Sci.*, no. December, pp. 722–731, 2004, doi: 10.1007/978-3-540-30217-9_73.

[47] Z. Wang and G. P. Rangaiah, “Application and Analysis of Methods for Selecting an Optimal Solution from the Pareto-Optimal Front obtained by Multiobjective Optimization,” *Ind. Eng. Chem. Res.*, vol. 56, no. 2, pp. 560–574, 2017, doi: 10.1021/acs.iecr.6b03453.

[48] S. S. Jin, S. Cho, H. J. Jung, J. J. Lee, and C. B. Yun, “A new multi-objective approach to finite element model updating,” *J. Sound Vib.*, vol. 333, no. 11, pp. 2323–2338, 2014, doi: 10.1016/j.jsv.2014.01.015.

[49] I. Das, “On characterizing the ‘knee’ of the Pareto curve based on normal-boundary intersection,” *Struct. Optim.*, vol. 18, no. 2–3, pp. 107–115, 1999, doi: 10.1007/bf01195985.

[50] T. Furukawa, S. Yoshimura, and Y. Mimura, “A human-like optimization method for constrained parametric design,” *Inverse Probl. Eng. Mech. IV*, vol. 2003, no. Isip, pp. 147–156, 2003, doi: 10.1016/B978-008044268-6/50020-X.

[51] K. Christodoulou, E. Ntotsios, C. Papadimitriou, and P. Panetsos, “Structural model

updating and prediction variability using Pareto optimal models," *Comput. Methods Appl. Mech. Eng.*, vol. 198, no. 1, pp. 138–149, 2008, doi: 10.1016/j.cma.2008.04.010.

[52] I. Y. Kim and O. L. De Weck, "Adaptive weighted-sum method for bi-objective optimization: Pareto front generation," *Struct. Multidiscip. Optim.*, vol. 29, no. 2, pp. 149–158, 2005, doi: 10.1007/s00158-004-0465-1.

[53] D. Y. Kparib, S. B. Twum, and D. K. Boah, "A Min-Max Strategy to Aid Decision Making in a Bi-Objective Discrete Optimization Problem Using an Improved Ant Colony Algorithm," *Am. J. Oper. Res.*, vol. 09, no. 04, pp. 161–174, 2019, doi: 10.4236/ajor.2019.94010.

[54] S. Stoilova, "An integrated multi-criteria and multi-objective optimization approach for establishing the transport plan of intercity trains," *Sustain.*, vol. 12, no. 2, 2020, doi: 10.3390/su12020687.

[55] X.-S. Yang, *Nature-Inspired Optimization Algorithms*, 1st editio., vol. 118. London, England: Elsevier, 2014.

[56] M. Zarepisheh and P. M. Pardalos, "An equivalent transformation of multi-objective optimization problems," *Ann. Oper. Res.*, vol. 249, no. 1–2, pp. 5–15, 2017, doi: 10.1007/s10479-014-1782-4.

[57] R. T. Marler and J. S. Arora, "Function-transformation methods for multi-objective optimization," *Eng. Optim.*, vol. 37, no. 6, pp. 551–570, 2005, doi: 10.1080/03052150500114289.

[58] J. Chi and Y. Liu, "Multi-objective genetic algorithm based on game theory and its application," *Proc. 2nd Int. Conf. Electron. Mech. Eng. Inf. Technol. EMEIT 2012*, pp. 2341–2344, 2012, doi: 10.2991/emeit.2012.520.

[59] S. Das, A. Abraham, and A. Konar, *Particle swarm optimization and differential evolution algorithms: Technical analysis, applications and hybridization perspectives*, vol. 116, no. May 2014. 2008.

[60] Z. W. Geem and J. H. Kim, "A new heuristic optimization algorithm: Harmony search," *A new heuristic Optim. algorithm Harmon. search*, vol. 76, pp. 60–68, 2001, doi: 10.1177/003754970107600201.

[61] S. Kirkpatrick, C. D. Gelatt, and M. P. Vecchi, "Optimization by simulated annealing,"

Science (80-.)., vol. 220, no. 4598, pp. 671–680, 1983, doi: 10.1126/science.220.4598.671.

[62] J. Naranjo-Pérez, M. Infantes, J. Fernando Jiménez-Alonso, and A. Sáez, "A collaborative machine learning-optimization algorithm to improve the finite element model updating of civil engineering structures," *Eng. Struct.*, vol. 225, 2020, doi: 10.1016/j.engstruct.2020.111327.

[63] J. L. Beck and K. V. Yuen, "Model Selection Using Response measurements: Bayesian Probabilistic Approach," *J. Eng. Mech.*, vol. 130. No. 2, no. February, pp. 192–203, 2004, doi: 10.1061/(ASCE)0733-9399(2004)130.

[64] B. Titurus and M. I. Friswell, "Regularization in model updating," *Int. J. Numer. Methods Eng.*, vol. 75, pp. 440–478, 2008, doi: 10.1002/nme.2257.

[65] Z. Yuan, P. Liang, T. Silva, K. Yu, and J. E. Mottershead, "Parameter selection for model updating with global sensitivity analysis," *Mech. Syst. Signal Process.*, vol. 115, pp. 483–496, 2019, doi: 10.1016/j.ymssp.2018.05.048.

[66] J. Jang and A. W. Smyth, "Model updating of a full-scale FE model with nonlinear constraint equations and sensitivity-based cluster analysis for updating parameters," *Mech. Syst. Signal Process.*, vol. 83, pp. 337–355, 2017, doi: 10.1016/j.ymssp.2016.06.018.

[67] A. J. Miller, *Subset Selection in Regression*, 2nd editio. New Delhi: Springer, 1995.

[68] P. Bruneau, O. Parisot, and B. Otjacques, "A heuristic for the automatic parametrization of the spectral clustering algorithm," *Proc. - Int. Conf. Pattern Recognit.*, vol. 2, no. 1, pp. 1313–1318, 2014, doi: 10.1109/ICPR.2014.235.

[69] T. A. N. Silva, N. M. M. Maia, M. Link, and J. E. Mottershead, "Parameter selection and covariance updating," *Mech. Syst. Signal Process.*, vol. 70–71, pp. 269–283, 2016, doi: 10.1016/j.ymssp.2015.08.034.

[70] P. Asadollahi, Y. Huang, and J. Li, "Bayesian finite element model updating and assessment of cable-stayed bridges using wireless sensor data," *Sensors (Switzerland)*, vol. 18, no. 9, 2018, doi: 10.3390/s18093057.

[71] Y. Li and L. Xu, "Unweighted multiple group method with arithmetic mean," *Proc. 5th Int. Conf. Bio-Inspired Comput. Theor. Appl.*, vol. 100, no. 2, pp. 830–834, 2010, doi:

10.1109/BICTA.2010.5645232.

[72] J. Chiachío, M. Chiachío, A. Saxena, S. Sankararaman, G. Rus, and K. Goebel, "Bayesian model selection and parameter estimation for fatigue damage progression models in composites," *Int. J. Fatigue*, vol. 70, pp. 361–373, 2015, doi: 10.1016/j.ijfatigue.2014.08.003.

[73] L. Mthembu, T. Marwala, M. I. Friswell, and S. Adhikari, "Finite element model selection using Particle Swarm Optimization," 2010.

[74] V. Arora, P. J. M. Van Der Hoogt, R. G. K. M. Aarts, and A. De Boer, "Identification of stiffness and damping characteristics of axial air-foil bearings," *Int. J. Mech. Mater. Des.*, vol. 7, no. 3, pp. 231–243, 2011, doi: 10.1007/s10999-011-9161-7.

[75] J. M. W. Brownjohn, "Structural health monitoring of civil infrastructure," *Philos. Trans. R. Soc. A Math. Phys. Eng. Sci.*, vol. 365, no. 1851, pp. 589–622, 2007, doi: 10.1098/rsta.2006.1925.

[76] T. Marwala, I. Boulkaibet, and S. Adhikari, *Probabilistic Finite Element Model Updating using Bayesian Statistics. Application to aeronautical and mechanical engineering*, First. Chichester, UK: John Wiley & Sons, Ltd Registered, 2017.

[77] J. Jang and A. Smyth, "Bayesian model updating of a full-scale finite element model with sensitivity-based clustering," *Struct. Control Heal. Monit.*, vol. 24, no. 11, pp. 1–15, 2017, doi: 10.1002/stc.2004.

[78] K. V. Yuen, "Recent developments of Bayesian model class selection and applications in civil engineering," *Struct. Saf.*, vol. 32, no. 5, pp. 338–346, 2010, doi: 10.1016/j.strusafe.2010.03.011.

[79] T. Yin, H. P. Zhu, and S. J. Fu, "Model selection for dynamic reduction-based structural health monitoring following the Bayesian evidence approach," *Mech. Syst. Signal Process.*, vol. 127, no. March, pp. 306–327, 2019, doi: 10.1016/j.ymssp.2019.03.009.

[80] E. Durmazgezer, U. Yucel, and O. Ozcelik, "Damage identification of a reinforced concrete frame at increasing damage levels by sensitivity-based finite element model updating," *Bull. Earthq. Eng.*, vol. 17, no. 11, pp. 6041–6060, 2019, doi: 10.1007/s10518-019-00690-5.

[81] A. Nozari, I. Behmanesh, S. Yousefianmoghadam, B. Moaveni, and A. Stavridis,

"Effects of variability in ambient vibration data on model updating and damage identification of a 10-story building," *Eng. Struct.*, vol. 151, pp. 540–553, 2017, doi: 10.1016/j.engstruct.2017.08.044.

[82] Y. Wu, R. Zhu, Z. Cao, Y. Liu, and D. Jiang, "Model updating using frequency response functions based on sherman-morrison formula," *Appl. Sci.*, vol. 10, no. 14, 2020, doi: 10.3390/app10144985.

[83] N. T. Davis and M. Sanayei, "Foundation identification using dynamic strain and acceleration measurements," *Eng. Struct.*, no. March, 2020, doi: 10.1016/j.engstruct.2019.109811.

[84] B. Jaishi and W.-X. Ren, "Structural Finite Element Model Updating Using Ambient Vibration Test Results," *J. Struct. Eng.*, vol. 131, no. 4, pp. 617–628, 2005, doi: 10.1061/(asce)0733-9445(2005)131:4(617).

[85] M. Razavi and A. Hadidi, "Assessment of sensitivity-based FE model updating technique for damage detection in large space structures," *Struct. Monit. Maint.*, vol. 7, no. 3, pp. 261–281, 2020, doi: 10.12989/smm.2020.7.3.261.

[86] B. Jaishi and W. X. Ren, "Finite element model updating based on eigenvalue and strain energy residuals using multiobjective optimisation technique," *Mech. Syst. Signal Process.*, vol. 21, no. 5, pp. 2295–2317, 2007, doi: 10.1016/j.ymssp.2006.09.008.

[87] X. Yang, H. Ouyang, X. Guo, and S. Cao, "Modal Strain Energy-Based Model Updating Method for Damage Identification on Beam-Like Structures," *J. Struct. Eng.*, vol. 146, no. 11, p. 04020246, 2020, doi: 10.1061/(asce)st.1943-541x.0002812.

[88] J. Liao, G. Tang, L. Meng, H. Liu, and Y. Zhang, "Finite element model updating based on field quasi-static generalized influence line and its bridge engineering application," *Procedia Eng.*, vol. 31, pp. 348–353, 2012, doi: 10.1016/j.proeng.2012.01.1035.

[89] S. P. Tchemodanova, M. Sanayei, B. Moaveni, K. Tatsis, and E. Chatzi, "Strain predictions at unmeasured locations of a substructure using sparse response-only vibration measurements," *J. Civ. Struct. Heal. Monit.*, no. September, 2021, doi: 10.1007/s13349-021-00476-x.

[90] S. Kim, K. Young, and J. Lee, "Bridge Finite Model Updating Approach By Static Load Input / Deflection Output Measurements : Field Experiment," 2016.

[91] M. Sanayei, G. R. Imbaro, J. A. S. McClain, and L. C. Brown, "Structural Model Updating Using Experimental Static Measurements," *J. Struct. Eng.*, vol. 123, no. 6, pp. 792–798, 1997, doi: 10.1061/(asce)0733-9445(1997)123:6(792).

[92] Y. Zhou, J. Zhang, W. Yi, Y. Jiang, and Q. Pan, "Structural Identification of a Concrete-Filled Steel Tubular Arch Bridge via Ambient Vibration Test Data," *J. Bridg. Eng.*, vol. 22, no. 8, p. 04017049, 2017, doi: 10.1061/(asce)be.1943-5592.0001086.

[93] E. Nazarian, F. Ansari, and H. Azari, "Recursive optimization method for monitoring of tension loss in cables of cable-stayed bridges," *J. Intell. Mater. Syst. Struct.*, vol. 27, no. 15, pp. 2091–2101, 2016, doi: 10.1177/1045389X15620043.

[94] L. Sun and Y. Xu, "Modal parameter identification and finite element model updating of a long-span aqueduct structure based on ambient excitation," *J. Vibroengineering*, vol. 22, no. 4, pp. 896–908, 2020, doi: 10.21595/jve.2020.21271.

[95] M. Sanayei, E. S. Bell, C. N. Javdekar, J. L. Edelmann, and E. Slavsky, "Damage Localization and Finite-Element Model Updating Using Multiresponse NDT Data," *J. Bridg. Eng.*, vol. 11, no. 6, pp. 688–698, 2006, doi: 10.1061/(asce)1084-0702(2006)11:6(688).

[96] J. D. Sipple and M. Sanayei, "Finite element model updating of the UCF grid benchmark using measured frequency response functions," *Mech. Syst. Signal Process.*, vol. 46, no. 1, pp. 179–190, 2014, doi: 10.1016/j.ymssp.2014.01.008.

[97] R. P. Bandara, T. H. Chan, and D. P. Thambiratnam, "Structural damage detection method using frequency response functions," *Struct. Heal. Monit.*, vol. 13, no. 4, pp. 418–429, 2014, doi: 10.1177/1475921714522847.

[98] Q. Pu, Y. Hong, L. Chen, S. Yang, and X. Xu, "Model updating–based damage detection of a concrete beam utilizing experimental damped frequency response functions," *Adv. Struct. Eng.*, vol. 22, no. 4, pp. 935–947, 2019, doi: 10.1177/1369433218789556.

[99] J. Wang and C. Wang, "Structural Model Updating of Frequency Response Function Based on Kriging Model," *Proc. - 2016 3rd Int. Conf. Inf. Sci. Control Eng. ICISCE 2016*, no. 1, pp. 640–644, 2016, doi: 10.1109/ICISCE.2016.142.

[100] S. Pradhan and S. V. Modak, "Damping Matrix Identification by Finite Element Model Updating Using Frequency Response Data," *Int. J. Struct. Stab. Dyn.*, vol. 17, no. 1, pp. 1–27, 2017, doi: 10.1142/S0219455417500043.

[101] B. K. Oh, D. Kim, and H. S. Park, “Modal Response-Based Visual System Identification and Model Updating Methods for Building Structures,” *Comput. Civ. Infrastruct. Eng.*, vol. 32, no. 1, pp. 34–56, 2017, doi: 10.1111/mice.12229.

[102] W. H. Wu, L. J. Prendergast, and K. Gavin, “An iterative method to infer distributed mass and stiffness profiles for use in reference dynamic beam-Winkler models of foundation piles from frequency response functions,” *J. Sound Vib.*, vol. 431, pp. 1–19, 2018, doi: 10.1016/j.jsv.2018.05.049.

[103] S. Zhou and W. Song, “Environmental-effects-embedded model updating method considering environmental impacts,” *Struct. Control Heal. Monit.*, vol. 25, no. 3, pp. 1–22, 2018, doi: 10.1002/stc.2116.

[104] J. Cui, D. Kim, K. Y. Koo, and S. Chaudhary, “Structural model updating of steel box girder bridge using modal flexibility based deflections,” *Balt. J. Road Bridg. Eng.*, vol. 7, no. 4, pp. 253–260, 2012, doi: 10.3846/bjrbe.2012.34.

[105] D. Dinh-Cong, T. Nguyen-Thoi, and D. T. Nguyen, “A FE model updating technique based on SAP2000-OAPI and enhanced SOS algorithm for damage assessment of full-scale structures,” *Appl. Soft Comput. J.*, vol. 89, p. 106100, 2020, doi: 10.1016/j.asoc.2020.106100.

[106] M. Rezaiee-Pajand, A. Entezami, and H. Sarmadi, “A sensitivity-based finite element model updating based on unconstrained optimization problem and regularized solution methods,” *Struct. Control Heal. Monit.*, vol. 27, no. 5, pp. 1–29, 2020, doi: 10.1002/stc.2481.

[107] F. L. Wang, T. H. T. Chan, D. P. Thambiratnam, and A. C. C. Tan, “Damage diagnosis for complex steel truss bridges using multi-layer genetic algorithm,” *J. Civ. Struct. Heal. Monit.*, vol. 3, no. 2, pp. 117–127, 2013, doi: 10.1007/s13349-013-0041-8.

[108] V. Srinivas, K. Ramanjaneyulu, and C. A. Jeyasehar, “Multi-stage approach for structural damage identification using modal strain energy and evolutionary optimization techniques,” *Struct. Heal. Monit.*, vol. 10, no. 2, pp. 219–230, 2011, doi: 10.1177/1475921710373291.

[109] E. Özer and S. Soyöz, “Vibration-based damage detection and seismic performance assessment of bridges,” *Earthq. Spectra*, vol. 31, no. 1, pp. 137–157, 2015, doi: 10.1193/080612EQS255M.

[110] J. Li, H. Hao, and Z. Chen, “Damage Identification and Optimal Sensor Placement for Structures under Unknown Traffic-Induced Vibrations,” *J. Aerosp. Eng.*, vol. 30, no. 2, pp. 1–10, 2017, doi: 10.1061/(asce)as.1943-5525.0000550.

[111] D. Feng and M. Q. Feng, “Model Updating of Railway Bridge Using In Situ Dynamic Displacement Measurement under Trainloads,” *J. Bridg. Eng.*, vol. 20, no. 12, p. 04015019, 2015, doi: 10.1061/(asce)be.1943-5592.0000765.

[112] H. Wang, A. Q. Li, and J. Li, “Progressive finite element model calibration of a long-span suspension bridge based on ambient vibration and static measurements,” *Eng. Struct.*, vol. 32, no. 9, pp. 2546–2556, 2010, doi: 10.1016/j.engstruct.2010.04.028.

[113] Y. S. Erdogan, M. Gul, F. N. Catbas, and P. G. Bakir, “Investigation of Uncertainty Changes in Model Outputs for Finite-Element Model Updating Using Structural Health Monitoring Data,” *J. Struct. Eng.*, vol. 140, no. 11, p. 04014078, 2014, doi: 10.1061/(asce)st.1943-541x.0001002.

[114] M. Sanayei, A. Khaloo, M. Gul, and F. Necati Catbas, “Automated finite element model updating of a scale bridge model using measured static and modal test data,” *Eng. Struct.*, vol. 102, no. January 2021, pp. 66–79, 2015, doi: 10.1016/j.engstruct.2015.07.029.

[115] S. Kim, N. Kim, Y.-S. Park, and S.-S. Jin, “A Sequential Framework for Improving Identifiability of FE Model Updating Using Static and Dynamic Data,” *Sensors (Switzerland)*, vol. 19, no. 23, 2019, doi: doi:10.3390/s19235099.

[116] H. Schlune, M. Plos, and K. Gylltoft, “Improved bridge evaluation through finite element model updating using static and dynamic measurements,” *Eng. Struct.*, vol. 31, no. 7, pp. 1477–1485, 2009, doi: 10.1016/j.engstruct.2009.02.011.

[117] B. Goller, J. L. Beck, and G. I. Schuëller, “Evidence-Based Identification of Weighting Factors in Bayesian Model Updating Using Modal Data,” *J. Eng. Mech.*, vol. 138, no. 5, pp. 430–440, 2012, doi: 10.1061/(asce)em.1943-7889.0000351.

[118] M. I. Friswell and J. E. Mottershead, *Finite Element Model Updating in Structural Dynamics*. Dordecht, Netherlands: Springer, 1995.

[119] F. Pacheco-Torgal, R. Melchers, X. Shi, N. De Belie, K. Van Tittelboom, and A. Saez, *Eco-efficient Repair and Rehabilitation of Concrete Infrastructure*. Kidlington, UK: Jonathan Simpson, 2017.

[120] Y. J. Cha and O. Buyukozturk, “Structural damage detection using modal strain energy and hybrid multiobjective optimization,” *Comput. Civ. Infrastruct. Eng.*, vol. 30, no. 5, pp. 347–358, 2015, doi: 10.1111/mice.12122.

[121] A. Osyczka, “An approach to multicriterion optimization problems for engineering design,” *Comput. Methods Appl. Mech. Eng.*, vol. 15, no. 3, pp. 309–333, 1978, doi: 10.1016/0045-7825(78)90046-4.

[122] O. Cuate and O. Schütze, “Pareto explorer for finding the knee for many objective optimization problems,” *Mathematics*, vol. 8, no. 10, pp. 6–15, 2020, doi: 10.3390/MATH8101651.

[123] Muhammad Nagy, Yasser Mansour, and Sherif Abdelmohsen, “Multi-Objective Optimization Methods as a Decision Making Strategy,” *Int. J. Eng. Res.*, vol. V9, no. 03, 2020, doi: 10.17577/ijertv9is030480.

[124] J. F. Jiménez-Alonso, J. Naranjo-Perez, A. Pavic, and A. Sáez, “Maximum Likelihood Finite-Element Model Updating of Civil Engineering Structures Using Nature-Inspired Computational Algorithms,” *Struct. Eng. Int.*, pp. 1–13, 2020, doi: 10.1080/10168664.2020.1768812.

[125] J. Naranjo-Pérez, J. F. Jiménez-Alonso, A. Pavic, and A. Sáez, “Finite-element-model updating of civil engineering structures using a hybrid UKF-HS algorithm,” *Struct. Infrastruct. Eng.*, vol. 17, no. 5, pp. 620–637, 2021, doi: 10.1080/15732479.2020.1760317.

[126] S. S. Jin, S. Cho, H. J. Jung, J. J. Lee, and C. B. Yun, “A new multi-objective approach to finite element model updating,” *J. Sound Vib.*, vol. 333, no. 11, pp. 2323–2338, 2014, doi: 10.1016/j.jsv.2014.01.015.

[127] N. F. Alkayem, M. Cao, Y. Zhang, M. Bayat, and Z. Su, “Structural damage detection using finite element model updating with evolutionary algorithms: a survey,” *Neural Comput. Appl.*, vol. 30, no. 2, pp. 389–411, 2018, doi: 10.1007/s00521-017-3284-1.

[128] D. Wang, Z. Tan, Y. Li, and Y. Liu, “Review of the application of finite element model updating to civil structures,” *Key Eng. Mater.*, vol. 574, pp. 107–115, 2014, doi: 10.4028/www.scientific.net/KEM.574.107.

[129] S. Waseda University, “Darwin ’ s Theory of Evolution by Natural Selection The Facts about Evolution,” pp. 1–31.

[130] J. Kennedey and R. Eberhart, “Particle Swarm Optimization,” in *Proceedings of ICNN’95 - International Conference on Neural Networks*, 1995, pp. 1942–1948, doi: 10.1002/9780470612163.

[131] E. Bassoli, L. Vincenzi, A. M. D’Altri, S. de Miranda, M. Forghieri, and G. Castellazzi, “Ambient vibration-based finite element model updating of an earthquake-damaged masonry tower,” *Struct. Control Heal. Monit.*, vol. 25, no. 5, pp. 1–15, 2018, doi: 10.1002/stc.2150.

[132] M. Jahangiri, M. A. Najafgholipour, S. M. Dehghan, and M. A. Hadianfard, “The efficiency of a novel identification method for structural damage assessment using the first vibration mode data,” *J. Sound Vib.*, vol. 458, pp. 1–16, 2019, doi: 10.1016/j.jsv.2019.06.011.

[133] H. Tran-Ngoc, S. Khatir, G. De Roeck, T. Bui-Tien, L. Nguyen-Ngoc, and M. Abdel Wahab, “Model updating for nam O bridge using particle swarm optimization algorithm and genetic algorithm,” *Sensors (Switzerland)*, vol. 18, no. 12, 2018, doi: 10.3390/s18124131.

[134] S. Qin, Y. L. Zhou, H. Cao, and M. A. Wahab, “Model Updating in Complex Bridge Structures using Kriging Model Ensemble with Genetic Algorithm,” *KSCE J. Civ. Eng.*, vol. 22, no. 9, pp. 3567–3578, 2018, doi: 10.1007/s12205-017-1107-7.

[135] A. M. Raich and T. R. Liszkai, “Improving the performance of structural damage detection methods using advanced genetic algorithms,” *J. Struct. Eng.*, vol. 133, no. March, pp. 449–461, 2007.

[136] N. F. Alkayem, M. Cao, and M. Ragulskis, “Damage localization in irregular shape structures using intelligent FE model updating approach with a new hybrid objective function and social swarm algorithm,” *Appl. Soft Comput. J.*, vol. 83, 2019, doi: 10.1016/j.asoc.2019.105604.

[137] F. Shabbir and P. Omenzetter, “Model updating using genetic algorithms with sequential niche technique,” *Eng. Struct.*, vol. 120, pp. 166–182, 2016, doi: 10.1016/j.engstruct.2016.04.028.

[138] D. E. Nasr and G. A. Saad, “Optimal Sensor Placement Using a Combined Genetic Algorithm–Ensemble Kalman Filter Framework,” *ASCE-ASME J. Risk Uncertain. Eng. Syst. Part A Civ. Eng.*, vol. 3, no. 1, p. 04016010, 2017, doi: 10.1061/ajrua6.0000886.

[139] J. F. Jiménez-Alonso and A. Sáez, "Model updating for the selection of an ancient bridge retrofitting method in Almeria, Spain," *Struct. Eng. Int.*, vol. 26, no. 1, pp. 17–26, 2016, doi: 10.2749/101686615X14355644771333.

[140] C. Costa, D. Ribeiro, P. Jorge, R. Silva, A. Arêde, and R. Calçada, "Calibration of the numerical model of a stone masonry railway bridge based on experimentally identified modal parameters," *Eng. Struct.*, vol. 123, pp. 354–371, 2016, doi: 10.1016/j.engstruct.2016.05.044.

[141] A. Sabamehr, C. Lim, and A. Bagchi, "System identification and model updating of highway bridges using ambient vibration tests," *J. Civ. Struct. Heal. Monit.*, vol. 8, no. 5, pp. 755–771, 2018, doi: 10.1007/s13349-018-0304-5.

[142] P. Pachón, R. Castro, E. García-Macías, V. Compan, and E. Puertas, "E. Torroja's bridge: Tailored experimental setup for SHM of a historical bridge with a reduced number of sensors," *Eng. Struct.*, vol. 162, no. September 2017, pp. 11–21, 2018, doi: 10.1016/j.engstruct.2018.02.035.

[143] A. M. Hernández-Díaz, J. Pérez-Aracil, J. F. Jiménez-Alonso, and A. Sáez, "Self-control of a lively footbridge under pedestrian flow," 2015.

[144] C. Gentilini, A. Marzani, and M. Mazzotti, "Nondestructive characterization of tie-rods by means of dynamic testing, added masses and genetic algorithms," *J. Sound Vib.*, vol. 332, no. 1, pp. 76–101, 2013, doi: 10.1016/j.jsv.2012.08.009.

[145] X. Yang, X. Guo, H. Ouyang, and D. Li, "A kriging model based finite element model updating method for damage detection," *Appl. Sci.*, vol. 7, no. 10, 2017, doi: 10.3390/app7101039.

[146] H. Sun, W. Chen, S. Cai, and B. Zhang, "Mechanical State Assessment of In-Service Cable-Stayed Bridge Using a Two-Phase Model Updating Technology and Periodic Field Measurements," *J. Bridg. Eng.*, vol. 25, no. 5, p. 04020015, 2020, doi: 10.1061/(asce)be.1943-5592.0001550.

[147] B. K. Oh, J. W. Hwang, S. W. Choi, Y. Kim, T. Cho, and H. S. Park, "Dynamic displacements-based model updating with motion capture system," *Struct. Control Heal. Monit.*, vol. 24, no. 4, pp. 1–16, 2017, doi: 10.1002/stc.1904.

[148] Y. Cui, W. Lu, and J. Teng, "Updating of structural multi-scale monitoring model based on multi-objective optimisation," *Adv. Struct. Eng.*, vol. 22, no. 5, pp. 1073–1088, 2019,

doi: 10.1177/1369433218805235.

[149] F. Y. Wang, Y. L. Xu, and S. Zhan, “Multi-scale model updating of a transmission tower structure using Kriging meta-method,” *Struct. Control Heal. Monit.*, vol. 24, no. 8, pp. 1–16, 2017, doi: 10.1002/stc.1952.

[150] H. T. M. Luong, V. Zabel, W. Lorenz, and R. G. Rohrmann, “Vibration-based Model Updating and Identification of Multiple Axial Forces in Truss Structures,” *Procedia Eng.*, vol. 188, pp. 385–392, 2017, doi: 10.1016/j.proeng.2017.04.499.

[151] V. Mosquera, A. W. Smyth, and R. Betti, “Rapid evaluation and damage assessment of instrumented highway bridges,” *Earthq. Eng. Struct. Dyn.*, vol. 41, pp. 755–754, 2012, doi: DOI: 10.1002/eqe.1155.

[152] H. Seon Park, J. H. Kim, and B. K. Oh, “Model updating method for damage detection of building structures under ambient excitation using modal participation ratio,” *Meas. J. Int. Meas. Confed.*, vol. 133, pp. 251–261, 2019, doi: 10.1016/j.measurement.2018.10.023.

[153] P. Jeenkour, J. Pattavanitch, and K. Boonlong, “Vibration-based damage detection in beams by genetic algorithm encoding locations and damage factors as decision variables,” *Vibroengineering Procedia*, vol. 16, pp. 35–40, 2017, doi: 10.21595/vp.2017.19345.

[154] S. Yu and J. Ou, “Structural Health Monitoring and Model Updating of Aizhai Suspension Bridge,” *J. Aerosp. Eng.*, vol. 30, no. 2, pp. 1–15, 2017, doi: 10.1061/(asce)as.1943-5525.0000653.

[155] R. Soman and P. Mainowski, “A real-valued genetic algorithm for optimization of sensor placement for guided wave-based structural health monitoring,” *J. Sensors*, pp. 1–10, 2019, doi: https://www.hindawi.com/journals/js/2019/9614630/.

[156] R. Hou, Y. Xia, Q. Xia, and X. Zhou, “Genetic algorithm based optimal sensor placement for L1-regularized damage detection,” *Struct. Control Heal. Monit.*, vol. 26, no. 1, pp. 1–14, 2019, doi: 10.1002/stc.2274.

[157] M. O. Okwu and L. K. Tartibu, “Particle Swarm Optimisation,” *Stud. Comput. Intell.*, vol. 927, pp. 5–13, 2021, doi: 10.1007/978-3-030-61111-8_2.

[158] H. Gökdağ and A. R. Yildiz, “Structural damage detection using modal parameters and

particle swarm optimization," *Mater. Test.*, vol. 54, no. 6, pp. 416–420, 2012, doi: 10.3139/120.110346.

[159] T. Marwala, "Finite-element-model updating using computional intelligence techniques: Applications to structural dynamics," *Finite-Element-Model Updat. Using Comput. Intell. Tech. Appl. to Struct. Dyn.*, pp. 1–250, 2010, doi: 10.1007/978-1-84996-323-7.

[160] S. C. Mohan, D. K. Maiti, and D. Maity, "Structural damage assessment using FRF employing particle swarm optimization," *Appl. Math. Comput.*, vol. 219, no. 20, pp. 10387–10400, 2013, doi: 10.1016/j.amc.2013.04.016.

[161] S. M. Seyedpoor, "A two stage method for structural damage detection using a modal strain energy based index and particle swarm optimization," *Int. J. Non. Linear. Mech.*, vol. 47, no. 1, pp. 1–8, 2012, doi: 10.1016/j.ijnonlinmec.2011.07.011.

[162] B. Nanda, D. Maity, and D. K. Maiti, "Crack assessment in frame structures using modal data and unified particle swarm optimization technique," *Adv. Struct. Eng.*, vol. 17, no. 5, pp. 747–766, 2014, doi: 10.1260/1369-4332.17.5.747.

[163] X. Zhang, R. X. Gao, R. Yan, X. Chen, C. Sun, and Z. Yang, "Multivariable wavelet finite element-based vibration model for quantitative crack identification by using particle swarm optimization," *J. Sound Vib.*, vol. 375, pp. 200–216, 2016, doi: 10.1016/j.jsv.2016.04.018.

[164] S. Gerist and M. R. Maheri, "Multi-stage approach for structural damage detection problem using basis pursuit and particle swarm optimization," *J. Sound Vib.*, vol. 384, no. October 2018, pp. 210–226, 2016, doi: 10.1016/j.jsv.2016.08.024.

[165] M. R. Nouri Shirazi, H. Mollamahmoudi, and S. M. Seyedpoor, "Structural Damage Identification Using an Adaptive Multi-stage Optimization Method Based on a Modified Particle Swarm Algorithm," *J. Optim. Theory Appl.*, vol. 160, no. 3, pp. 1009–1019, 2014, doi: 10.1007/s10957-013-0316-6.

[166] R. Perera, S. E. Fang, and A. Ruiz, "Application of particle swarm optimization and genetic algorithms to multiobjective damage identification inverse problems with modelling errors," *Meccanica*, vol. 45, no. 5, pp. 723–734, 2010, doi: 10.1007/s11012-009-9264-5.

[167] A. Cancelli, S. Laflamme, A. Alipour, S. Sritharan, and F. Ubertini, "Vibration-based damage localization and quantification in a pretensioned concrete girder using stochastic

subspace identification and particle swarm model updating," *Struct. Heal. Monit.*, vol. 19, no. 2, pp. 587–605, 2020, doi: 10.1177/1475921718820015.

[168] S. Chatterjee, S. Sarkar, S. Hore, N. Dey, A. S. Ashour, and V. E. Balas, "Particle swarm optimization trained neural network for structural failure prediction of multistoried RC buildings," *Neural Comput. Appl.*, vol. 28, no. 8, pp. 2005–2016, 2017, doi: 10.1007/s00521-016-2190-2.

[169] N. Metropolis, A. W. Rosenbluth, M. N. Rosenbluth, A. H. Teller, and E. Teller, "Equation of state calculations by fast computing machines," *J. Chem. Phys.*, vol. 21, no. 6, pp. 1087–1092, 1953, doi: 10.1063/1.1699114.

[170] R. I. Levin and N. A. J. Lieven, "Dynamic finite element model updating using simulated annealing and genetic algorithms," *Mech. Syst. Signal Process.*, vol. 12, no. 1, pp. 91–120, 1998, doi: 10.1006/mssp.1996.0136.

[171] T. Marwala, "Finite element model updating using response surface method," *Collect. Tech. Pap. - AIAA/ASME/ASCE/AHS/ASC Struct. Struct. Dyn. Mater. Conf.*, vol. 7, no. December, pp. 5165–5173, 2004, doi: 10.2514/6.2004-2005.

[172] S. S. Kourehli, "Damage diagnosis of structures using modal data and static response," *Period. Polytech. Civ. Eng.*, vol. 61, no. 1, pp. 135–145, 2017, doi: 10.3311/PPci.7646.

[173] A. T. Zimmerman and J. P. Lynch, "A Parallel Simulated Annealing Architecture for Model Updating in Wireless Sensor Networks," *IEEE Sens. J.*, vol. 9, no. 11, pp. 1503–1510, 2009, doi: 10.1109/JSEN.2009.2019323.

[174] H. F. Lam, J. H. Yang, and S. K. Au, "Markov chain Monte Carlo-based Bayesian method for structural model updating and damage detection," *Struct. Control Heal. Monit.*, vol. 25, no. 4, pp. 1–22, 2018, doi: 10.1002/stc.2140.

[175] Y. Huang, C. Shao, B. Wu, J. L. Beck, and H. Li, "State-of-the-art review on Bayesian inference in structural system identification and damage assessment," *Adv. Struct. Eng.*, vol. 22, no. 6, pp. 1329–1351, 2019, doi: 10.1177/1369433218811540.

[176] P. L. Green, "Bayesian system identification of a nonlinear dynamica system using a novel variant of Simulated Annealing," *Mech. Syst. Signal Process.*, vol. 52–53, no. 1, pp. 133–146, 2015, doi: 10.1016/j.ymssp.2014.07.010.

[177] D. Manjarres *et al.*, "A survey on applications of the harmony search algorithm,"

Engineering Applications of Artificial Intelligence, vol. 26, no. 8. pp. 1818–1831, 2013, doi: 10.1016/j.engappai.2013.05.008.

[178] X. Z. Gao, V. Govindasamy, H. Xu, X. Wang, and K. Zenger, "Harmony search method: Theory and applications," *Comput. Intell. Neurosci.*, vol. 2015, 2015, doi: 10.1155/2015/258491.

[179] Q. Long, X. Wu, and C. Wu, "Non-Dominated Sorting Methods for Multi-Objective Optimization: Review and Numerical Comparison," *J. Ind. Manag. Optim.*, vol. 17, no. 2, pp. 1001–1023, 2021, doi: 10.3934/jimo.2020009.

[180] J. Liu and X. Chen, "An improved NSGA-II algorithm based on crowding distance elimination strategy," *Int. J. Comput. Intell. Syst.*, vol. 12, no. 2, pp. 513–518, 2019, doi: 10.2991/ijcis.d.190328.001.

[181] K. S. Lee and Z. W. Geem, "A new meta-heuristic algorithm for continuous engineering optimization: Harmony search theory and practice," *Comput. Methods Appl. Mech. Eng.*, vol. 194, no. 36–38, pp. 3902–3933, 2005, doi: 10.1016/j.cma.2004.09.007.

[182] J. Naranjo-Pérez, M. Infantes, J. Jiménez-Alonso, and A. Sáez, "A collaborative machine learning-optimization algorithm to improve the finite element model updating of civil engineering structures," *Eng. Struct.*, vol. 225, 2020, doi: 10.1016/j.engstruct.2020.111327.

[183] A. Kaveh, S. M. Javadi, and M. Maniat, "Damage assessment via modal data with a mixed particle swarm strategy, ray optimizer, and harmony search," *Asian J. Civ. Eng.*, vol. 15, no. 1, pp. 95–106, 2014.

[184] L. F. F. Miguel, L. F. F. Miguel, J. Kaminski, and J. D. Riera, "Damage detection under ambient vibration by harmony search algorithm," *Expert Syst. Appl.*, vol. 39, no. 10, pp. 9704–9714, 2012, doi: 10.1016/j.eswa.2012.02.147.

[185] K. Boonlong, "Vibration-based damage detection in beams by cooperative coevolutionary genetic algorithm," *Advances in Mechanical Engineering*, vol. 2014. 2014, doi: 10.1155/2014/624949.

[186] O. Shallan, A. Eraky, T. Sakr, and M. Khozam, "Structural Damage Detection using Genetic Algorithm by Static Measurements," *Int. J. Trend Res. Dev.*, vol. 4, no. 1, pp. 324–329, 2017.

[187] F. Shabbir and P. Omenzetter, “Particle swarm optimization with sequential niche technique for dynamic finite element model updating,” *Comput. Civ. Infrastruct. Eng.*, vol. 30, no. 5, pp. 359–375, 2015, doi: 10.1111/mice.12100.

[188] Z. Luo and L. Yu, “PSO based Sparse Regularization Approach for Structural Damage Detection,” in *13th International Conference on Natural Computation, Fuzzy Systems and Knowledge Discovery (ICNC-FSKD 2017)*, 2017, no. 1, pp. 1033–1039.

[189] M. T. Vakil Baghmisheh, M. Peimani, M. H. Sadeghi, M. M. Ettefagh, and A. F. Tabrizi, “A hybrid particle swarm-Nelder-Mead optimization method for crack detection in cantilever beams,” *Appl. Soft Comput. J.*, vol. 12, no. 8, pp. 2217–2226, 2012, doi: 10.1016/j.asoc.2012.03.030.

[190] M. M. Saada, M. H. Arafa, and A. O. Nassef, “Finite element model updating approach to damage identification in beams using particle swarm optimization,” *Eng. Optim.*, vol. 45, no. 6, pp. 677–696, 2013, doi: 10.1080/0305215X.2012.704026.

[191] M. T. Vakil Baghmisheh, M. Peimani, M. H. Sadeghi, M. M. Ettefagh, and A. F. Tabrizi, “A hybrid particle swarm-Nelder-Mead optimization method for crack detection in cantilever beams,” *Appl. Soft Comput. J.*, vol. 12, no. 8, pp. 2217–2226, 2012, doi: 10.1016/j.asoc.2012.03.030.

[192] F. Kang, J. J. Li, and Q. Xu, “Damage detection based on improved particle swarm optimization using vibration data,” *Appl. Soft Comput. J.*, vol. 12, no. 8, pp. 2329–2335, 2012, doi: 10.1016/j.asoc.2012.03.050.

[193] J. Li and J. Chen, “Solving time-variant reliability-based design optimization by PSO-t-IRS: A methodology incorporating a particle swarm optimization algorithm and an enhanced instantaneous response surface,” *Reliab. Eng. Syst. Saf.*, vol. 191, no. July, 2019, doi: 10.1016/j.ress.2019.106580.

[194] R. S. He and S. F. Hwang, “Damage detection by a hybrid real-parameter genetic algorithm under the assistance of grey relation analysis,” *Eng. Appl. Artif. Intell.*, vol. 20, no. 7, pp. 980–992, 2007, doi: 10.1016/j.engappai.2006.11.020.

[195] S. F. Hwang and R. S. He, “Improving real-parameter genetic algorithm with simulated annealing for engineering problems,” *Adv. Eng. Softw.*, vol. 37, no. 6, pp. 406–418, 2006, doi: 10.1016/j.advengsoft.2005.08.002.

[196] R. Astroza, L. T. Nguyen, and T. Nestorović, “Finite element model updating using

simulated annealing hybridized with unscented Kalman filter," *Comput. Struct.*, vol. 177, pp. 176–191, 2016, doi: 10.1016/j.compstruc.2016.09.001.

[197] Q. Zhang, *Applied Game Theory and Strategic*. 2014.

[198] J. von Neuman and O. Morgenstern, *Theory of Games and Economic Behavior*, Fifth. Princenton: Princenton University Press, 1953.

[199] D. McNulty, "The Basics of Game Theory," *Investopedia*, 2019. https://www.investopedia.com/articles/financial-theory/08/game-theory-basics.asp.

[200] M. Jin, X. Lei, and J. Du, "Evolutionary game theory in multi-objective optimization problem," *Int. J. Comput. Intell. Syst.*, vol. 3, no. August 2013, pp. 74–87, 2010, doi: 10.1080/18756891.2010.9727754.

[201] S. Özyildirim and N. M. Alemdar, "Learning the optimum as a Nash equilibrium," *J. Econ. Dyn. Control*, vol. 24, no. 4, pp. 483–499, 2000, doi: 10.1016/s0165-1889(99)00012-3.

[202] R. Meng, Y. Ye, and N. G. Xie, "Multi-objective optimization design methods based on game theory," *Proc. World Congr. Intell. Control Autom.*, no. 070414154, pp. 2220–2227, 2010, doi: 10.1109/WCICA.2010.5554307.

[203] Y. R. Cheng, "Evolutionary Game Theoretic Multi-Objective Optimization Algorithms and Their Applications," University of Massachusetts Boston, 2017.

[204] K. K. Annamdas and S. S. Rao, "Multi-objective optimization of engineering systems using game theory and particle swarm optimization," *Eng. Optim.*, vol. 41, no. 8, pp. 737–752, Aug. 2009, doi: 10.1080/03052150902822141.

[205] R. Spallino and S. Rizzo, "Multi-objective discrete optimization of laminated structures," *Mech. Res. Commun.*, vol. 29, no. 1, pp. 17–25, 2002, doi: 10.1016/S0093-6413(02)00227-6.

[206] K. K. L. Wong, "Bridging game theory and the knapsack problem: a theoretical formulation," *J. Eng. Math.*, vol. 91, no. 1, pp. 177–192, 2015, doi: 10.1007/s10665-014-9742-1.

[207] R. Meng, K. H. Cheong, W. Bao, K. K. L. Wong, L. Wang, and N. gang Xie, "Multi-objective optimization of an arch dam shape under static loads using an evolutionary game method," *Eng. Optim.*, vol. 50, no. 6, pp. 1061–1077, 2018, doi:

10.1080/0305215X.2017.1378876.

[208] R. Meng, N. Xie, and L. Wang, “Multiobjective game method based on self-adaptive space division of design variables and its application to vehicle suspension,” *Math. Probl. Eng.*, vol. 2014, 2014, doi: 10.1155/2014/479272.

[209] H. Peters, *Game Theory: A multi-leveled approach*, First. Maastricht: Springer-Verlag Berlin Heidelberg, 2008.

[210] M. Bezoui, R. Euler, M. Moulai, and T. H. Boumediene, “A game theory approach to solve linear bi-objective programming problems : application to data collection in WSNs,” no. October, 2017.

[211] M. Xiao, X. Shao, L. Gao, and Z. Luo, “A new methodology for multi-objective multidisciplinary design optimization problems based on game theory,” *Expert Syst. Appl.*, vol. 42, no. 3, pp. 1602–1612, 2015, doi: 10.1016/j.eswa.2014.09.047.

[212] B. Chatterjee, “An optimization formulation to compute nash equilibrium in finite games,” *Proc. Int. Conf. Methods Model. Comput. Sci. ICM2CS09*, 2009, doi: 10.1109/icm2cs.2009.5397970.

[213] E. Holmberg, C. J. Thore, and A. Klarbring, “Game theory approach to robust topology optimization with uncertain loading,” *Struct. Multidiscip. Optim.*, vol. 55, no. 4, pp. 1383–1397, 2017, doi: 10.1007/s00158-016-1548-5.

[214] K.-B. Sim and J.-Y. Kim, “Solution of multiobjective optimization problems: coevolutionary algorithm based on evolutionary game theory,” *Artif. Life Robot.*, vol. 8, no. 2, pp. 174–185, 2004, doi: 10.1007/s10015-004-0308-6.

[215] J. S. Shamma, “Special Topic : Games in Control Systems Game theory , learning , and control systems,” vol. 7, no. 7, pp. 1120–1122, 2020.

[216] S. Mahjoubi and Y. Bao, “Game theory-based metaheuristics for structural design optimization,” *Comput. Civ. Infrastruct. Eng.*, vol. 36, no. 10, pp. 1337–1353, 2021, doi: 10.1111/mice.12661.

[217] N. Xie, N. Shi, J. Bao, and H. Fang, “Analysis and Application of Multi-object Decision Design Based on Game Theory,” *6Th World Congr. Struct. Multidiscip. Optim.*, no. June, 2005.

[218] Rui Meng, Ye Ye, and Neng-gang Xie, “Multi-objective optimization design methods

based on game theory," in *2010 8th World Congress on Intelligent Control and Automation*, Jul. 2010, no. 070414154, pp. 2220–2227, doi: 10.1109/WCICA.2010.5554307.

[219] A. K. Dhingra and S. S. Rao, "A cooperative fuzzy game theoretic approach to multiple objective design optimization," *Eur. J. Oper. Res.*, vol. 83, no. 3, pp. 547–567, 1995, doi: 10.1016/0377-2217(93)E0324-Q.

[220] M. S. Monfared, S. E. Monabbati, and M. Mahdipour Azar, "Bi-objective optimization problems with two decision makers: refining Pareto-optimal front for equilibrium solution," *OR Spectr.*, vol. 42, no. 2, pp. 567–584, 2020, doi: 10.1007/s00291-020-00587-9.

[221] S. S. Rao, "Game theory approach for multiobjective structural optimization," *Comput. Struct.*, vol. 25, no. 1, pp. 119–127, 1987, doi: 10.1016/0045-7949(87)90223-9.

[222] T. L. Vincent, "Game theory as a design tool," *J. Mech. Des. Trans. ASME*, vol. 105, no. 2, pp. 165–170, 1983, doi: 10.1115/1.3258503.

[223] W. Elsner, T. Heinrich, and H. Schwardt, "Tools II: More Formal Concepts of Game Theory and Evolutionary Game Theory," in *The Microeconomics of Complex Economies*, 2015, pp. 193–226.

[224] W. Elsner, T. Heinrich, and H. Schwardt, "Tools III: An introduction to simulation and Agent-Based Modeling," in *The Microeconomics of Complex Economies*, 2015, pp. 227–249.

[225] N. G. Xie, R. Meng, Y. Ye, L. Wang, and Y. W. Cen, "Multi-objective design method based on evolution game and its application for suspension," *Struct. Multidiscip. Optim.*, vol. 47, no. 2, pp. 207–220, 2013, doi: 10.1007/s00158-012-0815-3.

[226] M. Jin, X. Lei, and J. Du, "Evolutionary game theory in multi-objective optimization problem," *Int. J. Comput. Intell. Syst.*, vol. 3, pp. 74–87, 2010, doi: 10.1080/18756891.2010.9727754.

[227] D. Greiner, J. Periaux, J. M. Emperador, B. Galván, and G. Winter, "Game Theory Based Evolutionary Algorithms: A Review with Nash Applications in Structural Engineering Optimization Problems," *Arch. Comput. Methods Eng.*, vol. 24, no. 4, pp. 703–750, 2017, doi: 10.1007/s11831-016-9187-y.

[228] E. J. Hudson and P. Reynolds, “Design and Construction of a Reconfigurable Pedestrian Structure,” *Exp. Tech.*, vol. 41, no. 2, pp. 203–214, 2017, doi: 10.1007/s40799-016-0144-3.

[229] “Ansys | Engineering Simulation Software.” https://www.ansys.com/ (accessed Sep. 19, 2022).

[230] N. F. Alkayem, M. Cao, Y. Zhang, M. Bayat, and Z. Su, “Structural damage detection using finite element model updating with evolutionary algorithms: a survey,” *Neural Comput. Appl.*, vol. 30, no. 2, pp. 389–411, 2018, doi: 10.1007/s00521-017-3284-1.

[231] Y. F. Jin, Z. Y. Yin, W. H. Zhou, and X. Liu, “Intelligent model selection with updating parameters during staged excavation using optimization method,” *Acta Geotech.*, vol. 15, no. 9, pp. 2473–2491, 2020, doi: 10.1007/s11440-020-00936-6.

[232] G. H. Kim and Y. S. Park, “An improved updating parameter selection method and finite element model update using multiobjective optimisation technique,” *Mech. Syst. Signal Process.*, vol. 18, no. 1, pp. 59–78, 2004, doi: 10.1016/S0888-3270(03)00042-6.

[233] H.-P. Wan and W.-X. Ren, “Parameter Selection in Finite-Element-Model Updating by Global Sensitivity Analysis Using Gaussian Process Metamodel,” *J. Struct. Eng.*, vol. 141, no. 6, p. 04014164, 2015, doi: 10.1061/(asce)st.1943-541x.0001108.

[234] “Matlab 2022.” https://uk.mathworks.com/.

[235] W. T. Thomson and M. D. Dahleh, *Theory of Vibration with Applications*, 5th editio. Pearson Education Asia Limited and Tsinghua University Press, 2005.

Curriculum vitae

Suzana Ereiz was born in 1996 in Split, Croatia. She attended elementary school in Nova Bukovica and graduated from high school in Slatina. In 2014, she enrolled in undergraduate studies in civil engineering at the University of Zagreb, where she also pursuing her graduate studies in the Theory and Modelling of Structures programme. During her studies, Suzana received multiple awards from the Faculty and University for her academic and scientific achievements. She was also one of the few scholarship recipients at the University of Zagreb. In 2019, she was awarded the Rector's award for her scientific research in the field of structural dynamic and determination of axial force in tie rods of historical buildings under the guidance of Professor Ivan Duvnjak. In September 2019, Suzana graduated from the University of Zagreb with her master's thesis in the field of structural dynamics and model updating under the supervision of Professor Ivan Duvnjak. After her graduation she enrolled in postgraduate studies at the Faculty of Civil Engineering in the field of structural mechanics. During the same time, she has been employed in a private company that deals with the structural design.

Later, in February 2020, Suzana joined the Department of Engineering Mechanics at the Faculty of Civil Engineering, University of Zagreb, as research assistant on the project entitled "Autonomous system for assessment and prediction of infrastructure integrity, (ASAP)" founded by European structural and investment funds, Operational programme competitiveness and cohesion. During her work at the faculty, she has been involved in numerous professional projects of Laboratory of testing of structures mostly related to structural dynamic testing of existing structures. She spent a short period at Seville ETSI, Porto FEUP, Twente CME. To date, Suzana has published as author and co-author 6 research article in scientific journals and 6 conference papers.

JOURNAL PUBLICATIONS

A] Web of Science Core Collection (WoSCC), Current Contents

- Ereiz, Suzana; Jiménez-Alonso, Javier Fernando; Duvnjak, Ivan; Pavić, Aleksandar: Game theory-based maximum likelihood method for finite-element-model updating of civil engineering structures // Engineering structures, 277 (2022), 15; 115458, 15 doi:10.1016/j.engstruct.2022.115458
- Ereiz, Suzana; Duvnjak, Ivan; Jiménez-Alonso, Javier Fernando Review of finite element model updating methods for structural applications // Structures, 41 (2022), 684-723 doi:10.1016/j.istruc.2022.05.041
- Ereiz, Suzana; Duvnjak Ivan; Damjanović, Domagoj; Bartolac, Marko Analysis of Seismic Action on the Tie Rod System in Historic Buildings Using Finite Element Model Updating // Buildings, 11(10) (2021), 103390, 18
- Duvnjak, Ivan; Ereiz, Suzana; Damjanović, Domagoj; Bartolac, Marko Determination of Axial Force in Tie Rods of Historical Buildings Using the Model-Updating Technique // Applied Sciences-Basel, 10 (2020), 17; 6036, 15 doi:10.3390/app10176036

B] Web of Science Core Collection (WoSCC), Science Citation Index Expanded

- Ereiz, Suzana; Bartolac, Marko; Goričanec, Jurica; Orsag, Matko Application of UAVs for assessment of bridge infrastructure // Journal of the Croatian Association of Civil Engineers, 73 (2021), 11; 3254-2021, 12 doi:10.14256/JCE.3254.2021